ABSTRACT

Title of Dissertation: A PROCESS MODEL TO CHARACTERIZE AIRBORNE RADIONUCLIDE EMISSIONS AND TRANSPORT USING RADIOLOGICAL AND METEOROLOGICAL MEASUREMENTS

Dwight LeRoi Williams, Doctor of Philosophy, 2005

Dissertation directed by: Professor Gary A. Pertmer
Department of Nuclear Engineering

The radionuclide analysis model developed and validated in this study is the first one ever to integrate human judgment throughout the analytical process. Therefore, besides relating the generation, transport, and measurement of anomalous anthropogenic radionuclides, this model enables many associated tasks to be achieved that could not be performed using existing models. These tasks include thoroughly characterizing radionuclide detection sites, effectively processing qualitative data, and correcting data during processing. The study outlines the model as a highly detailed itemized procedure and validates the model through four case studies. Each case study is able to demonstrate a specific novelty of the model, although multiple novel and useful qualities of the model can be found in all of the case studies. Case Study 1 shows the model's ability to perform site characterizations by determining the presence of 50 radionuclides at a site where only seven had been identified previously. In Case Study 2, the model is shown to be able to isolate a specific emission location through the effective incorporation of

qualitative data. Case Study 3 demonstrates the model's ability to perform complicated radionuclide analysis completely independent of computational models. Through Case Study 4, the model is shown to be capable of processing errant data that could not be analyzed computationally. Besides the usefulness of each of the novelties, the model offers many practical values, including its ability to normalize analysis amongst radionuclide analysts with varied levels of experience -- effectively enabling junior level analysts to perform senior level analysis.

A PROCESS MODEL TO CHARACTERIZE AIRBORNE RADIONUCLIDE EMISSIONS AND TRANSPORT USING RADIOLOGICAL AND METEOROLOGICAL MEASUREMENTS

by

Dwight LeRoi Williams

Dissertation submitted to the Faculty of the Graduate School of the
University of Maryland, College Park in partial fulfillment
of the requirements for the degree of
Doctor of Philosophy
2005

Advisory Committee:

Associate Professor Gary A. Pertmer, Chair
Associate Professor Mohamad Al-Sheikhly
Professor Emeritus Joseph Silverman
Associate Professor Carol Smidts
Doctor Christopher Yeaw

I dedicate this dissertation to my Lord, Jesus Christ, who gave me
the guidance and instilled in me the perseverance
that enabled the completion of my
Doctor of Philosophy degree.

ACKNOWLEDGEMENTS

The completion of my doctoral degree was facilitated by the efforts of many organizations and individuals -- too many to be acknowledged in totality. Therefore, I will limit my acknowledgements to those whose support has been most tangible. The organizations whose assistance proved to be most substantial include the Office of the Deputy Assistant to the Secretary of Defense for Chemical Demilitarization & Threat Reduction (Dr. Steve Mangino), the Tri - University Meson Facility (Dr. John D'Auria), and the University of British Columbia (Dr. David Measday). Each of these organizations supplied data that was essential for the completion of my research. In addition, the financial support and educational resources provided by the Southern Regional Education Board Doctoral Scholars Program (led by Dr. Ansley Abraham) were invaluable.

The list of individuals whose support has been most meaningful must begin with my family members -- especially my wife (Sonja), my mother (Sharon Musa), and my father and mother in law (William and Solina Johnson). I am forever indebted to them for their love, encouragement, and multifaceted support. Outside of my family, my technical mentor and friend, Dr. Nelson DeGangi, helped me to think like a Ph.D. nuclear engineer and to keep work-related matters in perspective. Also, my special projects partner and friend, Dr. Jim Brangan, was steadfast in his encouragement and in helping me to plan ahead. I thank my advisory team (Drs. Pertmer, Al-Sheikhly, Silverman, Smidts, and Yeaw) for their guidance and availability; the UMCP staff for their valuable assistance; and all those who prayed on my behalf as I strived for this goal.

TABLE OF CONTENTS

LIST OF TABLES

LIST OF FIGURES

Chapter I: INTRODUCTION

Problem Statement

Purpose

The purpose of this project is to develop a process model that relates the generation, transport, and measurement of anomalous anthropogenic radionuclides. Given certain radiation or radionuclide measurements at a site, and possibly meteorological measurements, this model can be used to determine features associated with the source of the release, its transport, and the distribution of radionuclides at the detection site. Specifically, given the radionuclides and concentrations measured along with the prevailing local wind speeds and directions, this model will be able to estimate the emission time, duration, cause, source, radionuclides, and concentrations. Moreover, the source and transport estimations along with the measurement data trends at the detection site can be used to estimate anomalies, radionuclides that are present but not identified, and downwind concentrations. This model is ideally suited for real-world situations in which atmospheric radionuclides released from a site have been subsequently detected with radionuclide monitoring equipment. Even so, the novelties and uses associated with this model are broadly applicable and would add value to various types of technical analysis.

What Distinguishes This Research as being New?

The model developed introduces a revolutionary new approach to analyzing complex radionuclide monitoring data. This model is the first one ever to integrate human

judgment throughout the analytical process. As a result, this is the only model that is capable of:

- thoroughly characterizing a site based upon measured quantitative data (Note: In Case Study 1, existing techniques identified only 7 radionuclides; however, this model identified 50 radionuclides);
- analyzing complex radionuclide data without computational models;
- processing both qualitative and quantitative data with equal effectiveness; and
- correcting data as it is being processed (Note: Existing models are only able to correct data prior to input or following output; they cannot correct data during processing).

1. This model focuses on site characterization beyond the interpretation of measured data.

Quantitative models merely manipulate and interpret measured data. These models are unable to address specifics that have not been quantifiably measured and are therefore unable to achieve site characterization (since measured data represents only a subset of the total radionuclide data onsite). Because the model developed is the first ever that is able to systematically incorporate qualitative and other data -- in addition to the measured quantitative data -- it is the only model that is capable of achieving full radionuclide site characterization.

An associated novelty of this model is that it is the only one that can address <u>why</u> certain data measured (or not measured) is not consistent with ground truth. Computational

models are only able to provide insight into measured data consistencies with ground truth. Analysis of inconsistencies requires information beyond the measured data, and is therefore beyond the capability of computational models.

2. This process is the first that enables complex radionuclide monitoring data to be analyzed without computational models.

While computational models can facilitate the analytical processes of this model, they are not required in order to generate meaningful, generally accurate results. No other model in existence offers such repeatable results without the incorporation of computational models. (Note: Computational models yield "generally accurate" results as well, as a function of the input data. Certainly, the results of computational models are likely to be more precise, but not necessarily more accurate. Case Study 1 shows that this model can be more accurate than computational models, which offered no solution for the problem set in Case Study 1. Case Study 2 shows that this model can be more precise than computational models, which generated a broad area solution (southern Spain) instead of a facility-specific (Acerinox Smelting Plant) solution in Case Study 2.)

3. While computational models rely upon quantitative data as inputs, this model is the first to process both quantitative and qualitative data effectively.

Quantitative models have no way to accurately incorporate human factors, non-quantitative data media, etc. into their analysis. At best, this type of information is included as a statistical probability -- a number. While continued use of models utilizing this approach over time can generate results that normalize to reasonable approximations,

no subset of model runs is guaranteed to accurately account for the multifaceted variations of these qualitative data. The model developed is the first to thoroughly and accurately account for qualitative data inputs.

4. This radionuclide analysis model is the only one that corrects data as it is being processed.

Because existing models cannot incorporate human judgment into their processing, they are unable to recognize poor quality or inaccurate data and provide corrections. These models have no reasoning capability and are not designed to incorporate reason -- they simply process the quantitative data presented to them. It is this fact that led to the adage, "garbage in, garbage out." All data corrections must take place prior to data entry into the models or after the processed data has been output because the data cannot be corrected during processing. The model developed, on the other hand, is integrally dependent upon human judgment, and therefore is able to recognize and correct data as they are being processed.

In What Ways will This Research be Useful?

1. The model developed enables analysts of varying expertise and experience levels to reach normalized data analysis conclusions.

One of the principal benefits of this model is that it provides a peer-reviewed, standardized radionuclide analysis process from beginning to end. As a result, when a radionuclide detection system registers an anomalous reading -- be it the result of a complex radionuclide emission and transport, or a simple malfunction within the

processing equipment -- radionuclide analysts of varying knowledge and experience levels are able to systematically determine the cause of the reading in a repeatable, normalized manner. By thoroughly defining the analytical process in such a structured manner, junior analysts are able to perform senior level analysis, and analysts of all levels are able to follow the same comprehensive analytical sequence enabling them to reach normalized conclusions regarding the cause of the anomalous reading. In short, this model provides a mechanism for less experienced analysts to perform complicated radionuclide emission site characterizations as if they had years of experience.

2. This model enables definitive conclusions regarding the source of anomalous radionuclide detections to be determined.

Another benefit of the model is that it enables definitive conclusions to be reached through analysis. Typically, radionuclide analysis models are able to provide insight into particular anomalous readings by detection equipment; but no existing model is able to provide definitively accurate answers. Because these models are only able to process quantitative data and merely interpret the data entered into them, there is no way for the defining information, which includes qualitative data, to be incorporated adequately. Since the model developed incorporates qualitative data, several aspects related to the definitive "ground truth," which are not quantitative, can be included in the analysis. With the incorporation of all "ground truth" information into the analytical process, this model is able to trace a measured anomaly to its definitive source with a level of certainty that is not achievable with existing models.

3. If computational models are the desired analytical process, then this model can serve as a preprocessor of information prior to computational model use.

Due to the comprehensive, standardized processing of information in the early stages of this model, and the level of analysis that can be achieved without computational models, if computational models are the desired method for analysis, then this model can effectively serve as a preprocessor of data prior to computational model analysis. The early stages of the model enable measured data to be vetted and assumptions that will be incorporated into the analysis to be standardized. This preprocessing can prevent analysts from using the same computational model to analyze an anomalous reading and reaching varied conclusions that result from differing assumptions that have been incorporated.

4. This model can provide insight into the applicability of computational models in various circumstances.

In addition, because this model can serve to define the inputs and assumptions that will be incorporated into computational models, this model provides a systematic method for determining which computational models are and are not applicable for analyzing various situations. Therefore, this model can minimize the possibility that a computational model will be applied incorrectly to analyze an anomalous detection, resulting in suspect output.

5. This model can generate reasonable results based upon incomplete or inaccurate data.

Finally, since this model integrates human judgment into the analytical process, it enables reasonable estimates to be derived from incomplete or inaccurate measured quantitative

data. Existing models, which are incapable of adequately incorporating human judgment, provide little insight into anomalous radionuclide detection system readings without a reasonably complete data set. The output resulting from inaccurate or incomplete data can be quite inaccurate. However, the incorporation of human judgment, and therefore qualitative data, into this model's analysis enables it to draw from more information than the incomplete or inaccurate qualitative data measured, and provide reasonable results based upon the broader data analyzed.

Literature Review

This literature review is intended to serve as a knowledge baseline in the areas of atmospheric radionuclide emissions, atmospheric radionuclide transport, radionuclide collection/detection systems, and models that relate these phenomena. The purpose of this baseline is twofold. First, when considered in totality, this baseline will describe the radionuclide source-receptor models in existence and highlight the fact that none of these models incorporate human judgment throughout the analytical process. Therefore, no model is able to effectively process qualitative data, thoroughly characterize emission sites, correct for inaccurate or incomplete data during processing. Second, this baseline will provide reference information and characterization data that can be incorporated into the model developed in this study.

The structure of this review is relatively straightforward. First, each of the relevant phenomena (i.e., atmospheric radionuclide emissions, atmospheric radionuclide transport, and radionuclide collection/detection systems) is investigated. After the fundamental scientific phenomena have been introduced and addressed, relevant models that attempt to systematize these processes are investigated. It is through this final investigation that key knowledge voids are highlighted.

I. Atmospheric Radionuclides in the Environment and Their Sources

A. Nuclear Weapons Detonations

1. Introduction

2. Overt Atmospheric Detonation

3. Evasive Atmospheric Detonation

4. Underground Detonation

5. Underwater Detonation

6. Using Fission Products to Identify Nuclear Explosions

7. Activation Products Indicative of Nuclear Weapons Explosions

8. Broader Use of Radionuclides to Characterize Nuclear Explosions

9. Fractionation Effects that may Influence Nuclear Detonation Characterization

B. Medical Industry Emissions

1. Introduction

2. Radionuclides Detected by Atmospheric Radionuclide Sensors

C. Nuclear Reactor Emissions

1. Reactor Operation

2. Three Mile Island

3. Chernobyl

D. Reprocessing

1. Introduction

2. Decladding and Dissolution Phases

3. Off-gas Treatment

4. Reprocessing Facilities and Data

E. Other Processes

F. Natural Radionuclides

1. Introduction

2. Primordial Radionuclides

3. Primordial Radionuclide Daughters

4. Induced Radionuclides

II. Meteorological Influences

A. Introduction

B. Vertical Temperature Structure of Atmosphere

C. Instantaneous and Continuous Source Term Approximations

D. Characteristic Effluent Plumes

1. Fanning

2. Fumigation

3. Looping

4. Coning

5. Lofting

6. Caveats

E. Atmospheric Diffusion of Radionuclide Emissions

F. Diffusion Equations

1. Concentration Calculations -- Infinite Medium

2. Concentration Calculations -- Finite Medium

3. Additional Relationships

III. Collection/Detection Systems

A. Introduction

B. Radionuclide Collection Systems

1. General Methods for Airborne Sample Collection

Atmospheric Radionuclides in the Environment and Their Sources

Nuclear Weapons Detonations

Introduction

Historical studies have thoroughly evaluated radionuclide emissions that are generated by nuclear weapon explosions. The overwhelming majority of these studies are based upon nuclear weapons testing data and experience. The four nuclear weapons testing scenarios that have been evaluated in literature include overt atmospheric tests, evasive atmospheric tests, underwater tests, and underground tests. Because each scenario incorporates different environments and circumstances, the indicative radionuclides and corresponding quantities that are emitted vary according to the specific scenario. Table

1, which summarizes data found in literature, shows the percentage of particulate and gaseous radionuclides generated during a detonation that are detectable. Although there is no consistency between the scenario percentages, the detectable radionuclides can be categorized into one or more of the following sets: fissile material constituents, fission products, and activation products.

Table 1: Percentages of Detectable Radionuclides Based upon Nuclear Detonation Scenario

Scenario	**Detectable Particles**	**Detectable Gases**
Overt Atmospheric Detonation	15 - 100 %	100 %
Evasive Atmospheric Detonation	~ 0 - 10 %	5 - 15 %
Underground Detonation	0 - 15 %	1 - 100 %
Underwater Detonation	0 - 40 %	~ 0 - 100 %

Overt Atmospheric Detonation

Because of the quantity, variety, properties, airborne elevation, and atmospheric duration of radionuclides emitted during an overt atmospheric nuclear weapons detonation, this scenario has shown the greatest opportunity for radionuclide collection. Based upon the literature cited, an overt nuclear detonation is one in which few, if any, measures are taken to limit external awareness of the explosion. The most thoroughly studied overt atmospheric nuclear explosions have occurred either at or near the earth's surface (heights of burst ranging from 0 to 100 m).

As Table 1 shows, overt atmospheric nuclear explosions are most effectively detected via particulate radionuclide detection. Literature indicates that, on average, over 90% of the radionuclides generated in this manner are emitted into the atmosphere and are available for detection. Although in some special cases, upwards of 85% of the particulate radionuclides generated are suppressed and not detectable, because of the sheer volume of particulate nuclides generated, measuring particles frequently provides more data than measuring gases.

Extensive research has been conducted on the radionuclides that are detectable following an overt atmospheric nuclear weapons explosion. Several representative radionuclide sets are listed within Table 2. Differences between the sets are generally the result of several factors including how much they are based upon nuclear test data as opposed to theoretical calculations, the yield and type of nuclear device detonated, the height of burst, the assumed radionuclide sampling parameters, and the atmospheric conditions considered.

Of the wide variety of particulate radionuclides that serve as key indicators of an atmospheric nuclear weapons detonation (see Table 2), the most referenced was Ba-140. Others that were heavily referenced include Zr-95, Ru-103, Mo-99, and I-131. Ba-140 has been found to be most favorable because of the fission abundance of the mass 140 chain, its half-life relative to its precursors, its activity, and its ease of detection using gamma-ray spectroscopy. The 6.22% fission abundance of the mass 140 chain makes it the 12^{th} most abundant chain, well within the top 15% of all mass chains generated. The

three precursors of Ba-140, which are I-140, Xe-140, and Cs-140, have half-lives of 0.86 s, 13.6 s and 1.06 m, respectively. As a result, after approximately 10 minutes, Ba-140 exists independently, and because Ba-140 has a half life of 12.75 days, it can be detectable for months into the future. Ba-140 is easily detectable using gamma-ray spectroscopy because of the 100% abundant 537.3 keV gamma-ray it emits as it beta decays into La-140.

As Table 2 indicates, isotopes of xenon have been identified as the most conducive of the gases for radionuclide monitoring. Although other radionuclide gases are generated during an explosion (e.g., isotopes of krypton), these radioisotopes are generated with much lower abundances than radioxenons and can be more difficult to measure. Xe-133 has been commonly referenced as the gaseous key indicator of an atmospheric nuclear weapon detonation because of the fission abundance of the 133 mass chain (6.7%, the 3rd most abundant chain) and the distinct 81 keV gamma-ray (38% abundance).

Of the cases in which an overt atmospheric nuclear explosion could result in suppressed radionuclide signatures, a stratospheric detonation is most common. Because of the low mixing rates between the stratosphere and the troposphere, radionuclides can remain entrained in the stratosphere on the order of months before entering the troposphere in detectable quantities. As a result, Ba-140 is not an ideal indicator for these events since its half life would cause it to decay down to trace amounts within this time period. According to literature, the longer lived Zr-95 ($t_{1/2}$ = 62 days) and Ce-144 ($t_{1/2}$ = 284.6 days) are more suitable radionuclide indicators for a stratospheric nuclear detonation.

However, due to the relatively low activity of these radionuclides and their disbursed nature upon reentering the troposphere, detecting measurable quantities can still be difficult.

Evasive Atmospheric Detonation

The principal ways that nuclear weapons can be detonated in the atmosphere and generate minimal detectable radionuclide signatures are to use high strength containment chambers and conduct the detonation during heavy rain. Just as in the case of an overt detonation, the principal radionuclides that would likely be detectable are Ba-140 and Xe-133, although their measured concentrations would be diminished according to the effectiveness of the evasion efforts. For that matter all of the radionuclides listed in Table 2 would have the possibility of being detected following an evasive atmospheric detonation, but their likelihood of detection could be reduced to negligible amounts.

Although chambers exist that can fully contain radionuclide particulates generated by hydronuclear and low yield nuclear explosions (< 1 kt), for a high yield nuclear explosion, a containment chamber will only serve as an impediment to dispersion. Even though chambers are unable to contain a high yield explosion, the heavy metal chamber materials suppress the detectable radionuclide signatures by providing additional mass to the radionuclide cloud which reduces its dispersion height and increases gravitational settling thereby inhibiting long range detection. The added mass also enables more rapid cooling because the hot fission products are able to condense on the cooler chamber products that were vaporized during the detonation. Independent of the nuclear

detonation yield and the type of containment chamber used, a percentage of the radionuclide gases are released into the atmosphere.

Detonating a nuclear weapon in the atmosphere during a thunderstorm can suppress radionuclide signatures by entraining radionuclide particles in the rain water. Although studies agree that rain water can entrain these radionuclides, there is disagreement with respect to the level of entrainment. The studies that postulate rain to be an effective radionuclide particle suppressor estimate the effectiveness to be approximately 90%. Other studies question the theoretical nature of estimating radionuclide signature suppression, given the complexities of particle formation and dispersion, given no nuclear test data to support or refute the phenomenon. Scientists agree that rain is less effective at suppressing noble gas signatures than particulates signatures.

Underground Detonation

As Table 1 shows, although detectable radionuclide particles are an obvious result of an atmospheric nuclear detonation, in some cases, particles can be detected from underground and underwater detonations. Historical U.S. nuclear testing practices have shown that it is possible to contain all of the radionuclide particulates generated. Similarly, Russian experience indicates that half of their underground nuclear tests successfully contained all of the radionuclides generated, both particulates and gases.

Because effective containment practices are well known and necessary equipment is internationally accessible, it can be concluded that if radionuclides are allowed to escape

from an underground nuclear detonation, then it is the result of careless engineering practices or a deliberate decision to allow the release. Examples of carelessness include improper shaft construction, improper geological evaluation, and grossly inaccurate explosive yield calculations. Historically, deliberate radionuclide releases have been allowed due to prohibitive costs and domestic resources associated with full containment, a lack of concern whether full containment was achieved, and various experiments that investigated radionuclide release rates into the atmosphere following an underground nuclear explosion.

Generally, vertical shafts have been shown to contain radionuclides much better than horizontal shafts. This is likely because vertical shafts can be drilled to great depths, while the amount of overburden available for horizontal shafts is limited to the natural overburden in the topographical area. In addition, the geological response of the ground following a vertical shaft nuclear explosion (e.g., the creation of a subsidence crater) is also instrumental to suppressing radionuclides underground.

In cases where gases escape the ground and enter the atmosphere, xenon is the only gas of consequence. Experimentation at the Nevada Test Site showed that the total amount of xenon released is no greater that the prompt iodine and xenon radionuclide yields. All of the other customary contributors to the total xenon yield become entrenched in matrices underground and these matrices do not readily release the xenon once created. As a result, the xenon release duration spans on the order of days, corresponding to the half lives of the iodine and xenon.

Underwater Detonation

The opportunities for downwind collection of atmospheric radionuclide debris are least likely following an underwater nuclear detonation. As shown in Table 1, the total atmospheric radionuclide release can be near 0% in some cases -- especially for deeply submerged explosions. While the processes governing particulate entrainment in ocean water are well understood, the chemistry and physics noble gases dispersion through ocean water is more ambiguous. In general, if evasive techniques are used in conjunction with the underwater detonation, then the atmospheric release can be reduced by an additional two orders of magnitude.

Of course, relevant experimental data for underwater nuclear explosions was obtained though actual nuclear underwater weapons tests. Naturally, the largest quantity of radionuclides (5%) was released during the shallowest detonation (Crossroads Baker -- 25 m underwater). Other, deeper underwater (45 - 600 m) detonations released fewer radionuclides (~ 0.01 - 1%), and one underwater detonation is not known to have released any particulate or gaseous radionuclides into the atmosphere. The majority of radionuclides that escaped the surface were volatiles, radionuclides with condensation/evaporation temperatures below 1600K. Volatiles are known to escape because they approach the water surface in a gaseous state. Data regarding atmospheric xenon gas release quantities following an underwater nuclear detonation are poorly referenced in literature.

No experimental data exists regarding very shallow or very deeply submerged underwater detonations; therefore, theoretical estimations and extrapolations have been performed. The conclusion reached for a slightly submerged nuclear explosion was that approximately 40% of the particulate radionuclides and possibly all of the gases would be released and detectable. In cases where the detonation is so deep that it collapses upon itself before reaching the water surface, scientists estimate that radionuclide releases would be negligible.

In both the experimental and theoretical cases, the entrained radionuclides can remain submerged below the water surface indefinitely. Gamma-rays emitted from radionuclides that migrate to shallow depths can be detectable above the water in the local vicinity of the detonation for approximately one week. However, these radionuclides will not contribute to any downwind measurements unless they are released from the water's surface.

Using Fission Products to Identify Nuclear Explosions

Prototype International Data Center (PIDC) scientists found that nuclear weapon detonations could best be identified using two intersecting sets of radionuclides. The first, more comprehensive set was the radionuclide library which consisted of all radionuclides that would have a reasonable possibility of detected with gamma-ray spectroscopy following a nuclear weapon detonation. This list is shown in Column A of Table 2. Factors affecting detectability include the nuclear detonation environment, radionuclide yield, half-life, decay mode, and decay physics. The second, limited set

consisted of radionuclides that would be most likely detectable by gamma ray spectroscopy following a nuclear weapon detonation. This list of most likely radionuclides was established by the international Conference on Disarmament in Working Paper CD/NTB/WP.224, published in March 1995. This list is shown as Column B of Table 2. All of the radionuclides listed are fission products that are of relatively high abundance. Radionuclide sets from Germany, the Pacific Northwest National Laboratory (PNNL), and the Russian Federation have also been listed.

Table 2: Radionuclides Used to Identify Nuclear Weapons Detonations

Radionuclide	**A. PIDC Library**	**B. WP.224**	**C. Germany**	**D. PNNL**	**E. RFNC**
Ag-110				X	
Ag-111	X		X	X	
Ag-113	X				
As-77	X		X		
Ba-140	X	X	X	X	X
Cd-115	X		X	X	
Cd-115m	X				
Ce-141	X		X	X	
Ce-143	X	X	X		
Ce-144	X		X	X	X
Cs-134	X	X	X	X	
Cs-136	X	X	X		

Cs-137	X	X	X	X	
Eu-155	X				
Eu-156	X		X		
Eu-157	X		X		
Gd-159	X				
Ge-77	X				
I-131	X	X	X	X	X
I-132			X	X	
I-133	X	X	X	X	
I-135	X		X		
Kr-85m			X		
Kr-88			X		
La-140	X		X	X	X
La-141	X		X		
Mo-99	X	X	X	X	X
Nb-95	X	X	X		X
Nb-95m	X		X		
Nb-96	X				
Nd-147	X		X	X	
Pd-109	X		X		
Pd-112	X		X		
Pm-149	X		X		
Pm-150	X				

Pm-151	X		X		
Pr-145	X				
Rh-105	X		X		
Ru-103	X	X	X	X	X
Ru-105	X		X		
Ru-106	X		X		X
Sb-125	X				
Sb-126	X		X		
Sb-127	X		X	X	
Sb-128	X		X		
Sb-129	X		X		
Sm-153	X		X		
Sm-156	X		X		
Sn-123	X				
Sn-125	X		X		
Sr-91	X		X		
Sr-92	X		X		
Tb-161	X				
Tc-99m	X		X		
Te-129m	X				
Te-131m	X		X		
Te-132	X	X	X	X	
Xe-131m	X	X	X		

Xe-133	X	X	X		X
Xe-133m	X	X	X		
Xe-135	X		X		X
Y-92	X		X		
Y-93	X		X		
Zr-95	X	X	X	X	X
Zr-97	X	X	X	X	

Having identified sets of radionuclides useful for determining whether or not a nuclear detonation had occurred, PIDC scientists were able to develop criteria for determining when a nuclear weapons test had likely NOT occurred. They concluded that unless two of the anthropogenic radionuclides within the library were identified, at least one of which being a fission product, then the source of the radionuclides likely was not a nuclear weapons test. Certainly, at least one of the radionuclides was expected to be a WP.224 radionuclide, but this was not a criterion.

Once the likely occurrence of the event had been established, independent analysis was conducted at multiple laboratories around the world. One of the principal methods of analysis at these laboratories was to analyze certain fission product ratios to further characterize the event. Some of the ratios that are preferred by various international laboratories are listed in Table 3. As the table shows, several sets of ratios can be useful. Based on these lists, each laboratory appears to have a differing philosophy regarding the use of fission product ratios. For example, Germany's list seems quite inclusive, as was

the German list of characteristic fission products provided in Table 2. On the other hand, PNNL prefers to avoid radionuclide ratios that incorporate two different elements due to distortions that could result from fractionation effects. Russia's list seems to incorporate only the most telling of the ratios; however, it should be noted that Russia relies on other ratios including activation product and fissile material ratios. Some scientists question the effectiveness of ratios that incorporate Nb-95 and Pm-149 (e.g., Nb-95m/Nb-95, Zr-95/Nb-95, and Pm-151/Pm-149) because the scientists have found that the gamma-rays used for quantification can be obscured by other gamma-rays likely to be present in spectra. As of 2001, the final set of certified international laboratory requirements, which would include a standardized set of radionuclide ratios for characterization, had not yet been established.

Table 3: Key Fission Product Ratios

Ratio	**A. Germany**	**B. PNNL**	**C. RFNC**
Ba-140/La-140	X		X
Ce-143/Ce-141	X	X	
Ce-143-Ce-144		X	
Ce-144/Ce-141	X	X	
Cs-137/Cs-136	X		
I-133/I-131	X		
Nb-95m/Nb-95	X		
Pm/151/Pm-149	X		
Ru-106/Ru-103	X		

Te-131m/Te/132	X		
Xe-133m/Xe-135	X		
Xe-135/Xe-133	X		
Zr-95/Nb-95	X		X
Zr-97/Zr-95	X	X	

Activation Products Indicative of Nuclear Weapons Explosions

Although fission products are the principal indicators of a nuclear weapons explosion, activation products can be equally as informative. These radionuclides are formed as neutrons escape the fissile material and interact with the nuclear weapon structural materials and other externals (e.g., soil, earth, etc.). While the presence of activation products alone does not indicate that a nuclear explosion has occurred, when coupled with the detection of fission products, the activation products can aid in characterizing the explosion.

As in the case with fission product evaluation, the activation product radionuclides that are used by various international scientists differ. The principal radionuclides that are universally considered include are Co-60 and Fe-59. These radionuclides are formed by neutron bombardment of the iron, nickel, and cobalt, materials in the weapon. The nuclear reactions are shown in Equation 1. Cs-134 is also considered to be an informative activation product; however, because the 134 mass chain is the most abundant of all fission mass chains, Cs-134 is normally listed as a fission product. The

Cs-134 activation reaction is shown in Equation 2. Other frequently referenced activation products are listed in Table 4.

Co-59 (n,γ) Co-60; Note: natural abundance of Co-59 is 100% Equation 1a

Ni-60 (n,p) Co-60; Note: natural abundance of Ni-60 is 26.2% Equation 1b

Fe-58 (n,γ) Fe-59; Note: natural abundance of Fe-58 is 0.26%, but overwhelming majority of structural materials are iron based Equation 1c

Cs-133 (n,γ) Cs-134; Note: natural abundance of Cs-133 is 100% Equation 2

Table 4: Activation Products Used to Identify Nuclear Weapons Detonations

Radionuclide	**A. PIDC Library**	**B. Germany**	**C. RFNC**
Ag-110m	X	X	
Am-241	X		
Br-82			X
Ce-137	X		
Ce-139	X		
Co-57	X	X	
Co-58	X	X	X
Co-60	X	X	X
Cr-51	X	X	
Cs-134	X	X	
Eu-152	X		

Eu-152m	X		
Fe-59	X	X	X
Hf-181		X	
Hg-203	X		
I-123	X		
I-126			X
K-42			X
Mn-54	X	X	
Na-22		X	X
Na-24			X
Np-239	X	X	X
Pa-233		X	
Sb-124		X	
Te-123m	X	X	
U-237	X	X	
Zn-65	X	X	

Broader Use of Radionuclides to Characterize Nuclear Explosions

While fission product ratios are most commonly used to determine the fissile material composition of a nuclear weapon and identify the date and location of a nuclear weapon explosion, several measured activation products and fissile material quantities are used to further characterize the detonation. Ratios involving either Mo-99, Zr-95, or Ce-144, and either Pu-239, Pu-240 or U-234 can be used to analyze energy release values due to

fission reactions. While the fission product quantities can be determined by gamma-ray spectroscopy, the transuranic quantities can be found by radiochemical or alpha particle analysis. To determine neutron energy distributions and fluence, gamma-ray spectroscopy can be used to quantify amounts of Np-239, Fe-59, Co-58, Co-60, Na-22, Na-24, K-42, Br-82, or I-126. Additionally, quantities of H-3 and Np-239 can be used, as well as the ratios U-235/U-234, U-234/U-238, Pu-238/Pu-239, Pu-238/Pu-240, Am-241/Am-239, and Am-241/Am-240, in order to assess the content of the special nuclear material used in the weapon. These values are determined by gamma-ray and radiochemical analyses. If the fissile material in the weapon was known to be plutonium, then the Am-241/Pu-241 ratio, which can be evaluated using alpha particle and gamma-ray spectroscopy, can provide information about the age of the plutonium. Finally, statistically Be-7 measurements have been known to provide insight into the sophistication of the nuclear weapon design; however, due to the significant magnitude of the Be-7 background around the globe, statistically significant measurements are uncommon.

Fractionation Effects that may Influence Nuclear Detonation Characterization

As PNNL has noted, using ratios involving differing chemical species can lead to inaccurate results due to fractionation effects. Fractionation is any change from the original set of radionuclides that are expected following a nuclear detonation. For instance, radionuclide quantity measurement variations that are the result of normal radioactive decay is not considered fractionation. On the other hand, chemical reactions that are partial to a particular radionuclide species and therefore perturb the quantities

from what would have been measured if the radionuclides had been in isolation is considered fractionation. Therefore, fractionation effects are caused by interaction of the nuclear explosion product radionuclides with their external environment. Fractionation effects can significantly and independently affect the quantities of radionuclides measured from a nuclear weapon detonation. As a result, they can cause meaningful inaccuracies in radionuclide ratio measurements.

Several factors can increase fractionation effects. For example, when condensation occurs more rapidly than normal, because a number of more volatile radionuclides exist within a select, few fission product mass chains, these mass chains can be affected by the rapid condensation differently than other mass chains. Similarly, the interaction of heavy particles, such as ejected soil or containment chamber materials blown up during the detonation, with the fission product radionuclides can enhance fractionation. Heavier particles tend to enhance condensation and settle more rapidly and therefore can skew downwind measurements. Other fractionation-prone influences include varying solubilities of radionuclides in water, radionuclide uptake by microorganisms, and the affinity of certain radionuclides toward specific sample collection processes.

For atmospheric detonations, if the fireball does not reach the ground, then fractionation effects tend to be minimal. However, in situations where external influences were more pronounced (e.g., during a rain storm), even if the fireball does not touch the ground, considerable fractionation can occur. Underwater nuclear explosions tend to experience more fractionation that air bursts. Even so, initial fractionation effects in water have been

moderate -- similar to the limited fractionation that occurs in air (likely because air and water demonstrate fluid-like properties). Later fractionation effects in water can be significant. When a nuclear weapon explodes underground, it can result in extreme fraction effects. These effects, however, are predictable based upon years of underground nuclear testing experience.

Medical Industry Emissions

Introduction

Radioisotope use within the medical industry has increased significantly over the past two decades. Medical radioisotopes are used around the world in over 13 million procedures per year to palliative, diagnostic, and treatment purposes. The most commonly used radioisotopes are listed in Table 5. As a result of the continued growth in radioisotope production, use, and disposal, radioisotopes have been periodically detected by airborne radionuclide monitoring systems. A number of medical radioisotopes are also indicative of a nuclear detonation. These radionuclides are bolded with a carrot (^) in Table 5. The six radionuclides that have been detected by the international network of sensors analyzed by the Prototype International Data Center (PIDC) are bolded and italicized with an asterisk in Table 5.

Table 5: Commonly Used Medical Radionuclides

Nuclide	**$t_{1/2}$**	**Nuclide**	**$t_{1/2}$**	**Nuclide**	**$t_{1/2}$**	**Nuclide**	**$t_{1/2}$**
Ac-225	10.0 d	**Cu-64^**	**12.7 h**	Mn-52	5.59 d	Sm-145	340 d
Ac-227	21.8 y	Cu-67	61.9 h	**Mo-99^**	**65.9 h**	**Sm-153^**	**2.00 d**

Am-241^	**432 y**	Dy-165	2.33 h	N-13	9.97 m	Sn-117m	13.6 d
As-72	26.0 h	**Eu-152^**	**13.4 y**	**Nb-95^**	**35 d**	Sr-85	65.0 d
As-74^	**17.8 d**	**Eu-155^**	**4.73 y**	O-15	122 s	Sr-89	50 d
At-211	7.21 h	F-18	110 m	Os-191	15.4 d	Sr-90	29.1 y
Au-198^	**2.69 d**	Fe-55	2.73 y	Os-194	6.00 y	Ta-178	9.3 m
Be-7	53.2 d	**Fe-59^**	**44.5 d**	P-32	14.3 d	Ta-179	1.8 y
Bi-212	1.10 h	Ga-64	2.63 m	P-33	25 d	Ta-182	115 d
Bi-213	45.6 m	Ga-67	78.3 h	**Pb-203^**	**2.16 d**	Tb-149	4.13 h
Br-75	98 m	Ga-68	68.1 m	Pb-212	10.6 h	Tc-96	4.3 d
Br-77	57 h	Gd-153	242 d	Pd-103	17 d	***Tc-99m^****	***6.01 h***
C-11	20.3 m	Ge-68	71 d	**Pd-109^**	**13.4 h**	Th-228	720 d
C-14	5730 y	H-3	12.3 y	Pu-238	2.3 y	Th-229	7300 y
Cd-109	462 d	I-122	3.6 m	Ra-223	11.4 d	***Tl-201^****	***73.1 h***
Ce-139	138 d	***I-123^****	***13.1 h***	Ra-226	1.6E3 y	**Tm-170^**	**129 d**
Ce-141^	**32.5 d**	I-124	4.17 d	Rb-82	1.27 m	Tm-171	1.9 y
Cf-252	2.64 y	I-125	59.9 d	Re-186	3.9 d	W-188	69.4 d
Co-55	17.5 h	***I-131^****	***8.04 d***	Re-188	17 h	Xe-127	36.4 d
Co-57^	**272 d**	I-132	2.28 h	**Rh-105^**	**35.4 h**	***Xe-133^****	***5.25 d***
Co-60^	**5.27 y**	In-111	2.81 d	Ru-97	2.89 d	**Y-88^**	**107 d**
Cr-51^	**27.7 d**	In-115m	4.49 h	**Ru-103^**	**39 d**	Y-90	64 h
Cs-130	29.2 m	Ir-191m	6 s	S-35	87.2 d	**Y-91^**	**58.5 d**
Cs-131	9.69 d	**Ir-192^**	**73.8 d**	**Sc-46^**	**84 d**	Yb-169	32 d
Cs-137^*	***30.2 y***	Kr-81m	13.3 s	**Sc-47^**	**3.34 d**	Zn-62	9.22 h

Cu-61	3.35 h	Lu-177	6.68 d	Se-72	8.4 d	**Zn-65^**	**244 d**
Cu-62	4.7 m	Mn-51	46.2 m	Se-75	120 d	**Zr-95^**	**64.0 d**

Radionuclides Detected by Atmospheric Radionuclide Sensors

Relatively few studies have investigated radionuclide effluents that result from medical industry processes. The PIDC is one organization that has devoted research to this issue and presented experimental results in peer reviewed technical publications. Consequently, the overwhelming majority of the literature cited in this area originated at the PIDC.

The PIDC monitored an international network of radionuclide sensors that could detect and quantify radionuclides from any industrialized continent. This type of global coverage made the PIDC network ideal for monitoring radionuclide effluents associated with the medical industry because medical radioisotope development and use has historically been most prevalent on industrialized continents. As table 1 indicates, the medical radionuclides identified by the network includes I-123, I-131, Tc-99m, Tl,-201, Cs-137, and Xe-133, and all of the medically-relevant detections were collect locally. In other words, there is no known global background concentration of radionuclides that has resulted from the medical radioisotope industry. Because PIDC analyses indicated that the Cs-137 and Xe-133 detections were unrelated to the medical isotope production or use, only the remaining four are addressed in this section.

I-123 is a radionuclide that is used for medical diagnostics purposes. The primary I-123 gamma-ray (159 keV, 83.3% abundance) is useful for cerebral imaging. I-123 is generated in a cyclotron through the proton bombardment of Xe-124 and subsequent decay of Cs-123. The reaction is listed in Equation 3.

$$\text{Xe-124 (p,2n) Cs-123} \xrightarrow{5.94\ \text{m}} \text{Xe-123} \xrightarrow{2.08\ \text{h}} \text{I-123} \qquad \text{Equation 3}$$

I-123 was measured at only one of the international network of sensors; however, it was measured with some regularity (in approximately one-third of all analyzed spectra) over the three year history of the monitoring site. The quantities measured were miniscule and orders of magnitude below national safety standards. Although quantities were minute, I-123 is generally easy to detect because its primary gamma-ray is not in the vicinity of any other relevant gamma-rays. As a result of the abundance of radionuclide data, PIDC scientists were able to use analytical techniques to trace the I-123 from the sensor back to the origin -- a cyclotron producing I-123 for medical purposes.

I-131 is a fission product radionuclide that is most commonly used in the treatment of thyroid disorders. As a medical radioisotope, it is produced in reactors specifically for use within the medical industry. Because I-131 is a fission product, it has been detected on all of the continents where radionuclide monitoring sensors report data to the PIDC. While the overwhelming majority of these detections were directly to the nuclear power industry and nuclear research, a few may have been related to the medical industry.

Tc-99m is one of the most commonly used isotopes in the medical industry and is regularly used as a tracer for imaging purposes. It is estimated that over 80 percent of all medical procedures involving the use of radioisotopes utilize Tc-99m. This radionuclide is produced onsite at medical facilities by separating it from its fission product parent, Mo-99.

As a result of the broad use of Tc-99m, it is readily available and has been detected worldwide. Correspondingly, as in the case of I-131, Tc-99m has been detected on every continent that has sensors that report to the PIDC. Also like I-131, because Tc-99m is a fission product, not all detections of Tc-99m can be directly linked to the medical industry. Even so, medical facilities were identified as likely sources for multiple Tc-99m detections on two continents.

Tl-208 is used in cellular viability analyses. It is a generated by proton bombardment of Tl-203 in a cyclotron and emits a 167.4 keV gamma-ray with 100% abundance. The Tl-208 generation equation is shown in Equation 4. Like I-123, only one radionuclide sensor has confirmed the presence of Tl-201, but the radionuclide has been detected at the site on several occasions. PIDC scientists identified the likely source of the detection as a local medical facility.

$$\text{Tl-203 (p,3n) Pb-201} \xrightarrow{9.4\ \text{h}} \text{Tl-201} \qquad \text{Equation 4}$$

Nuclear Reactor Emissions

Reactor Operations

During the normal operation of light water reactors, gaseous and particulate radionuclide waste products are generated through the fission process and the activation of non-fissile materials in the reactor core. The overwhelming majority of these waste products never escape the system due their short half-lives and various chemical processing techniques; nevertheless, an infinitesimal fraction of these wastes are released into the atmosphere. The most common radionuclide emissions into the atmosphere consist of noble gases, iodine, tritium, and particulates. History has shown these processes to take place in all manner of nuclear reactor systems including PWRs, BWRs, HWRs, GCRs, LWGRs, and FBRs. However, due to differing operational processes and regulations around the world governing effluent releases, the effluent quantities can vary greatly. Table 6 lists the average activity emitted from nuclear facilities worldwide, normalized per year from 1990 through 1994. As a comparison, Table 7 shows the same information from 1995 through 1997.

Table 6: Worldwide Average Activities Normalized per year (1990 - 1994), (TBq $(GW\ y)^{-1}$)

Reactor Type	**Noble Gases**	**Tritium**	**I-131**	**C-14**	**Other Particulates**
PWR	27	2.3	0.33	0.22	0.18
BWR	354	0.94	0.81	0.51	178
HWR	2050	650	0.35	1.4	0.051
GCR	1560	4.7	1.4	1.6	0.30

LWGR	1720	26	6.8	1.3	14
FBR	380	49	0	0.12	12

Table 7: Worldwide Average Activities Normalized per year (1995 - 1997), (TBq $(GW\ y)^{-1}$)

Reactor Type	**Noble Gases**	**Tritium**	**I-131**	**Particulates**
PWR	13	2.4	0.17	0.13
BWR	171	0.86	0.33	351
HWR	252	329	0.11	0.048
GCR	1 240	3.9	0.42	0.17
LWGR	465	26	6.9	8.4
FBR	209	49	0	1.0

Tables 8 and 9 express the noble gas and iodine radionuclides emitted from U.S. PWRs and BWRs in detail along with their activity fractions based on data obtained throughout 1982.

Table 8: Noble Gases Activity Fractions resulting from U.S. PWR and BWR Operations (1982)

Radionuclide	**Half-life**	**PWR Act. Fract.**	**BWR Act. Fract.**
Ar-41	1.8 h	0.005	0.029
Kr-85m	4.5 h	0.0042	0.061
Kr-85	10.8 y	0.0162	0.013

Kr-87	76 m	0.0086	0.083
Kr-88	2.8 h	0.0039	0.143
Xe-131m	12 d	0.0063	0.034
Xe-133m	2.2 d	0.0059	0.0071
Xe-133	5.3 d	0.806	0.198
Xe-135m	15 m	0.002	0.056
Xe-135	9 h	0.139	0.171
Xe-138	14 m	0.003	0.195

Table 9: Radioiodines Activity Fractions resulting from U.S. PWR and BWR Operations (1982)

Radionuclide	**Half-life**	**PWR Act. Fract.**	**BWR Act. Fract.**
I-131	8 d	0.272	0.065
I-133	21 h	0.68	0.27
I-135	6.6 h	0.043	0.658

In atypical situations more significant quantities of radionuclides and radiation can be released. The two most prominent examples in recent history are the Three Mile Island accident in 1979 and the Chernobyl accident in 1986. Because these accidents were so different in their scope and their overall radiological effects, they are effective at reflecting the range of radiological consequences that can result from nuclear reactor accidents.

Three Mile Island

The Three Mile Island (TMI) power plant, near Harrisburg, Pennsylvania, consisted of two PWRs, TMI-1 and TMI-2. The 800 MWe TMI-1 began operation in 1974 and is amongst best performing units in the US, according to the NRC. TMI-2 was rated at 900 MWe and almost new at the time of the accident.

The TMI-2 accident occurred at 4:00 am on March 28, 1979 when the reactor experienced a relatively minor malfunction while operating at 97% power. In response to this malfunction in the secondary cooling circuit, the primary coolant temperature increased. As a result, the reactor automatically shut down after only one second. However, due to a relief valve that was stuck in the open position, much of the primary coolant drained out of the core which limited heat removal and caused severe damage to the core and fuel rods. Because of a faulty display, the operators were unable to properly diagnose and respond to the unplanned automatic shutdown of the reactor. Because of the misdiagnosis and subsequent time delay, radioactive material was released into the cooling water.

Two and one-half hours after the onset of the accident, the operators were able to stop the coolant loss through the relief valve. But superheated steam and gases that had been generated blocked the coolant flow through the core cooling system. The problem persisted well into the afternoon when operators began injecting high-pressure water into the cooling system to increase pressure and to collapse steam bubbles. By 7:50 pm,

enough water and pressure had been restored to the core that a reactor coolant pump could be restarted.

Over the next two days, operators were able to shift the gas into waste gas decay tanks using various pipes and compressors. However, due to leaky compressors, some radioactive gases were released into the environment. Moreover, small amounts of radiation were likely released as operators vented a hydrogen bubble that had formed in the containment vessel.

Although the accident and the environmental consequences were studied in detail by the NRC, the EPA, the predecessor organization to the Department of Health and Human Services, and several independent organizations, radionuclide release levels were so low that they are scarce in literature. Average radiation dose levels were estimated to be 1 millirem for the 2 million residents in the vicinity, one percent of the annual background in the area. The maximum dose to a hypothetical person at the TMI site boundary was estimated to be less than 100 millirem. Therefore, the TMI-2 accident serves as a representative example of the lower boundary of environmental releases that can result from nuclear reactor accidents.

Chernobyl

The Chernobyl nuclear accident was far more severe and had much more serious environmental consequences than the TMI accident. The accident occurred in April 1986 in the Ukrainian Republic of the Former Soviet Union. At the time, the Chernobyl

nuclear power plant consisted of four RBMK-1000 graphite nuclear reactors (Soviet LWGRs) that were rated at 1000 MWe. The accident occurred in Unit 4, which was constructed in 1983.

On April 25, the day before the accident, Unit 4 was scheduled for a maintenance shutdown. During the reactor shutdown period, an emergency electrical power capability test was to be conducted. The test, similar to previous tests, was slated to investigate whether the turbines coasting down would provide sufficient power to initiate emergency equipment. To conduct this test, the power was to be reduced from full power to 25% power (250 MWe - 300 MWe) and the emergency core cooling system (ECCS) was to be disconnected.

The experiment began uneventfully with the initiation of power reduction and the disconnection of the ECCS. However, during the power reduction phase, a need for power within the power grid arose, so instead of steadily decreasing down to 25% power, the power reduction was paused at 50% power for approximately 9 hours. In addition to disconnecting the ECCS, the automated neutron flux (reactivity) regulator was also disconnected. This enabled Xe-135, a reactor poison, to build up in the core during the 9 hour delay, which greatly reduced the neutron flux. Because the automated reactivity control system was not operating, the reactor became unstable and power dropped to 10 MWe before leveling at 60 MWe. However, because of the Xe-135 concentration and low neutron flux, the power could not be increased. Had the reactor been shut down at this point, as safety instructions required, the accident would have been avoided. But

instead, the operators apparently tried to "jump start" the reactor, and increased the power so quickly that a steam explosion occurred, which led to a secondary hydrogen explosion. The hydrogen explosion led to parts of the nuclear reactor core to be ejected into the surroundings, and a graphite fire in Unit 4 which burned for over 10 days. The graphite fire led to the most significant quantities of radionuclide effluents to be released and emissions that reached altitudes on the order of 1 km. .

Approximately 3.5% of the total fuel inventory (6 tons of fuel) was dispersed into the atmosphere. In contrast, about half of the more volatile particulates, including isotopes of cesium, iodine, and tellurium, were released. At the other end of the spectrum, 100% of the noble gases were released. The radionuclides emitted were in the various forms including gases, aerosols, and particles. Table 10 compares the quantities of selected radionuclides available in the rector core with the quantity of radionuclides released.

Table 10: Radionuclide Quantities in Core vs. Radionuclide Quantities Released

Core inventory on 26 April 1986			**Total release during the accident**	
Nuclide	**Half-life**	**Activity (PBq)**	**Percent of inventory**	**Activity (PBq)**
Xe-133	5.3 d	6 500	100	6500
I-131	8.0 d	3 200	50 - 60	~1760
Cs-134	2.0 y	180	20 - 40	~54
Cs-137	30.0 y	280	20 - 40	~85
Te-132	78.0 h	2 700	25 - 60	~1150
Sr-89	52.0 d	2 300	4 - 6	~115

Sr-90	28.0 y	200	4 - 6	~10
Ba-140	12.8 d	4 800	4 - 6	~240
Zr-95	1.4 h	5 600	3.5	196
Mo-99	67.0 h	4 800	>3.5	>168
Ru-103	39.6 d	4 800	>3.5	>168
Ru-106	1.0 y	2 100	>3.5	>73
Ce-141	33.0 d	5 600	3.5	196
Ce-144	285.0 d	3 300	3.5	~116
Np-239	2.4 d	27 000	3.5	~95
Pu-238	86.0 y	1	3.5	0.035
Pu-239	24 400.0 y	0.85	3.5	0.03
Pu-240	6 580.0 y	1.2	3.5	0.042
Pu-241	13.2 y	170	3.5	~6
Cm-242	163.0 d	26	3.5	~0.9

Figure 1 illustrates the activity release rates with respect to time. The initial release was largely the result of the reactor fuel that was disbursed during the explosion and the emission of the more volatile gases and particulates. The sustained increased release rate between days 7 and 10 was associated with the core melt. After day 10, the release rates dropped significantly. This was likely due to a rapid cooling of the reactor fuel as the core melted and began interacting with other materials. Subsequent release rates were relatively low and persisted for an additional month.

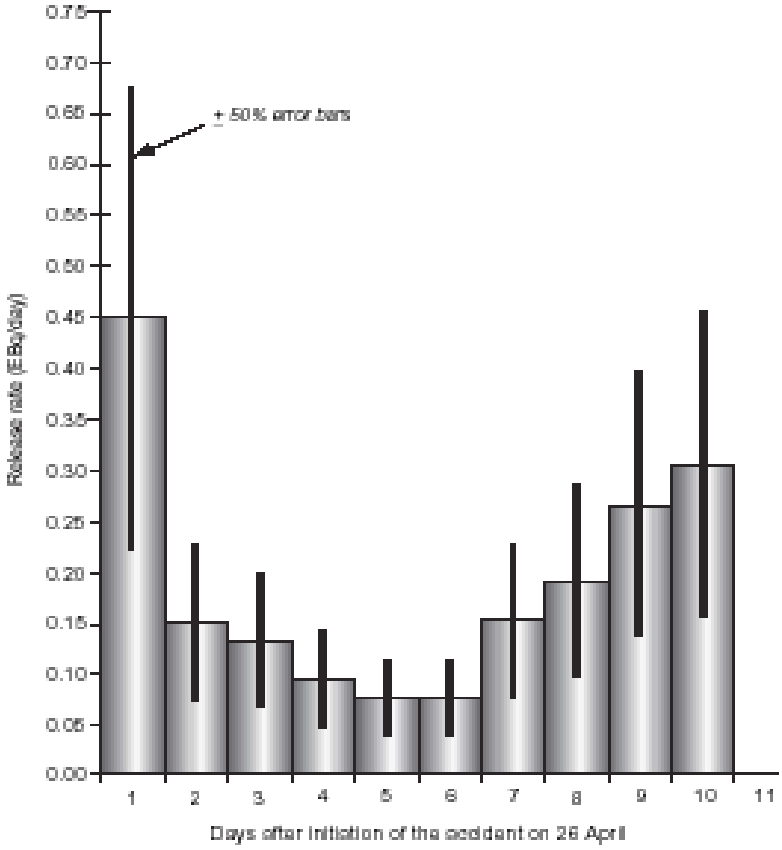

Figure 1: Activity Release Rates with respect to Time

Two particle size distributions were evident amongst the emissions. The smaller particles generally ranged between 0.3 and 1.5 µm in diameter and the larger particles had diameters of approximately 10 µm. Between 80 and 90% of the nonvolatile radionuclide activity was present amongst the larger particles. Contributing radionuclides included transuranics, Zr-95, Nb-95, La-140, and Ce-144. These larger particles were deposited close to the accident site, while the smaller particles were dispersed more widely. Vaporized fuel constituents, such as ruthenium isotopes, condensed and formed metallic particles. These, as well as the smallest of the fuel particles, were disbursed even further. Corresponding activities ranged between 0.5 and 10 kBq for the ruthenium particles and

0.1 and 1 kBq for fuel fragments. The particles containing I-131 and Cs-137 ranged from 0.4 to 0.7 μm in diameter.

Behavior of Deposited Radionuclides

The distributions and interactions of radionuclides deposited in the environment were a function of several factors including: the physical and chemical characteristics of the radionuclides, whether the fallout was dry or wet, the particle size and shape, etc. For example, when comparing particles generated directly via the explosion with those that originated as gases and were converted into particles via chemical reactions, nucleation, condensation, or coagulation, the explosion generated particles tended to be larger and less soluble. As a result, these particles interacted differently than those generated by the gas-to-particle conversion process. The large, 10 μm fuel particles containing uranium, plutonium, refractory elements (Zr, Mo, Ce, etc.), Ru, Ba, and Sr were deposited primarily by gravitational settling within 100 km of the accident site. On the other hand, the small particles, consisting of the more volatile elements (I, Te and Cs) were more widely dispersed to distances on the order of thousands of kilometers and primarily deposited through rainfall. Due in part to the easy measurability of Cs-137, it was the principal radionuclide used to characterize ground deposition quantities.

The result of the varied competing influences led to the formation of three hotspot locations of unusually high deposition. The central hotspot included the 30 km region surrounding the reactor site where Cs-137 measurements exceeded 1500 kBq/m^2. The northeastern hotspot was centered 200 km away from the accident site. This region was

formed because of rainout that occurred on the 28th and 29th of April. Although the amount of radioactivity emanating from the reactor was relatively low on those days, the rainout processes served to concentrate the emissions, resulting in ground depositions of 5000 kBq/m^2. These concentrations were the highest measured as a result of the accident -- over three times higher than concentrations measured adjacent to the reactor site. The same precipitation system on April 28th and 29th led to the formation of the third hotspot, as well. The third hot spot was formed 500 km to the northeast of the accident site. Cs-137 ground deposition concentrations were 600 kBq/m^2. In addition to the three hotspots, deposition concentrations ranging from 40 kBq/m^2 to 200 kBq/m^2 were prevalent in the European region of the Soviet Union.

Chernobyl's plume of radioactivity traveled across the European portion of the Soviet Union and then across Europe (Figure 2). Beyond Soviet borders, radioactivity from the accident was first measured at a Swedish nuclear power station. The initial southeasterly winds led to deposition in Scandinavia, the Netherlands, Belgium and Great Britain. Then the plume shifted south and caused deposition in central Europe, the northern Mediterranean region, and the Balkans. Cs-137 and Cs-134 were the radionuclides deposited throughout most of Europe. The deposition was higher (40 - 185 kBq/m^2) in certain countries where rainfall occurred. These countries included Austria, Switzerland, Germany, and Scandinavia. On average, most countries in Europe received Cs-137 depositions on the order of 50 kBq/m^2. Countries receiving the least Cs-137 deposition (on the order of 0.02 kBq/m^2) included Spain, France, and Portugal. Although the airborne plume was detectable throughout the northern hemisphere, including North

America and Japan, only minimal deposition was measured beyond Europe. No deposition was measured across the equator in the southern hemisphere.

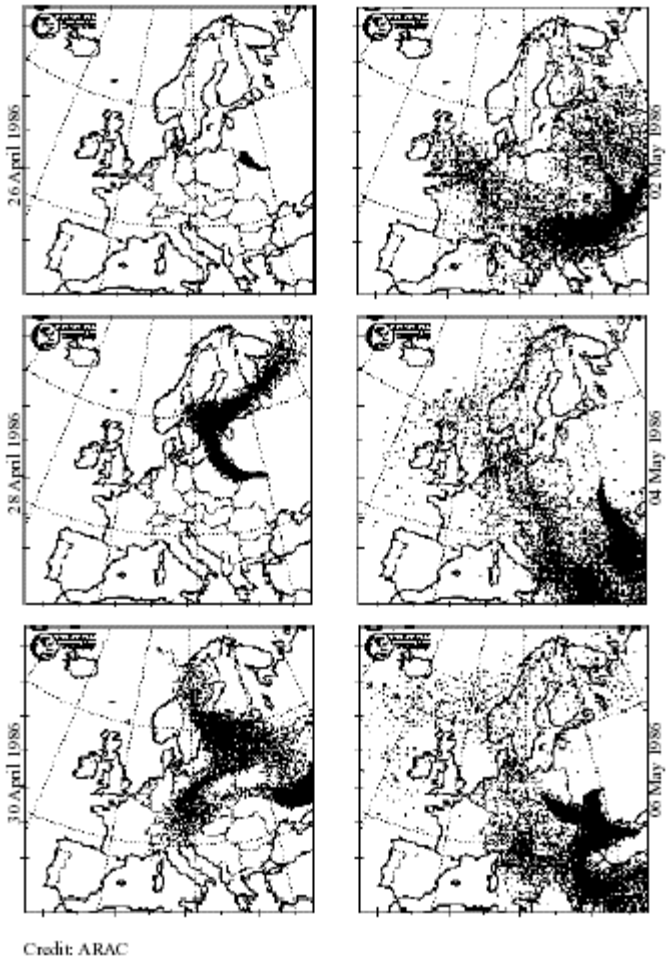

Figure 2: Areas where Radioactive Plume Traveled

At present, no significant quantities of deposited radionuclides are transferred into less contaminated areas through resuspension; however, resuspension has played a role in times past. One year after the incident, a storm resuspended radioactivity that had been deposited in the highly contaminated central hotspot (within 30 km of the reactor). As a result, the airborne radioactivity concentration increased by three orders of magnitude to

300 Bq/m^3. Forest fires have also led to notable increases in airborne radioactivity. For example, in 1992, a forest fire near the 30 km central hotspot caused airborne radioactivity measurements to increase by two orders of magnitude to between 20 and 70 Bq/m^3. In addition, radioactivity measurements were increased at remote monitoring stations as well. Although contamination levels trended downward following the accident, due to the decay of the shorter lived radionuclides and the persistence of the longer lived Cs-137 (with a half-life of 30.17 years), the contamination levels seem to be decreasing less rapidly. Historically, environmental radionuclide contamination can be expected to persist in statistically significant quantities for 10 half-lives. In the case of the Cs-137 from the Chernobyl accident, the contamination would be expected to continue for another 300 years.

Nuclear Fuel Reprocessing

Introduction

Once nuclear fuel has been discharged from a reactor, it can be reprocessed to recover useful fission products, byproduct transuranics, and the remaining fissile material that can be used as nuclear fuel in the future; to isolate detrimental fission products from the recoverable materials; and to convert the radioactive waste products into a form suitable for long-term storage. Although nuclear fuel is generally designed to be stored on the order of 150 days, in the near term, most fuel will be stored for much longer periods of time because of the significant backlogs. One benefit of the long storage times is that it enables all of the radionuclide gaseous to decay to insignificant levels except for C-14 compounds, H-3, Kr-85, I-129, and I-131.

Equation 5 shows the key C-14 generation equation. Table 11 lists the specific activities of H-3, Kr-85, I-129, and I-131 for several types of reactors following 150 days of storage. It should be noted that the Table 11 values reflect the relative dominance of radionuclide activities. Because most reprocessing facilities service multiple reactors, actual activity levels entering a given reprocessing facility can be much higher.

N-14 (n,p) C-14; Note, N-14 exists as a contaminant in the fuel Equation 5

Table 11: Radionuclide Specific Activity 150 Days after Discharge

Specific Activity 150 Days after Discharge	**PWR (33 MWd/kg; 30 MW/Mg)**	**LMFBR (37 MWd/kg; 49.3 MW/Mg)**	**HTGR (95 MWd/kg; 64.6 MW/Mg)**
H-3 (Ci/Mg)	690	1050	1090
Kr-85 (Ci/Mg)	11,000	8430	60,800
I-131, I-129 (Ci/Mg)	2.22	3.55	4.07

The overall activity of Kr-85 far exceeds the activities of H-3, I-129, and I-131. Accordingly, Kr-85 is the greatest contributor to airborne gamma-ray activity measurements that result from reprocessing. C-14 and H-3 are strict beta emitters, and I-129 is principally a beta emitter. Although I-131 is a gamma-ray emitter like Kr-85, I-131 discharges are minimal in comparison to the amount of Kr-85 released. In most cases, the small amounts of I-131 that are released are indistinguishable from

background. However, literature indicates that when fuel has been reprocessed for military applications, the cooling time can be greatly reduced, thereby increasing the significance of the I-131 concentration. Moreover, it is also important to note that while all of the Kr-85 present is gaseous, approximately half of the tritium is entrained within the zircaloy cladding and is not readily releasable, and the physical properties of iodine enable I-129 and I-131 the be present as either a gas or a liquid.

A historical review of literature revealed eleven methods for reprocessing nuclear fuel. The established processes identified include Bismuth Phosphate, Redox, Trigly, Butex, Purex, and Thorex. Other approaches include aqueous, nonaqueous, pyrometallurgical, pyrochemical, and fluorine volatility processes. Because of the wealth of literature available regarding the Purex process and its broad international use, it will serve as the model for nuclear fuel reprocessing in this analysis.

Decladding and Dissolution Phases

By and large, off-gases are generated at the front end of the Purex process during the decladding and dissolution phases. During the decladding phase, fuel assemblies containing zircaloy or steel clad fuel rods are fed into a mechanical shearer and cut into pieces between approximately 1 and 5 cm long, thereby exposing the irradiated fuel pellets. In cases where the cladding remained fully intact prior to shearing, the shearing process can release up to ten percent of the xenon and radiokrypton contained in the fuel and a small portion of the H-3, molecular C-14 in the form of CO_2, and other volatile fission products. In addition, all of the helium injected between the cladding and fuel

pellets during fabrication to enhance heat transfer is released. Once generated, these gases travel through the off-gas treatment system where iodine and other entrained solids are collected. It is possible for krypton isotopes to be collected, as well; but H-3 and C-14 collection processes are not generally used.

Although H-3 is not generally collected, it can be removed from the gas stream through a chemical process called voloxidation. The voloxidation process, developed by Oak Ridge National Laboratory, involves oxidizing the sheared fuel in a rotating kiln, which converts the denser UO_2 to the less dense U_3O_8. The change in density causes the fuel to swell and ultimately pulverizes it. As a result, the occluded tritium is exposed to oxidizing gases and converted into tritiated water. Voloxidation can release over 99 percent of the H-3 and all of the remaining Kr-85 from the fuel. The process ends by converting the unreacted hydrogen to water, cooling it, and collecting the tritiated water with a molecular sieve or anhydrous calcium sulfate. Voloxidation is not an essential part of fuel reprocessing operations; but if the process is used, it occurs after the shearing phase to exploit the optimized fuel exposure, and prior to dissolution to avoid mixing the tritium with the deluge of hydrogen that is evolved in this phase.

The dissolution phase involves reacting the fuel and cladding conglomeration with hot nitric acid. This phase is principally intended accomplish three tasks: to dissolve the uranium and plutonium, fully separate the fuel from the cladding, and chemically prepare all of the fuel constituents for further separation. The majority of the dissolution off-gases consist of air, nitrogen oxides, and steam. The steam is contaminated with tritium

if voloxidation was not used. These gases also contain the remaining nuclides of interest including Kr-85, elemental and compound forms of C-14, and the overwhelming majority of the I-129 and I-131. It should be noted that not all of the iodine within the system is present as a gas. Some of the iodine exists in aqueous form as iodides, iodates, and elemental iodine.

The two primary nitric acid reactions that occur in the dissolution phase are listed below.

$$UO_2 + 4HNO_3 \rightarrow UO_2(NO_3)_2 + 2NO_2 + 2H_2O \qquad \text{Equation 6}$$

$$3UO_2 + 8HNO_3 \rightarrow 3UO_2(NO_3)_2 + 2NO + 4H_2O \qquad \text{Equation 7}$$

The dominance of either reaction is generally a function of the nitric acid concentration. By flooding the dissolution environment with oxygen, the generation of off-gas reaction products can be essentially eliminated; however, the gaseous fission products will persist. The governing reaction is shown below.

$$2UO_2 + 4HNO_3 + O_2 \rightarrow 2UO_2(NO_3)_2 + 2H_2O \qquad \text{Equation 8}$$

Off-gas Treatment

Prior to stack discharge into the environment, radionuclide gases from the decladding, voloxidation, and dissolution phases undergo radioiodine absorption and sometimes krypton retention procedures. Gases generated during later reprocessing phases also

experience radioiodine absorption, but no krypton retention. C-14 and H-3 retention is not generally practiced.

Radioiodine removal is a complicated process due to the variety of reprocessing phases that liberate it and the varied chemical forms in which it is present. Approximately one percent of the radioiodine present is released during the decladding phase; a portion is also released during voloxidation, if used. Most of the radioiodine is released during the dissolution phase, but a small percentage continues into other phases of the reprocessing system. The radioiodine may be present as a gas or a liquid, and may exist in elemental or organic forms, as HI or HIO, or as HIO_3 in nitric acid.

Iodine is normally removed by drawing the decladding and voloxidation off-gases into iodine absorbers, and distilling the iodine present within the dissolution mixture. Experimental studies have shown that distilling 20 percent of the nitric acid solution can remove 99 percent of the iodine present. Some of the remaining traces of iodine are released amongst the other dissolution gases.

Several other iodine removal methods have been pursued, as well. Elemental iodine and HI can be removed by adsorption by aqueous NaOH; however, disposing of the spent solution can be challenging. The Oak Ridge National Laboratory's Iodox method used absorption in boiling concentrated nitric acid to convert all elemental and compound forms of iodine into the solid, nonvolatile I_2O_5. In another Oak Ridge process, nitric acid containing small amounts of $Hg(NO_3)_2$ is boiled and absorbs elemental and compound

forms of iodine as HgI_2. The solution is then evaporated from vermiculite, leaving the iodine in a stable, storable form. At Hanford, silver nitrate coated berl saddles were used to remove elemental iodine and HI from dissolution off-gases. However, research conducted at Idaho Nuclear and in Karlsruhe, Germany have demonstrated that a more effective way to use silver is to impregnate it with a zeolite catalyst. In a humid environment at 150^{o}C, all volatile iodines are absorbed as silver iodide, a stable compound that is suitable for permanent storage.

As Table 11 shows, Kr-85 generates a significant portion of the gaseous product activity prior to reprocessing. As in the iodine case, several methods for removing krypton for reprocessing off-gases have been pursued. Some of the notable approaches are listed below in Table 12. Each process listed below has been proven to achieve a 99 percent krypton removal efficiency.

Table 12: Kr-85 Off-gas Removal Processes

Process	**Status/Comments**
Room temperature adsorption on charcoal or molecular sieves	In nuclear power plants, process used for xenon decay storage; simple operation principle; large beds required; charcoal poses flammability hazard
Low temperature adsorption on charcoal or silica gel	Pilot tested at reprocessing facility; smaller beds required; charcoal poses flammability hazard
Permselective membrane separation	Pilot tested; small equipment; no flammability hazard

Cryogenic distillation	Pilot tested; small equipment; ozone explosion hazard
Chlorofluoromethane absorption	Pilot tested; small equipment; no flammability hazard

Nuclear power plants have proven the use of room temperature adsorption to retain krypton contained in off-gases. The process impedes the flow of all the gases long enough to allow the non-inert radionuclide gases to decay to insignificant quantities. In order to retain Kr-85, large beds would be required along with a complex system for bed regeneration. Because of the flammability hazard posed by treating reprocessing off-gases with charcoal, both oxygen and NO_x would need to be extracted from the off-gases prior to entering the retention system.

Cryogenic adsorption requires smaller beds, but the off-gases must be pretreated beforehand to remove condensables. This method has been tested on a pilot plant scale at a reprocessing facility. As with room temperature adsorption, the beds pose a flammability hazard. As a matter of fact, the risk of ignition may be more severe due to the possible adsorption of ozone generated through oxygen radiolysis.

Using permselective membranes is another process that has been investigated for the removal of krypton from reprocessing off-gases. However, the future of this method for reprocessing applications is not promising. Disadvantages include the deterioration that

results from radiation, ozone, and NO_x exposure and the severe consequences of mechanical failures.

One of the most promising krypton removal methods was tested widely at the Idaho Chemical Processing Plant. This process begins by purifying the incoming off-gases from the reprocessing system. CO_2 and NO_2 are removed by scrubbing with a NaOH solution. Although the CO_2, containing C-14, could be collected by using lime to precipitate $CaCO_3$, this step is generally not practiced. By passing the off-gas over a 650°C rhodium catalyst, N_2O can be separated into N_2 and O_2. After the off-gas is purified, regenerators are used to cool the gas to -160°C, which condenses H_2O, NO_x, and the remaining traces of CO_2. The now purified off-gas is then washed with liquid nitrogen to condense the krypton, which is later concentrated by fractional distillation. The two chief concerns with this process are that solid H_2O, CO_2, and NO_x can clog the low temperature equipment, obstructing the gas flow; and the proximity of the accumulating solid hydrocarbons and the condensed oxygen and ozone poses an explosion risk.

The other promising method, absorption in halogenated solvents, was studied at both Brookhaven and Oak Ridge. In this process, the reprocessing system off-gases are compressed to almost 1 MPa and cooled to approximately -30°C in a cold trap, which removes the majority of the H_2O, NO_2, diatomic iodine, and iodine compounds. The rest of the off-gas continues through an absorber-fractionater column that contains -28°C R-12 refrigerant at the top and is reboiled at 31°C at the bottom. N_2 and O_2 are removed at

the top of the system, and an R-12 solution containing Kr, CO_2, and N_2O, and traces of N_2, O_2, NO_2, H_2O, and iodine compounds is removed from the bottom. The bottom contaminants are then fed into a stripper where the Kr, CO_2, and N_2O are removed. These stripper products can then be processed further to separate and package the C-14 and Kr-85. Benefits of this absorption process are that flammability and explosion hazards are minimal, the gas does not need to be purified prior to processing, the process does not require extremely low temperatures, and the process offers some level of flexibility. Disadvantages include the need for high-pressure operations, the fairly complicated process flow, and the need for an auxiliary system to fully separate the C-14 from the Kr-85.

Reprocessing Facilities and Data

As of 1979 in the U.S., five reprocessing facilities had been built, each using some variation of the Purex process. Basic information about these facilities is contained in Table 13. As Table 13 shows, only two facilities were operating in 1979. As a result in a shift in U.S. governmental policy, the Barnwell facility remains unused even today.

Table 13: Principal U.S. Reprocessing Facilities as of 1979

Facility Location	**Owner**	**Initial Operation**	**Status**
Hanford, WA	U.S. Atomic Energy Commission; U.S. Department of Energy	1944 initially; 1956 upgrade	Inactive since 1974

Idaho Chemical Processing Plant; Idaho National Engineering Lab	U.S. Atomic Energy Commission; U.S. Department of Energy	1953	Operating
Savannah River, SC	U.S. Atomic Energy Commission; U.S. Department of Energy	1954	Operating
West Valley, NY	Nuclear Fuel Services, Inc.	1966	shut down in 1972
Barnwell Nuclear Fuel Plant; Barnwell, SC	Allied General Nuclear Services	n/a	no license issued

Internationally, seven major reprocessing facilities had been planned or operated by 1979, not including sites in the Former Soviet Union. Basic information about these plants is included in Table 14. Smaller facilities have been operated in India, Italy, and probably in other countries.

Table 14: Principal Reprocessing Facilities Overseas as of 1979

Facility Location	**Owner**	**Initial Operation**	**Status**
Marcoule, France	Cogema	1958	Operating
Windscale (Sellafield), UK	British Nuclear Fuels, Limited	Site 1, 1964; Site 2, planned	1, operating; 2, n/a

Mol, Belgium	Eurochemic	1966	Shut down
La Hague, France	Cogema	Site 1, 1967; Site 2, 1976	1, operating; 2, operating
Karlsrule, (West) Germany	KFK/GWK	1971	Operating
Tokai-Mura, Japan	Power Reactor and Nuclear Fuel Development Corporation	1975	Operating
Hessen, (West) Germany	DKW	Planned for 1992	n/a

Research conducted in Europe and Asia indicate that the total quantity of radionuclides emitted into the atmosphere during normal reprocessing plant operations can be insignificant. One study determined that the annual emission quantities for Japanese facility corresponded to a mere 1 mSv/y dose equivalent. Averaged atmospheric reprocessing emission quantities are shown for each of Europe's three reprocessing facilities in Table 15.

Table 15: Airborne Radionuclide Releases from European Reprocessing Plants from 1980-1985 (all units are TBq/GWy(e))

Effluent	**Sellafield, UK**	**La Hauge, France**	**Marcoule, France**
Kr-85	1.4 E4	1.2 E4	1.4 E4

H-3	1.2 E2	3.2	5.7 E1
C-14	3.5	n/a	n/a
Beta emitting particulates	6.3 E-2	4.5 E-5	2.9 E-4
Alpha emitting particulates	2.3 E-4	7.5 E-6	n/a

Other Processes

In addition to the aforementioned processes that cause radionuclides to be emitted into the atmosphere, radionuclides can be generated through front-end uranium fuel cycle processing, high energy physics experiments, and traditionally non-nuclear processes, as well. Of course, these processes, even when considered in collectively, only contribute to a fraction of the overall radioactivity that includes the more dominant processes. Because of the stringent containment requirements on radioactive wastes, their contribution to the overall concentration of radionuclides emitted into the atmosphere is negligible.

The front-end processes related to the uranium fuel cycle include mining, milling, conversion, enrichment and fabrication. The mining and milling process is the initial phase of the fuel cycle. Although these processes are distinctly different, they are grouped because they are normally collocated. The two principal mining methods are underground mining and open pit mining. Rn-222 is the chief radionuclide that is released into the atmosphere from mining. Because Rn-222 is a gas, it is much more

readily disbursable than particulate releases. During the ore granulation and concentration associated with milling, particulates containing natural uranium daughters can be emitted into the air. Although the same particulates can be released through mining, their concentrations are infinitesimal when compared to Rn-222 emissions. Mill tailings, if not sufficiently contained, can be blown into the air by the wind or release additional radon gas. Table 16 lists normalized atmospheric releases that result from the mining and milling process and the other front-end processes as well.

Table 16: Atmospheric Releases Resulting from Front-End Uranium Fuel Cycle Processing (all units are MBq/GWy(e))

	U-238	**Th-230**	**Ra-226**	**Rn-222**	**Pb-210**
Mining				2.0 E 7	
Milling	6.6 E 2	7.4 E 1	4.0 E 1	8.8 E 5	4.0 E 1
Mill Tailings	7.0 E -1	1.5 E 1	1.5 E 1	1.0 E 6	1.5 E 1
Conversion	7.4 E 1	7.4 E -1	7.0 E -2	8.1 E 3	
Enrichment	3.7 E 1	7.4			
Fabrication	7.4 E -1				

The concentrated ore, called yellow cake (U_3O_8), that results from the milling phase is typically converted to uranium hexafluoride (UF_6) and enriched by gaseous centrifuges or gaseous diffusion to increase the relative percentage of U-235. Afterwards, in preparation for the fuel fabrication process, the uranium is converted into uranium metal

(U) or uranium dioxide (UO_2) so that it can be used as nuclear reactor fuel. As Table 16 shows, these processes result in much less atmospheric radioactivity than the mining and milling process.

High energy physics experiments typically involve linear accelerators or cyclotrons that accelerate heavy charged particles (protons, deuterons, alpha particles, etc.) into a known target material to generate a reaction. Depending on the type of particles being accelerated, the target material, the energy of impact, and other factors, the resulting reaction may involve the target material absorbing the particles, the formation of a large product (on the scale of the target atoms) and a small product (on the scale to the particles), or the formation of several products. In general, radionuclides resulting from accelerator applications are proton rich and neutron poor with respect to either their stable counterparts or the reactants. These product radionuclides generally emit gamma-rays which can facilitate their characterization. High energy physics experiments are not known to play a major role in atmospheric radionuclide emissions. In rare situations, product radionuclides have been quantifiable above background locally; however, even in these cases, the measured concentrations were near zero.

Naturally Occurring Radionuclides

Introduction

Radionuclides that exist within nature can generally be grouped into one of three categories: primordial radionuclides, primordial radionuclide daughters, and induced radionuclides. Primordial radionuclides are those that exist with half-lives on the order of

the age of the universe (~10^8 years or greater). There are many more primordial radionuclide daughters in nature than primordial radionuclides. In general, these daughter radionuclides have half-lives shorter than their primordial parents. Induced radionuclides can be found within the atmosphere and are principally the result of cosmic proton and neutron interactions with stable natural elements.

Primordial Radionuclides

There are two distinct categories of primordial radionuclides. The first category includes radionuclides that decay directly into stable nuclides and those that parent short decay chains before reaching stable nuclides. This first category can be generalized as "singular" primordials because of the dominance of radionuclides with stable daughters. The second category, called "series" primordial principals, includes radionuclides that exist as the parent of an extended decay chain. Singular primordials consist of alkali metals, transition metals, metalloids, lanthanides, and non-metals. The list of singular primordial radionuclides and relevant properties are shown in Table 17. Series primordial principals, on the other hand, are far fewer in number and only contain actinides, specifically U-238, U-235, and Th-232. The series primordial principals are listed in tabular form with their daughters in Tables 18, 19, and 20.

Table 17: Singly Occurring Primordial Radionuclides

Radionuclide	**Half-Life (y)**	**Radiations**	**Daughters**	**Typical Terrestrial Concentration (Bq/kg)**
K-40	1.26 E9	β^-, γ	Ar-40, Ca-40	630

V-50	6 E 15	γ	Ti-50	2 E-5
Rb-87	4.8 E 10	β^-	Sr-87	70
Cd-113	> 1.3 E 15	β^-	In-113	< 2 E-6
In-115	6 E 14	β^-	Sn-115	2 E-5
Te-123	1.2 E 13	X-rays	Sb-123	2 E-7
La-138	1.12 E 11	β^-, γ	Ce-138, Ba-138	2 E-2
Ce-142	> 5 E 16	not reported	n/a	< 1 E-5
Nd-144	2.4 E 15	α	Ce-140	3 E-4
Sm-147	1.05 E 11	α	Nd-143	0.7
Sm-148	7 E 15	α	Nd-144	9 E-6 6000ppbwt
Gd-152	1.1 E 14	α	Sm-148	7 E-6
Hf-174	2.0 E 15	α	Yb-170	2 E-7
Lu-176	2.2 E 10	β^-, γ	Hf-176	0.04
Ta-180	> 1.2 E 15	γ	Hf-180	< 1.3 E-8 1700ppbwt
Re-187	4.3 E 10	β^-	Os-187	1 E-3
Os-186	2 E 15	α	W-182	1 E-9 1.8ppbwt
Pt-190	6.9 E 11	α	Os-186	7 E-8
Pt-192	1 E 15	α	Os-188	3 E-6
Bi-209	> 2 E 18	α	Tl-205	< 4 E-9

Primordial Radionuclide Daughters

Series primordial principals and their daughters, along with the singular K-40, are the most significant contributors to external radioactive background. The series radionuclide daughters are all similar in that they originate from a uranium or thorium parent with a half-life of at least 10^8 years. In addition, each of the daughter decay chains generally consists of the same elements including thorium, actinium, radium, radon, polonium, bismuth, thallium, culminating in stable lead. The three decay series, the uranium series, the thorium series, and the actinium series, are listed in tables 2 through 4 respectively. As the tables show, none of the series share any isotopes and daughter half-lives range from fractions of a microsecond to approximately 10^5 years. Moreover, many of the radionuclides emit multiple types of radiation. While α and γ radiation decay emissions dominate, a substantial number of radionuclides emit β particles as well.

Table 18: The Uranium Series (parents listed immediately above daughters)

Nuclide	**Historical Name**	**Half-Life**	**Major Radiations**
U-238	Uranium	4.47 E9 y	α, < 1% γ
Th-234	Uranium	24.1 d	β, γ
Pa-234m	Uranium	1.17 m	β, < 1% γ
Pa-234	Uranium	21.8 y	β, γ
U-234	Uranium	244500 y	α, < 1% γ
Th-230	Ionium	7.7 E4 y	α, < 1% γ
Ra-226	Radium	1600 y	α, γ

Rn-222	Emanation Radon	3.8 d	α, < 1% γ
Po-218	Radium A	3.05 m	α, < 1% γ
a) Pb-214	Radium B	26.8 m	β, γ
b) At-218	Astatine	2 s	α, γ
Bi-214	Radium C	19.9 m	β, γ
a) Po-214	Radium C'	164 μs	α, < 1% γ
b) Tl-210	Radium C"	1.3 m	β, γ
Pb-210	Radium D	22.3 y	β, γ
Bi-210	Radium E	5.01 d	β
a) Po-210	Radium F	138.4 d	α, < 1% γ
b) Tl-206	Radium E"	4.2 m	β, < 1% γ
Pb-206	Radium G	stable	none

Table 19: The Thorium Series (parents listed immediately above daughters)

Nuclide	**Historical Name**	**Half-Life**	**Major Radiations**
Th-232	Thorium	1.4 E10 y	α, < 1% γ
Ra-228	Mesothorium I	5.75 y	β, < 1% γ
Ac-228	Mesothorium II	6.13 h	β, γ
Th-238	Radiothorium	1.91 h	α, γ
Ra-224	Thorium X	3.66 d	α, γ
Rn-220	Emanation Thoron	55.6 s	α, < 1% γ

Po-216	Thorium A	0.15 s	α, < 1% γ
Pb-212	Thorium B	10.64 h	β, γ
Bi-212	Thorium C	60.55 m	α, γ
a) Po-212	Thorium C'	0.305 μs	α
b) Tl-208	Thorium C"	3.07 m	β, γ
Pb-208	Thorium D	stable	none

Table 20: The Actinium Series (parents listed immediately above daughters)

Nuclide	**Historical Name**	**Half-Life**	**Major Radiations**
U-235	Actinouranium	7.04 E8 y	α, γ
Th-231	Uranium Y	25.5 h	β, γ
Pa-231	Proactinium	2.28 E4 y	α, γ
Ac-227	Actinium	21.77 y	β < 1% γ
Th-227	Radioactinium	18.72 y	α, γ
Fr-223	Actinium K	21.8 m	β, γ
Ra-223	Actinium X	11.43 d	α, γ
Rn-219	Emanation Actinon	3.96 s	α, γ
Po-215	Actinium A	1.78 ms	α, < 1% γ
a) Pb-211	Actinium B	36.1 m	β, γ
b) At-215	Astatine	~0.1 ms	α, < 1% γ
Bi-211	Actinium C	2.14 m	α, γ

a) Po-211	Actinium C'	0.516 s	α, γ
b) Tl-207	Actinium C"	4.77 m	$\beta < 1\% \gamma$
Pb-207	Actinium D	stable	none

Induced Radionuclides

Induced radionuclides in the atmosphere are normally generated through cosmic radiation interactions (principally high energy protons and high energy neutrons) with elements in the earth's atmosphere. It follows that all of the radionuclides listed in Table 21 are produced through cosmic radiation interactions with nitrogen, oxygen, and argon, since these elements constitute over 99% of the earth's atmosphere by weight and by volume. The two radionuclides that have shown the greatest influence on the environment are H-3 and Be-7. Although H-3 is listed as the third most abundant radionuclide by activity concentration, given its 12.33-year half-life (which is orders of magnitude longer than the two more abundant radionuclides), H-3 is clearly the most abundant of the atmospherically induced radionuclides when considering total atomic concentration. Be-7's effect on the environmental is largely due to its relatively high atmospheric concentration (0.01 Bq/kg) which is an order of magnitude greater than any of the other induced radionuclides in the troposphere.

Table 21: Induced Radionuclides

Nuclide	**Half-Life**	**Major Radiations**	**Target Element**	**Typical Tropospheric Concentration (Bq/kg)**
H-3	12.33 y	β	N,O	1.2 E-3

Na-22	2.60 y	γ	Ar	1 E-6
S-35	87.4 d	β	Ar	1.3 E-4
Be-7	53.3 d	γ	N, O	0.01
Ar-37	35.0 d	X-ray	Ar	3.5 E-5
P-33	25.3 d	β	Ar	1.3 E-3
P-32	14.28 d	β	Ar	2.3 E-4

Meteorological Influences on Radionuclide Transport

Introduction

The atmospheric release and dispersal of radionuclides is a key method through which they are introduced into the environment. Even so, radionuclide emissions constitute only an infinitesimal fraction of the total quantity of pollutants released into the atmosphere. Numerous studies have documented the dispersal of gaseous and particulate effluents in the atmosphere and the subsequent deposition on the ground. Due to the complexity of spatial and temporal meteorological dynamics, developing highly detailed descriptions of atmospheric radionuclide dispersions is impractical, if not impossible. However, simplified models based on statistical data and time or statistical averages are able to approximate atmospheric dispersion to varying degrees of accuracy under certain conditions.

Most atmospheric radionuclide emissions from nuclear sources can be effectively approximated as either a continuous flow or an instantaneous puff from a point source.

Various configurations of this nature have been investigated both theoretically and experimentally to assess downwind radionuclide and activity concentrations and patterns. Although considering the nuclear component of airborne radionuclide emissions adds a level of complication to the overall problem, some complexities, like urban pollution considerations, do not need to be evaluated as thoroughly because they are so infrequently encountered in the nuclear arena.

Virtually all radionuclide releases originate from sources within the planetary boundary layer (altitudes less than 1 km) within the troposphere, which ranges from 0 to approximately 10 km altitude. Similarly, nearly all radionuclide and radiation sensors exist within the planetary boundary layer, as well. Because very little vertical mixing occurs between the troposphere and higher levels of the atmosphere, radionuclides released within the troposphere typically remain within the earth's proximity. Correspondingly, most meteorological studies related to anthropogenic nuclear emissions focus on dynamics within the planetary boundary layer and the troposphere.

There are also limits to the horizontal distances radionuclides emitted within the planetary boundary layer can travel before their concentrations are diluted to negligible levels. Consequently, a wealth of research has been conducted to characterize radionuclide releases within a few kilometers of the emission location. Far fewer techniques are available to address releases that travel over 10 km.

Vertical Temperature Structure of Troposphere

For centuries, scientists have understood that temperature generally decreases with height within the troposphere. Therefore, if a parcel of air travels upwards in the atmosphere slowly enough such that a quasi-equilibrium state can be maintained with its surroundings, then the parcel will experience a decrease in temperature. However, in reality, atmospheric motions can occur so rapidly that the quasi-equilibrium state is not reached. In these cases, very little heat is exchanged between the parcel and the surrounding atmosphere. As a matter of fact, such a negligible amount of heat is exchanged that the process is said to be adiabatic -- that is, with no heat exchange whatsoever.

Adiabatic processes are commonly assumed within meteorology. As a result, the adiabatic lapse rate, the rate at which a parcel of air cools as it rises without exchanging heat with the surrounding atmosphere, is used as a frame of reference for other meteorological processes including atmospheric stability characterizations. The adiabatic lapse rate in one U.S. Standard Atmosphere is $0.98^{o}C/100m$. By comparison, the normal, or standard, lapse rate lapse rate is $0.65^{o}C/100m$.

Several lapse rates are displayed in Figure 3. The adiabatic lapse rate is identified as a dashed line. The normal lapse rate is subadiabatic, generally characterized by more stable atmospheric conditions. An isothermal lapse rate is one in which temperatures do not change with respect to height. As the figure shows, inversion conditions indicate an atmospheric temperature profile that is upside down with respect to adiabatic and normal

lapse rate conditions. Inverted lapse rates are indicative of some of the most stable atmospheric conditions, characterized by stratified horizontal atmospheric flow. In contrast, superadiabatic lapse rates generally imply unstable atmospheric conditions, which are turbulent in all three dimensions.

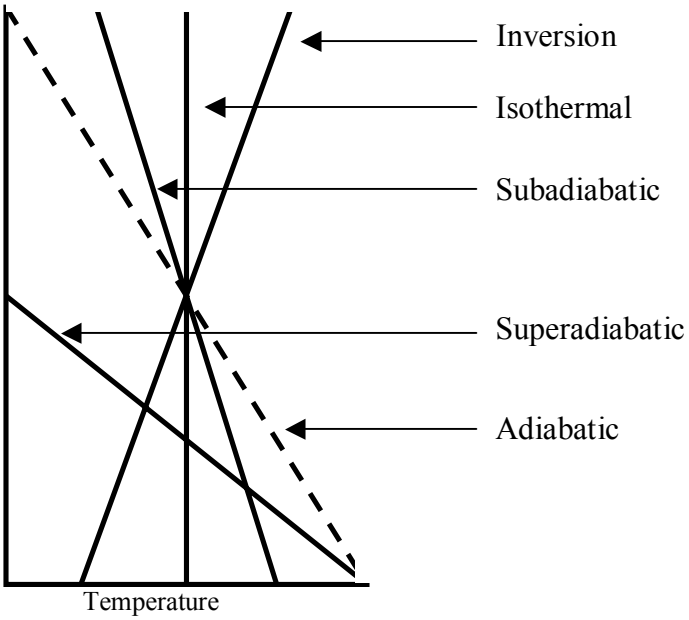

Figure 3: Atmospheric Lapse Rates

Instantaneous and Continuous Source Term Approximations

The overwhelming majority of all radionuclide emissions can be approximated as originating from either instantaneous point sources or continuous point sources. Events that are reasonably approximated as instantaneous point sources include explosions and other short venting emissions. Instantaneous represents the chronological portion of the approximation, since a finite amount of time expires during any short venting emission. Similarly, considering a point source is a spatial approximation, since all radionuclide

emission sources have some finite area, if not volume. Once the instantaneous emission is generated, its movement from the source location is governed by the speed and direction of the wind at the moment of release, assuming negligible buoyancy, particle settling velocity, or other external effects. As time progresses and the puff travels into other wind fields, its average speed and direction will change accordingly. In addition, the puff will expand about its center over time as its edges interact and become diluted with the surrounding atmosphere. Customarily, when an instantaneous point emission occurs, the amount of material released is quantified in terms of total mass or activity released. Downwind, the puff is usually described in terms of exposure or a time integrated concentration as it passes over a specified observation point.

The continuous point source emission has been studied more thoroughly by diffusion meteorologists. This approximation adequately models stack emissions and structural leaks where radionuclides are released into the atmosphere. A continuous emission is essentially an infinite sequence of instantaneous puff emissions released with a differential time increment between each puff. Like the instantaneous point source approximation, these releases are initially governed by the wind properties upon their release. However, because of the time duration associated with the release, the amount of material released is expressed as a mass or an activity rate. As the puff travels downwind, it is described as an average volumetric concentration. The cross-sectional area of a continuous source plume tends to increase as it travels downwind because of transverse wind influences. As a result, the plume's centerline concentration decreases as its distance from the source increases.

Most radionuclides that enter the atmosphere via continuous atmospheric emissions are released at an elevation through stacks. The ground concentration distribution that would be expected following a continuous stack emission is shown as a function of longitudinal and transverse distance in Figure 4. Although the airborne concentration is highest at the stack release, the ground concentration at the base of the stack is essentially zero. The ground concentration then typically rises to a peak value in the local vicinity of the stack, and gradually decreases as the distance from the stack increases. As Figure 4 illustrates, at any point downwind from the stack, a cross-section of the ground concentration distribution will be Gaussian in shape. The peak concentration is principally a function of the downwind distance traveled, and the standard deviation is primarily a function of the wind's turbulent effects on the plume.

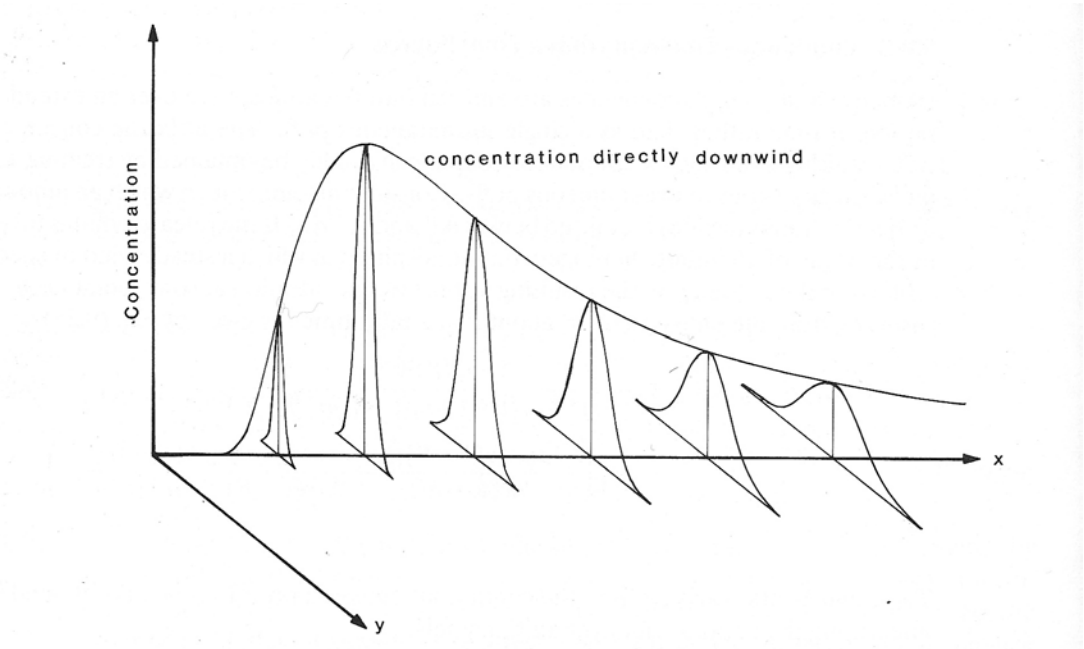

Figure 4: Ground Concentration Distribution Downwind from an Elevated Continuous Source

Characteristic Effluent Plumes

Fanning

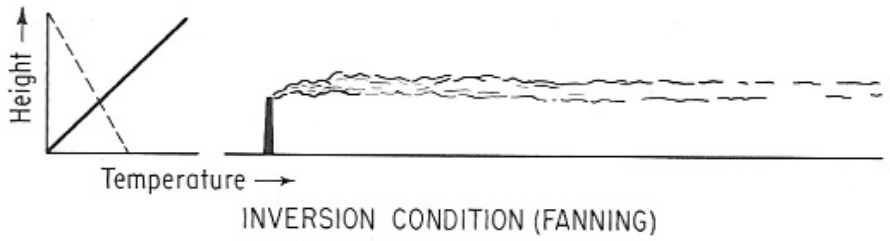

Figure 5: Fanning Plume Illustration and Vertical Temperature Profile

When a vertical temperature inversion inhibits vertical mixing, thereby creating very stable atmospheric conditions, plumes are limited to effectively one-dimensional horizontal diffusion in a manner called fanning. During these inverted lapse rate conditions, the extent of the transverse spreading is determined by shearing within the horizontal winds. This shear may be significant at night. If the prevailing horizontal winds are light, the fanning plume might be narrow and ribbon-like, meandering in an oscillating manner. Because the spreading of the plume is minimal, the plume may hold its form for tens of kilometers -- orders of magnitude greater than distances that would be expected in less stable atmospheric conditions, for example, during windy, daytime conditions.

Fanning plumes are very difficult to model because they are most affected by localized atmospheric variations and other unique factors that are not statistically governed. Even so, because of the distance they tend to travel without ground deposition, stack emanations during stable, inversion conditions can be desirable. A fanning plume may

be undesirable in situations where the emissions stack does not generate the plume above local obstructions like buildings, trees, or mountains. In addition, fanning plumes are not well suited for radionuclide emissions. Because of the limited spreading, the radionuclide flow can effectively act as an airborne line or planar source that delivers radiation exposures to the ground downwind even though the ground level radionuclide concentrations are zero. However, it should be noted that the stable conditions needed to generate true fanning plumes are quite rare, especially over great distances.

Fumigation

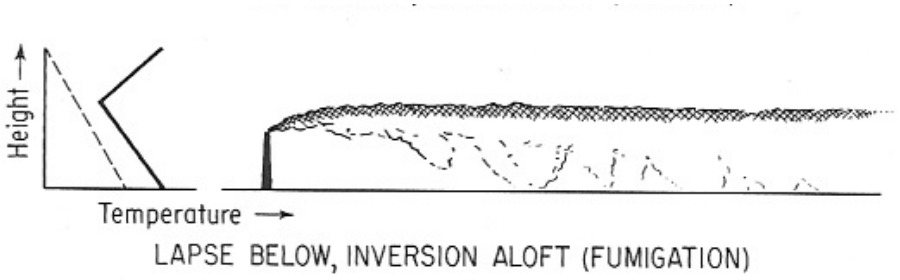

Figure 6: Fumigation Plume Illustration and Vertical Temperature Profile

When the sun rises on a clear day, the earth's atmosphere is normally heated from the ground upwards. As the atmosphere in heated, the inversion conditions that were present overnight are replaced by neutral or unstable atmospheric conditions. At some point in time, the newly generated daytime atmospheric conditions are present at the height of the emission stack. Therefore, the stable inversion layer exists just above the stack, and the less stable daytime conditions exist below. The result of these conditions is a fumigation plume. Fumigation plumes may also be formed through sea breeze conditions which generally occur during the late morning or early afternoon.

Fumigation plumes can deliver the greatest ground level concentrations when compared to all other types of effluent plumes. This is because a) the concentrated fanning plumes are able to dump their full concentrations into the ground level air, and b) the above ground inversion keeps subsequent emissions from fully spreading vertically restricting them to ground level air. Depending of the speed of the inversion layer dissipation, the fumigation conditions can persist for hours for considerable distances.

Looping

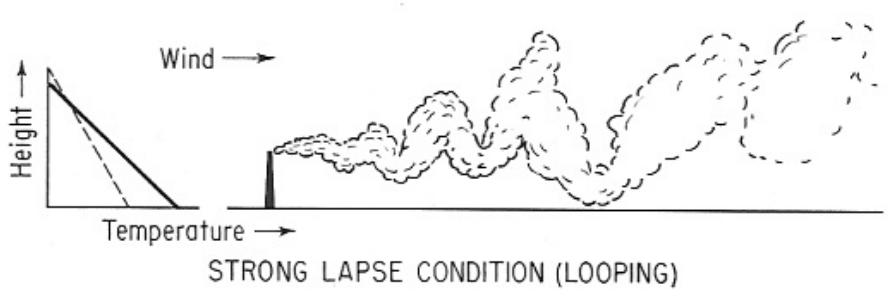

Figure 7: Looping Plume Illustration and Vertical Temperature Profile

As the day progresses and the lower layers of the atmosphere continue to become warmer, remnants of the overnight temperature inversion completely vanish. During the hottest parts of clear days in warm seasons, the resulting temperature profile can be very unstable due to the strong lapse rate. This can lead to large vertical eddy flows that generate looping plumes, which can cause the stack emissions to chaotically be brought down to the ground in large puffs. In some cases, the thermally induced downdrafts can bring the plume to the ground in close proximity to the emission location. However,

since the principal cause of such chaotic flow is atmospheric turbulence, which also contributes to ample mixing, when the looping plumes reach ground level, they tend to be more diffuse than fumigation plumes and also dissipate more quickly. Even so, it is possible to produce high average effluent concentrations on the ground simply because the deposition locations are so close to the stack emission point where the plume is most concentrated.

Coning

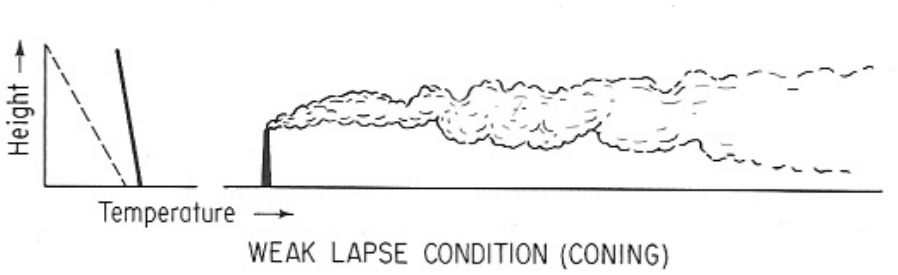

Figure 8: Coning Plume Illustration and Vertical Temperature Profile

During normal or weak lapse rate conditions, stack plumes tend to form cones oriented horizontally. Ground deposition from these coning plumes generally occurs at shorter distances than fanning plumes, but longer distances than looping plumes. This is because the thermally induced turbulence below a coning plume is between that of the other two plume types. Coning plumes can occur in the day or night and are most frequently present during cloudy or windy conditions. As a matter of fact, in climates that are characterized by cloudiness, coning plumes may be the most abundant of all plume types. On the other hand, in dry climates, they may be more seldom.

Lofting

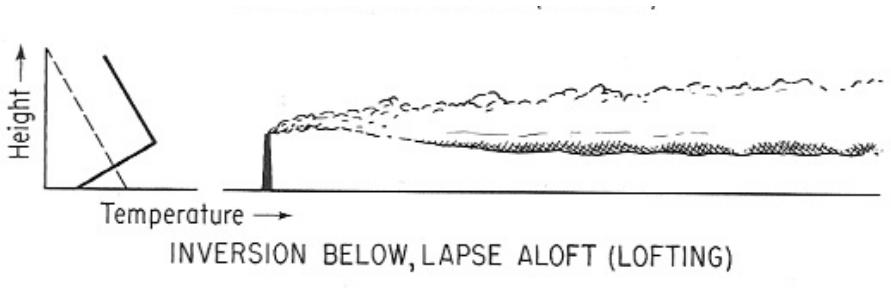

Figure 9: Lofting Plume Illustration and Vertical Temperature Profile

Lofting plumes are characteristically observed around sunset as the atmosphere transitions from unstable daytime conditions to the very stable night time conditions. The persistence of the lofting conditions is a function the stack height and the rate of change from the strong lapse rate to the inversion conditions. Therefore, lofting plumes may exist from time scales on the order of minutes to those on the order of hours. In rare cases, lofting plumes can persist throughout the entire night. Lofting plumes are ideal for minimizing ground deposition concentrations. Because the lower levels of the atmosphere are dominated by the inversion conditions, plumes can travel long distances before deposition is likely. Moreover, since mixing is occurring at higher levels, when deposition does occur, concentrations are likely to be relatively dilute.

Caveats

Each of the preceding plumes has been idealized for purposes of description and general analysis. However, in reality, several of the features that have not been considered in this section would need to be addressed if detailed calculations were necessary. For example, while none of the plumes considered an emission velocity of the effluents as they exit the

stack and enter the atmosphere, in actuality, all effluent plumes exiting a stack have a vertical velocity associated with them. In addition, the effluents being emitted may have a temperature that is higher than the surrounding atmosphere, which will lead to an increased plume rise and other buoyancy effects. Moreover, the plume constituents may not have the same material density as the surrounding air into which it is emitted. Therefore, in the case of more dense constituents, the plume would have a downward motion component not previously addressed. Furthermore, once a portion of a plume comes in contact with the ground, downwind plume depletion and resuspension of deposited particles must be considered. Other meteorological factors not addressed by the characteristic plumes include precipitation scavenging, ground boundary reflection, and building wake effects on diffusion. Finally, radionuclide generation and decay, atmospheric fractionation effects, and other phenomena not specifically related to meteorology would need thorough consideration as well for these approximations to approach reality.

Atmospheric Diffusion of Radionuclide Emissions

Radionuclide particles and gases emitted into the atmosphere experience random collisions with other atmospheric constituents and are influenced by wind fluctuations. These interactions cause the radionuclide emissions to become more dilute over time. While the wind influences have proven to be difficult to model from a strict mathematical perspective, the random mixing portion of the problem has been studied for decades and found to have a more straightforward mathematical solution. The random mixing of effluents emitted into the atmosphere has been shown to be adequately described by

diffusion theory. Therefore, in homogeneous atmospheric conditions when the wind is still, diffusion theory can accurately describe radionuclide dispersion in the atmosphere. However, these conditions are extremely rare when considering atmospheric diffusion distances.

The principal mechanism governing the dispersion and mixing of radionuclides in the atmosphere is turbulent airflow. The corresponding winds are the result of eddy flow and exhibit heterogeneous speeds and directions, but tend to fluctuate around some central value. The driving eddies are largely dependent upon the stability of the atmosphere and terrain effects. Unlike the well-characterized diffusion theory description of ambient dispersion, to date, no exclusively mathematical explanation for turbulent flow and mixing has been developed. All existing descriptions are dependent upon empirical data.

The eddy flows governing plume dispersion can generally be classified in two categories. Small scale eddies are much smaller than plume diffusion distances. These eddies tend to cause mixing amongst the plume's constituents and dilution as outside air is mixed into the plume. The net result is an overall size increase of the plume. Large scale eddies are larger than plume diffusion distances. These eddies do not mix or dilute the plume, rather they shift the overall direction of the plume's migration. The net result of these eddies is the meandering, sometimes oscillating track that most plumes display. Both plume spreading and the meandering track are illustrated in Figure 10.

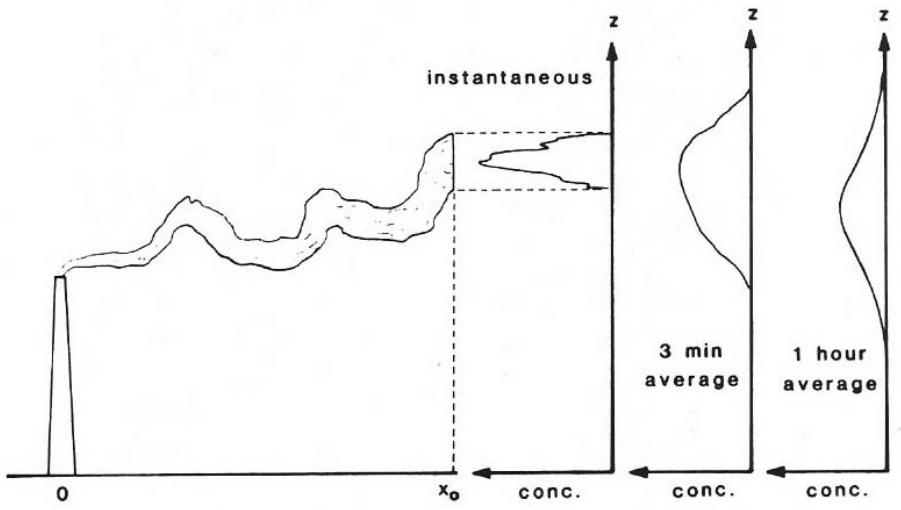

Figure 10: Plume Spreading and Meandering as a result of Eddy Flow

Figure 10 also shows vertical concentration distributions at some downwind location, identified as x_0. The instantaneously measured distribution shows irregular concentration fluctuations within the plume. In addition, the peak concentration of the plume rests at a specific height at that instant. However, if the plume is not measured at a specific instant in time, but as an averaged value over some time interval, the plume shows fewer internal concentration fluctuations. Similarly, if the averaging time is increased further, the concentration profile within the plume becomes smoother and more Gaussian in appearance. In addition, the figure shows that the position of peak concentration shifts towards the center of the distribution as the length of time increases.

Diffusion Equations

Concentration Calculations -- Infinite Medium

Because the diffusion of atmospheric pollutants is well studied, equations describing atmospheric diffusion are well established. The general diffusion equation which expresses the concentration of a pollutant instantaneously released into an infinite medium of air is shown in Equation 9. In this equation, C_{air} represents the pollutant concentration in air, Q represents the quantity of pollutant released, the release point of (x_0, y_0, z_0) is used in standard Cartesian space, and σ_x, σ_y, and σ_z are the standard deviations of the plume spread, called diffusion parameters.

$$C_{air} = \frac{Q}{(2\pi)^{\frac{3}{2}}\sigma_x\sigma_y\sigma_z}\exp\left[-\frac{(x-x_0)^2}{2\sigma_x^2}-\frac{(y-y_0)^2}{2\sigma_y^2}-\frac{(z-z_0)^2}{2\sigma_z^2}\right] \qquad \text{Equation 9}$$

Of course, if steady winds are active in an arbitrary direction (for example, the x direction), then the diffusion equation is modified slightly to reflect the influence. The modified equation is shown in Equation 10. In this equation, u represents the average wind velocity, t represents the duration of diffusion, and the diffusion parameters remain constant with respect to time.

$$C_{air} = \frac{Q}{(2\pi)^{\frac{3}{2}}\sigma_x\sigma_y\sigma_z}\exp\left[-\frac{((x-x_0)-ut)^2}{2\sigma_x^2}-\frac{(y-y_0)^2}{2\sigma_y^2}-\frac{(z-z_0)^2}{2\sigma_z^2}\right] \qquad \text{Equation 10}$$

By integrating with respect to time and approximating, the diffusion equation for a continuously emitting source into an infinite atmosphere with a constant wind can be found. This result is shown as Equation 11. For convenience, the point of origin is defined as (0,0,0), the diffusion parameters are assumed to be constant with respect to the x direction, and .

$$C_{air} = \frac{Q}{2\pi u \sigma_y \sigma_z} \exp\left[-\frac{y^2}{2\sigma_y^2} - \frac{z^2}{2\sigma_z^2} \right] \qquad \text{Equation 11}$$

Concentration Calculations -- Finite Medium

When considering non-infinite media, the influence of contaminant reflection arises. Contaminant reflection is the property of certain types of contaminants to remain in the atmosphere even after they have interacted with a surface boundary. For example, if, during atmospheric dispersion, a contaminant touches the ground does not settle due to gravity, is not absorbed, and is not adsorbed, and is therefore still a part of the atmospheric diffusion process, then contaminant reflection has occurred. To address contaminant reflection given a continuous emission from a stack of height $z - z_0 = h$, an imaginary source is emitted from a height -h and is assumed to follow identical idealized diffusion patterns. Because contaminant reflection can vary from 0% to 100%, the value α (ranging from 0 to 1, respectively) is used as a scaling factor for the amount of reflection occurring. This configuration is shown in Figure 11.

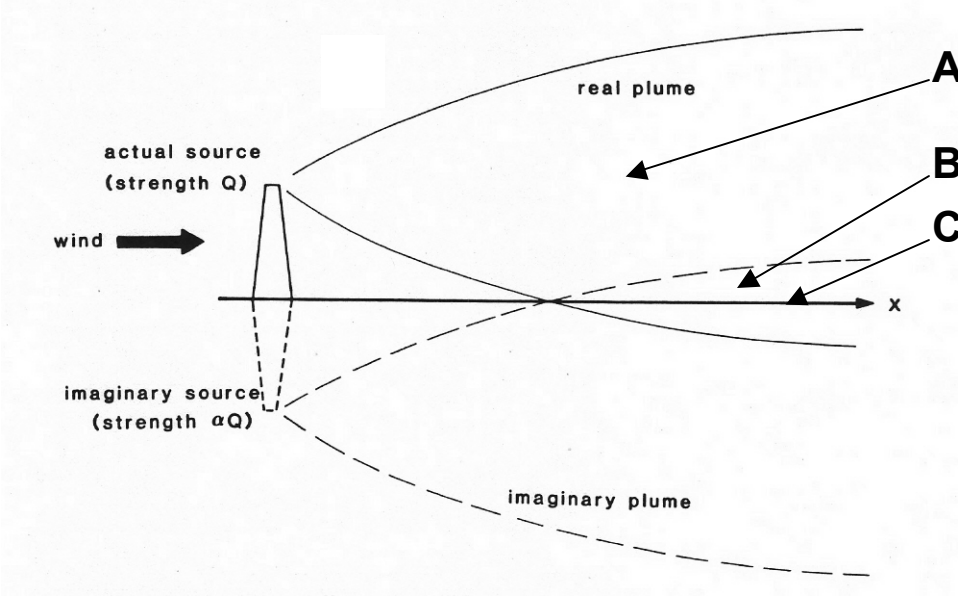

Figure 11: Plume Reflection

The corresponding concentrations of contaminants in the three regions identified as A, B, and C are shown in Equation 12A, 12B, and 12C, respectively. In region A, the contaminant concentration is simply the standard concentration determined by Equation 11.

$$C_{air} = \frac{Q}{2\pi u \sigma_y \sigma_z} \exp\left[-\frac{y^2}{2\sigma_y^2} - \frac{z^2}{2\sigma_z^2} \right] \qquad \text{Equation 12A}$$

In region B, relatively close to the ground at greater distances, the airborne concentration calculation is much more complicated. It includes the standard concentration in air (Equation 12A) plus the additional concentration added by the reflected plume contribution.

$$C_{air} = \frac{Q}{2\pi u \sigma_y \sigma_z} \exp\left[-\frac{y^2}{2\sigma_y^2} - \frac{z^2}{2\sigma_z^2} \right] + \frac{\alpha Q}{2\pi u \sigma_y \sigma_z} \exp\left[-\frac{y^2}{2\sigma_y^2} - \frac{(2h-z)^2}{2\sigma_z^2} \right] \quad \text{Equation 12B}$$

On the surface of the ground, region 3, where z = h, Equation 12B simplifies to Equation 12C.

$$C_{ground} = \frac{Q(1+\alpha)}{2\pi u \sigma_y \sigma_z} \exp\left[-\frac{y^2}{2\sigma_y^2} - \frac{h^2}{2\sigma_z^2} \right] \quad \text{Equation 12C}$$

Considering the extremely conservative estimate of $\alpha = 1$, which means that none of the atmospheric contaminants are extracted when the plume interacts with the ground, Equation 12C reduces to the well known Sutton Equation. The Sutton Equation, introduced in 1953, expresses the ground level concentration downwind from a continuous point source emission and is listed as Equation 13.

$$C_{ground} = \frac{Q}{\pi u \sigma_y \sigma_z} \exp\left[-\frac{y^2}{2\sigma_y^2} - \frac{h^2}{2\sigma_z^2} \right] \quad \text{Equation 13}$$

Additional Relationships

Of the many relationships that can be derived from the various concentration equation variables, one of the most practical is the relationship between the distance a plume has traveled and its ground level concentration, given a certain emission height and

atmospheric conditions. In order to develop these correlations, it is useful to normalize the ground level concentration with the emission rate and wind speed. These normalized relationships are shown for release heights of 0 m (a surface level release), 30 m, and 100 m in Figures 12, 13, and 14 respectively.

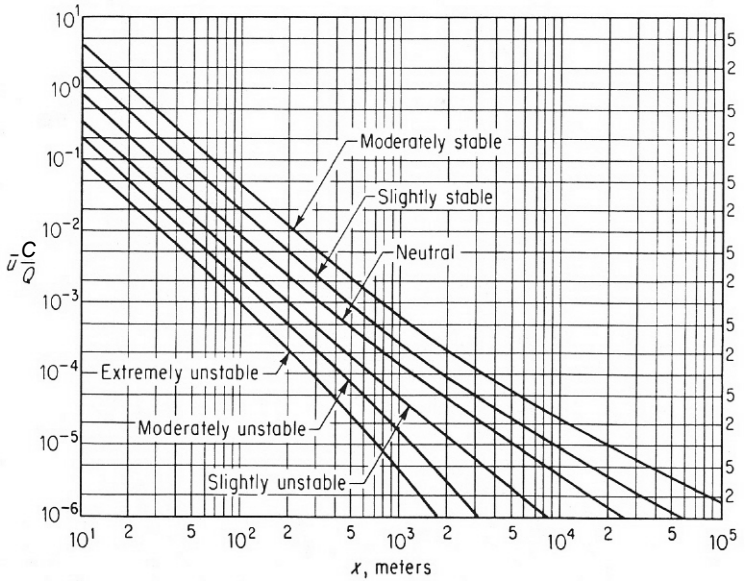

Figure 12: Normalized Ground Level Concentrations following Surface Level Release

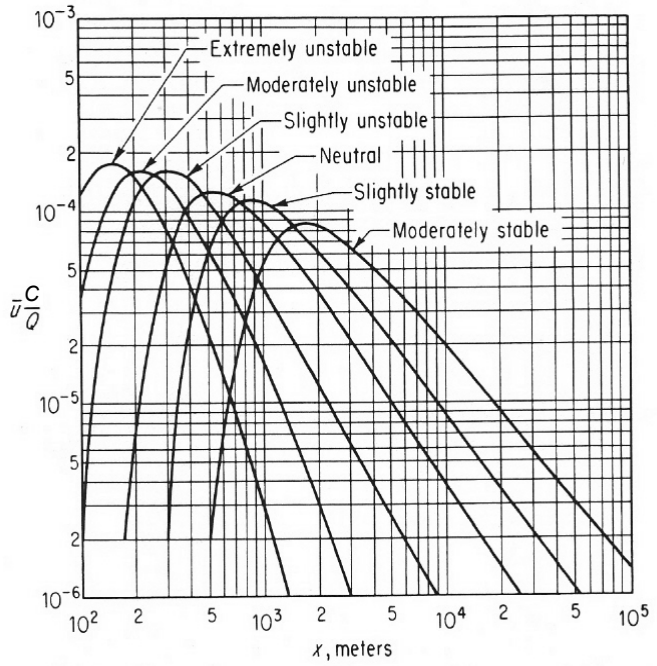

Figure 13: Normalized Ground Level Concentrations following Release from 30 m Altitude

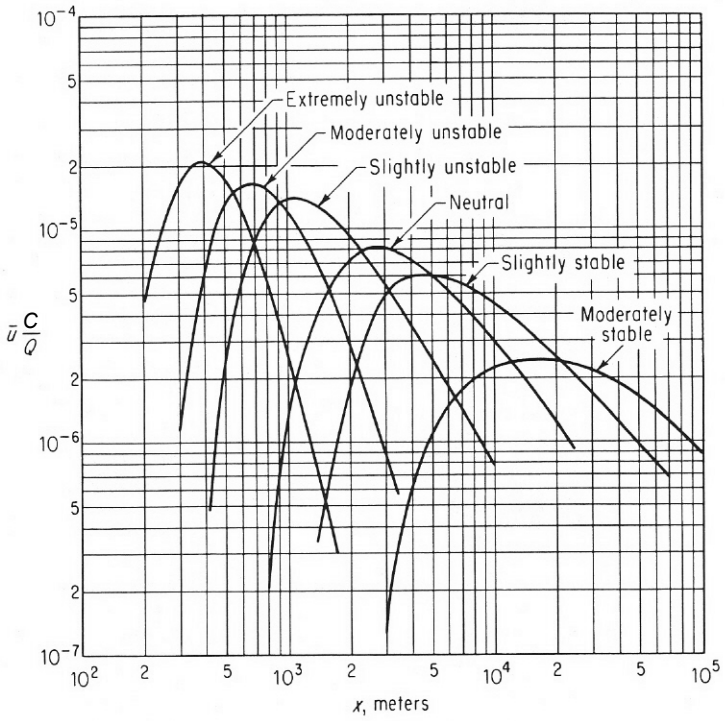

Figure 14: Normalized Ground Level Concentrations following Release from 100 m Altitude

In all of the concentration calculations that have been noted, the diffusion coefficients are assumed to be known. Literature has shown that an efficient, effective way to determine the diffusion coefficients is to use standardized charts. Recall from the derivation Equation 11 that diffusion in the direction of the blowing winds can be assumed to be constant (i.e., $\sigma_x = 0$). The charts for σ_y and σ_z determination are shown as Figures 15 and 16, respectively.

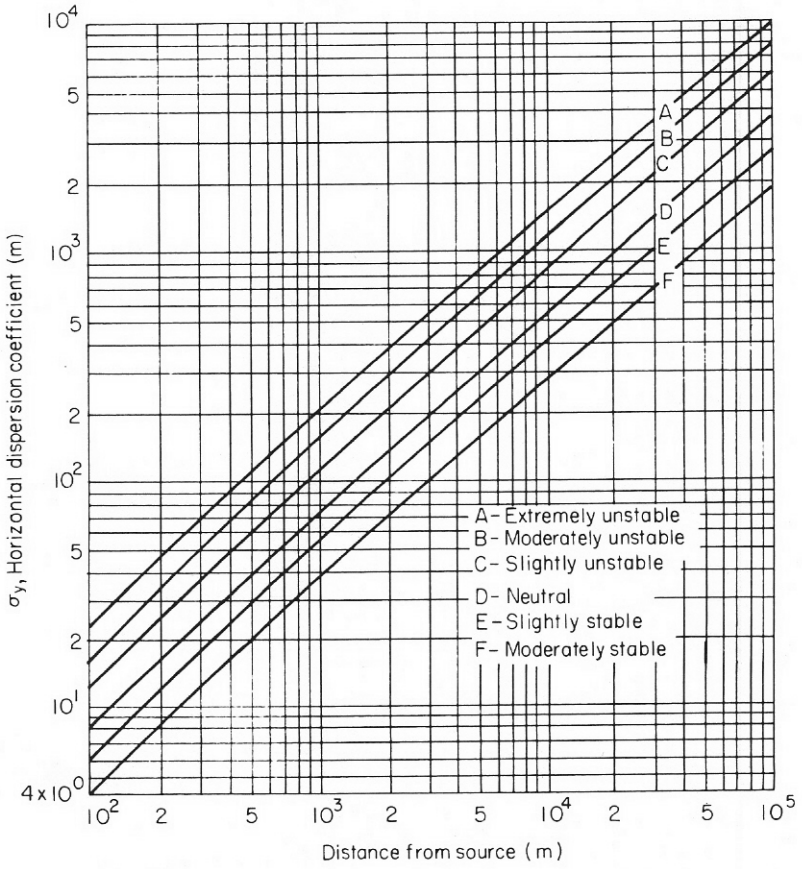

Figure 15: σ_y as a Function of Diffusion Distance in x Direction

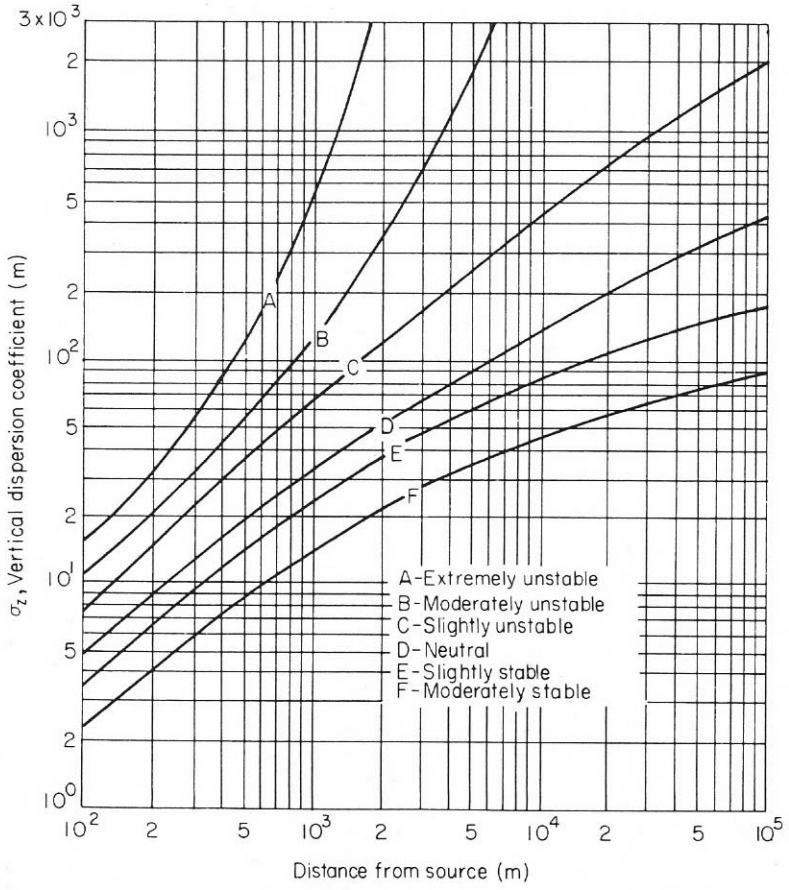

Figure 16: σ_z as a Function of Diffusion Distance in x Direction

Figures 12 through 16 all show multiple curves, each related to a different atmospheric condition. These atmospheric conditions were defined by Pasquill and are listed in Table 22. Table 23 shows how the atmospheric conditions relate to various meteorological phenomena.

Table 22: Atmospheric Stability Category Conditions

Atmospheric Stability Conditions	**Pasquill Category**	**Δ T (^{o}C) / altitude (km)**
Extremely Unstable	A	< -19
Moderately Unstable	B	-19 to -17
Slightly Unstable	C	-17 to -15
Neutral	D	-15 to -5
Slightly Stable	E	-5 to +15
Moderately Stable	F	> +1.5

Table 23: Relationship between Atmospheric Conditions and various Meteorological Phenomena

Surface Wind Speed (m/s)	**Daytime Insolation**			**Nighttime Conditions**	
	Strong	**Moderate**	**Slight**	**Thin Overcast (≥ 4/8 cloudiness)**	**≤ 3/8 cloudiness**
< 2	A	A - B	B	-	-
2	A - B	B	C	E	F
4	B	B - C	C	D	E
6	C	C - D	D	D	D
> 6	C	D	D	D	D

Collection and Detection Systems

Introduction

Generally, radionuclide levels within the environment are quantified onsite directly or collected and quantified in a laboratory environment. Several factors can govern which method is best for any given set of circumstances including the type of radiation(s) being measured, the time sensitivity of the measurements, the fidelity of information needed, etc. The discussion below addresses various radionuclide collections systems and radiation detection systems -- some of which are suitable for field use and others are suitable for laboratory use.

Radionuclide Collection Systems

General Methods for Airborne Sample Collection

In general, there are six ways in which airborne radionuclide samples are collected. These methods are filtration, volumetric sampling, bowed flow collection, adsorption, condensation, dynamic flow sampling. Although in some situations, multiple methods could prove to be effective, each method listed offers unique benefits given certain limitations that may be present.

Filtration air sampling is the most common method used to capture airborne particulates. While this method is effective at efficiently collecting particulates, it is ineffective as a gas collector. This simple process involves drawing air through some sort of filtration medium, thereby concentrating the airborne contaminants in the medium. After a set amount of time has elapsed with a measured flow rate of air passing through the filtration

medium, the filtration medium can be removed, and the captured radionuclide particulates can be measured and analyzed. Knowing the average flow rate of air through the filtration medium, the amount of time the medium collected particulates, and the amount of radioactive material measured on the medium, the corresponding airborne radioactivity can be calculated.

Numerous filtration media are available. Several factors can influence which medium is ideal in specific situations. These factors include the required particulate collection efficiency, porosity of the medium, durability, cost, cross-sectional size, air flow resistivity, inherent background radioactivity, and chemical solubility. The most commonly used filters are glass fiber filters, cellulose-asbestos filters, and membrane filters. Because membrane filters are soluble in organic solvents, they work well when the radioactivity collected will be measured by a liquid scintillation counter. Radiation entrained within the other two types of filters is typically measured by standard radiation counting practices or by radiochemical assay.

Volumetric sampling simply involves drawing air and interspersed contaminants into a container. This method can be used to collect particulates or gases. Some of the more common ways to draw the contaminant-laden air into the sampler include pre-evacuated container collection, vacuum pump collection, and dynamic evacuation collection. The pre-evacuated container collection process involves evacuating the container in a remote location with a vacuum pump. When the evacuated container is brought to the collection site and opened, the negative pressure gradient draws air into the container. The now air-

filled container can then be sealed and removed to a remote location for analysis. Vacuum pump collection uses a pump to draw air into the container. One disadvantage of this method is that some of the air drawn into the container by the pump is likely to be drawn through the container into the pump, possibly causing a portion of the contaminants to be lost. In the dynamic evacuation collection process, a container filled with a liquid is brought to the sampling site. The liquid is then poured out, which dynamically draws air into the container to fill the volume. As in all of the other methods, the air filled contained can be analyzed remotely.

In the bowed flow collection process, particulate contaminants are collected in the flow stream at a location where the direction of flow changes abruptly. The momentum of the particles in the airflow prevents them from changing directions as quickly as the air in which they are carried. At the location within the flow stream where particles are likely to be collected, the inner wall of the flow mechanism is typically coated with a coagulant or an adhesive to improve collection efficiency. Bowed flow collectors may incorporate various stages with differing airflow speeds to tailor their collection to particulates of specific sizes.

Adsorption sampling involves collecting contaminants on a medium within the airflow path through chemical bonding processes. These collectors are traditionally used as gaseous radionuclide samplers. They can be used to collect particulates, but they do so with poorer efficiency than other processes. To maximize the available surface area for trapping the gaseous contaminants, the adsorption medium is porous or granulated.

Common adsorber materials include silica gel, activated charcoal, and silver zeolite. Silica gel is typically used to collect tritium oxide (T_2O) vapor. Activated charcoal can be used to collect radioiodine, xenon, krypton, and argon. Silver zeolite is used to collect radioiodine exclusively, with no noble gases.

Condensation sampling, also known as dehumidifier sampling, uses a cold trap to condense water vapors within the sampled air. The condensate liquid is then analyzed for radioactive contaminants -- often with a liquid scintillation counter. When calculations related to the radioactivity of the condensate are performed, the temperature and relative humidity of the air drawn into the sampler must be known to determine the concentration of radiation per unit volume of air. The condensation surface can be cooled any number of ways. Cryogenic and liquid nitrogen cooling are frequently used options. This sampling method is generally used to sample tritium oxide and tritiated water (HTO) vapors.

In dynamic flow sampling, air is drawn directly over or through a detection system so that real time measurements can be taken obtained. This method is used when the radionuclides being studied are difficult to collect or when measurements are needed on a continuous or an instantaneous basis. One drawback to this method is that the detection system efficiency and operation can be hampered because of the accumulation of particulates and the condensation of certain gases. To prevent this from occurring, particulates are filtered and gases are adsorbed before the flow stream reaches the

detector. These detectors are useful for detecting tritium through its low energy gamma-rays.

Airborne Radionuclide Samplers and Monitors

High volume air samplers, also called high flow rate air samplers, are known for their ability to provide accurate estimates of airborne radioactivity concentration at a particular location for a set duration of time. These noisy samplers typically operate at flow rates of at least 500 cubic feet per hour. They use a vacuum system to draw air from the atmosphere across a filter that collects entrained particulates. In addition to particulate filters, these samplers can be equipped with greased plate for bowed flow collection or activated charcoal inserts for adsorption collection. Although high volume air samplers have been known to run for several days for collection operations, they are generally stopped for brief periods of time to replace the filter, so that the used filter can undergo remote radionuclide analysis. A limited number of advanced high volume air samplers are able to perform the radionuclide analysis automatically within the sampler.

Low volume air samplers, or low flow rate samplers, operate similarly to their high volume counterparts. However, these systems operate more quietly due to the reduced power requirement that results from the lower flow. Low volume samplers are typically used in situations when the collection period needs to span a longer duration of time, or as backup collection systems.

Continuous air monitors (CAMs) are low flow rate sampling systems that are equipped with radiation detectors that monitor the airflow. These systems can be designed to detect are report alpha, beta, or gamma radiation activity, radioiodine activity, or noble gas activity. Traditionally, they are used in radiation safety alarm systems and provide some type of display or other indication of the instantaneously measured or averaged radiation.

Personal air samplers (PASs) are small, portable devices which unobtrusively sample air near a worker's nose and mouth. These battery-powered systems estimate the airborne radioactivity concentration present in a cumulative manner while they are in operation. They contain a battery-powered pump that operates at a flow rate of approximately 20 liters/minute which simulates the breathing rate of a moderately active worker.

Radiation Detection Systems

Gas-filled Detection Systems

Gas-filled detection systems are typically those that detect direct ionization radiation as it passes through and excites gas molecules in the system. The three main types of gas-filled detectors are ionization chambers, proportional counters, and Geiger-Mueller counters. Each of the systems uses progressively strong electric fields to create ion-pairs. The created ion pairs are then used to quantify the amount of radiation present. Figure 17 graphically depicts the voltage regions for the three gas-filled detector processes.

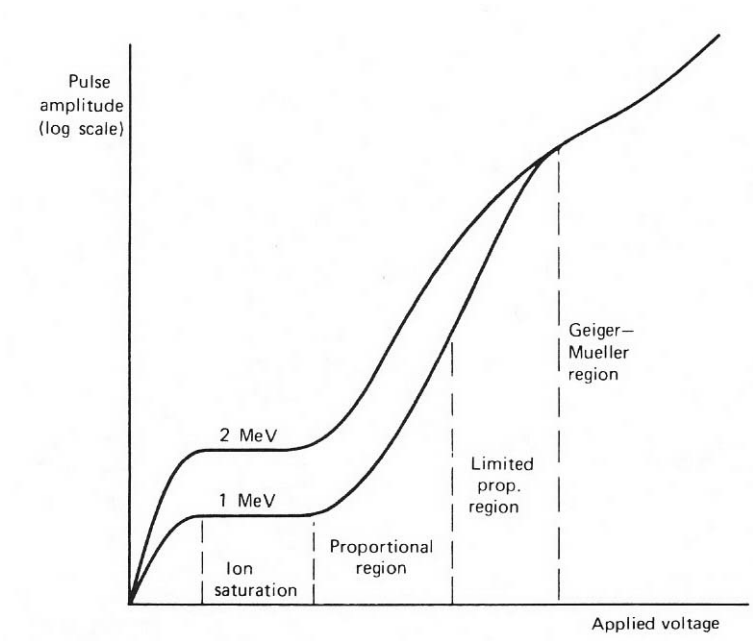

Figure 17: Voltage Relationships of Gas-Filled Detectors

An ionization chamber, also known as an ion chamber, is the simplest of the gas-filled detection systems. These detectors use an air filled chamber and can be designed with a small voltage drop either coaxially or across two parallel plates. The radiation that enters the system directly ionizes the gas inside the chamber. The resulting ion pairs are then accelerated and collected through the voltage drop and either electrical pulses or the current associated with the charge migration is measured. Ion chambers can be used to detect radiation per unit time for alpha particles, beta particles, gamma rays, and x-rays.

A proportional counter is typically used in a laboratory. The standard proportional counter is equipped with a counting tray for the radioactive sample being analyzed and a flowing "proportional gas" of argon or methane. Depending on the arrangement of the detector, it can be used to detect, alpha, beta, x-ray, and gamma radiation, as well as

neutrons. To detect neutrons, the standard proportional gas is changed to either boron triflouride (BF_3) or helium-3 (He-3). Because of the common use of these modified proportional counters, they are generally referenced as BF_3 counters and He-3 counters. These detectors rely on the B-10(n,α)Li-7 and He-3(n,p)H-3 reactions, respectively. BF_3 counters are limited to detecting slow neutrons only, while the He-3 counters are able to detect both slow and fast neutrons.

The Geiger-Mueller Counter is a historic gas-filled radiation detection device that still has broad applicability and use today. The system is known by several names including a Geiger Counter, a G-M Counter, and a G-M Tube. A Geiger Counter operates by using an electric field that generates an electrical signal when radiation interacts with either the gas inside the tube or the tube wall. The electrical pulses are then converted to a display measurement reading and sometimes an audible clicking sound. G-M Counters typically measure radiation per unit time but are limited to low count rates since they have the disadvantage of long dead times which can cause high count rate measurements to be underestimated. Because G-M counters cannot measure energy, they are not especially useful for identifying radioisotopes. They can be used to detect x-rays, gamma-rays, alpha particles and beta particles, but it is unable to distinguish between them.

Scintillation Counters

A scintillation counter detects radiation through light that is emitted as ionizing radiation interacts with certain materials. The emitted light can then be transformed into an electrical pulse. The pulse amplitude is a function of the number of electrons that were

excited during the interaction and therefore scale with the amount of radiation that generated the scintillation. These detectors have several benefits including a compact size and the ability to detect alpha, beta, gamma, x-ray, and neutron radiation.

Some of the most popular scintillation detectors are the liquid scintillation counter, the sodium iodide (NaI(Tl)) detector, and the bismuth germinate (BGO) scintillator. Liquid scintillation counters are typically used in a laboratory. With the appropriate configuration, these counters can achieve low background counts and correspondingly low minimum detectable activities. Sodium iodide detectors are known for their high light yield. These detectors have become the standard scintillator systems for performing gamma-ray spectroscopy. They can be used in a laboratory or in the field. Although the NaI(Tl) crystal can be fragile, it can be useful in the field because it does not need cooling. BGO detectors are similar in principle to sodium iodide detectors. However, they have the disadvantage of lower light yields than sodium iodide detectors. The chief functional difference between the BGO detector and the NaI(Tl) detector is the ruggedness of the BGO system. Because of its durability, it is more suitable for use in the field than NaI(Tl) detectors.

Integral to the functionality of scintillator detectors is the ability to convert the weak light outputs into detectable electrical signals. The two types of devices that are used to accomplish this are photomultiplier tubes (PMTs) and photodiodes (PDs). PMTs convert the emitted scintillation light into a small number of low energy electrons. These electrons then proceed through the electron multiplier portion of the tube which results in

an amplified, detectable output electrical signal. Photodiodes can be used as an alternative to PMTs and offer the advantage of increased ruggedness, smaller sizes, and decreased power needs. In addition, unlike PMTs, PDs are virtually insensitive to magnetic fields which enable them to be used in circumstances where magnetic fields may be present.

Other Detectors

Thermoluminescent detectors (TLDs) are the most widely used personal radiation detection devices. As opposed to most detectors that offer count rate data, TLDs serve as integral counters and provide information regarding radiation exposure over a duration of time. In order to measure the amount of exposure, TLDs must be heated. The heating process causes light to be generated that corresponds to the amount of TLD radiation exposure. In addition to enabling a quantifiable measurement of exposure, the heating process effectively anneals the exposed portions of the detector which enables the detector to be fully reused. Through the process of use and heating, a TLD can be reused many times.

High-purity germanium (HPGe) detectors are useful for detecting x-rays and gamma-rays principally in a laboratory environment, but increasingly in the field. HPGe detectors offer good detection efficiency and high energy resolution. As a result, these detectors are an ideal choice for performing x-ray and gamma-ray spectroscopy -- especially in situations where the spectra have been generated by multiple radiation sources or may have other complexities. Although these detectors must operate cooled for proper

performance, they can be allowed to heat up between uses with essentially no performance degradation. Now that cooling mechanisms are becoming more compact, HPGe detectors are increasing in their field use.

Radionuclide Concentration Calculation

Calculating radionuclide concentrations collected on filter paper can be a relatively straightforward process. The governing equation describing the change in filter paper activity with respect to time is expressed as Equation 14. As Equation 14 shows, the total plume activity with respect to time is calculated by multiplying the plume activity concentration with the flow rate of sampled air through the filter. Both the plume activity and the flow rate may be time dependent.

$$\frac{dA}{dt} = Q(t)F(t) - \lambda A \qquad \text{Equation 14}$$

where, A = Activity on Filter Paper (disintegrations/time)

Q = Plume Activity Concentration (disintegratons/(time · volume)

F = Sampler Flow Rate (volume/time)

λ = Decay Constant (1/time)

The number of counts generated by a radionuclide collected onto the filter paper, which corresponds to its peak area, is simply the time dependent integral of the filter paper activity equation, Equation 14. However, because the filter paper activity is not readily measurable, the number of counts must be related to the plume activity concentration and

flow rate. Because the time varying nature of the plume concentration and flow rate can lead to solutions that cannot be addressed analytically, time averaging can be used to generate constant, average values. This greatly simplifies matters and results in a standard first order differential equation in terms of filter paper activity. This equation can be integrated with respect to the sampling time, the independent variable in Equation 14. Then it can be integrated with respect to the decay time, the time between the radionuclide collection onto the filter paper and counting the sample using a radionuclide detection system. The result can then be integrated with respect to the counting time in the detection system. Because the decay time and counting time are independent of one another and all other processes considered, integrating with respect to these variables is also straightforward. The result of these three integrations is shown as Equation 15.

$$C\ (T,\mu,\phi) = \frac{\varepsilon \gamma Q F}{\lambda^2}\left(1-e^{-\lambda T}\right)\left(1-e^{-\lambda \mu}\right)e^{-\lambda \phi} \qquad \text{Equation 15}$$

where, C = Number of Counts (Area) Generated by Specific Radionuclide (disintegrations)

Q = Plume Activity Concentration (disintegratons/(time · volume)

F = Sampler Flow Rate (volume/time)

λ = Decay Constant (1/time)

T = Sampling Time (collecting airborne particulates onto filter paper)

ϕ = Decay Time (neither collecting nor counting)

μ = Counting Time (generating spectra based upon filter paper activity)

ε = Energy Dependent Efficiency of Detector (scalar)

γ = Gamma-Ray Branching Ratio (scalar)

Relevant Models

Introduction

Numerous models have been developed to track the generation and dispersion of airborne radionuclide contaminants. A search of the available literature has led to over thirty atmospheric radionuclide generation and dispersion models that have been used or are in use by the U.S. and foreign governments -- each model reportedly offering differing types of output and benefits. The U.S. Government has identified a select set of these models as being functional and reliable enough for use within regular emergency response and site characterization procedures. The models most widely used within the Government include RASCAL, developed for use by the Nuclear Regulatory Commission (NRC); HPAC, developed for use by the Defense Threat Reduction Agency (DTRA); SHARC, developed for use by Sandia National Laboratories (Sandia); and ARAC and HOTSPOT, both developed for use by Lawrence Livermore National Laboratories (LLNL). While some of these radionuclide models have broad applications including nuclear, chemical, and biological dispersion phenomena (e.g., HPAC and ARAC), others are specifically intended to address nuclear-related phenomena alone (i.e., RASCAL and HOTSPOT).

A review of these models highlights the novelty and utility of the model developed. The principal void within this body of models is that none of these models fully integrates

human judgment throughout the analytical process. As a result, these models are dependent upon quantitative inputs and are incapable of processing qualitative data. One effect of these limitations is that none of these models are able to achieve site characterization because they are only able to analyze data that have been input into them -- a subset of total quantity of data available. Another effect is that none of the models identified are able to correct themselves during analysis. If inconsistent or incomplete data is input into these models, they are likely to either fail during analysis or output an errant result. Because human judgment is fully integrated into the model developed, it is the only one that is capable of overcoming the shortfalls identified within existing models.

Principal Radionuclide Dispersion Models Used within U.S. Government

ARAC

LLNL's Atmospheric Release Advisory Capability (ARAC) was developed to assess the consequences of radiation releases by modeling plume movements in near-real time. ARAC offers sophisticated modeling capabilities and is able to simulate complex terrain effects, multi-location, real-time wind field data, etc. Because the model operates in near-real time, it is able to effectively estimate the spread of radioactive contaminants for emergency response applications. three-dimensional atmospheric flows, and dispersion of releases on all scales of interest, from local to global

ARAC's dispersion component uses a Lagrangian stochastic, Monte Carlo method to solve the three-dimensional advection-diffusion equation. This component simulates

numerous processes including radioactive decay and generation, mean wind advection, turbulent diffusion, and wet and dry deposition as a function of aerosol spatial and dimensional distributions. The decay and corresponding generation of radionuclides within decay chains is calculated during the simulation. Because of the versatility of the source and emission mechanism specifications including point, line, area, or volume sources, and continuous or instantaneous emissions, the model can address stack emissions with momentum and/or buoyant plume rise, fires, and explosions. For aerosol sources, the mass, activity, and particle size distributions can be predetermined with tabular or lognormal distribution input parameters. Moreover, due to ARAC's robustness, multiple, time-dependent sources can be applied during each run. One of ARAC's unique features is that it can address time-varying emission of radionuclide mixtures and time-dependent decay and generation of radionuclides within decay chains during atmospheric transport.

The ARAC model is linked to a system that automatically accesses global databases of geographical data including terrain elevation, high-resolution land use and coverage data, real-time meteorological observations and forecasts, and population data. In addition, the system accesses both radionuclide decay chain and dose factor databases. As a result, ARAC is able to output varying air and ground concentrations, doses, and dose rates. The doses can be calculated in a time-averaged or time-integrated manner. The overall output of the ARAC model and its supporting resources is an explanation of the nature of the release, a description of the assumptions used in the calculations, and a summary of the predicted effects.

The principal strength of the ARAC model is its robustness. The code has been proven to be both versatile and effective through thousands of assessments, exercises, and emergency response applications ranging over a period of twenty years. The key weakness of the code is its difficulty in handling sparse data. For example, the diagnostic wind fields can have large errors if sparse data is input into the model. Errors within such a fundamental parameter can be easily perpetuated and lead to significant errors in the overall output.

HPAC

DTRA's Hazard Prediction & Assessment Capability (HPAC) Gaussian puff model which is capable of treating the dispersion of contaminants wide variety of atmospheric conditions. HPAC can be used to evaluate nuclear, biological, chemical, and radiological dispersal events. HPAC models the atmospheric dispersion of gases, particulates, and liquid aerosols from multiple sources, and is functional with varying levels of meteorological input ranging from an individual wind speed and direction to spatial and time dependent wind and temperature fields. One of the principal objectives of HPAC is to assess the consequences of weapons of mass destruction. The model also assists the military with selecting the optimum targeting options when nuclear, biological, and chemical materials are in the vicinity. Another customary use of HPAC involves providing support during accidents or after terrorist events involving nuclear, biological, and chemical materials. Due to the complexity of the program, HPAC users must be trained and obtain a license prior to running HPAC on a personal computer.

HPAC's modules perform four principal functions: source term generation, meteorological data retrieval, plume transport and dispersion, and effects estimations. The source term modules applicable include nuclear facilities and devices with defaults for nuclear power stations, nuclear weapon accidents, and yield generating nuclear detonations. HPAC is able to access a climatology database for its meteorological input. HPAC Meteorological Data Servers accounts are available for emergency response purposes. These data servers provide access to both real-time observations and forecast models. With a few meteorological inputs, sufficient to enable the code to perform interpolations and extrapolations, a three-dimensional time-varying wind field can be initialized. The wind field may be developed either with or without terrain considerations. If the terrain consideration is chosen, a terrain database with approximately a one kilometer resolution coordinate system can be used.

HPAC uses the Second-order Closure Integrated PUFF (SCIPUFF) model to for dispersion calculations. SCIPUFF uses a series of Gaussian puffs that are released and tracked in either a stationary or moving frame of reference. The puff approach is flexible enough to allow plumes to split and merge depending meteorological influences. Other associated phenomena that can be addressed include radionuclide decay, plume rise due to buoyancy and momentum, dense gas effects, and wet and dry deposition.

HPAC users have a choice of two modes of operation. The operational mode uses default source terms, while the advanced mode allows the user to specify relevant source term parameters. Advanced mode operation of HPAC can accommodate almost all varieties

of source terms; however, due to the complexity of this mode, a high level of training and experience with HPAC is needed to successfully use this mode.

HPAC can output mapped plots of dose and deposition and can highlight lethality values. One of HPAC's more unique features is its Hazard Area plot, which is presented as the probability of that a specified dose level is exceeded. All of HPAC's plotted outputs are able to show city and national boundaries from a 1:1,000,000 database. These products may be exported in into other types of computer software, such as ARCInfo.

HPAC has several strengths. First, it uses a second-order turbulence closure model within its dispersion calculations. Therefore, it tends to be reasonably accurate for dispersions that travel long distances. The model has been especially useful determining the radiological impacts that result from nuclear reactor accidents. Next, the SCIPUFF portion of HPAC is able to address complex terrain by using a terrain-following coordinate system within the model. Finally, the code considers varying dynamic effects in an integrated manner which gives it the capacity to more accurately extrapolate results. Even so, weaknesses exist within the model, as well. For example, HPAC does not address dispersions at high altitudes (above 30 km) or complicated localized aerodynamic flow patterns like flow within a forest or around buildings. In addition, HPAC is not suitable for emergency response situations because it does not accept real-time meteorological data inputs. HPAC also assumes that the density of the atmospheric releases to be similar to that of air. Therefore, radionuclide releases of high buoyancy or density may be modeled inaccurately.

RASCAL

The Radiological Assessment System for Consequence AnaLysis (RASCAL) was developed for use by the U.S. Nuclear Regulatory Commission (NRC). The model is designed for emergency response teams who respond to nuclear power reactor accidents and other radiological emergencies at NRC licensed facilities. The NRC favors the RASCAL over other dose assessment models because RASCAL can estimate releases based strictly upon accident progressions and can therefore address releases from unmonitored pathways. By using RASCAL, the NRC is able to conduct analyses that are completely independent of EPA analyses and can have an added level of confidence in its results.

RACSAL consists of four subprograms. First, the Decay Calculator computes the decay and corresponding generation of radionuclides. Although it does not integrate the total activity over the decay period, it can calculate time-dependent activities. The Decay Calculator also accesses the RASCAL radionuclide database and can display decay series in a tabular or graphical format.

Next, the Field Measurement to Dose (FMDose) portion of the model uses empirical measurements to calculate emergency response team safety limits, and acute and residual doses. Because FMDose utilizes real-time measurements for its calculations, the empirical field data must be acquired from the accident site to be useful. Like the Decay

Calculator, FMDose is able to access the RASCAL radionuclide database and can display decay series in a tabular or graphical format.

Then, the Meteorological data Processor subprogram uses manually entered meteorological data within atmospheric transport and diffusion models. Meteorological data can be entered for the release location onsite and up to 35 additional meteorological observation locations for subsequent use by the final subprogram, STDose. Entering data from multiple stations will cause a two-dimensional surface wind field to be generated by using a simple distance weighting of station data. Moreover, if the meteorological data is provided by an NRC-regulated facility, then the surface fields can be further refined to include mass consistency using known topographic data in the vicinity.

The final portion of the RASCAL model, the Source Term to Dose (STDose) subprogram, computes doses from radionuclide releases by using a Gaussian plume-puff transport and diffusion model. While a steady-state Gaussian plume model is used in the vicinity of the release (at distances up to approximately 1 km), at later travel distances a time-dependent Gaussian puff code calculates the dispersion. STDose also evaluates plume rise, wet and dry deposition, and radionuclide decay. This subprogram also incorporates time-dependent source emission rates for several predetermined scenarios. For example, nuclear power reactor releases can be characterized by evaluating the plant type and conditions or from assessing measured release data. Other predetermined scenarios include spent fuel sources, which can be stored in a wet or dry storage environment, UF6 canisters, uranium oxide fires and explosions, criticality accidents, and other direct radionuclide releases. STDose allows the user to input the quantity and types

of radionuclides in the source term in the direct release scenario. STDose output includes plots of dose contours and tables of dose vs. downwind distance.

HOTSPOT

The HOTSPOT set of health physics codes was developed by LLNL for emergency planners and emergency response personnel. HOTSPOT was designed to provide these individuals with fast, portable software tools to enable a more effective evaluation of accidents involving radioactive materials. It is most effective in evaluating a localized release within a few hours of the emission with steady winds over flat terrain. Because of HOTSPOT's effectiveness, it is used for emergency planning at several Department of Energy facilities, and for civil defense purposes internationally. The model is also useful for performing safety analyses of nuclear material handling facilities.

The HOTSPOT model is a first-order approximation of the radiation effects related to the release of radioactive materials into the atmosphere. The Gaussian Plume Model that is incorporated into HOTSPOT has been used widely for initial emergency assessments of radionuclide releases and for safety analysis planning. Therefore, HOTSPOT is reasonably accurate for initial assessment purposes.

Given basic user input values for atmospheric stability and wind speed and direction, HOTSPOT computes downwind assessments of atmospheric radionuclide releases using one of four subprograms: PLUME, EXPLOSION, FIRE, and RESUSPENSION. These subprograms can address continuous or puff releases, explosive releases, fuel fires, and

area contamination incidents in the vicinity where the basic input are applicable. Therefore, complicated meteorological dynamics can impair the accuracy of the output. Other options can expedite preliminary nuclear weapon accident assessments by addressing tritium, uranium, and plutonium releases. Moreover, if certain radionuclides are known to be present, HOTSPOT enables the user to manually enter them for evaluation.

The EXPLOSION subprogram calculates the effects of nuclear weapon detonated on the earth's surface. These include prompt effects such as neutron, gamma, blast, and thermal effects, as well as delayed effects like fallout information. The fallout data calculated include arrival time, and dose rate upon arrival. In addition, the subprogram can compute integrated dose contours for several time intervals and display these contours on geographic maps.

The principal strength of the HOTSPOT model is its simplicity. Because HOTSPOT is based on simple, first-order approximations, it is easy to use, it operates quickly, and it can be applied in a variety of situations. Although other models can provide more data than the HOTSPOT model, due to the limited amount of input data that is typically available in emergency response situations, the accuracy of the additional data may be questionable. On the other hand, the more limited amount of data generated by HOTSPOT is quite reliable. The main limitation of HOTSPOT is its inaccuracy when addressing complex terrain, meteorological conditions, or aerodynamics.

SHARC

The Sandia Hazard Assessment Response Capability, SHARC, models and assesses the effects of weapons of mass destruction by using field-portable codes. SHARC principally consists of the following subprograms: AIRRAD, ERAD, NUKE, BLAST, and SHARC. The BLAST subprogram evaluates general blast effects and predicts distance ranges for these effects. NUKE uses well-established computational methods to estimate prompt effects related to a nuclear detonation including blast overpressure, thermal output, and gamma and neutron effects including electromagnetic pulse influences. The Explosive Release Atmospheric Dispersal subprogram, ERAD, computes the atmospheric dispersion of materials that were emitted by the detonation of high explosives. AIRRAD models the transport of radionuclide fallout. This subprogram estimates the fallout arrival time and duration, dose rate, and integrated dose. Finally, the SHARC subprogram provides the user with dialog boxes to operate the other subprograms and enables output contours to be displayed on maps.

Other U.S. Radionuclide Dispersion Models

GENII

Originally developed in 1990, GENII is an older, general purpose environmental health physics model. GENII was designed to incorporate internal dosimetry models recommended by the International Commission on Radiological Protection (ICRP) into updated versions of existing environmental pathway analysis models. Although GENII was developed for use at DOE's Hanford facility, it is said to be flexible enough to be applicable to a variety of generic sites. The name GENII originates from the fact that at

the time that the code was developed, it was considered to be a second generation environmental dosimetry computer code; hence, the name Generation II, or GENII.

GENII can be used to determine radiation doses to populations from both acute and chronic atmospheric releases, as well as releases that might emanate from a spill or a waste disposal site. The Gaussian plume model that is used is capable of addressing air transport in one of several manners including the use of an effective stack height and/or the calculation of plume rise from momentum or buoyancy effects. GENII is also versatile enough to incorporate building wake effects and seasonal effects in acute atmospheric release scenarios. More recently, a stochastic version of GENII was developed, GENII-S, as a combined product of Pacific Northwest National Laboratory and Sandia National Laboratories.

GXQ

GXQ is a PC-based model that uses a straight-line Gaussian plume model to calculate atmospheric dispersion coefficients for instantaneous and continuous atmospheric releases. The model was developed by Westinghouse safety analysts for use at DOE's Hanford facility to supplement the GENII downwind dispersion and radiological dose calculations. GXQ utilizes several subprograms that enable it to address plume meander, rise, depletion, building wake effects, and gravitational settling. The model is essentially a compilation of various aspects of several relevant industrial models. The primary strength of GXQ is its ability to address such a wide variety of sources, including nuclear

and non-nuclear releases. However, the model cannot be run independently and can only provide meaningful assessments when run in conjunction with GENII and other codes.

AIRISK

The AIRISK radiological assessment model was developed by Los Alamos National Laboratories to facilitate ground contamination and health consequence analyses related to possible Hanford high-level radioactive waste tank explosions. AIRISK models the atmospheric transport of radionuclides to determine doses downwind and the related acute and latent health effects. Because this DOE model was developed for use in the DOE complex, its radiological assessment capabilities are quite suited for accident scenarios that would be expected at DOE facilities. In addition to the DOE-specific nature of AIRISK, it is strong in that it can incorporate terrain effects into the model. However, for complex releases, the model may be limited because it can only address releases of up to forty radionuclides.

ERAD

Sandia National Laboratory developed the Explosive Release Atmospheric Dispersion (ERAD) model to provide near-real time assessments of localized radiological hazards that could be caused by explosions involving hazardous materials. ERAD models turbulent atmospheric transport and diffusion in three-dimensions. To characterize and model the emission of warm and other buoyant gases, ERAD utilizes an integral plume rise technique. A discrete time Lagrangian Monte Carlo method is used to model particle dispersion stochastically. Using the Monte Carlo approach enables a more realistic

treatment of spatially variant meteorological conditions, calm wind conditions, and buoyancy effects. Although Monte Carlo methods traditionally require substantial computing power, ERAD's three-dimensional simulation is relatively low because it relates each Monte Carlo particle to a small puff that spreads horizontally based upon Gaussian law. Although ERAD is user-friendly, because it can only address one radionuclide at a time, it can become cumbersome for complex releases involving multiple isotopes.

DOSEEP

DOSEEP, a Gaussian plume model, was developed by NOAA in the 1970s to predict centerline radiation exposures downwind from gaseous radionuclide emissions following underground nuclear weapons tests. The model was developed to address radionuclide gases that had migrated to the surface and into the atmosphere after several nuclear weapons had been detonated underground. This model was used along with PIKE, a gaseous and particulate venting model, to predict the exposure due to radionuclide gases and particulates following actual nuclear weapons tests. DOSEEP has been useful when addressing both unplanned releases and planned gaseous releases from underground nuclear weapons tests. Because these gaseous emissions typically migrate to the surface rather slowly, they generally reach the surface with no thermal buoyancy. Therefore, DOSEEP does not address buoyancy phenomena. DOSEEP is easy to use and requires only basic input to operate such as a source term, wind speed, and atmospheric stability. However, because of the general nature of the model, it cannot incorporate terrain effects,

does not have any deposition calculation capabilities, and only predicts centerline radiation exposures, likely overestimating them at great distances.

PIKE

PIKE is a 1960s NOAA analog model that estimates the quantity of gases and particulates energetically released into the atmosphere resulting from severe underground nuclear explosion venting. Because these releases occur within minutes of the detonations, both heat and pressure must be modeled as a part of the release process. As a result, as PIKE calculates fallout patterns and radiation exposure levels, buoyancy is considered along with standard meteorological phenomena. PIKE has also been designed to plot the predicted fallout patterns on map of the Nevada Test Site area and surrounding locales due to the abundance of underground nuclear weapon tests that have been conducted there. Strengths of the PIKE model include its simple input capabilities and its ability to incorporate readily available meteorological data. Weaknesses of the model include the fact that it is heavily based on a limited amount of historic data, local terrain is only marginally considered, and no scavenging, precipitation, or other dynamic meteorological effects are considered.

CATS

The Consequences Assessment Tool Set (CATS) was jointly developed in 1993 by the Defense Special Weapons Agency and the Federal Emergency Management Agency. This broadly applicable model predicts the consequences of natural, industrial, and technological catastrophic events. CATS' two operational modes, express and detailed,

enable both novice and expert analysts to predict the consequences of nuclear, biological, and chemical (NBC) events. Express mode operation uses prescribed terrorist or military explosion data along with current weather data. It enables the inexperienced user to input basic information and generate radiation intensity and concentration distributions. The detailed mode is much more flexible and allows the experienced user to vary the type of NBC material, explosive, and deployment mechanism. Moreover, complex environmental data can be incorporated into this mode, even multi-dimensional wind fields.

The primary purpose of the CATS model is to calculate and analyze consequences; therefore, its graphical display capabilities are minimal. However, because it operates within a graphical information system, it has robust graphical output capabilities. Because of the usefulness of the CATS model, it has been used in a variety of fora within the U.S., including the 1996 Summer Olympics in Atlanta, Georgia.

ARCON96

ARCON96 was developed jointly by the U.S. Nuclear Regulatory Commission (NRC) and the Pacific Northwest National Laboratory. This model has been used by the NRC to calculate radiation concentrations in nuclear power plant control rooms and in urban areas under accident conditions. For urban area calculations, ARCON96 uses meteorologically data averaged hourly to simulate both point and area source releases. However, questions exist regarding the accuracy of this model. One source of inaccuracy is the relative coarseness of hourly averaged data when evaluating urban dispersions.

Moreover, constant accident release rates and wind fields are assumed, which introduce further inaccuracies. The model was designed to address releases that traverse under 10 km from a release height of no more then 100 m.

BNLGPM

BNLGPM was developed by the DOE's Brookhaven National Laboratory to provide emergency response estimations of downwind particulate and gaseous radionuclide doses following an accidental emission from the onsite 60 MWt High Flux Beam Reactor (HFBR) stack. Because this model was developed for use at only one site, it is able to incorporate site-specific data, like the topography onsite and readings from the 100-meter tall emissions stack. BNLGPM uses local meteorological data along with user-input values, such as Pasquill-Gifford-Turner stability class. In addition, the model makes use of a steady state, straight-line Gaussian dispersion model. The BNLGPM model is fast, user friendly, and generally effective in calculating downwind doses from the HFBR; however, because the model was specifically developed for HFBR emissions, it is not readily applicable to other sites, emission mechanisms, or radionuclides.

GAUS1

GAUS1 is a Gaussian plume model that was developed by LANL to be run on a handheld graphical calculator. This model estimates radiological doses resulting from resuspension, wet and dry deposition, and complicated flow patterns, such as in building wakes. It also computes plume rise with buoyancy and momentum effects, and long range transport. Because of the calculator-based portability of GAUS1, it is especially

convenient during emergencies. The model has also been used to assess radiological risks at both LANL and Cape Canaveral. However, since the model is somewhat complicated, it is best suited for experienced users.

CAP88-PC

The Clean Air Act Assessment Package - 1988 (CAP88-PC) was developed in the late 1970's by the Environmental Protection Agency. The model was later finalized with assistance from Oak Ridge National Laboratory and DOE Headquarters. This model was designed to estimate average radionuclide dispersions from up to six sources by using a modified Gaussian plume equation. CAP88-PC originated as the rather limited AIRDOS model and was later expanded to address radionuclide emissions with the addition of the RADRISK and DARTAB components.

CAP88-PC is robust in its ability to address a broad variety of sources including elevated emission stacks and area sources. The model can use either a momentum-based or a buoyancy-based plume rise to determine airborne radionuclide concentrations and ground deposition rates within an 80 km radius of the emission location. However, the model does not address varying terrain heights, certain localized atmospheric phenomena, like building wake effects, and radionuclide decay during transport.

TRIAD

TRIAD was developed by NOAA in the late 1980's for use by the NRC and DOE to model the accidental dispersion of uranium hexafluoride (UF_6) gas into the atmosphere.

TRIAD is capable of modeling both reactive and non-reactive gases at distances less than 30 km. The model's Gaussian puff dispersion algorithm can calculate dry deposition rates while addressing multiple, non-stationary sources, and dispersions that traverse variable terrain elevations. However, the model is limited in that it assumes wind directions that are constant with height and that the puff is only transported by winds at the effective release height. Other limitations include the model's inability to treat large puffs that split into smaller puffs, chemical reactions, and complex terrains including building wakes and cavities.

TRAC RA/HA

This modification of the Terrain Responsive Atmospheric Code (TRAC) was specifically developed to focus on both risk assessments and hazard assessments (RA/HA) in complex terrain. The original TRAC model was developed in the mid 1980s to address the complex atmospheric flows associated with the Rocky Flats Environmental Technology Site (RFETS). Because of the complexity of the terrain, straight-line Gaussian plume models were not able to accurately characterize the atmospheric airflow. As a result, TRAC employed a three-dimensional Lagrangian model to address the complex atmospheric airflow. TRAC RA/HA uses the same type of Lagrangian model and has expanded it to include risk assessment and hazard assessment capabilities.

TRAC RA/HA has broad applications and is capable of modeling releases of plutonium, enriched and depleted uranium, fission products, and other non-reactive radiological particulates and gases. It is robust enough to consider the generation and decay of

radionuclides and their daughters within the plume, time-varying emission rates, wet and dry deposition, and gravitational settling. The model provides deposition and dose contours along with statistical summaries of each for distances up to 100 km. However, TRAC RA/HA is unable to address emissions originating from energetic releases and fires.

VENTSTAR XL

VENTSAR XL is a user-friendly dose assessment model developed and used at the Savannah River Technology Center Site to calculate short term atmospheric release doses. This straight-line Gaussian plume model is able to incorporate the effects of plume rise and buildings into its atmospheric dispersion calculations. The plume rise can be evaluated as a function of either buoyancy or momentum. The building effects that can be addressed include recirculation cavities, high turbulence zones, and wakes beyond the building. The model outputs doses that are calculated at various distances specified by the user. A key limitation of this model is that it does not incorporate the decay and generation of radionuclides within the plume.

RSAC-5

The Radiological Safety Analysis Computer Program (RSAC-5) was developed by the Idaho National Engineering and Environmental Laboratory (INEEL) and Lockheed Martin Idaho Technologies to calculate the both acute and chronic effects of airborne radionuclide releases. RSAC-5 uses a Gaussian plume diffusion model that can be used in combination with the Pasquill-Gifford and other auxiliary models. One special feature

of RSCA-5 is its ability to model fumigation conditions (stability Class F), the meteorological condition that results in the highest ground level concentrations following an elevated atmospheric emission.

This model has many strengths, including its ability to correct for plume rise, building wakes, and ground depletion during transport. In addition, the model is able to calculate radionuclide generation and decay during transport. A fission product library is incorporated into the model, and the user can modify the library, or import actinide and activation product libraries from other models if desired. Atmospheric radionuclide concentrations can be modified to simulate fractionation, processing, or filtration. The fractionation and other options can be evaluated in a simple manner (e.g., by calculating a percentage of the total radionuclide concentration), or using more complex approaches (e.g., as a function of the chemical group or element). Therefore, RSAC-5 is capable of evaluating complex emission and transport scenarios.

PUFF-PLUME

The PUFF-PLUME model was developed by Pacific Northwest Laboratory in the early 1970s and was later revised by the Savannah River Site approximately a decade later. This Gaussian atmospheric transport diffusion model can address puff and plume dispersions of both radionuclide and chemical emissions. The model uses real-time meteorological measurements and forecasts as it estimates wet deposition, dry deposition, and doses. PUFF-PLUME uses Pasquill horizontal diffusion parameters and Briggs vertical diffusion parameters which enable the model to address atmospheric turbulence

on a fundamental level. The model is also able to address radioactive decay during transport. Aside from the robustness of the model, its principal strengths are its simplicity and its speed of operation. However, the model is limited in that it is unable to model three dimensional wind fields, dense gas dispersions, or short duration atmospheric transport.

AXAIRQ

AXAIRQ was originally developed by the Nuclear Regulatory Commission in the early 1980s and was enhanced by the Savannah River Technology Center (SRTC) in 1995. The AXAIRQ model is used to assess doses from atmospheric radionuclide releases at SRTC. Although the atmospheric transport portion of this model is limited in that it is unable to address plume rise, the dose calculation features are robust in that it can calculate plume shine, ground shine, and inhalation doses. Population doses are automatically calculated out to a radius of 80 km and the position of maximum dose is noted. The user is also able to specify dose calculation distances outside of 80 km.

HARM-II

HARM-II was developed by the National Oceanic and Atmospheric Administration for use by the U.S. Department of Energy Oak Ridge Operations Office. This emergency management dose assessment model was designed to predict the effects of accidental radionuclide and chemical emissions within 50 km of the release location. One of the benefits of this model is that it is able to address particulate emissions, passive gas releases, and heavy gas releases. Therefore, it can model gaseous uranium hexafluoride

(UF_6) plumes. Another benefit of HARM-II is that it is able to accommodate time varying emission rates that can be input by the user, via a mathematical function, or using direct readings from an emissions stack. HARM-II uses a Gaussian model for particulate and passive gas emissions, and a Colenbrander-type dispersion algorithm for heavy gas emissions and modeling. The model is especially suited for uranium fuel cycle releases in that it incorporates the production of UO_2F_2 and HF by the reactions between UF_6 and water. Finally, the HARM-II meteorological modeling capabilities enable it to address radionuclide source depletion, dry deposition, and gravitational settling.

AXAOTHER XL

The Savannah River Site originally developed the AXAOTHER XL model to be run on an IBM mainframe in the early 1980s. It was later modified into its current PC-capable form in 1996. This model was designed to estimate doses following acute atmospheric radionuclide emissions during extreme wind conditions, specifically, during tornadoes or high-velocity straight line winds. Doses within an 80 km radius are calculated, as well as the maximum offsite dose. AXAOTHER XL uses its 500 radionuclide library and Gaussian plume dispersion modeling capabilities to automatically calculate radionuclide concentrations air within its straight-line wind calculations. However, for tornado condition calculations, radionuclide concentrations must be provided by the user. The chief limitation of AXAOTHER XL is that it does not calculate the generation and decay of radionuclides during transport.

SLAB

The SLAB dense gas dispersion model was first made public in 1985 by Lawrence Livermore National Laboratory. Although the model does not calculate source release rates, it is able to determine gaseous radionuclide transport from area sources, horizontal jets, and vertical jets. The model simplifies horizontal transport by assuming that all of the emitted radionuclides are uniformly affected by the prevailing winds; hence, the name, SLAB. However, in compensating for this simplification, the model incorporates thermodynamic effects, such as latent heat exchanges that result from the condensation or evaporation of liquids. SLAB's output includes the location of the maximum radionuclide concentration and the time required to reach the maximum concentration.

PAVAN

The PAVAN model was developed by the Pacific Northwest National Laboratory for use by the U.S. Nuclear Regulatory Commission as it estimates ground level concentrations downwind of accidental radionuclide releases from nuclear facilities into the atmosphere. The model can accommodate radionuclide releases from building vents as well as emission stacks, and calculates relative radionuclide air concentrations as a function of time and direction. Although PAVAN is unable to address multiple emission sources, it is able to model advanced plume dispersion processes such as those cause by building wakes. The PAVAN model is limited in that it cannot accommodate complex terrains and is not well suited for emergency response applications.

MACCS2

The MELCOR Accident Consequence Code System, version 2 (MACCS2) was developed by the Nuclear Regulatory Commission to model and perform consequence analyses of accidental radionuclide releases into the atmosphere. MELCOR, which provides the initial conditions for the MACCS2 code, simulates the progression of severe light water nuclear power reactor accidents. MACCS2 uses the output of the MELCOR to analyze the subsequent atmospheric transport, diffusion, and wet and dry deposition in time-dependent meteorological conditions.

MAACS2 is most effective when it is applied to nuclear reactors and other facilities that emit radionuclides from ground level. Moreover, it is comprehensive in that it incorporates emission, transport, environmental pathway, and dose models as it estimates the release effects of all radionuclides that may be generated during nuclear reactor accidents. The key weakness within the MACCS2 model is the fact that it uses a straight line Gaussian plume model for atmospheric transport and diffusion calculations.

Radionuclide Dispersion Source Term Models

KBERT

In 1995, the U.S. Department of Energy (DOE) released KBERT to analyze worker safety risks during accidents at DOE nuclear facilities. KBERT is most often used to during the risk estimation process inside a facility, but the model can also be used to predict that source term for radioactivity releases that escape the facility are enter the atmosphere. As with most accident and emergency response models, KBERT is easy to

use, runs fast, and is broadly applicable. However, weaknesses of the model include its need to have all flow rates defined, which may require data that is not available during accident conditions, and its inability to account for turbulence.

MELCOR

MELCOR was developed by Sandia National Laboratories for use by the Nuclear Regulatory Commission in the analysis of severe light water nuclear reactor accidents that result in core damage. MELCOR models the progression of a variety of severe accidents and can address several features including thermal hydraulic responses within the reactor coolant system, containment, and confinement buildings; the overheating and degradation of the reactor core; hydrogen and radionuclide generation, internal release, and transport within the system; and how safety features affect the system thermal hydraulics. Benefits of this model include its fast run time, and its ability to model sprays, multiple flow paths into control volumes, and two-phase flow. A chief weakness of this model is its inability to incorporate ventilation components into the system.

FIRAC

The FIRAC model was developed jointly by the Nuclear Regulatory Commission and the U.S. Department of Energy and is currently administered through Los Alamos National Laboratory. This model predicts fire-induced flows, thermal and material transport, and radioactive source terms within facilities. It is able to address facilities that do and do not have ventilation systems, so it is well suited to provide source term information for radiation releases that escape a facility and enter the atmosphere. FIRAC's fire modeling

capabilities inside buildings include an ability to compute fuel mass consumption rates and energy generation rates, fire growth and smoke transport, and generation rates and size distributions of radioactive particles made airborne because of the fire. FIRAC is a fast running, user friendly code that is able to address multiple flow paths and indoor aerosol transport problems. The model can be run on a personal computer and can generate both tabular and graphical outputs. However, diffusion, turbulence, and other multi-dimensional flow effects are not accurately addressed.

FIRAC/FIRIN

The FIRAC/FIRIN model was collaboratively developed by the NRC, LANL, PNNL, New Mexico State University, and Westinghouse. The model was originally developed in 1985 and was regularly updated during the 1990s. FIRAC/FIRIN is intended to predict measurable system parameters (i.e., pressures, temperatures, flow rates) in networked systems or spaces where radioactive materials are involved. It accomplishes this through submodels that address fire conditions, gas dynamics, material transport, and heat transfer.

It can model airflow in any enclosed area that would be encountered in the workspaces of a nuclear facility including, glove boxes, rooms, and ventilation systems. The airflow modeling capability enables radionuclides to be tracked as they traverse through various compartments. Therefore, the model is useful for calculating atmospheric emission source terms that could result from a nuclear accident. It is also useful for determining the rate at which radionuclide effluents are generated and their size distributions. So the

FIRAC/FIRIN model effectively predicts the accident condition source terms releasing radionuclides within a nuclear facility and releasing radionuclides from a nuclear facility.

The strengths of this model include its user friendliness, its ability to address all HVAC components within a facility ventilation system, and its ability to address complicated network configurations. Because of these strengths, FIRAC/FIRIN is used throughout the DOE complex. Even so, the model does have limitations. First, its approximations of spatial variations are quite general and provide few details. Next, the fire submodel is limited in that it can only model one fire at a time and no fire mitigation parameters are included. Finally, the ventilation systems are modeled only include unidirectional flows.

CONTAIN

CONTAIN was developed by Sandia National Laboratories for the NRC in 1995 to characterize the radiological, physical, and chemical conditions inside a nuclear power plant containment building after a severe primary coolant system accident. The model accomplishes these tasks through submodels that address ventilation systems, closed systems such as glove boxes and workspaces, radionuclide diffusion, turbulent transport, and spray phenomena. Through these calculations, CONTAIN is able to generate effective source terms for atmospheric dispersions that could result from these accident conditions. It is applicable to any number of commercial nuclear reactor and DOE facilities with and without ventilation systems. CONTAIN has many strengths. It is fast, versatile, and robust in its ability to address multiple flow paths, two phase flow, and

sprays. However, the model is limited in its inability to address spatial acceleration within momentum balance analyses.

Foreign Radionuclide Dispersion Models

COSMYA

Germany and the United Kingdom jointly led the development of the Code System from the Methods for Assessing the Radiological Impact of Accidents (COSYMA) model. Originally released in 1990, COSMYA is the European equivalent to the MACCS model. Like MACCS, COSYMA performs offsite consequence analyses of accidental radionuclide releases into the atmosphere. COSMYA can be used to model numerous radionuclides, but it cannot be used for modeling related to tritium.

The COSYMA model is a compilation of subprograms and data sets. Its three accident consequence subprograms are designed to be applied at various distances and time durations following the release. The Near Early subprogram is useful for localized calculations of both initial health effects and the influence of emergency response actions. Like the Near Early subprogram, the Near Late subprogram is applicable in the vicinity of the accident. However, the Near Late subprogram is different in that it evaluates delayed health effects and mitigating actions. The Far Late subprogram addresses delayed health effects and the influence of mitigating actions far from the accident site. COSYMA's five different atmospheric dispersion options include both Gaussian plume and Gaussian puff models. Even so, COSYMA has difficulty modeling radionuclide releases in regions of complex terrain.

UFOTRI

The German UFOTRI model was developed in 1991 for evaluating the consequences of accidental tritium releases from nuclear facilities. Because the model specializes in tritium releases, it is capable of treating addressing tritium as tritiated water vapor (HTO) and tritiated gas (HT). The UFOTRI model can be run in a deterministic manner by using one weather sequence, or for probabilistic assessments by processing up to approximately 150 sequences. UFOTRI and COSYMA can be used in conjunction with one another for a comprehensive assessment of accidental releases of all radionuclides, including tritium. Due to the effectiveness of the UFOTRI model, it is used as the reference model for tritium releases from the International Thermonuclear Experimental Reactor (ITER) facility.

PC-AQPAC

The Personal Computer-based Air Quality Package (PC-AQPAC) is a chemical and radiological consequences model originally developed by the Canadian Atmospheric Environment Service.

Although PC-AQPAC has been principally geared to characterize chemical accidents, because radioactive materials exist in the PC-AQPAC database, some limited radiological assessments are possible. PC-AQPAC incorporates both Gaussian plume and Gaussian puff models, can address both heavy and buoyant gases, and can be used in emergency response situations. However, the model is limited in that it uses straight-line plume calculations and cannot incorporate topographical effects.

ETMOD

The Environmental Tritium Model (ETMOD) was released by Ontario Hyrdo in Canada in 1991. The model can simulate several tritium-related phenomena including the atmospheric transport of tritiated water vapor (HTO) and tritiated gas (HT) and ground deposition of HT. ETMOD is also able to incorporate plume deposition depletion and the generation of HTO from HT oxidation within the plume within its analyses. Like its German counterpart, UFOTRI, ETMOD is only capable of analyzing tritium releases. ETMOD is known as a user-friendly model that provides generous amounts of output data.

Meteorological Dispersion Models

HYSPLIT

In 1982, the Hybrid Single-Particle Lagrangian Integrated Trajectory (HYSPLIT) was developed by NOAA as a coarse atmospheric dispersion model. Today, HYSPLIT is much more advanced and is able to simulate a wide range of long range gaseous and particulate transport scenarios. The current version of the model is extremely robust in its capabilities and is useful for emergency response, routine atmospheric dispersion and air quality assessments, and forecasting. HYSPLIT simulates transport and dispersion by integrating puff and particle dispersion model techniques. The principal strength of HYSPLIT is its versatility; however, it tends to be less accurate when modeling transport at distances less than 300 m.

OMEGA

The OMEGA atmospheric dispersion model, developed by the Science Applications International Corporation, became operational in 1995. This dispersion model also has the capability to serve as a weather prediction model. OMEGA is an extremely robust model and can track the dispersion of atmospheric pollutants through both Eulerian and Lagrangian operational modes. The model is functional in complex terrains and in situations where only a limited amount of data is available. Moreover, OMEGA can be operated in either a forecast mode or in a mode that facilitates the investigation of historical meteorological activities. OMEGA can be coupled with several databases that have supplemental data (e.g., land/water fractions, soil type, land use, etc.), and the model can operate at resolutions down to 1 km. Due to the functionality of this model, it has been used worldwide to support military, environmental, and homeland security activities.

INPUFF

The Integrated Puff (INPUFF) meteorological model was developed by the Environmental Protection Agency in the late 1980s to facilitate atmospheric dispersion modeling associated with incineration ships. This model is useful for simulating both short and long duration point source releases in variable winds. Because INPUFF was developed to analyze ship-based releases, it is able to accommodate moving emission sources. One of INPUFF's greatest strengths is its ability to model time dependent release rates. However, the model is unable to address dense gas dispersions or buoyant releases.

RAPTAD

The Random Puff Transport and Diffusion (RAPTAD) model was developed in the 1980's by Los Alamos National Laboratory and the YSA Corporation. This model is a Lagrangian random puff model that can be used to predict the diffusion and transport of airborne pollutants over complex terrains. A key advantage of the random puff model is the speed and accuracy of the computations. The type of puff model requires much fewer puffs (1% - 10%) to be released than similar particle methods. RAPTAD is frequently used with the HOTMAC model to predict the transport of pollutants over complex terrains in situations where other models are less reliable. When RAPTAD and HOTMAC are used in conjunction with one another, they are able to model mesoscale meteorological activities and time-dependent transport and diffusion in the midst of three-dimensional winds.

CTDMPLUS

The Complex Terrain Dispersion Model Plus Algorithms for Unstable Situations (CTDMPLUS) was developed by the Environmental Protection Agency in the late 1980's to serve as a refined air quality model that can accommodate the full range of atmospheric stability conditions and complex terrains. CTDMPLUS models the plume trajectory at regularly scheduled, prespecified time intervals. The output of the interval computations incorporates the terrain and deforms the airborne plume accordingly. The principal weakness of this model is its inability to address dense gas plume dispersions.

Chapter II: ITEMIZED PROCEDURE

1. Initial Condition -- Obtain Anomalous Radionuclide Measurement

(Note 1: An anomaly only needs to be evident in one feature of the radionuclide measurement. Therefore, no insight into the cause of the anomaly -- be it the presence of atypical radionuclides, issues related to the collection or detection system, or another catalyst -- is necessary in order to assess that a measurement is anomalous.)

(Note 2: Although several radionuclide measurements may be initially obtained that appear to be associated with the same event, only one is necessary as an initial condition. The others can be incorporated in section 4.1.3 during the Environmental Characterization.)

2. Evaluate Accuracy of Measurement, Highlight Anomalies, and Make Superficial Corrections as Needed

2.1 Assess directly measurable initial data relevant to aggregate data quantification

2.1.1. Note sampling time

2.1.2. Note decay time

2.1.3. Note counting time

2.1.4 Note total volume of air sampled

2.1.5. Note all emission lines identified

2.1.5.1. Evaluate accuracy of peak curve fits

2.1.5.1.1. Note FWHMs

2.1.5.1.2. Ensure that peak areas > Net Peak Detection Threshold (PDT_n, see Appendix 5)

2.1.5.1.3. Verify that peak areas of overlapping peaks (multiplets) are accurately fit

2.1.5.2. Evaluate accuracy of baseline continuum fit

2.1.5.2.1. Closely evaluate step functions and other baseline features

2.1.5.2.2. Verify that baseline of overlapping peaks (multiplets) are accurately fit

2.1.6. Note radionuclide identifications based upon emission lines

2.1.6.1. Note customary emission lines with no apparent radionuclide association discrepancies

2.1.6.2. Note emission lines with multiple radionuclide identifications

2.1.6.3. Note emission lines with no radionuclide identifications

2.1.6.4. Note apparent patterns or anomalies regarding radionuclide identifications (i.e., all isotopes of same element, set of radionuclides identified obviously incomplete, etc.)

2.2. Assess derived data relevant to radionuclide identification and quantification

2.2.1. Determine flow rate from sampling time and total volume

2.2.2. Verify soundness of automated calibrations

2.2.2.1. Observe energy vs. channel calibration

2.2.2.2. Observe efficiency vs. energy calibration

2.2.2.3. Observe resolution vs. energy calibration

2.2.3. Identify complete and accurate set of radionuclides present based upon emission lines identified

2.2.3.1. Evaluate relative radionuclide abundance of emission lines associated with radionuclides identified

2.2.3.2. Note whether relative abundances are significantly different than expected, and if so, check for single line emitters and other possible obscurants

2.2.3.3. Hypothesize radionuclide associations with all true emission lines identified but not associated with radionuclides

(Note: Hypotheses should be based strictly upon energies of gamma-ray emissions identified. Physical, environmental, and other factor should not be considered at this stage.)

2.2.3.4. Determine whether key line peak areas or the relative average areas of all of peaks associated with each radionuclide (average line peak areas) should be used to calculate radionuclide concentrations

2.2.4. Determine accuracy of radionuclide concentration calculations

2.2.4.1. Verify radionuclide concentrations and supporting calculations

2.2.4.2. Note influence of radionuclides likely present but not identified based upon step 2.2.3.2 and 2.2.3.3)

2.2.5. Determine parent and progeny radionuclides possibly present based upon radionuclides identified

2.2.5.1. Determine whether half-lives of parents and progeny are appropriate for detection

2.2.5.2. Determine whether concentrations of radionuclides identified correspond to detectable quantities of parents and progeny

2.2.6. Perform preliminary analysis

2.2.6.1 Perform preliminary classification of the types of radionuclides identified

2.2.6.2 Evaluate and correlate directly measurable and derived data to determine whether the quantities are within reason

3. Incorporate Data about Collection and Measurement Mechanisms and Procedures into Analysis

3.1. Incorporate details regarding type of radionuclide sampler used

3.1.1. Incorporate details regarding specific collection mechanism

3.1.1.1. Note specific processes regarding radionuclide collection

3.1.1.1.1 Note whether cooling is required for collection

3.1.1.1.2 Note whether active or passive collection occurs

3.1.1.1.3 Note whether high volume or low volume collection occurs

3.1.1.1.4 Note whether discontinuous or continuous collection occurs

3.1.1.2. Note and investigate any data or hardware that indicates malfunction

3.1.1.2.1 Pay close attention to output related to electrical and mechanical systems associated with collection mechanism

3.1.1.2.2. If malfunction apparent, estimate effects of malfunction on collection processes and data

3.1.1.2.3 If total air volume (step 2.1.4), flow rate (step 2.2.1), or other relevant data show statistically significant inconsistencies, investigate potential causes for inconsistencies

3.1.1.2.4. If data or hardware anomalies are present, compare potential hardware malfunction effects (step 3.1.2.2.2) and data inconsistency catalysts (step 3.1.2.2.3) with reality

3.1.2. Note physical state of radionuclides collected (gas vs. particulate)

3.1.2.1. Verify that all radionuclides identified are consistent with physical state of radionuclides being collected

3.1.2.2. As follow-up to step 2.2.3.3 and step 2.2.5, limit list of parents and progeny likely collected based upon physical state

3.2 Incorporate information regarding surroundings and type of radionuclide detection and analysis

3.2.1. Determine whether internal or external background impairs meaningful data acquisition

(Note: Internal background is largely the result of detector contamination. External background is generally the result of radiation sources in the vicinity.)

3.2.2. Incorporate details regarding specific detection and analysis mechanisms

3.2.2.1. Note specific processes involved in detection and analysis

3.2.2.1.1 Note whether cooling is required for proper detection

3.2.2.1.2 Note whether sample and system isolation are required for proper detection

3.2.2.1.3 Note level of automation of analysis

3.2.2.2 Note and investigate any data or hardware that indicates malfunction

3.2.2.2.1 Pay close attention to output related to electrical, mechanical, and software systems associated with detection and analysis mechanisms

3.2.2.2.2. If malfunction apparent, estimate effects of malfunction on detection and analysis processes and data

3.2.2.2.3. If data, hardware, or software anomalies are present, compare potential malfunction effects (step 3.2.2.2.2) with reality

3.2.3. Determine whether decay time is too long for meaningful data acquisition

3.2.3.1. Determine minimum half-life detectable based upon decay time

3.2.3.2. Verify that radionuclides identified meet half-life threshold for detection

3.2.3.3. As follow up to step 3.1.1.2, determine which radionuclides likely not detected due to limited half-lives and which radionuclides should have been detectable if present

4. Characterize Environment

4.1. Identify other sensors in the region

4.1.1. Identify sensors within geographic vicinity of detection sensor

4.1.1.1. Identify all types of facilities where sensors may be present

4.1.1.1.1. Determine whether sensor data is available for external observation/analysis

4.1.1.1.2. Determine type of data collected with sensors (e.g., radionuclide data, integrated activity, etc.)

4.1.1.1.3. Gather sensor data

4.1.1.1.3.1 Follow steps 2 (Evaluate Accuracy of Measurement, Highlight Anomalies, and Make Superficial Corrections as Needed) and 3 (Incorporate Data about Collection and Measurement Mechanisms and Procedures into Analysis) as closely as possible for each sensor

4.1.1.1.3.2. Evaluate veracity of original sensor detection in light of other sensors in vicinity

4.1.1.1.3.3. Cross reference data from other sensors to determine veracity of sensor detections in vicinity

4.1.1.2. Identify all stand-alone sensors

4.1.1.2.1. - 4.1.1.2.3.3. Follow steps 4.1.1.1.1 - 4.1.1.1.3.3

4.1.2. Identify sensors within continuous similar terrain as terrain of detection sensor

4.1.2.1. - 4.1.2.2.3.3. Follow steps 4.1.1.1 - 4.1.1.1.3.3

4.1.3. Identify sensors that indicate detections that may be relevant to detection at detection sensor

4.1.3.1. - 4.1.3.2.3.3. Follow steps 4.1.1.1 - 4.1.1.1.3.3

4.1.4. For all sensors identified where data is available, gather data for time periods preceding and following time period when original detection was noted

4.2. Characterize natural environment

4.2.1. Characterize terrain

4.2.1.1. Identify type of land in vicinity of detection sensor based upon regions identified in steps 4.1.1, 4.1.2, and 4.1.3

4.2.1.2. Identify bodies of water in vicinity of detection sensor

4.2.1.2.1. Identify size of water body

4.2.1.2.2. Identify customary motion/activity level of water body

4.2.1.2.3. Estimate effects of water body on surrounding environment (sea breeze, directionally consistent prevailing winds, etc.)

4.2.1.3. Determine layout of terrain

4.2.1.3.1. Develop general description of terrain(s) in vicinity of detection sensor

4.2.1.3.2. Determine various altitudes of ground levels in vicinity

4.2.1.3.3. Identify and characterize impediments to airflow

4.2.1.3.3.1. Identify impediment heights

4.2.1.3.3.2. Characterize impediment density

4.2.1.3.3.3. Characterize seasonal features of impediments (trees vs. buildings, etc.)

4.2.2. Characterize meteorology to fullest extent possible

4.2.2.1. Identify fundamental meteorological parameters in vicinity during time period preceding and following sensor detection

4.2.2.1.1. Identify geospatial and chronological temperature distributions on earth surface and at various altitudes in atmosphere

4.2.2.1.2. Identify geospatial and chronological distributions of wind speeds and directions on earth surface and at various altitudes in atmosphere

4.2.2.1.3. Identify geospatial and chronological distributions of barometric pressure

4.2.2.1.4. Identify geospatial and chronological distributions of humidity

4.2.2.1.5. Identify general weather conditions in sensor detection and surrounding areas

4.2.2.2. Identify vertical temperature of troposphere

4.2.2.2.1. Estimate lapse rate

4.2.2.2.2. Estimate lapse rate trend from preceding time periods

4.3. Draw preliminary conclusions based upon environmental determinations

4.3.1. Codify list of radionuclides likely present at detection site based upon step 3.2.3.2 and 3.2.3.3

4.3.2. Determine whether any chronological correlations can be determined

4.3.3. Based upon radionuclide concentration distributions in region, estimate likelihood of various source regions in manner similar to source-receptor method (from very likely to very unlikely)

4.3.3.1. Further clarify likelihood of source regions based upon radionuclide source emission requirements

4.3.3.2. Especially in case when minimal number of sensors detect radionuclides, further clarify likelihood of source regions by incorporating chronological factors (e.g.,

peak spreading over time and distance causes radionuclide sensor to be exposed to plume for longer period of time, required time of emission, required time of plume transport, etc.)

4.4. Identify potential radionuclide emission sources

4.4.1. Consider all radionuclide emission sources in vicinity

4.4.1.1. Identify radionuclide emission sources in geographic vicinity as detection sensor

4.4.1.2. Identify radionuclide emission sources in similar terrain as detection sensor

4.4.1.3. Remember to consider that certain radionuclide emission sources are portable

4.4.2. Consider all radionuclide emission sources in most likely regions from step 4.3.3

4.4.2.1. If too few sources are identified in this region, consider radionuclide sources in less likely regions

4.4.2.2. If too many sources are identified, narrow the list by incorporating radionuclide source emission requirements from step 4.3.3.1 and possibly chronological requirements from step 4.3.3.2

4.4.2.3. Remember to consider that certain radionuclide emission sources are portable

5. Characterize Possible Sources

5.1. Reference radionuclides and categories noted in step 4.3.1, step 2.1.6.4, and step 2.2.6

5.2. Given consolidated list, reevaluate to determine whether any trends are apparent in radionuclide categories

5.3. Determine types of radionuclide emission sources that could have emitted radionuclide categories and half-lives

5.4. Eliminate all emission sources from step 4.4 that do not fit categories identified in step 5.3

5.4.1. Remember to include portable sources from steps 4.4.1.3 and 4.4.2.3

5.4.2. If possible, use radionuclide ratios to further refine list of possible candidate sources

5.5. Develop preliminary rank for each emission source identified in step 5.4 based upon estimated likelihood that emission source was source of detection

5.5.1. Consider reasonableness of source emission requirements identified in step 4.3.3.1

5.5.2. Consider reasonableness of chronological factors identified in step 4.3.3.2

5.5.3. Consider reasonableness of types of radionuclide emission sources as they relate to radionuclide categories identified in step 5.3

6. Develop Characterizations of Possible Sources

6.1. Investigate historical releases from each radionuclide source (empirical)

6.1.1. Characterize customary releases

6.1.1.1. Characterize radionuclide emissions

6.1.1.1.1. Identify radionuclides released

6.1.1.1.2. Identify radionuclide quantities released

6.1.1.1.2.1. Determine average quantities released

6.1.1.1.2.2. Determine maximum and minimum quantities released

6.1.1.1.3. Characterize chronological factors

6.1.1.1.3.1. Characterize radionuclide generation rates in order to generate quantity of radionuclides released during customary emissions

6.1.1.1.3.2 Characterize any residence time between radionuclide generation and emission

6.1.1.1.3.3. Characterize radionuclide emission rates and durations

6.1.1.2. Identify frequency of customary releases

6.1.2. Characterize anomalous releases

6.1.2.1. Identify frequency of anomalous events

6.1.2.1.1. Identify frequency of anomalous events that led to release

6.1.2.1.2. Identify frequency of similar anomalous events that did not lead to release

6.1.2.1.3. Distinguish between process paths that led to releases and paths that did not

6.1.2.2. Characterize radionuclide emissions

6.1.2.2.1. Identify radionuclides released

6.1.2.2.2. Identify radionuclide quantities released

6.1.2.2.3. Characterize chronological factors

6.1.2.2.3.1. Characterize radionuclide generation rates in order to generate quantity of radionuclides released during emissions

6.1.2.2.3.2 Characterize any residence time between radionuclide generation and emission

6.1.2.2.3.3. Characterize radionuclide emission rates and durations

6.1.2.3. Identify processes that led to release

6.1.2.3.1. Determine likelihood of reoccurrence

6.1.2.3.1.1. Determine whether mitigation mechanisms have been incorporated since anomalous event

6.1.2.3.1.2. Determine need for human intervention in mitigation process

6.1.2.3.2. Determine whether any alternate sequences of events could have generated same or similar release

6.2. Identify processes involved in each radionuclide emission source that may contribute to release mechanism (theoretical)

6.2.1. Identify mechanical processes

6.2.1.1. Determine likelihood of processes leading to release

6.2.1.2. Determine radionuclides that would be released given specific processes

6.2.2. Identify processes requiring human involvement

6.3. Identify physical parameters relevant to emission

6.3.1. Characterize boundary conditions at emission-atmosphere interface

6.3.1.1. Identify stack height

6.3.1.2. Identify cross-sectional area of emission

6.3.1.2.1. Identify whether individual or multiple release points are necessary

6.3.1.2.2. If multiple release points are necessary, identify whether releases can be considered as one collective release or as multiple releases

6.3.2. Note effluent temperature

6.3.2.1. Note whether effluent temperature is above or below ambient air temperature (from step 4.2.2.1.1)

6.3.2.2. Note whether effluent temperature is consistent cross-sectionally and over time

6.3.3. Note humidity of emission

6.3.4. Note total volume of emission

6.3.5. Note average density of emission

6.3.6. Note momentum/internal energy of emission

6.3.7. Note duration of emission

6.3.8. Note any directionality of emission

6.4. Estimate physical, chemical, and nuclear properties relevant to emission

6.4.1. Estimate physical state of emission

6.4.2. Estimate full chemical constituency of emission

6.4.3. Estimate activity and radionuclides associated with emissions

6.5. Incorporate related data

6.5.1. Review current and historical news reports

6.5.2. Acquire additional relevant historical and contextual data

6.5.3. Analyze possible release, transport, and detection scenarios using various established computerized models

7. Use Source Characterizations and Natural Environmental Data to Estimate Chains of Events from Most Likely Sources based upon Step 3, Step 6, and Step 4

7.1. Use emission precursor actions (from step 6.2) as initial conditions for each likely radionuclide emission source

7.2. Estimate emission parameters and their effects for each likely radionuclide emission source

7.2.1. Start with determinations from steps 6.3 and 6.4

7.2.2. Narrow range of possible parameters by considering likelihood of various combinations of parameters

7.2.3. Estimate effects

7.2.3.1. Estimate particle size distribution of emission

7.2.3.2. Estimate average and maximum initial height of plume rise

7.2.4. Summarize chronology of emission

7.3. Estimate transport parameters and their effects for each likely radionuclide emission source

(Note: This section is likely to be accomplished through established models.)

7.3.1. Start with natural environmental determinations from step 4.2

7.3.2. Narrow range of possible parameters by considering likelihood of various combinations of parameters

7.3.3. Estimate average and maximum height of plume rise

7.3.4. Estimate plume appearance and structure

7.3.5. Estimate radionuclide generation and decay during transport

7.3.6. Estimate chemical and physical transformations that occur during transport

7.3.7. Estimate effects

7.3.7.1. Estimate wet and dry depositions and deposition rates

7.3.7.2. Estimate downwind concentration contours

7.3.8. Summarize chronology of transport

7.4. Estimate collection and data acquisition parameters

7.4.1. Start with data about measurement mechanisms from step 3 and collected radionuclide data from step 4.1.4

7.4.2. Compare radionuclides likely detectable from transport calculations in step 7.3 with radionuclides identified at sensor locations

7.4.3. If possible, calculate radionuclide ratios that should be detectable based upon transport parameters their effects in step 7.3 and collection mechanisms in step 7.4.1

7.4.4. Summarize chronology of collection and data acquisition

8. Use Estimated Chains of Events to Determine Most Likely Radionuclide Emission Source

8.1. Rank possible radionuclide emission sources based upon reasonableness of chain of events

8.2. Select highest ranking radionuclide emission source as most likely source of detection at sensor location

8.3. Develop possible explanations for data, aspects of sequence of events, and additional factors that appear to be inconsistent with overall analysis

9. Recreate Most Likely Chain of Events

9.1. Characterize most likely release source and mechanism

9.1.1. Identify most likely source location

9.1.2. Identify most likely radionuclide emission source (facility/portable)

9.1.3. Identify most likely release mechanism

9.1.4. Identify most likely chronology of emission (duration, etc.)

9.2. Characterize radionuclide transport

9.2.1. Identify initial conditions of emission once release enters atmosphere

9.2.2. Characterize prevailing meteorological influences

9.2.3. Characterize dominant terrestrial factors

9.2.4. Determine chronology of transport

9.2.5. Identity plume spread during transport

9.2.6. Identify chemical/nuclear transformations that occur during transport

9.2.7. Characterize plume deposition/depletion during transport

9.3. Characterize radionuclide collection/data acquisition mechanism at source detection location

9.3.1. Identify relevant parameters of detection sensor

9.3.2. Verify relevant parameters of acquisition mechanism

9.3.3. Verify correlation between radionuclides detected and radionuclides identified as present

9.3.4. Explain why some radionuclides identified as present were not detected

9.4. Identify and address any additional information relevant to sequence of events

Chapter III: CASE STUDY 1 -- SITE CHARACTERIZATION

Highlights

Section 1, Initial Condition: The initial condition was the detection of several anomalous gamma-ray peaks that could not be associated by the automated processing system measured at a radionuclide detection facility in Vancouver, British Columbia, Canada.

Section 2, Validate and Superficially Correct Data: The measurements were validated as sound. A model novelty revealed in this section is the introduction of seven candidate radionuclides as the sources for the atypical peaks measured. Moreover, a rationale for the presence of these radionuclides was identified. The computational model used identified the presence of these radionuclides as impossible. Moreover, because the varying senior scientists used differing analytical processes that were not comprehensive, they all arrived at incorrect conclusions.

Section 3, Validate Hardware and Software Operation: All hardware and software systems appeared to operate properly. A novelty of this model was revealed in this section through the estimation of minimum detectable half-lives. Although the estimation was rough (± 26%), no other model was able to perform such an estimation.

Section 4, Characterize Environment: The low density of radionuclide detectors and possible emission sources in the detection region reduced the utility of the meteorological and other portions of this section. Even so, this section highlighted a novelty in that it revealed critical qualitative data that proved to be instrumental to thoroughly

characterizing the radionuclide detection site. Moreover, because of the incorporation of qualitative data, a likely source region was identified in this section when none of the computer models queried were able to generate solutions because of the incomplete data available.

Section 5, Characterize Possible Sources: Three possible emission sources were identified, one of which, the Vancouver International Airport is a nontraditional radionuclide emission location. The incorporation of nontraditional source locations is an additional benefit of this model. Moreover, this section also isolates the likely radionuclide emission source that caused the anomalous detections, which served as the initial condition. Making this determination based on such a limited amount of measured quantitative data is possible because of the incorporation of human judgment into the analytical process.

Section 6, Develop Characterizations of Possible Sources: This section revealed the most important output based upon the human judgment novelty. This section specifically identified the radionuclide emission source facility, which was based largely upon qualitative data. No existing model was able to output the emission source with specificity. In addition, this section demonstrates that this model is the only one that was able to thoroughly characterize the detection site. While only seven radionuclides were identified and believe to exist prior to analysis with this model, this model revealed the presence of 50 radionuclides and the reasons why the 43 undetected radionuclides were not identified through the spectral processing system.

Section 7, Estimate Likely Chain of Events: This section codifies the factors governing the generation, emission, transport, collection, and detection of the radionuclides identified. In addition, this section highlights the characterization of the detection site. Neither of these outputs is possible with existing models.

Section 8, Determine Most Likely Emission Source: This section was combined into section 7 since only one source was identified as likely.

Section 9, Recreate Most Likely Chain of Events: This section was combined into section 7 since only one source was identified as likely.

1. Initial Condition -- Obtain Radionuclide Data Measurement

The initial condition for this case study occurred from March 14 through March 23, 1997 when several anomalous gamma-ray peaks were measured in addition to the peaks customarily present within spectra at the CA002 monitoring station located on the campus of the University of British Columbia in Vancouver, British Columbia, Canada. The increase in the total number of gamma-ray peaks identified was over 50%. Table 24 lists all of the peaks that were identified during the period in question. In addition, the table contrasts the gamma-rays generally present in CA002 spectra with the atypical peaks that serve as the initial conditions for this case study. Figure 18 contrasts the typical and atypical spectra graphically by overlaying a representative region of each.

Finally, Table 25 lists the automated peak areas in counts for some of the more notable atypical peaks.

Table 24: Gamma-Rays Present in CA002 Spectra

Generally Present Peaks	**Atypical Peaks**
Energy (keV)	Energy (keV)
74.79	
77.07	
87.16	
89.88	
115.17	
159.02	
238.64	
252.56	
	270.04
277.33	
	287.04
287.99	
295.22	
300.14	
	311.60
327.92	

	338.41
351.93	
	374.74
415.22	
	440.01
452.97	
477.58	
	505.39
510.76	
	516.24
	522.46
	538.51
	545.07
569.73	
583.16	
609.3	
	670.28
	687.83
727.27	
	742.67
763.29	
	781.79
785.49	

	790.36
	803.29
	807.32
	820.11
860.49	
	881.05
	883.97
893.43	
	899.16
911.13	
916.95	
	918.01
969.12	
	983.91
	992.33
	1016.20
	1032.54
	1078.34
1078.74	
1093.64	
1238.42	
1368.45	
1460.74	

1512.67	
1592.24	
1620.6	
1718.78	
1764.52	
2103.36	

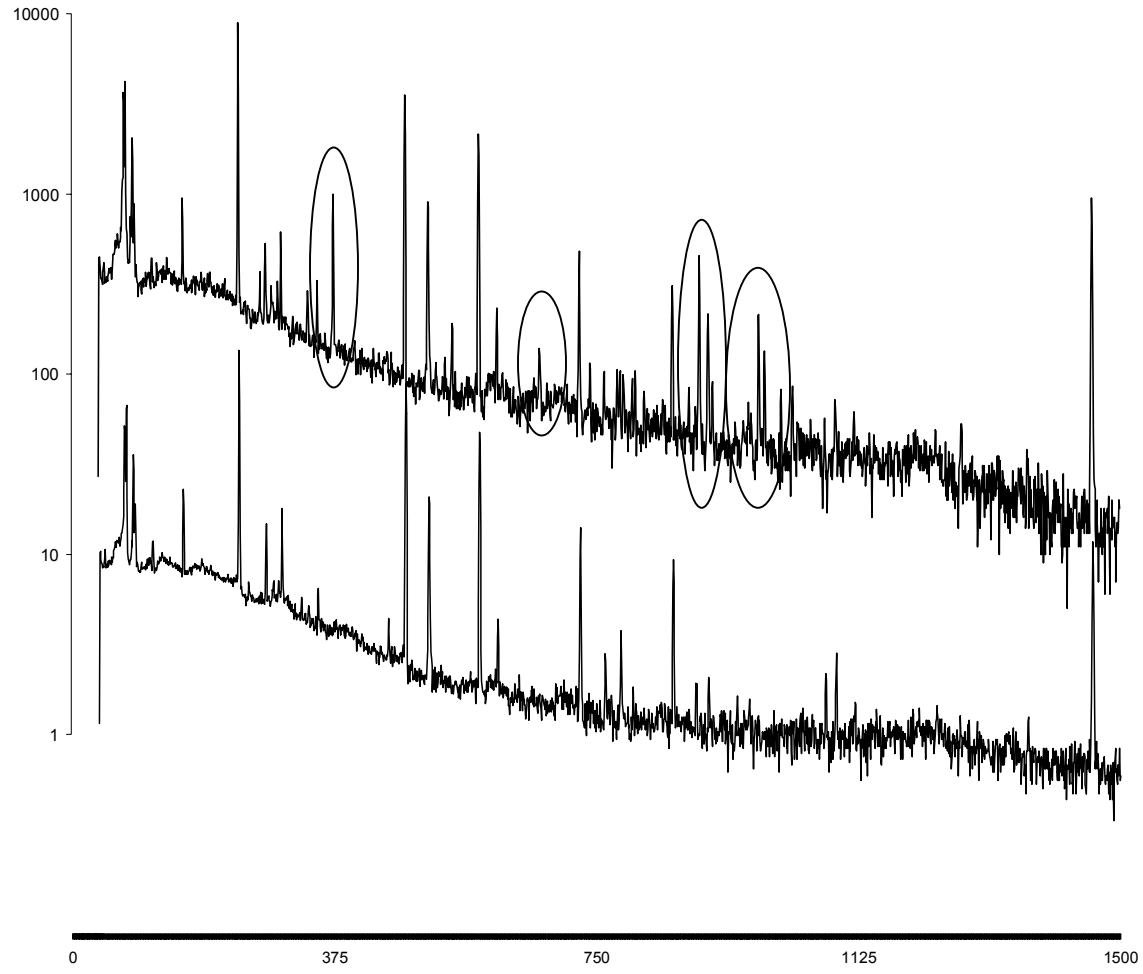

Figure 18: Overlay of Representative Regions of Typical and Atypical CA002 Spectra

Table 25: Peak Areas for Most Notable Atypical Peaks

Date	**Automated Peak Energy (keV) / Peak Area (Counts)**					
	545	**803**	**884**	**899**	**992**	**1032**
14 March 2004						
15 March 2004	270.94			921.77	277.76	236.46
16 March 2004						
17 March 2004		199.60		789.10	243.15	347.62
18 March 2004	181.61			320.35	81.40	
19 March 2004	278.08	90.85	77.65	1090.66	225.27	144.62
20 March 2004				280.66		71.45
21 March 2004				326.72	71.58	
22 March 2004	214.05			841.17	509.43	296.76
23 March 2004						

2. Evaluate Accuracy of Measurement, Highlight Anomalies, and Make Superficial Corrections as Needed

Assess Directly Measurable Initial Data Relevant to Aggregate Data Quantification

Note sampling time, decay time, counting time, and total volume of air sampled

Because these gamma-ray measurements are intended for scientific analysis, they are accompanied by a wealth of fundamental, directly measurable data including sampling time, decay time, counting time, and volume of air sampled. Historical station data indicate that the operational goals for these values are 24 hours, 4.25 hours, and 19.5 hours, for the respective chronological measurements. Because of the dependence of air volume on sampling time, no real operational goals for air volume exist. The actual values measured are shown in Table 26. Table 26 also lists equivalent data in italics for the days preceding and following the period in questions for comparative purposes. Obvious anomalies (deviations greater that 10% from operational goals) are highlighted with asterisks (*).

Table 26: Fundamental Data Directly Measurable

Date	**Sampling Time (h)**	**Decay Time (h)**	**Counting Time (h)**	**Air Volume (m^3)**
11 March 2004	*46.07**	*4.47*	*19.5*	*49005*
12 March 2004	*24.05*	*4.42*	*19.5*	*23965*
13 March 2004	*24.94*	*4.28*	*19.5*	*24412*
14 March 2004	24.17	4.26	19.5	23689
15 March 2004	24.95	4.23	19.5	24461

16 March 2004	23.83	4.25	19.5	21661
17 March 2004	24.16	4.27	19.5	23572
18 March 2004	23.78	4.24	18.21	22735
19 March 2004	22.42	4.26	19.5	21336
20 March 2004	28.28*	4.24	17.23*	16909
21 March 2004	21.48*	4.25	18	20936
22 March 2004	22.26	4.24	19.5	21683
23 March 2004	25.96	4.26	18.38	25277
24 March 2004	*22.64*	*4.26*	*19.50*	*22103*
25 March 2004	*24.57*	*4.26*	*19.50*	*23758*
26 March 2004	*24.20*	*4.26*	*17.89*	*23261*

Although the overwhelming majority (3 out of 4) anomalies listed in Table 26 occur during the period in question, the anomalies are too infrequent to be directly linked to the anomalous gamma-rays measurements during the period.

Note all emission lines identified and radionuclide identifications based upon emission lines

Upon reviewing the spectral emission lines identified, all of the questionable peaks look similar in size, shape, baseline, and full width at half maximum (FWHM) to the peaks customarily present. A representative spectrum is shown in Figure 19. The complete set of spectra for the time period in question is shown graphically in Appendix A.

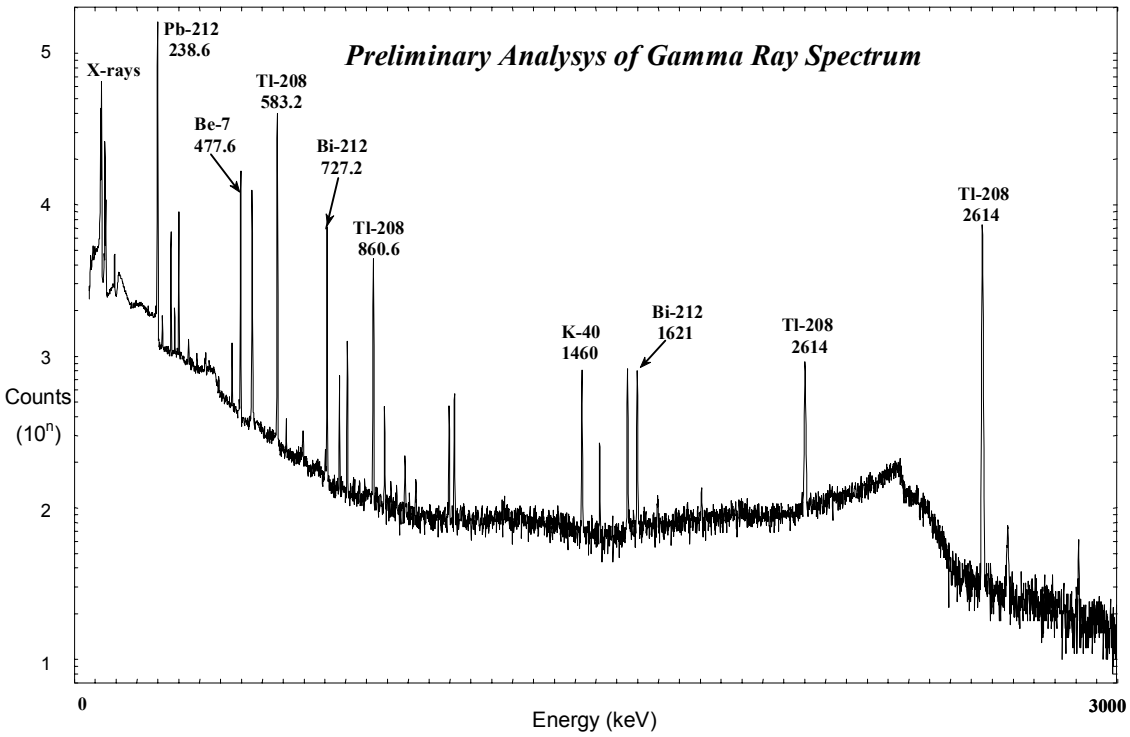

Figure 19: Typical CA002 Spectrum with Key Radionuclide Associations Identified

Figure 19 also highlights key radionuclides associated with the peaks customarily present. The actual radionuclides associated with the peaks identified by the automated spectral processing system are shown in the Peak Search Results section of the Atmospheric Radionuclide Measurement Reports (ARMRs) in Appendix B. The percentage of unassociated peaks is substantial, generally over 20%, for these spectra. Of course, the unusually high percentage of unassociated peaks was the anomaly that originally drew these spectra into question. A representative sample of typical CA002 spectra, with unassociated peak percentages ranging between 3% and 12%, are shown in ARMRs included within Appendix 3. In addition to the increase in percentage of unassociated peaks for the spectra during the period in question, there was also an increase in the number of peaks that had multiple radionuclide associations. While the

value was marginally over 2 during the baseline periods, it jumped to 3.5 during the period in question.

Assess Derived Data relevant to Radionuclide Identification and Quantification

Determine flow rate from sampling time and total volume

The collection flow rate is the easiest property that can be derived from the directly measurable data. The flow rate is determined by dividing the total sampling volume by the total collection time. Therefore, it serves as a normalizing property that can be used to evaluate the state-of-heath of the collection process. Flow rate values for the period in question are listed in Table 27. As in Table 26, these values are preceded and followed by baseline values in italics for context. Anomalous values, those differing by more than 10% from the customary flow rate of 975 m^3/h, are identified with an asterisk (*).

Table 27: CA002 Flow Rates

Date	**Collection Flow Rate (m^3/h)**
11 March 2004	*1063.71*
12 March 2004	*996.45*
13 March 2004	*978.83*
14 March 2004	980.10
15 March 2004	980.40
16 March 2004	908.98
17 March 2004	975.66

18 March 2004	956.06
19 March 2004	951.65
20 March 2004	597.91*
21 March 2004	974.67
22 March 2004	974.08
23 March 2004	973.69
24 March 2004	*976.28*
25 March 2004	*966.95*
26 March 2004	*961.20*

The March 20 flow rate is clearly below normal. Table 26 indicates that several aspects of the operational process deviated from normal values including the higher than normal sampling time, the unusually low volume of air that was collected, and the shorter than normal counting time. The counting time was probably shortened to compensate for the long sampling time so that the data could be transmitted on schedule. However, there is no known reason for the low volume of air which led to the low flow rate. Obvious possibilities include an air flow impediment or blockage, or a problem with the motor that drew the air through the collection system.

Verify Soundness of Automated Calibrations

All of the automatically generated calibration equations for the CA002 spectra appear to be in order. The three calibration equations that are incorporated into each spectral analysis are the energy vs. channel calibration, resolution vs. energy calibration, and

efficiency vs. channel calibration. Of course, serious inconsistencies in any of these equations would have led to noticeable problems in the spectra and the spectral analysis. Therefore, given the sound appearance of the spectra, the satisfactory calibration equations are to be expected.

Identify complete and accurate set of radionuclides present based upon emission lines identified

A review of the ARMRs reveals that the automated spectral processing system was able to identify the presence of many radionuclides that are regularly seen at CA002. These radionuclides include Bi-212, Bi-214, K-40, Pb-214, Tl-208, Be-7, Pb-212, I-123, and Ac-228. The key lines for these radionuclides appeared intact. Further evaluation of these spectra reveals that the relative radionuclide abundances of most peaks identified were sound. However, a few of the secondary peaks associated with radionuclides were not consistent with expected gamma-ray abundances. A more detailed investigation draws these inconsistent abundances into question, given the broad accuracy of the primary and other peak abundances in the spectra. Considering the broad energy range covered by the anomalous peaks that serve as the initial conditions for this study, it may be that some anomalous gamma-rays are superimposed onto the secondary peaks, altering their apparent abundances.

Because the key lines of the radionuclides identified appear to be intact, using radionuclide key lines to determine concentrations is likely to be more accurate than using the average of all peaks associated with a particular radionuclide. Using the

average of abundances calculated from all peaks associated with a particular radionuclide is more likely to incorporate some of the peaks with inconsistent abundances into the calculation, while using the key lines, which appeared to be unaffected by these occurrences, offers a greater opportunity for overall accuracy.

An analysis of the gamma-rays not associated with radionuclides reveals that they are the key lines and strong secondary lines of the following radionuclides: At-209, Po-207, Bi-206, Po-206, Bi-204, Po-204, and Bi-203. Relevant information for these radionuclides is included in Table 28. Even so, there is no known presence of these radionuclides in the local environment, nor is there any known reason why they would be present within the samples collected. Therefore, without additional information, relating the unassociated gamma-rays with these radionuclides exclusively is premature. However, these radionuclides serve as a reasonable set of candidates to be evaluated further.

Table 28: Relevant Data regarding Atypical Radionuclides

Radionuclide	**Half-Life**	**Primary Gamma-Rays**	**Relative Abundance**
Bi-203	11.76 h	820.3	30%
Bi-204	11.22 h	899.15	98%
		374.72	82%
		984.02	59%
		911.78	13.5%
		670.75	11.4%
		912.22	11.1%

		918.15	10.8%
		791.19	3.26%
Po-204	3.53 h	883.984	29.9%
		270.068	27.8%
		1016.31	24.1%
Bi-206	6.243 d	803.10	99%
		881.01	66.2%
		516.18	40.7%
		1718.70	31.8%
Po-206	8.8 d	1032.26	32.9%
		511.36	24.1%
		286.410	23.8%
		807.38	22.7%
		338.44	19.2%
		522.47	15.7%
		980.23	7.08%
		311.56	4.24%
		860.93	3.54%
Po-207	5.80 h	992.33	59.3%
		742.64	28.2%
At-209	5.41 h	545.0	91%
		781.9	83.5%
		790.2	63.5%

Another point of interest regarding these unassociated gamma-ray peaks is that they appear to be somewhat consistent in several of the spectra in question. Assuming that the anomalous peaks are associated with gamma-ray emitting radionuclides -- a reasonably sound assumption given the apparent soundness of the overall spectra -- then using key lines will increase the likelihood of sound their radionuclide quantifications. Using the average gamma-ray abundance process could easily become unreasonably complex since none of the radionuclides, nor their sources, are known.

Determine accuracy of radionuclide concentration calculations

Because the intended purpose of the CA002 monitoring station is to measure for evidence of nuclear weapons testing and the radionuclides measured are not indicative of nuclear explosions, the overwhelming majority of these radionuclides are not quantified. Be-7 and Pb-212 are quantified because they offer an ongoing baseline of atmospheric and terrestrial radionuclide levels, respectively, to enable more elaborate quantifications, if necessary. The Be-7 and Pb-212 concentrations are shown in Table 29. The I-123 identified is known to be associated with a medical radioisotopes manufacturing facility within 2 km of the station, and is therefore not quantified either.

Table 29: CA002 Be-7 and Pb-212 Concentrations Measured

Date	**Be-7 Concentration ($\mu Bq/m^3$)**	**Pb-212 Concentration ($\mu Bq/m^3$)**
11 March 2004	*1.6E+03*	*3.2E+03*
12 March 2004	*2.4E+03*	*2.7E+03*

13 March 2004	*2.8E+03*	*2.8E+03*
14 March 2004	2.2E+03	3.9E+03
15 March 2004	2.5E+03	4.6E+03
16 March 2004	2.1E+03	2.7E+03
17 March 2004	3.8E+03	2.8E+03
18 March 2004	3.5E+03	1.7E+03
19 March 2004	1.1E+03	1.4E+03
20 March 2004	2.9E+03	1.3E+03
21 March 2004	3.4E+03	2.9E+03
22 March 2004	3.3E+03	5.3E+03
23 March 2004	3.5E+03	3.4E+03
24 March 2004	*1E+03*	*5.6E+03*
25 March 2004	*5.8E+03*	*5.6E+03*
26 March 2004	*3.9E+03*	*3.8E+03*

Of the seven radionuclides that may be associated with the atypical peaks, three (At-209, Po-207, and Bi-203) appear to have no relationship with any other radionuclides known to be or possibly present. While the remaining four radionuclides do not have any relationship with any of the radionuclides known to be present, they do have relationships amongst one another. Po-206 decays into Bi-206 with a branching ratio of 100% and Po-204 decays into Bi-204 with a branching ratio of 99.3%. Because the operational scheme of the CA002 monitoring station is geared towards measuring fission products indicative of a nuclear weapon detonation, most of which have half lives on the order of hours and

days, the radionuclides detected by the system typically have half-lives in this range. The fact that all seven radionuclides possibly associated with the anomalous peaks have half-lives ranging from 3.5 hours to 8.8 days lends credibility to their presence. At this point, although no source of these atypical radionuclides is known, it is reasonable to conclude that they are the source of the anomalous peaks. This conclusion is based upon the fact that the atypical peaks correspond to gamma-rays that would be identifiable if the radionuclides were present; the clear parent daughter relationships amongst a subset of the radionuclides; and the half lives that are ideally suited for detection. If any of these circumstances was different, such a conclusion may be suspect.

Determine parent and progeny radionuclides possibly present based upon radionuclides identified

Given that the sampling system is geared towards collecting particulates with half lives that range between hours and days, it is possible that many other radionuclides not identified were present. These radionuclides may not have been identified because they were not collected due to their gaseous states (i.e., radons), or they may have been collected but not detected due to a half-life that was either too long or too short. A listing of the parents and daughters of the known anomalous radionuclides that may have been present but not detected are listed in Table 30. As Table 30 shows, the number of nuclides possibly present but not detected is much larger than the number of anomalous radionuclides detected, outnumbering them by 3 to 1.

Table 30: Parent and Daughter Radionuclides possibly present at CA002 but not Identified

Nuclides not Collected due to Gaseous State	**Nuclides with Half-lives too Short for Detection**	**Nuclides with Half-lives too Long for Detection or Stable**
Rn-211 (parent of Po-207)	At-208 (parent of Bi-204)	Bi-209 (granddaughter of At-209)
Rn-210 (parent of Po-206)	At-207 (parent of Po-207; parent of Bi-203)	Pb-207 (granddaughter of Po-207)
Rn-209 (parent of At-209)	At-206 (parent of Po-206)	Bi-207 (daughter of Po-207)
Rn-208 (parent of Po-204)	Pb-205 (granddaughter of At-209)	Pb-206 (granddaughter of Po-206; daughter of Bi-206)
Rn-207 (grandparent of Bi-203; grandparent of Po-207)	At-204 (parent of Po-204; grandparent of Bi-204)	Tl-205 (great granddaughter of At-209)
Rn-206 (grandparent of Po-206)	At-203 (grandparent of Bi-203)	Pb-204 (daughter of Bi-204)
Rn-204 (grandparent of Po-204)	Po-203 (parent of Bi-203)	Tl-203 (granddaughter of Bi-203)
Rn-203 (great grandparent of Bi-203)		

The apparent relationship between the noble gas, radon, and the anomalous radionuclides is particularly interesting because of its potential similarity to local emissions that led to the I-123 activation product detections. The I-123 became airborne because minute

quantities of the noble gas, Xe-123, escaped from a local facility. After the xenon escaped, it decayed directly into iodine, which was subsequently detected. It is possible that minute quantities of gaseous radon escaped from a local facility and decayed into the anomalous radionuclides detected; however, at this point, there is no evidence to support this hypothesis.

The parent daughter relationships between these nuclides are shown in Figure 20. All of the nuclides referenced in Table 30, with direct relationships to the anomalous radionuclides, are identified in black font in the figure. The radionuclides shown in white font are a) those that are not directly related to the anomalous radionuclides but could be present, and b) those that would have likely been present, given the known presence of the anomalous radionuclides and the possible presence of nuclides listed in Table 30, but for some reason were not identified.

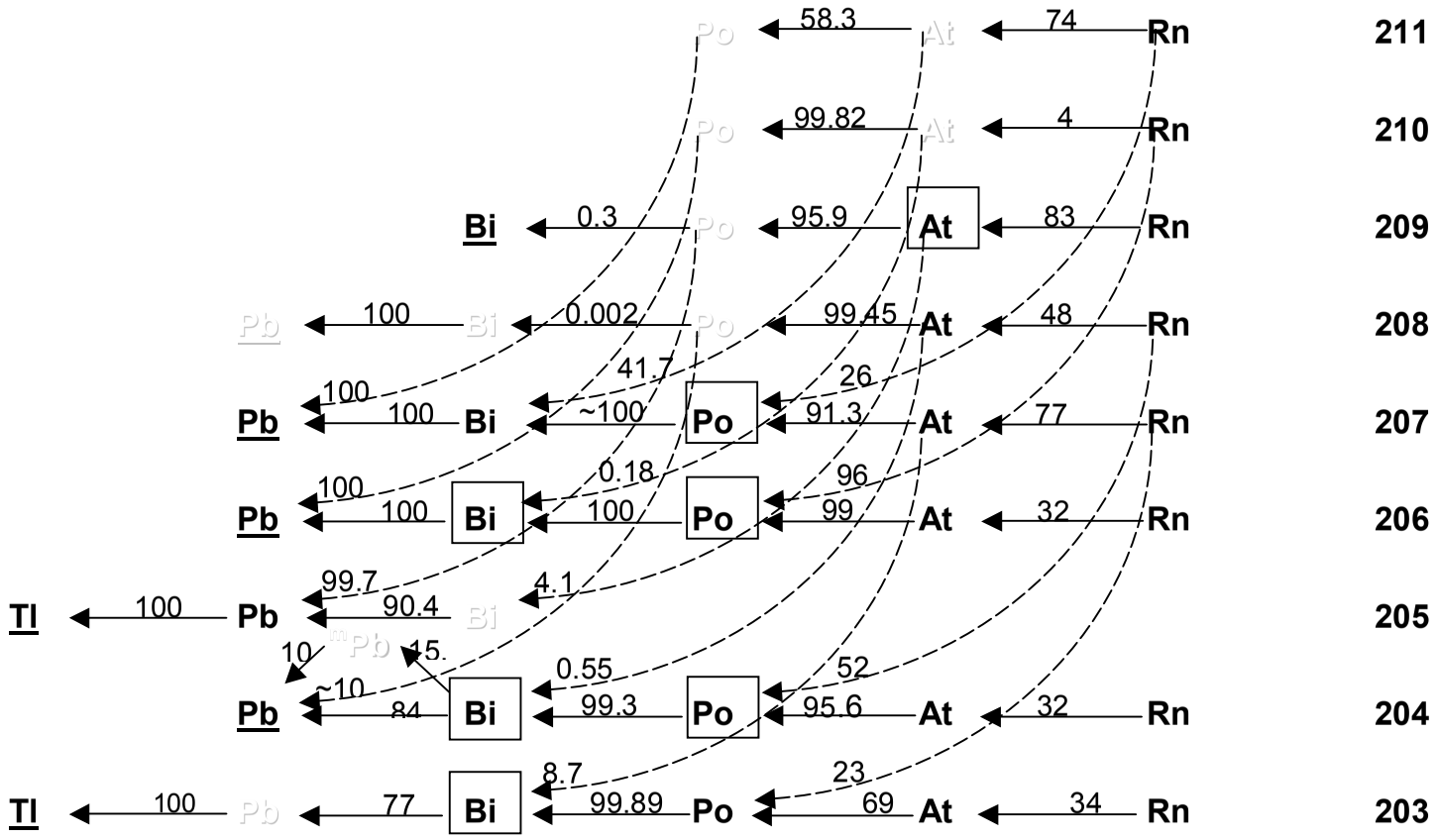

Figure 20: Parent - Daughter Relationships between Nuclides

Perform preliminary analysis

Because all of the atypical radionuclides are neutron depleted, it is reasonable to conclude that they are activation products. The I-123 that is periodically measured at CA002 is also an activation product, so anthropogenic activation products are not uncommon at the CA002 monitoring station. Finally, all the other radionuclides detected at the CA002 station are natural radionuclides. K-40 is a singular primordial. Be-7 is an induced radionuclide. Ac-228, Pb-212, Bi-212, and Tl-208 are radionuclides from the thorium series, and Bi-214 and Pb-214 are uranium series radionuclides.

3. Incorporate Data about Collection and Measurement Mechanisms and Procedures into Analysis

Incorporate details regarding type of radionuclide sampler used

The CA002 monitoring station utilizes a high volume particulate radionuclide sampler to extract radionuclides from the air at the full range of ambient temperatures. The sampler draws air via a 1100 m^3/h blower in 24 hour time blocks to accomplish nearly continuous sampling. A representative picture of the sampler is shown in Figure 21. The collection flow rate is controlled by a variable speed motor, which is shown in Figure 21 at the base of the thinner vertical pipe. The motor is able to maintain constant flow by increasing its speed to compensate for the flow as the flow becomes increasingly impeded with collected debris. Typical flow rates average approximately 975 m^3/h, which correspond to an air volume of 23400 m^3.

Figure 21: High Volume Particulate Radionuclide Sampler

The white cube shaped box shown in Figure 21 holds a high efficiency, glass fiber, particulate collection filter that measures 60 cm x 60 cm. The collection filter collects 1.0 micron diameter particles with an efficiency of 99.99%. This size of interest is in direct response to the fact that nuclear weapons testing debris that traverses large distances typically range from 0.1 to 5 microns in diameter.

Based upon this information, the collection system appears to have operated properly. This is evidenced by the generally consistent 975 m^3/hr flow rates noted in Table 27, and the fact the only radionuclides in particulate form appear to have been collected.

After the collection process is complete, each filter paper is manually isolated in a wax paper sleeve and pressed into the form of a hockey puck (r = 3.2 cm, z = 1.3 cm) in

preparation for subsequent analysis. It is in this form that the short lived background radionuclides collected are allowed to decay.

Incorporate information regarding surroundings and type of radionuclide detection and analysis

After the decay period has been completed, the compressed filter paper is manually placed inside the detection system for counting. Two pictures of the detection system used are shown in figures 22 and 23. Figure 22 shows the coaxially mounted, 40% efficient, cryogenically cooled HPGe detectors with the low background shield closed, and Figure 23 shows the two detectors fully exposed, with no external shield. The detectors are calibrated for 15 minutes with a known check source for quality control purposes. Given the presence of the low background shield that minimizes the influence of external radionuclides, it is unlikely that the anomalous radionuclides exist outside the counting apparatus. In addition, given the inconsistent presence of the anomalous radionuclides, it is unlikely that they are the result of detector contamination.

Figure 22: CA002 Detection System with Low Background Cover Closed

Figure 23: Representative Example of Detection System Uncovered

In addition to the equipment specifically used for radionuclide sample collection and detection, auxiliary equipment including an ambient dose rate meter and a local weather conditions monitor is present at the collection site. The equipment is enclosed in a 20 ft x

8 ft x 8 ft trailer an is powered by an uninterruptible power supply which can supply up to 4 hours of continuous battery operation, if necessary.

In general, conservative estimations assess that environmentally collected radionuclides are considered to have decayed to insignificant levels after eight half-lives and are considered to be essentially nonexistent after ten half-lives. Therefore, given the 4 hour (240 minute) decay time, radionuclides with half lives of 30 minutes or less would be generally indistinguishable from background, and radionuclides with half lives of 24 minutes or less would have essentially decayed away. All of the anomalous radionuclides exceed these half-life criteria.

The PDT_n, a concept derived in Appendix 4, can also be used to estimate the minimum half-life detectable based upon the station's standard operational parameters. Assuming various background counts per channel of 500, 100, 50 and 20 at various points within each spectrum, the corresponding PDT_n values are 76.27, 35.61, 25.97, and 17.42 respectively. In order to calculate the minimum half-lives, several values will need to be estimated. The most sound estimations deal with the operational parameters of the collection system and include the sampling time, decay time, counting time, and flow rate. These values were chosen as 24 h, 4 h, 19.5 h, and 975 m^3/h, respectively, based upon the standard operational parameters for the station. The energy dependent detector efficiency was chosen based upon the energy location in the spectrum where each background value typically occurs. The minimum peak width was chosen to be five channels, and the branching ratio was conservatively chosen to be one. Of course, the

minimum half-life detectable is directly dependent upon the airborne concentration present. The relationship between the airborne concentration and the minimum half-life detectable for each of the background count values chosen are plotted in Figure 24. Because typically measured airborne radionuclide concentrations for this station range between 1E3 and 1E4, the figures show that the minimum half-lives measurable are more thoughtfully estimated to vary between 1.15 and 1.95 hours for these airborne concentration ranges.

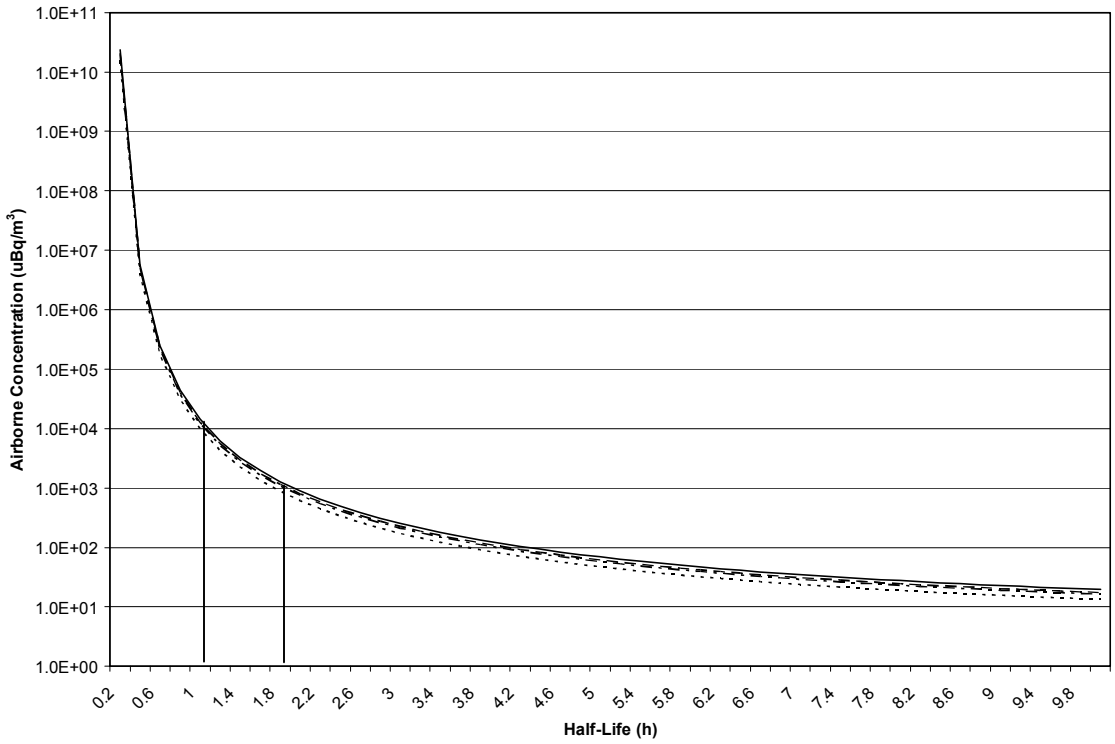

Figure 24: Aggregate Plot showing Minimum Half-Life to Detect Peak over 500, 100, 50, and 20 Background Counts per Channel

4. Characterize Environment

Identify other sensors in the region

This case study is rather unique due to the low density of nuclear infrastructure in the region. Correspondingly, as Figure 25 shows, the national network of radiation monitoring stations operated by the Health Canada Radiation Protection Bureau is of similarly low density in this region. The network includes only one site in British Columbia -- the Vancouver station where the anomalous data was originally measured. Other sites where environmental radiation sensors are located are shown in figures 25 through 28. Each of these figures highlights the fact that there are no sensors close to the Vancouver site. As a result, no other sensor data related to the atypical radionuclide detections is available.

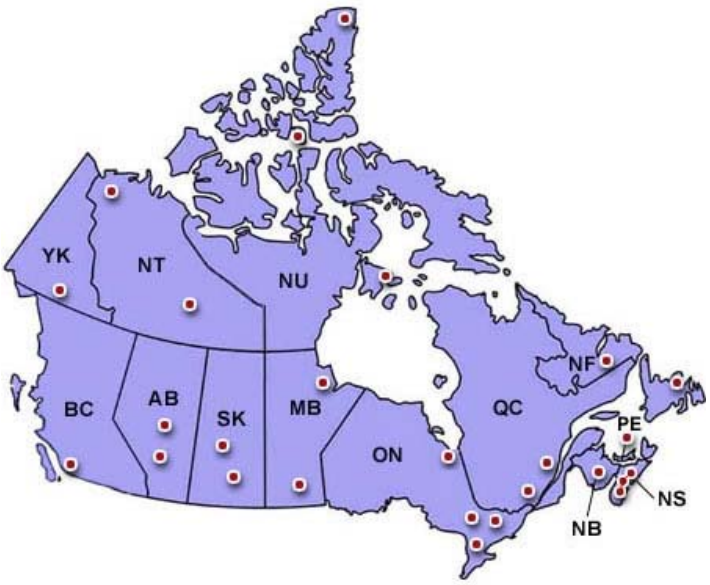

Figure 25: Health Canada Radiation Protection Bureau network of monitoring stations

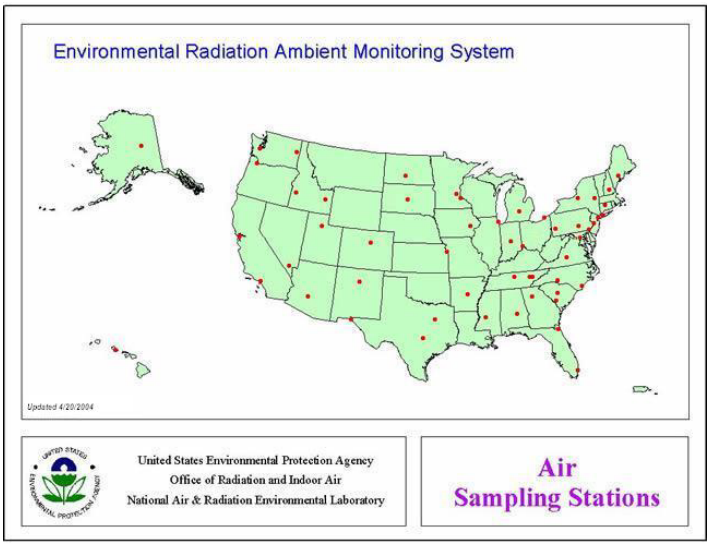

Figure 26: EPA Radiation Ambient Monitoring System Air Sampling Stations

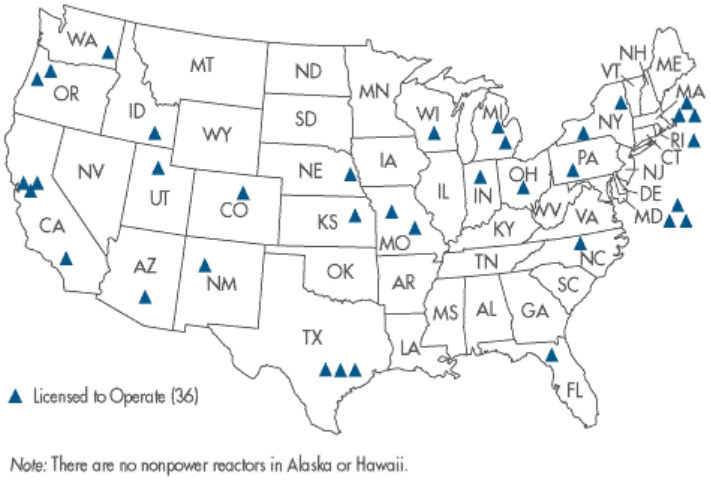

Note: There are no nonpower reactors in Alaska or Hawaii.

Figure 27: U.S. Nuclear Research Reactors with Standard Environmental Radiation Monitoring Sensors (NRC)

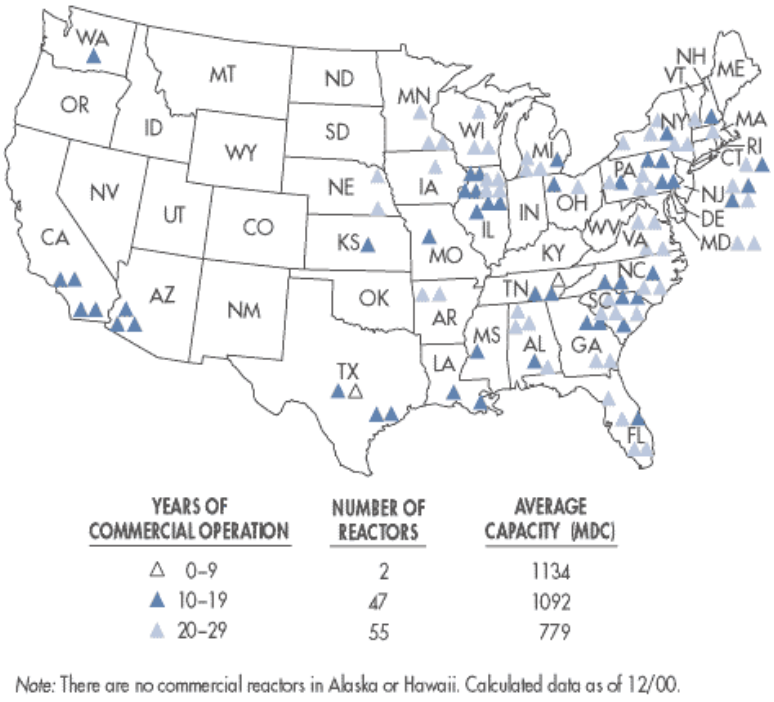

Figure 28: U.S. Nuclear Power Reactors with Standard Environmental Radiation Monitoring Sensors (NRC)

Characterize natural environment

Characterize terrain

The detection site, shown in Figure 29, is located in an open grassy area on the University of British Columbia campus. Therefore, there are no major impediments to airflow in the immediate vicinity of the monitoring station. Trees and buildings of varying heights can be randomly found on the order of one hundred meters from the station. As a result, no dynamic meteorological conditions that affect the station are created due natural or anthropogenic ground barriers.

Figure 29: Immediate terrain of collection site

Considering the terrain from a broader perspective, the UBC campus, on which the monitoring station is located, is bordered on the south and west by a cliff that drops approximately 1000 meters to flowing water below. The water below is the point at which the Frasier River flows into the larger the Strait of Georgia. The Frasier River is immediately adjacent to the coast and flows from southeast to northwest. At the point where the Frasier River meets the Strait of Georgia, on the order of a kilometer offshore, the Strait flows due south. This dynamic is shown in Figure 30. The broader region to the north includes forest and some buildings until coastline is reached. The forest and buildings are also present to the east. The layout of these surroundings is shown in Figures 31 and 32.

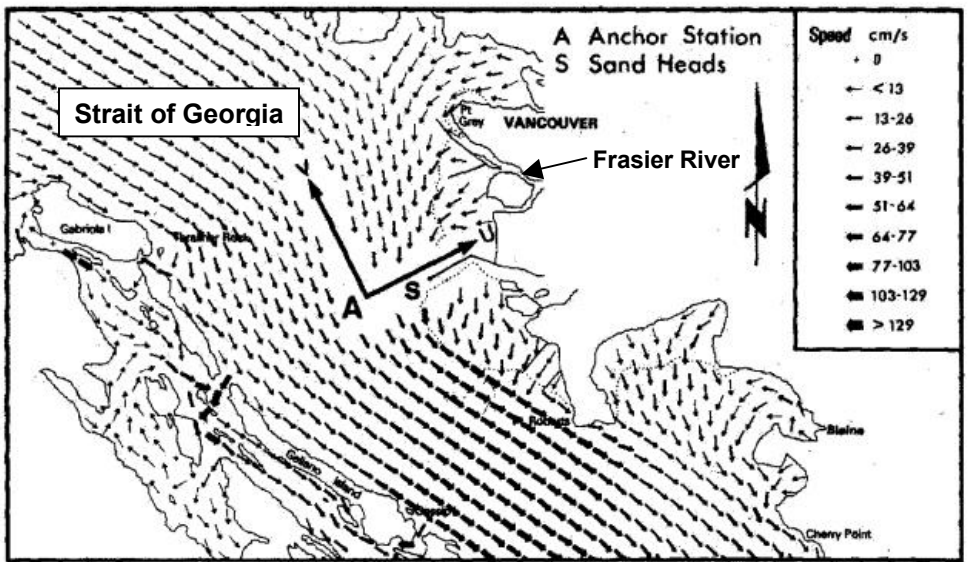

Figure 30: Location of UBC campus (Port Grey) with respect to Frasier River and Strait of Georgia. (Note: Flow arrows correspond to water velocities. Also, the v, u, A, and s, coordinates are essentially arbitrary coordinates that were used to gather the data.)

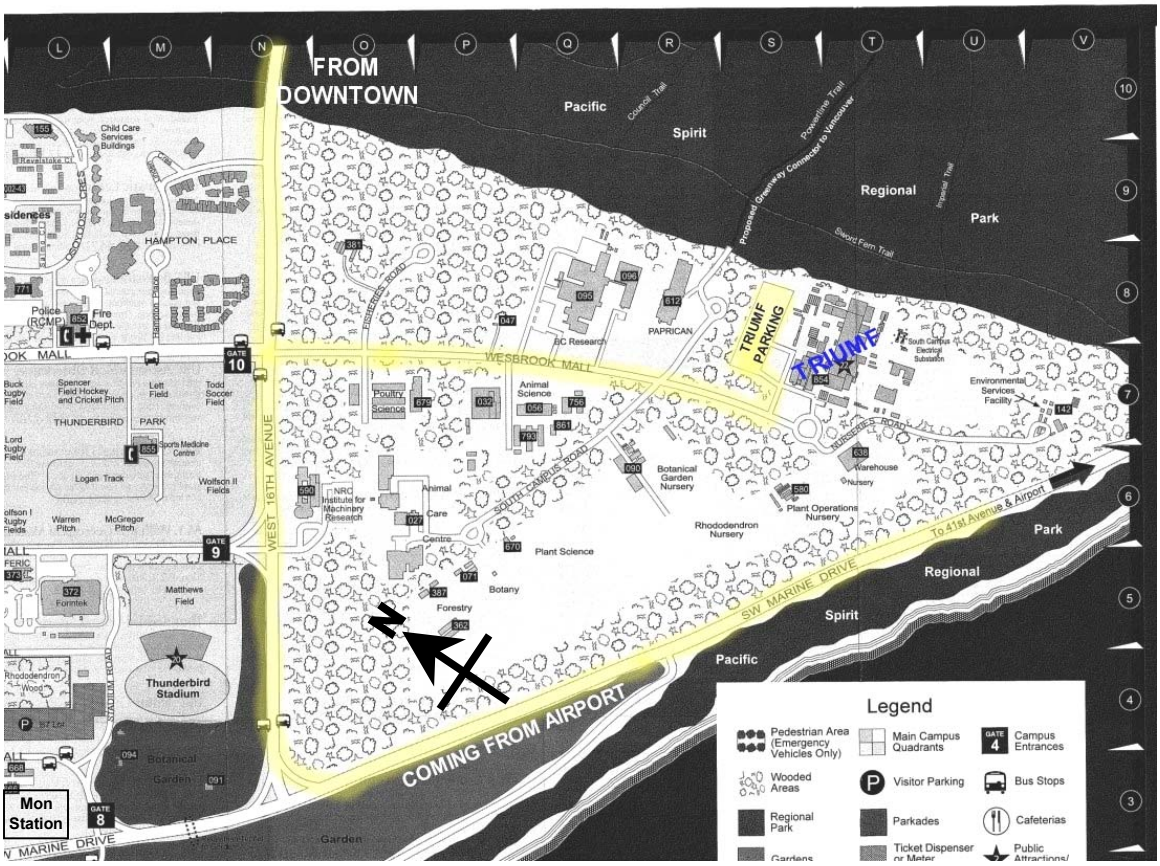

Figure 31: Immediate northeast and southeast surroundings of monitoring station (lower left)

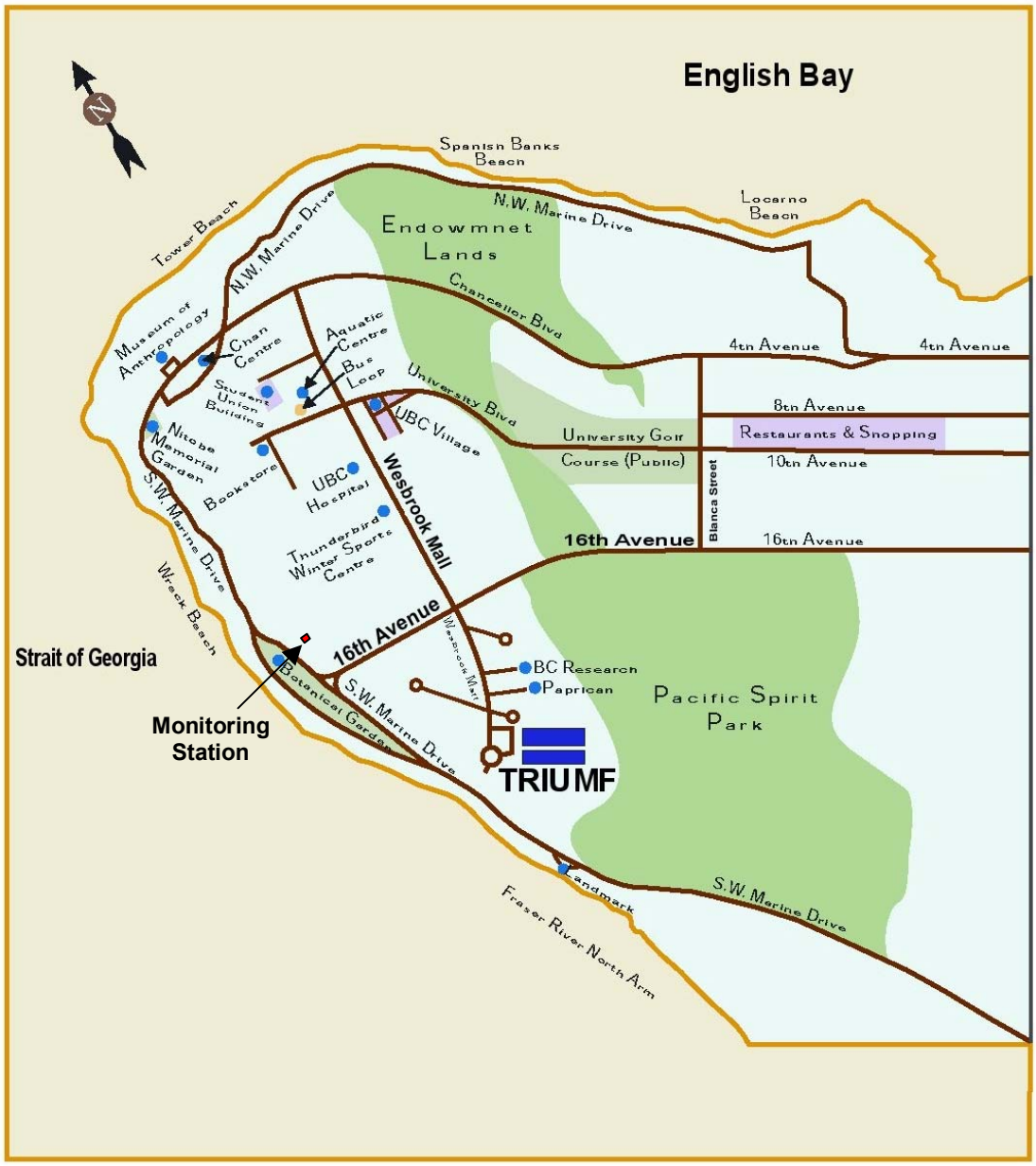

Figure 32: Immediate regional surroundings of monitoring station in all directions

When considering the region from as even broader perspective, to the south and west, beyond the Strait of Georgia, a strip of land approximately 100 km wide by 500 km long, is oriented from northwest to southeast. The land appears to be dominated by high terrain on the order of 1000 meters. Despite the size of this land mass with respect to the size of

the Strait of Georgia and the Frasier River, the flowing water likely impacts the detection site environment more significantly due to the dynamic nature of the water flow. A map which displays these features is shown in Figure 33. The figure also shows the broader northern and eastern regions, which is characterized by mountains approximately 1500 meters in height.

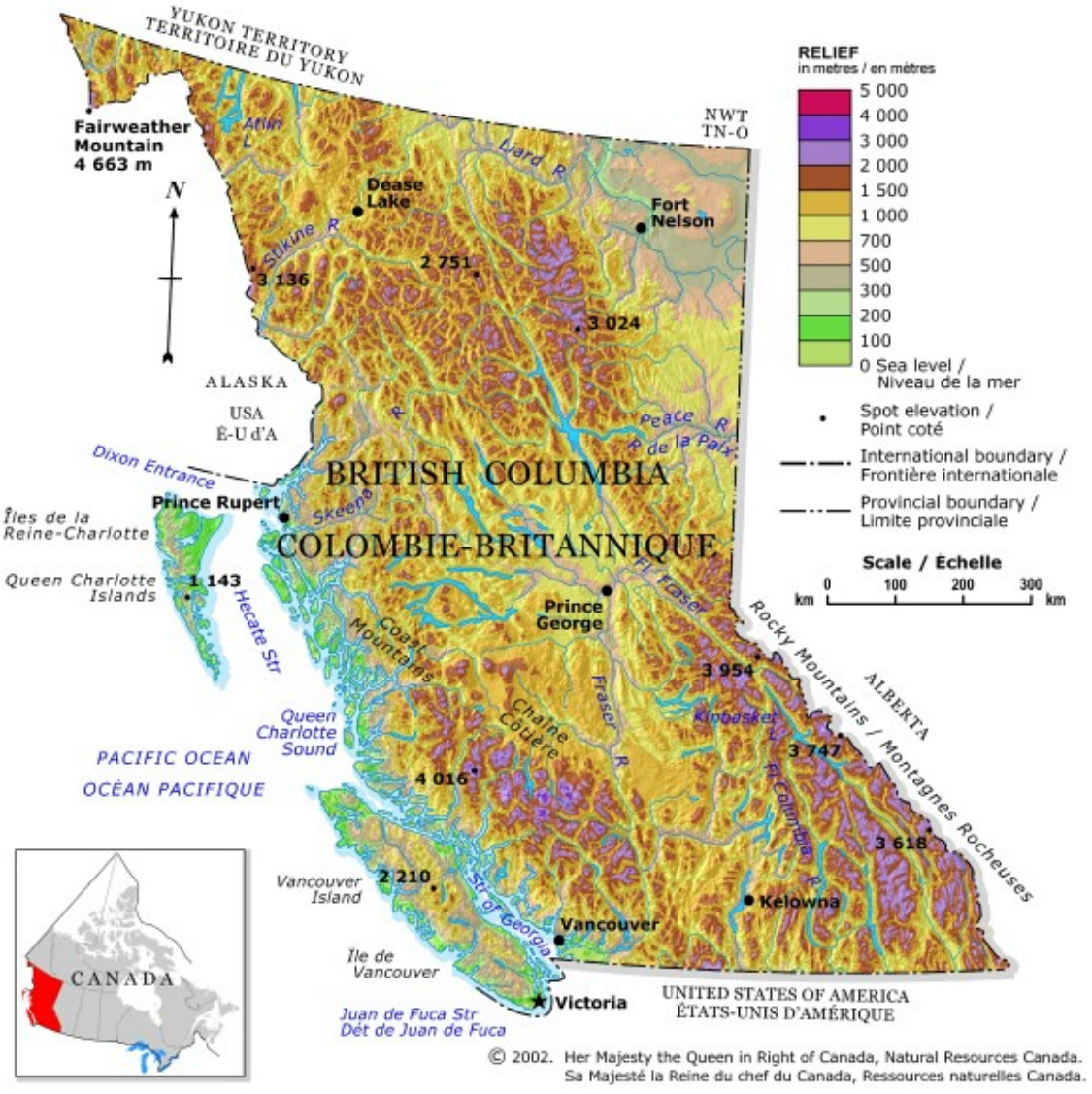

Figure 33: Relief Map of Vancouver and British Columbia Region

Characterize meteorology to fullest extent possible

The meteorological station that is integrated into the detection station has limited capabilities, reliably providing wind speed and direction at the site. Therefore, all tangible meteorological data must be obtained from nearby stations. Because a number of meteorological stations exist in Vancouver, some meteorological information was obtained by using data from the closest nearby station, while in other cases, when possible, a weighted average was used to estimate the actual values at the detection site. The annual average wind rose for the detection site is shown in Figure 34, and the average annual precipitation for the region is shown in Figure 35.

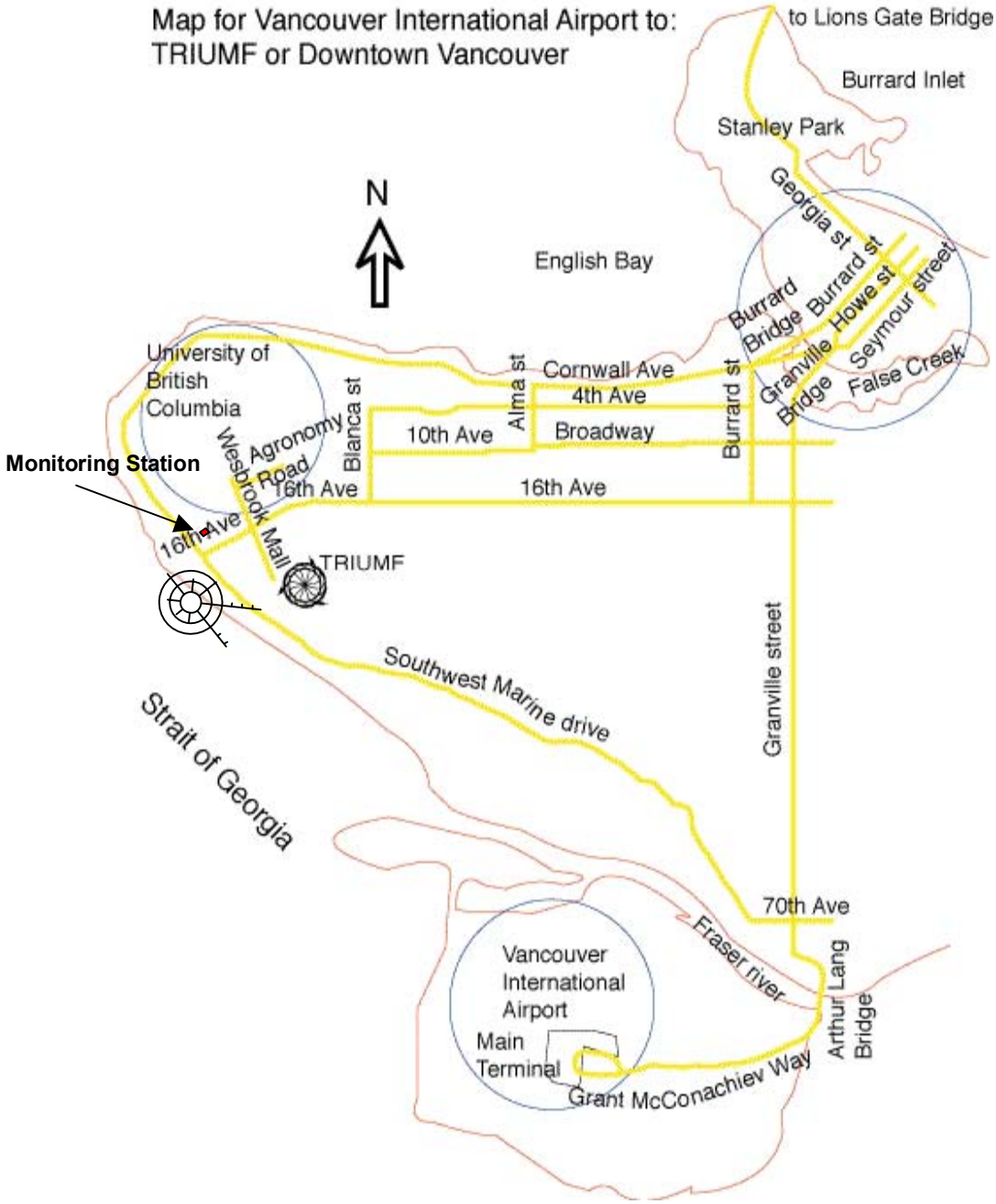

Figure 34: Average Annual Wind Rose for Detection Site

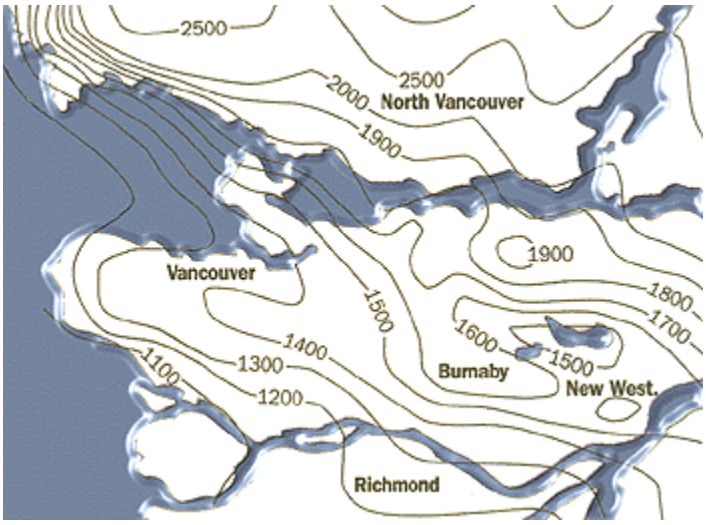

Figure 35: Mean Annual Precipitation for Greater Vancouver (mm/yr)

Appendix E shows representative meteorological data, satellite imagery, meteorological trajectory models, and airborne concentration dispersion models for the detection site. Based on all of the meteorological data evaluated along with the radionuclide detection data and sensor location information, no conclusive correlations were derivable. First, given the detected concentrations and the amount of concentration reduction during dispersion, any radionuclides that reached another sensor would likely have been too diffuse to measure. In addition, given the forward and backtracking trajectories, there are no consistencies between trajectories and measured concentrations at the detection site. Therefore, either the atypical radionuclides originated from a highly localized source, or they traversed mesoscale distances but were to diffuse to be detected. However, given the inconsistent mesoscale meteorological data coupled with the general consistency of detection, the localized source option is most reasonable.

Draw preliminary conclusions based upon environmental determinations

Based on analysis to this point, Figure 20 still represents the most likely set of atypical radionuclides present at the detection site. Moreover, the detection site is likely close to the source location -- not only due to the meteorological analysis, but also because of the short half-lives of some of the atypical radionuclides detected. For example, the half-life of Po-204 is 3.53 hours. If, as Figure 20 suggests, the polonium is the result of a Rn-204 ($t_{1/2}$ = 1.24 m) decay into At-204 ($t_{1/2}$ = 9.1 m), which then decays into Po-204, then the radon and astatine have decayed to insignificant levels in approximately 1.5 hours, leaving the polonium as the principal remaining parent in the decay chain. Therefore, the source and detection sites must be close enough for the short-lived Po-204 to be atmospherically dispersed, decay in transit, and be detected effectively. Based upon the wind speeds indicated in Figure 34 at the detection site, the source location may be located within mere miles, possible five, of the detection site. However, the quantities and concentrations released drive this rough estimation.

According to Figure 34, the two most likely source locations are the TRIUMF high energy physics site and the Vancouver International Airport. Another possible source is the University of British Columbia teaching hospital located 1 km to the northeast of the detection site. Given the estimated close proximity of the source and detection sites, this set of possible source locations is reasonable.

It should be noted that the resolution of the NGM atmospheric model used has a resolution of 2 km. That means that the smallest dimension of each parcel used in the

model's evaluation is 2 km. While this is not uncommon amongst mesoscale meteorological models, the resolution causes the model to be of no analytical utility if the radionuclide source is the TRIUMF site, 2 km southeast of the detection site, or the UBC hospital, and limited utility if the source is the Vancouver International Airport located 10 km southeast of the detection site.

5. Characterize Possible Sources

Recall that the atypical radionuclides detected are At-209, Po-207, Bi-206, Po-206, Bi-204, Po-204, and Bi-203. These radionuclides are activation products with half-lives ranging from 3.5 hours to 8.8 days. Moreover, as Figure 20 shows, these radionuclides are all daughters, grand daughters, and great grand daughters of various radon isotopes. The only reasonable source for such combinations of short-lived activation product radionuclides is the TRIUMF high energy physics site. Neither history nor logic supports short-lived airborne activation products originating from any portable or permanent airport equipment. Similarly, it would be unprecedented for a hospital to generate such a multifaceted set of environmentally detectable airborne activation products. Therefore, the most likely source for the anomalous radionuclides detected is the TRIUMF site. An aerial picture of the TRIUMF site is shown in Figure 36.

Figure 36: Aerial View of TRIUMF Site

Because only one viable source location exists, the ranking of possible sources in Section 8, Use Estimated Chains of Events to Determine Most Likely Radionuclide Emission Source, will not be necessary. Therefore, in this case study, the Section 8 evaluation will not be conducted.

6. Develop Characterizations of Possible Sources

Infinitesimal radionuclide releases are not uncommon for the TRIUMF site. The most common radionuclide released is Xe-123, with varying concentrations of I-123 as an impurity. Xe-123 is a byproduct of the process used to generate I-123, which is used for to manage thyroid cancer and to image cardiac and neurological disorders. The production equations are shown in Equation 16.

$$Xe-124(p,2n)Cs-123 \xrightarrow{5.94m} Xe-123 \xrightarrow{2.08h} I-123 \qquad \text{Equation 16a}$$

$$Xe-124(p,2n)Cs-123m \xrightarrow{1.62s} Xe-123 \xrightarrow{2.08h} I-123 \qquad \text{Equation 16b}$$

Releases generally occurred daily on days when I-123 was being produced. The typical schedule was either four straight days of production with three days of inactivity, or five straight days of production with two days of inactivity. Because the releases occurred following a decay period intended to increase the quantity of I-123 generated, thereby reducing the amount of Xe-123, directly correlating production and emission rates is challenging. The releases are best approximated as instantaneous emissions of low activity.

Besides the regularly occurring Xe-123 releases, atypical releases have been associated with the TRIUMF site. The two radionuclides that have been referenced in literature are Kr-77 and Ne-24. Kr-77 may have been released one or two times from the site; however, to date, no correlations have yielded conclusive results. On the other hand, the Ne-24 emissions are much more conclusive, having occurred and the effects having been measured on the order of 100 times.

The primary commonality between all three releases associated with the site is that they all involved an infinitesimal amount of gas escaping the particulate scrubber system. In each case, the gases decayed into particle progeny which was detected at the detection site. In the case of the Xe-123, it decayed and was detected as I-123; Kr-77 was detected as Br-77; and Ne-24 was detected as Na-24. Given that all of the atypical radionuclides detected are the progeny of various isotopes of gaseous radon, it is possible, and may be likely, that the same process took place. If the same process did indeed take place, then the set of radionuclides emitted are more closely represented by the radon isotopes listed in Figure 37, as opposed to the more limited set shown in Figure 20. Again, as in Figure 20, the seven detected radionuclides are shown in boxes.

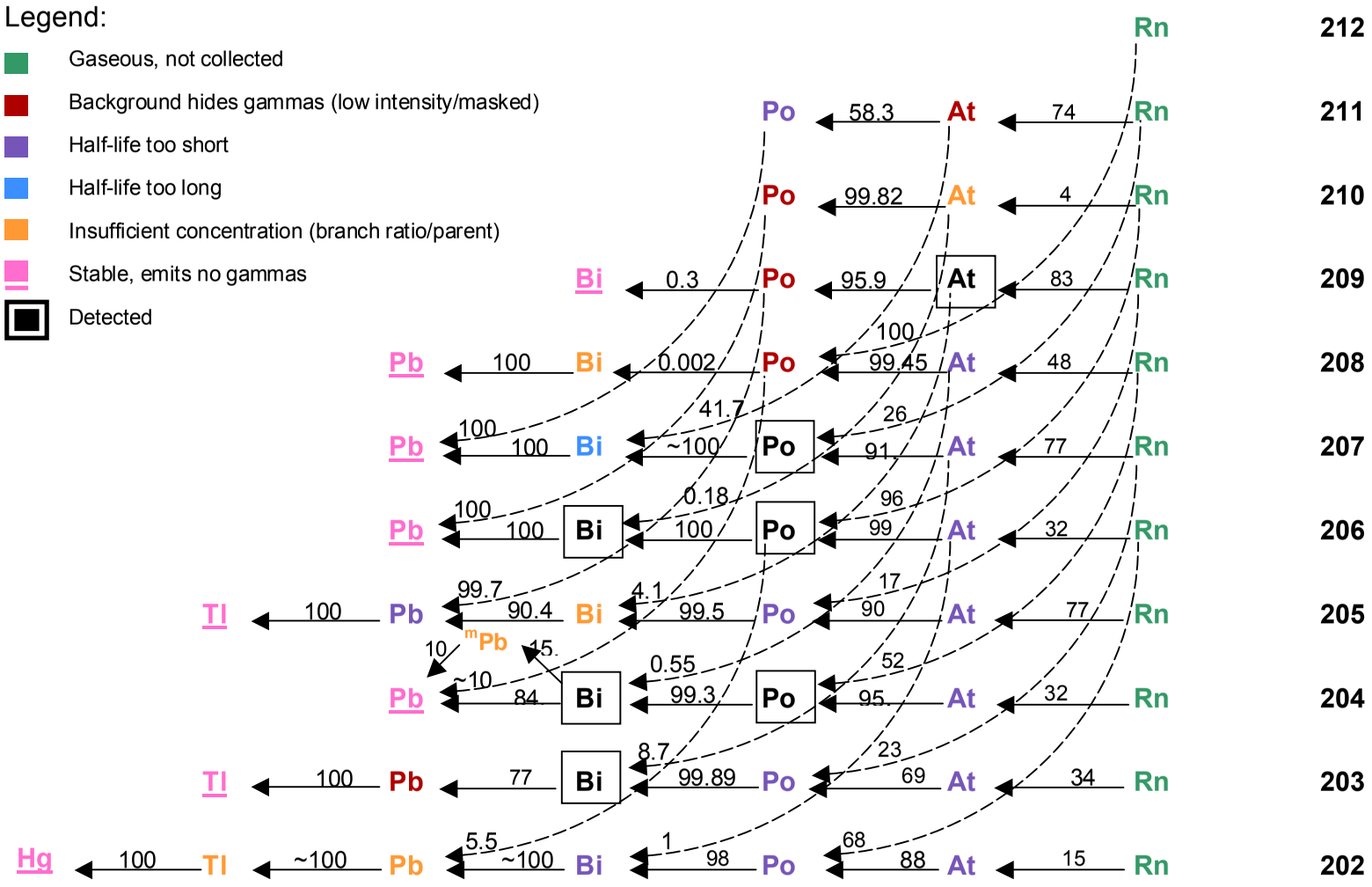

Figure 37: Updated Parent - Daughter Relationships between Nuclides

Regarding the physical parameters relevant to the emission, a picture of one of the primary buildings on the TRIUMF site is shown in Figure 38. The height of the emissions stacks and their cumulative area can be estimated based upon this figure. The height of the emission stacks is approximately 35 feet and their cumulative area is approximately 5 square feet. Based upon the picture, all emissions would have occurred in the vertical plane with at least nominal internal energy and momentum. Given the height of the surrounding trees, it is reasonable to deduce that effluents emanating from the stacks were able to be dispersed without significant obstruction from the trees.

Figure 38: Picture of building on TRIUMF site

Further investigations corroborated the hypothesis that the TRIUMF facility was the source of the atypical radionuclides detected, and that the hypothesized decay processes

from radon to the multitude of progeny actually occurred. A member of the TRIUMF staff indicated that on the days in question, the facility was being used to bombard thorium carbide targets with 500 MeV protons to make isotopes of francium. Based upon research conducted by CERN, shown in Figure 39, involving the bombardment of thorium carbide targets with 600 MeV protons, the staff member concluded that a suite of radon isotopes are generated through this process. Although the radon isotopes listed in the figure range from Rn-198 through Rn-227, because the figure is a semi-log plot, the peak abundances are orders of magnitude above lesser values. A clear break on both sides of the peak appears to occur at 10E6 atoms per second, leaving isotopes of radon ranging from 203 through 223 as most likely to have progeny collected and detected. In addition, this also means that although no progeny of the other radons indicated in the figure are listed, they may indeed be present but undetectable due to their low concentrations.

Isotopes of other gaseous radionuclides are also generated through the bombardment including krypton and xenon. However, according to Figure 37, none of these progeny, or progeny of radon isotopes ranging from 220 - 223 was detected at the monitoring station. Further investigations revealed that the krypton and xenon progeny were either stable or pure beta emitters, rendering them undetectable by the gamma-ray detection system in place at the monitoring station. Regarding the highly abundant isotopes of radon whose progeny were not detected, the lack of detection may be related to the unusually short half lives of the progeny, many on the order of seconds.

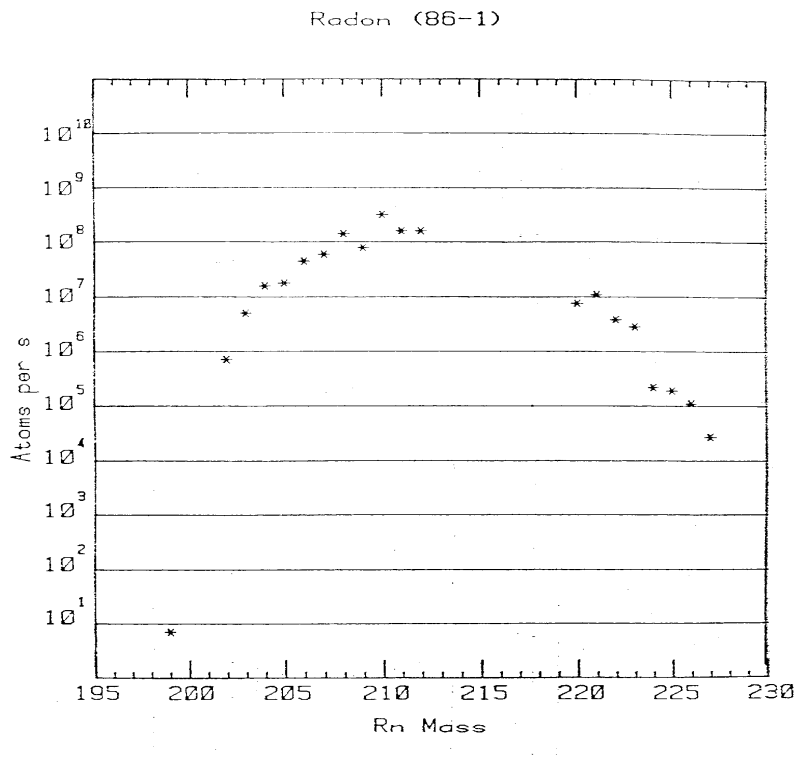

Figure 39: Distribution of Radon Isotopes following 600 MeV proton bombardment of thorium carbide, generated by CERN

7. Likely Chain of Events

At the conclusion of Section 5, it was noted that since only one viable source location existed, there was no need to conduct the Section 8 analysis. Another consequence of having only one feasible source is that it enables the evaluations in Section 7, Use Source Characterizations and Natural Environmental Data to Estimate Chains of Events from Most Likely Sources, and Section 9, Recreate Most Likely Chain of Events, to be combined. Therefore, Section 9 will not appear as a separate evaluation.

The initial conditions for the source term of this case study involved high energy physics experiments that were conducted at the TRIUMF site in Vancouver British Columbia on

the University of British Columbia (UBC) campus. Protons were being used to bombard thorium carbide in an effort to produce francium. As a result of the bombardments, a wide variety of secondary nuclides were generated -- including radons ranging in mass from 197 to 227 amu, as shown in Figure 39. These, and other radionuclide products not specifically related to the experiment, were held in an emissions system where the overwhelming majority of radionuclides decayed to nondetectable levels.

TRIUMF staff performed a brief daily venting of the airborne emissions system after the decay period. Therefore, the radionuclides releases occurred under controlled conditions. While the decay period was long enough for the overwhelming majority of particulate and gaseous radionuclides present to decay to insignificant levels, some minute quantities of longer lived radionuclides remained. The scrubbers associated with this experiment's emissions system seem to have satisfactorily prevented particulates from escape; however, gaseous products, principally radon isotopes, were released through the stacks in minute quantities.

The release point of the emission stacks stood approximately 35 feet above ground level. The momentum of the gas upon release was likely sufficient to carry it over the surrounding trees (shown in Figure 38) without significant interference. Once airborne, the radionuclides were carried by the prevailing winds, which blew from the east-southeasterly direction, towards the detection site. The prevailing wind direction and the emission location relative to the detection site are shown in Figure 34. During transit, the radon products released continued their natural radioactive decay processes into

daughters, grand-daughters, and subsequent progeny -- all of which are particulates. The most significant radon isotopes emitted and their progeny are shown in Figure 37.

The radionuclide collection mechanism generally operated continuously in 24 hour blocks of time. It was designed to capture 1 μm diameter particulates with an efficiency of 99.99%. Therefore, gases and smaller diameter particulates that were likely present were not collected as effectively.

After material collection, the captured radionuclides experienced a 4 hour decay period prior to radionuclide data acquisition using an HPGe detector. The decay period enabled the shorter lived radionuclides present to decay to nondetectable levels. Based upon historical airborne concentrations measured at the site, the minimum half-life detectable ranged between 1 and 2 hours. Therefore, although all of the radionuclides shown in Figure 37 are present at the detection at some concentration, only the subset identified in the figure was detectable.

Chapter IV: CASE STUDY 2 -- QUALITATIVE DATA INCORPORATION

Highlights

Section 1, Initial Condition: The initial condition was the detection of an anomalously high Cs-137 concentration at a radionuclide detection site in Schauinsland, Germany.

Section 2, Validate and Superficially Correct Data: The limited amount of data available prevented effective data validation. It was interesting to note that only Cs-137 was measured. Had the Cs-137 originated from an atmospheric release of fission products, other fission products would likely have been identified, as well. The Cs-137 identified may have been the result of detector contamination or some other non-atmospheric source.

Section 3, Validate Hardware and Software Operation: No hardware or software malfunction is apparent; but given the limited amount of data accompanying the noted detection, no definitive conclusions can be determined.

Section 4, Characterize Environment: The large number of candidate radionuclide sources and detection sites in the region are overwhelming. Other detection sites in the region detected anomalous Cs-137 concentrations, as well. This fact served as validation of the initial condition of this case study and effectively eliminated the possibility that the detection was the result of detector contamination. Based upon the chronology and location of the detections, the likely radionuclide emission location was in the region of

southern Spain. Based upon existing computational models, this is the most refined source determination available.

Section 5, Characterize Possible Sources: Although over 1000 candidate radionuclide sources were identified, after analyzing the chronology and location of the detections, none of the candidate source facilities were likely. The benefit of human judgment in this section was that it enabled unlikely sites to be eliminated from consideration even though they were in the region of possible sources. These sites were eliminated through an analytical assessment of their likely outputs.

Section 6, Develop Characterizations of Possible Sources: This section revealed the most important output based upon the human judgment novelty. This section specifically identified the radionuclide emission source facility, which was based largely upon qualitative data, press reporting in this case. No existing model was able to output the emission source with specificity. Moreover, this section revealed the model's ability to identify a radionuclide emission source even when the source was not known as a radionuclide emission facility and had no known history of radionuclide emissions.

Section 7, Estimate Likely Chain of Events: This section codifies the factors governing the generation, emission, transport, collection, and detection of the Cs-137 identified. In addition, this section definitively characterizes the detection site. No existing model was able to conclusively identify that Cs-137 was the only radionuclide present at the

detection site. At best, they were only able to say that Cs-137 was identified as being present.

Section 8, Determine Most Likely Emission Source: This section was combined into section 7 since only one source was identified as likely.

Section 9, Recreate Most Likely Chain of Events: This section was combined into section 7 since only one source was identified as likely.

1. Initial Condition -- Obtain Radionuclide Data Measurement

The initial condition for this case study occurred on June 8, 1998 when an atypically large Cs-137 gamma-ray peak was measured in addition to the peaks customarily present within spectra at the DE002 monitoring station located in Schauinsland, Germany. Cs-137 is regularly measured at the DE002 station and is associated with airborne resuspension of Chernobyl fallout. The June 8 peak was easily noticeable, as it corresponded to a concentration 10 times normal Cs-137 concentrations measured at this station. However, it is important to note that the concentration measured corresponded to a dose equivalent 10 orders of magnitude below ICRP limits.

2. Evaluate Accuracy of Measurement, Highlight Anomalies, and Make Superficial Corrections as Needed

Historical station data indicate that the operational goals for sampling time, decay time, and counting time are 168 hours, 48 hours, and 120 hours, respectively. The measured

values for the spectrum in question are 165 hours, 52 hours, and 124 hours, respectively. These values correspond to differences of 2%, 8%, and 3%, respectively. Therefore, the operational parameters for the spectrum in question appear to be consistent with historical values for the monitoring station. The nominal air collection flow rate is 500 m^3/hr for this station; however, the measured flow rate was not available for evaluation in this study. Given the consistency of the other operational values measured, it is reasonable to conclude that the flow rate was also consistent.

Due to the limited amount of onsite data available for this case study, the only radionuclide identified as being present is Cs-137. Natural radionuclides are known to have been present but their identifications were not preserved because their quantities were within normal bounds. Only measurements of anthropogenic radionuclides and atypical quantities were preserved.

Cs-137 essentially emits one gamma-ray with an energy of 661.7 keV. Therefore, the only practical way to evaluate the concentration is through the key line. The calculated Cs-137 concentration was 17.0 $\mu Bq/m^3$. Supporting information was not available to validate the accuracy of the concentration, so its accuracy must be accepted until refuting data is made available. In addition, because Cs-137 essentially decays directly into stable Ba-137, no parent daughter relationships can be correlated.

Based upon the preliminary information available, it is difficult to determine whether the Cs-137 concentration measured is valid or is not valid. The concentration is an order of

magnitude above of historical station Cs-137 concentration measurements. However, because the measurements have been so consistent over time (± 1.5 $\mu Bq/m^3$), such a substantial deviation can reasonable be viewed with a level of skepticism.

Perform preliminary analysis

Because only Cs-137 was detected, it is unlikely that a fission event was the cause. Had the emission been the result of a fission event, at least one of several other fission products would have likely been detected in addition to Cs-137. These other radionuclides include Cs-136, Cs-134, Ba-140, I-131, and I-133. Because none of these or any other fission product radionuclides were detected, nuclear reactors and nuclear detonations are not likely sources. Similarly, because Cs-137 is a fission product, rich in neutrons, it is not likely to have originated from an accelerator facility. The detected Cs-137 was likely separated prior to its emission.

3. Incorporate Data about Collection and Measurement Mechanisms and Procedures into Analysis

The DE002 monitoring station utilizes a high volume particulate radionuclide sampler to extract radionuclides from the air at the full range of ambient temperatures. The sampler draws air via a 1000 m^3/h blower in 7 day time blocks to accomplish nearly continuous sampling. Radionuclides from the drawn air are entrained onto polypropylene filters. Typical flow rates average approximately 500 m^3/h, which correspond to an air volume of 84000 m^3.

There is no evidence that a hardware malfunction occurred. The collection of Cs-137, a particulate, is consistent with the designed operation of the station. Moreover, the HPGe data acquisition system worked well enough to be able to identify the Cs-137 peak and enable concentration quantification based upon the measured peak area.

4. Characterize Environment

Identify other sensors in the region

The radionuclide monitoring stations throughout the region are shown as white dots on the map in Figure 40. The detection site is indicated by the yellow triangle. Through these detection sites, it was revealed that the higher than normal Cs-137 concentrations were observed throughout Europe during this time period. The highest concentration was measured in France, at 2400 μBq/m3. The collection period for this sample lasted 8 days, from 25 May 1998 through 2 Jun 1998.

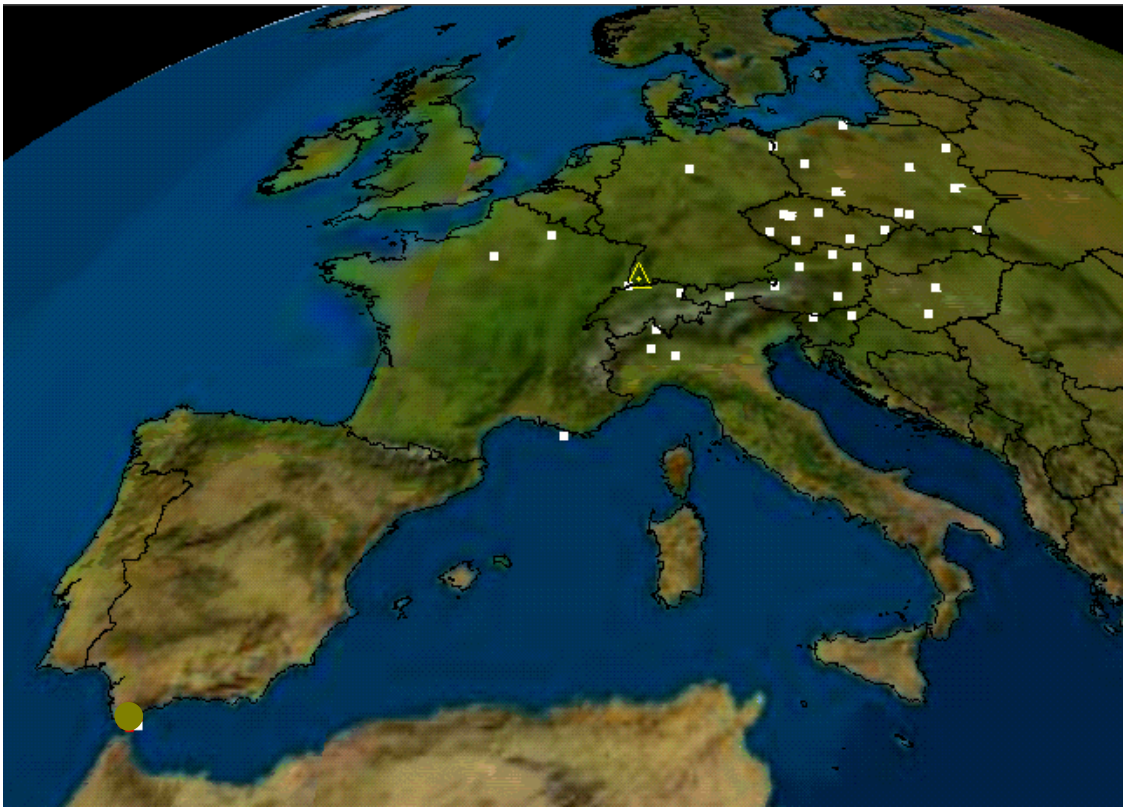

Figure 40: Radionuclide Monitoring Stations in Vicinity of Detection Site

Characterize natural environment

Characterize terrain

The detection site, shown in Figure 41, is located in a somewhat enclosed grassy area in the Black Forest. Trees approximately ten meters tall can be randomly found on the order of tens of meters from the station. Therefore, while there are no major impediments to airflow in the immediate vicinity of the monitoring station, no extended, laminar airflow paths are likely to intersect the station.

Figure 41: Immediate terrain of DE002 Collection Site

Considering Germany's Schauinsland and Black Forest regions from a broader perspective, they lie in the southwest corner of Germany. The region is sporadically covered with dense patches of pine and fir trees. The hundred mile stretch of rolling hills and mountainous land, which borders both Switzerland and France, lies along the eastern bank of the Rhine River. However, due to the terrain, the river's airflow does not govern the airflow in the immediate vicinity of the station. The highest peak in the region is Feldberg at 1495 meters. A relief map and a picture of this region are shown in Figures 42 through 44. The location of the German monitoring station relative to the French monitoring station that measured the high detection is shown in Figure 45.

Figure 42: Relief Map of Schauinsland and Black Forest Regions

Figure 43: Picture of Schauinsland and Black Forest Regions

Figure 44: Another Picture of Schauinsland and Black Forest Regions

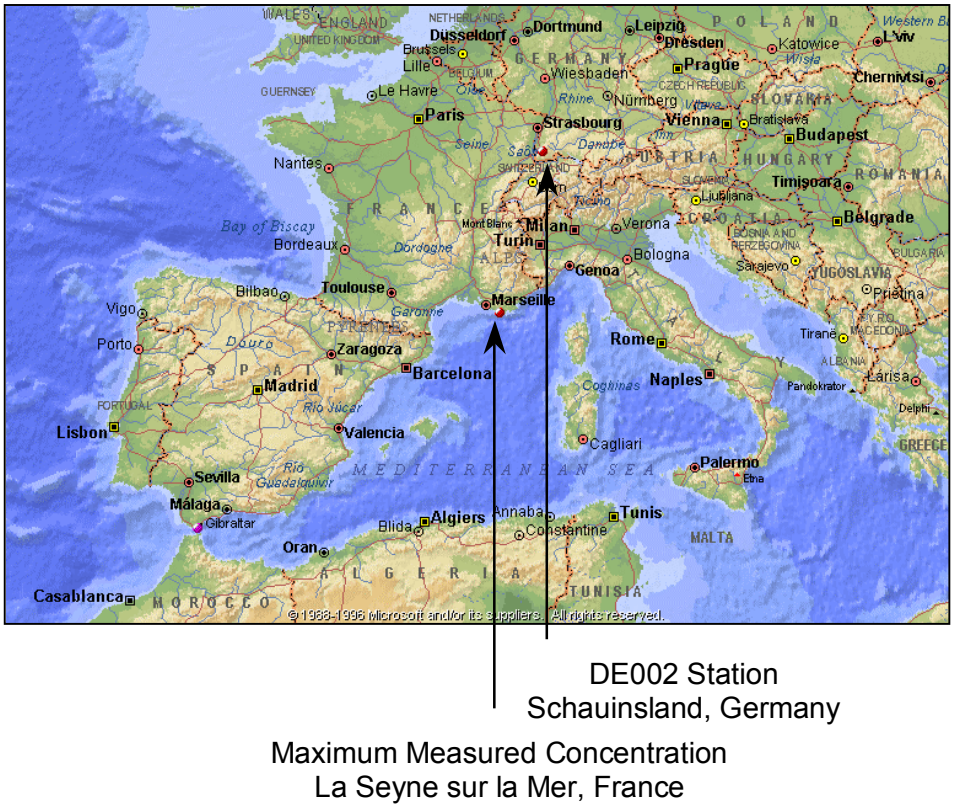

Figure 45: Location of German monitoring station relative to French monitoring station

Characterize meteorology to fullest extent possible

The meteorology of the region is characterized by rain in the late spring and summer months, during the time period of the anomalously high Cs-137 detection. June and July are the rainiest months during the year and the average annual rainfall in the area is approximately 1300 mm. Temperatures in this region are generally cool. July is the warmest month of the year with temperatures averaging 65^{O}F.

Draw preliminary conclusions based upon environmental determinations

Because of the 7 day radionuclide collection period at the DE002 station, very little insight into the source location is gained through meteorological modeling. Figure 46 shows the OMEGA meteorological model's assessment of the likely source region based upon the wind trajectories during the 7 day collection period. The region clearly extends into central Europe. In addition, it stretches into the Atlantic Ocean and into Africa; however, these areas were simply cropped by the display.

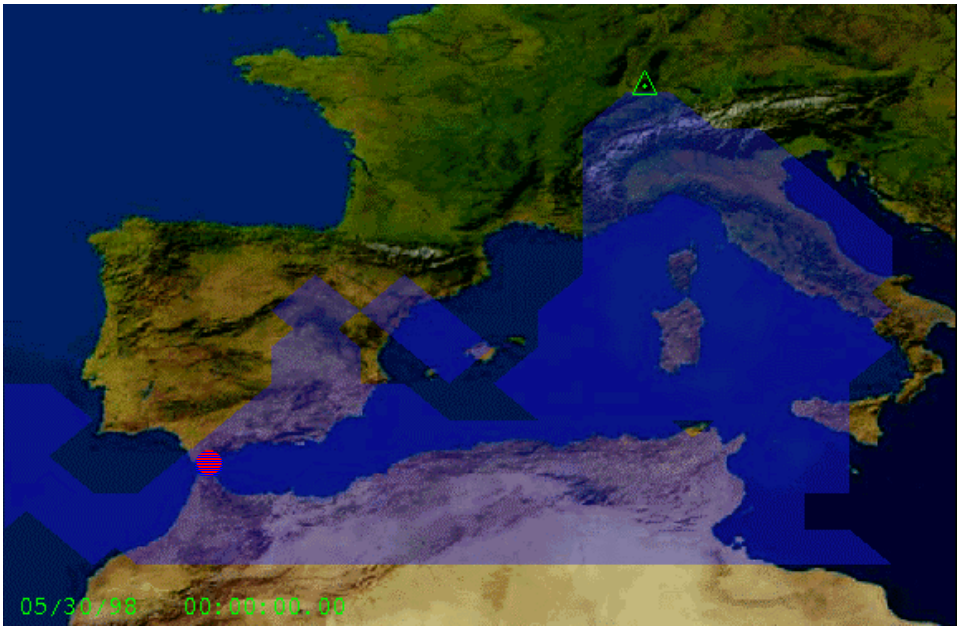

Figure 46: 7 day Field of Regard based upon June 8, 1998 Cs-137 Detection at DE002 (shown as Green Triangle)

Given that plumes tend to dilute as they traverse, because of the airborne concentration measured in France that was two orders of magnitude higher than the DE002 concentration measured, there is a good chance that the French station is closer to the source location than the German station. A secondary conclusion based upon this fact, and the fact that the French station's collection time ended towards the beginning of the DE002 collection time, is that the emission likely did not begin during the end of the DE002 radionuclide collection period. Therefore, the emission probably occurred on or before June 6, 1998 (a date arbitrarily chosen at 48 hours prior to the end of the DE002 air sampling time). If the emission was from an instantaneous puff source, then it probably occurred towards the overlapping periods of the sampling times, maybe between May 30 and June 2, 1998. On the other hand, if the emission was from a continuously emitting source, then it may have begun towards the end of the French

detector's collection period and ended during the German station's collection period, possibly from May 30 through June 6, 1998. These relationships are shown in Figure 47.

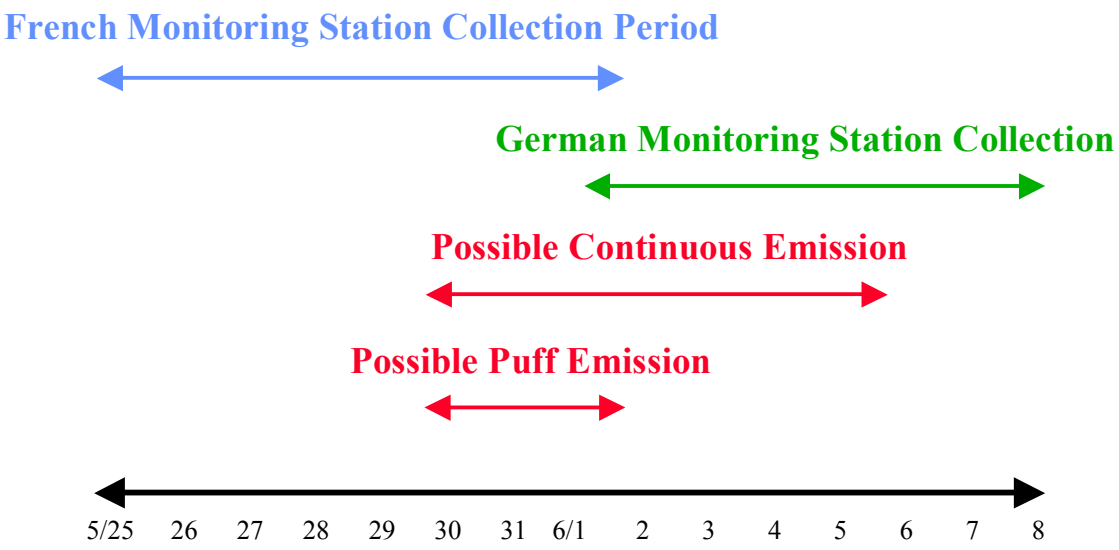

Figure 47: Relationships between Collection Periods and Possible Emission Periods

Considering the continuous emission possibility, the relevant collection period for the DE002 monitoring station ranges from June 1 (the start of the DE002 collection period) through June 6 (the end of the postulated emission period). Considering this adjusted time period, the corresponding regions of likely emission sources change from the ones shown in Figure 45 to those shown in Figure 48.

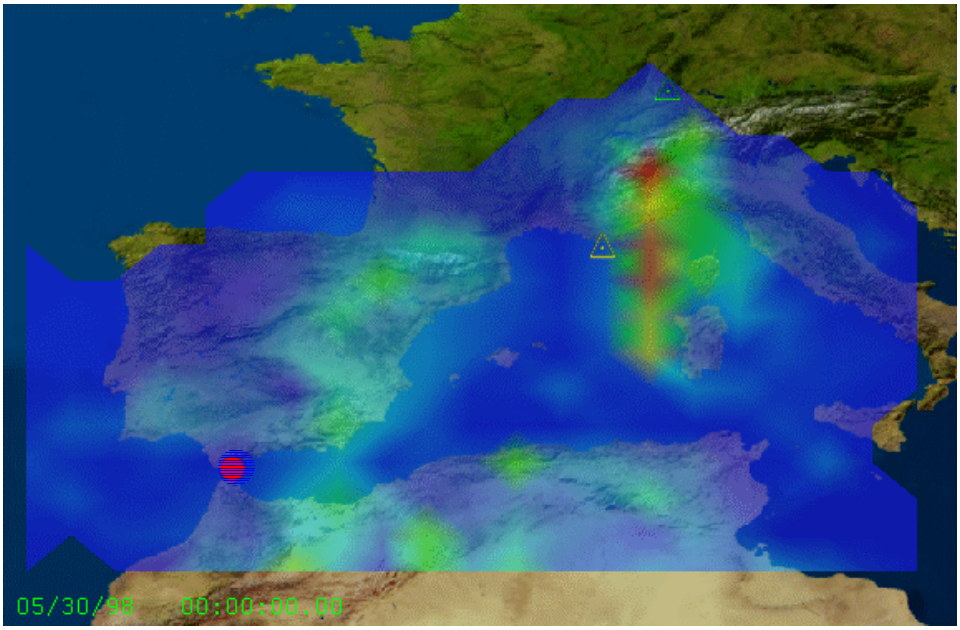

Figure 48: Field of Regard based upon postulated June 1 through June 6, 1998 Cs-137 Detection at DE002 (shown as Green Triangle)

Similarly, the continuous emission source regions for the French monitoring station, which corresponds to the dates May 30 through June 2, 1998 are shown in Figure 49.

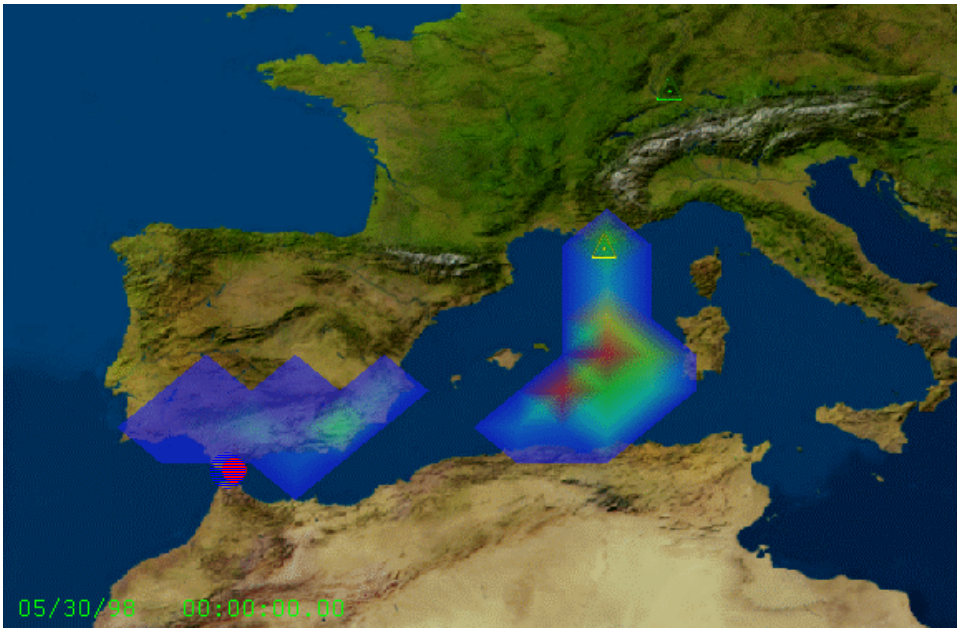

Figure 49: Field of Regard based upon postulated May 30 through June 2, 1998 Cs-137 Detection at DE002 (shown as Yellow Triangle)

Because the postulated continuous emission includes the entire time period from May 30 through June 6, 1998, the likely source term regions can be represented by superimposing the German and French monitoring stations (Figures 48 and 49). This superimposition is shown as Figure 50.

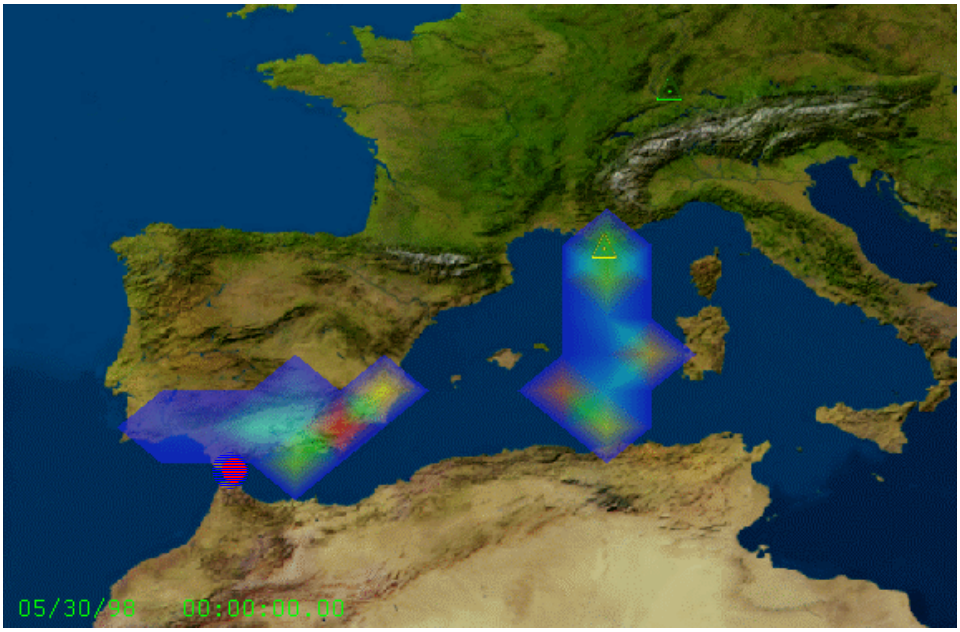

Figure 50: Combined Field of Regard based upon German and French continuous emission Fields of Regard

The same compound display of likely source regions (Figure 53) can also be derived for the instantaneous puff emission assumption. This can be accomplished by combining the postulated puff source regions from the German monitoring station (Figure 51) and the French monitoring station (Figure 52), both assumed to be 24 hours long.

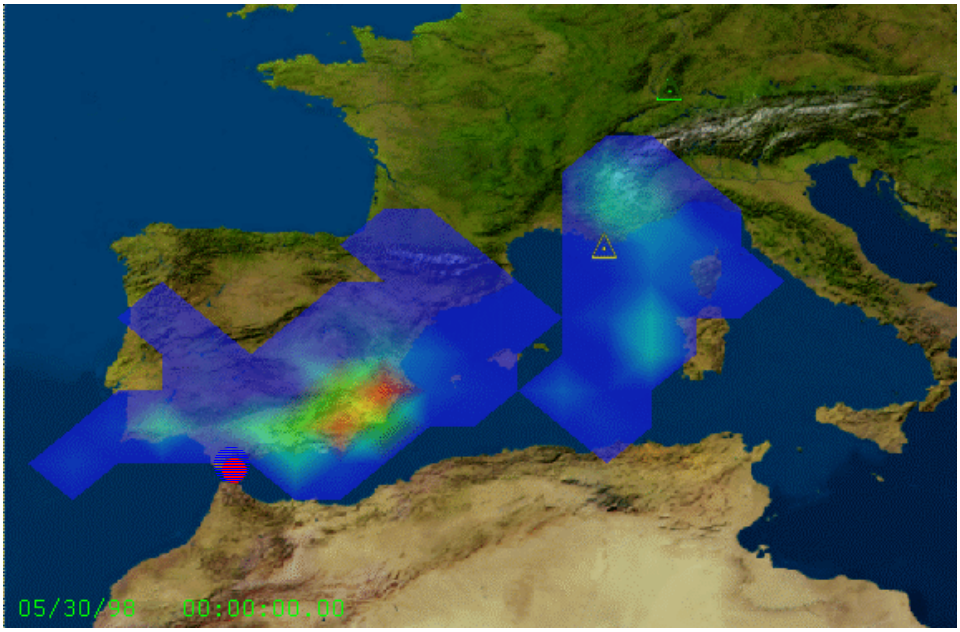

Figure 51: Field of Regard based upon postulated puff emission of Cs-137 Detection at DE002 (shown as Green Triangle)

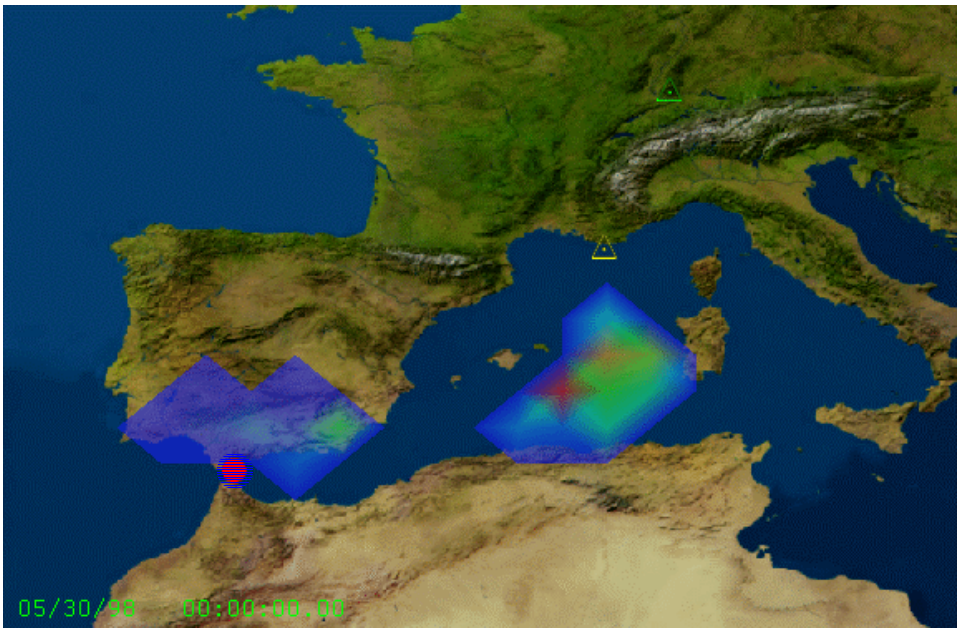

Figure 52: Field of Regard based upon postulated puff emission of Cs-137 Detection at French Monitoring Station (shown as Yellow Triangle)

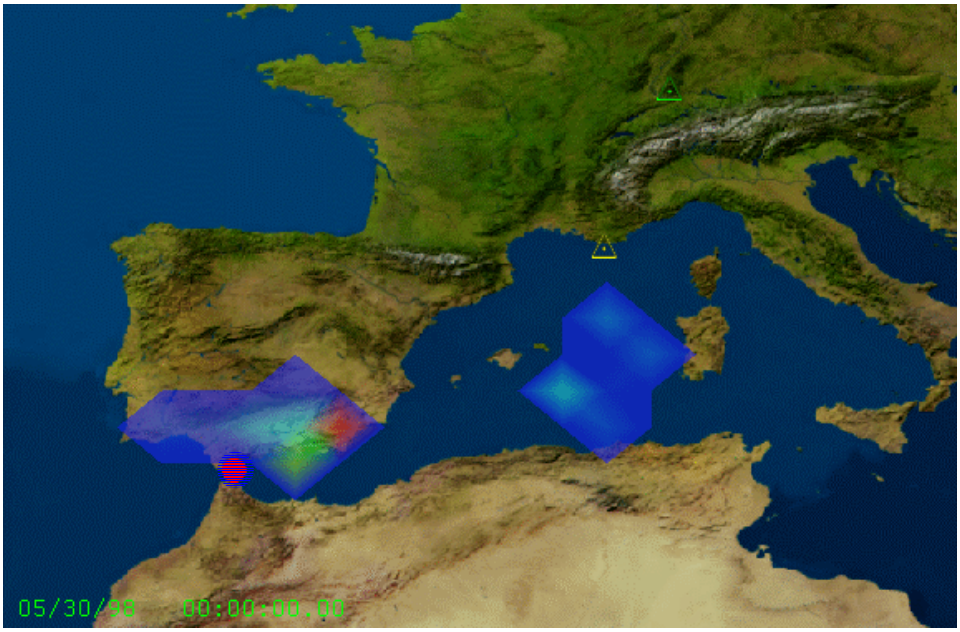

Figure 53: Combined Field of Regard based upon German and French puff emission Fields of Regard

It is interesting to note that the only land mass essentially identified as a source region exists in southern Spain.

Based upon the meteorological analysis performed, depending on the postulated emission duration and start date, several source regions are reasonable candidates. If we consider the region indicated through meteorological analysis related to the week long German monitoring station detection, then the source region includes portions of Europe, Africa and the Atlantic. If we consider a continuously emitting source that influenced both the French and German monitoring station detections, then we may be looking at a smaller region, including a small section of south central Europe and much of southern Spain. Finally, if we consider a more instantaneous puff source, then the source region includes

even a smaller section of southern Spain. However, at this point, no potential source facilities have been identified.

Identify potential radionuclide emission sources

The list of radionuclide sources initially considered includes the over one thousand sources throughout Europe. A representative sample is shown in Appendix 6. These facilities include nuclear power reactors, nuclear research reactors, nuclear research facilities, and hospitals that may use radioactive sources in patient care. Because plotting all of these facilities on a figure would be difficult to interpret, a representative subset is included in Figures 54 and 55. In addition to the nuclear facilities shown in Figure 54, an African seismic event is shown as well. This is shown in the event that it might be correlated with a nuclear detonation.

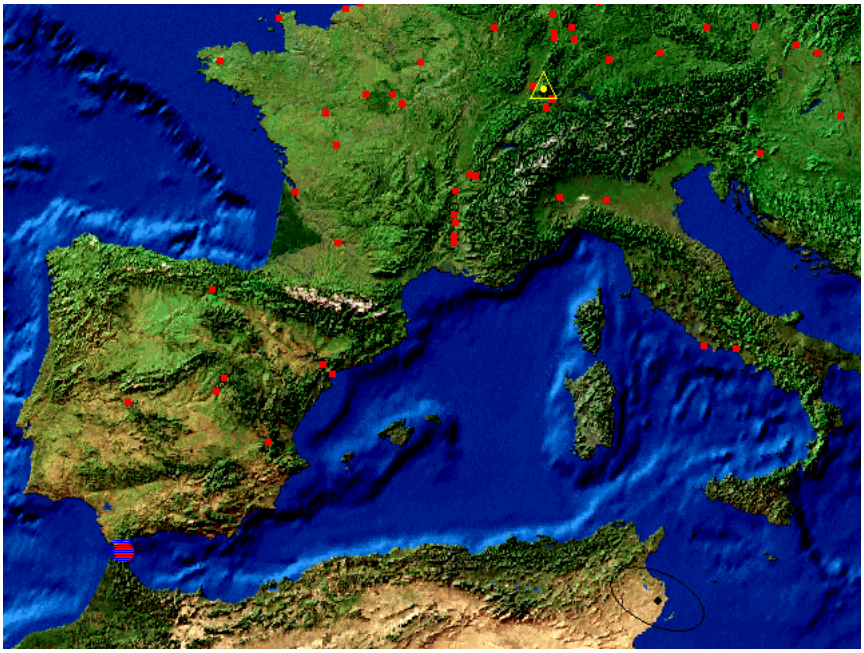

Figure 54: Representative Distribution of Candidate Radiological Emission Sources

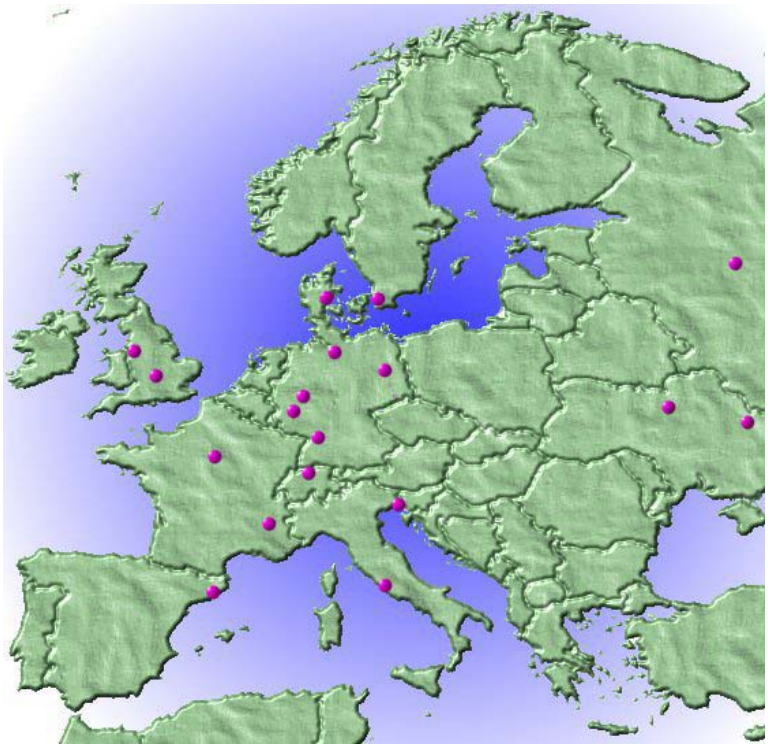

Figure 55: Selected Nuclear Research Facilities in Europe

5. Characterize Possible Sources

Recall that the Cs-137 was detected in isolation with no other fission products. The overwhelming majority of the facilities listed as candidates are nuclear reactors, which would emit other fission products along with a Cs-137 emission. So these reactors are likely not the source of the Cs-137 detected. Similarly, it is unlikely that a hospital would emit the type of Cs-137 concentration that was detected in France. Therefore, the hospitals probably are not the source either. Moreover, because Cs-137 is a neutron rich isotope, it is unlikely that any of the accelerator facilities, which generally produce neutron depleted nuclides, are the source. Thus, out of the over one thousand candidate radionuclide source facilities throughout Europe, none are likely.

6. Develop Characterizations of Possible Sources

Identify physical parameters relevant to emission

While there are no likely candidate sources that can be analyzed in greater detail at this point, certain features associated with the release can be more definitively determined. Based upon the high concentration measured at the French monitoring station, and the stark reduction in concentration by the time the plume reached the relatively nearby German monitoring station, it is likely that the emission originated from a source relatively close to the French monitoring station (i.e., from a European or North African coastal location) at a time more conducive to the French station's detection schedule (between May 25 and June 2, 1998). However, it is also possible that the plume originated at a time closer towards the end of the French monitoring station's collection periods and the beginning of the German station's collection period. If this was the case, then the stark difference in concentrations could simply be the result of the difference in terrain of the two stations. According to Figure 45, the French station is located on the Mediterranean coast, easily accessible to most plumes in the region, while the German station is located in the mountainous forest and may be less accessible to plumes. Based upon these chronological considerations, the chronologies and source regions postulated in Section 4 seem reasonable.

The plume may have been emitted at above ambient temperatures or with substantial momentum or internal energy. Otherwise, the plume might not have had the buoyancy needed to pass above the mountains to be detected by the German station.

Because the French monitoring station likely registered the Cs-137 plume prior to the German monitoring station (based upon the sampling schedules of the two stations), and the French station measured a concentration so much higher than the German station, it is likely that the plume was traveling from south to north. More confidence in the extrapolated detection chronology yields the possibility that the plume was traveling from southwest to northeast.

Incorporate related data

In an effort to validate or eliminate some of the numerous estimations and assumptions made to this point, it is useful to incorporate additional data -- even data that is merely tangentially relevant -- that can add credibility to the suppositions or refute them. Throughout the analysis, the two governing sets of assumptions have been associated with the chronology of the release and the likely location of the release. Because these two sets of assumptions are not independent, the most logical way to investigate them is to begin with the most restrictive chronological and geographical parameters, and work outwards to scenarios with broader parameters. Ultimately, associated data regarding the entire European continent may be incorporated if sufficiently relevant data are not discovered earlier.

The most restrictive chronological and geographic case involves an instantaneous emission that occurred towards the end of the French stations monitoring period and the beginning of the German stations monitoring period -- a total of 48 hours. The corresponding terrestrial source region includes only southern Spain (Figure 53). An

interesting series of news and technical reports from this time period and region revealed that a Cs-137 emission had taken place on May 30, 1998. Representative reports and excerpts are shown in Appendix 7. According to the reports, a Cs-137 source of at least one Curie had inadvertently been smelted in a batch of scrap metal at the Acerinox Plant in Algeciras, Spain (Figure 56). Although radiation detectors are present at the land and sea entrances of the facility to prevent radioisotopes from entering, the sea based radiation detector had been inoperable since May 25, 1998. Therefore, it is possible that the Cs-137 entered through this entrance unbeknownst to the operators. Based upon this information related to the timely Acerinox smelting facility accident, it is likely that the facility is the source of the plume emission that was detected.

Acerinox Plant
Algeciras, Spain

Figure 56: Location of Cs-137 Likely Plume Emission Source

7. Most Likely Chain of Events

Because only one viable alternative exists, Section 7 (Use Source Characterizations and Natural Environmental Data to Estimate Chains of Events from Most Likely Sources), Section 8 (Use Estimated Chains of Events to Determine Most Likely Radionuclide Emission Source), and Section 9 (Recreate Most Likely Chain of Events) can be combined. Therefore, Sections 8 and 9 will not appear as separate sections.

The chain of events for this case study is relatively straight forward. A Cs-137 source of at least one Curie entered a Spanish smelting facility located on the southern coast of Spain and was smelted with a batch of metal on May 30, 1998. During the smelting process, Cs-137 effluents were ejected into the atmosphere and were carried towards the northwest. These effluents were subsequently detected by the DE002 German radionuclide monitoring station and many other European radionuclide monitoring facilities. While Cs-137 was the only radionuclide detected at the DE002 monitoring station, the analysis showed that it indeed was the only radionuclide present.

Chapter V: CASE STUDY 3 -- COMPLICATED RADIONUCLIDE ANALYSIS

Highlights

Section 1, Initial Condition: The initial condition was the detection of several anomalous gamma-ray peaks that could not be associated by the automated processing system measured at a radionuclide detection facility in Charlottesville, Virginia. The spectrum was clearly an inauthentic sample prepared to test the capabilities of the human analysts and computational models in use at the Prototype International data Center, the data processing headquarters for the Comprehensive Test Ban Treaty.

Section 2, Validate and Superficially Correct Data: One novelty of this model revealed in this section is its utility in perform complicated radionuclide analysis without computational models. In addition, although the manual implementation of this model is more labor intensive than its computational counterparts, it is shown to reveal more information.

Sections 3 - 9 were not needed in order to complete this analysis.

1. Initial Condition -- Obtain Radionuclide Data Measurement

The initial condition for this case study occurred on June 9, 1997 when several anomalous gamma-ray peaks were measured in addition to the peaks customarily present within spectra at the US001 monitoring station located on the campus of the University of Virginia in Charlottesville, Virginia. Because of the combination of typical and atypical spectral features, this spectrum was clearly a manufactured test spectrum sent to evaluate

the abilities of the analysts and the computational models in use at the Prototype International Data Center, the data processing headquarters for the Comprehensive Test Ban Treaty. The total number of gamma-ray peaks identified was four times the normal amount -- a total of 120 peaks. All of the customary peaks appeared to be present along with several associated with fission products of U-235. The majority of peaks present were not associated with radionuclides.

2. Evaluate Accuracy of Measurement, Highlight Anomalies, and Make Superficial Corrections as Needed

Much of the relevant data regarding this anomalous spectrum was not preserved so evaluating the accuracy of the accompanying data is not possible. However, a preliminary analysis may prove to be revealing.

Given that U-235 and a number of fission products were identified as present, it may be instructive to determine whether some of the other unidentified gamma-ray peaks are associated with fission products. As a matter of fact, if the sample is associated with the fission of U-235, then the set of radionuclides present is well defined according to the U-235 fission yields associated with the chart of the nuclides. Although the process would be highly involved, the fission products present and those identifiable can be calculated by hand. The hand calculations used determine the radionuclides present are included within Appendix H.

Based upon the U-235 fission yield abundance for each mass family of fission products and the half-lives of the radionuclides in each family, the fission product radionuclides that should have been identified are shown below.

Table 31: Radionuclides that Should Have Been Present

Typical Radionuclides Present
Be-7
K-40
Th-232 Series
Ac-228
Pb-212
Bi-212
Tl-208
Th-234
Bi-214
Ra-226
Anthropogenic Radionuclides Present
Sr-91
Y-91m
Y-93
Zr-95
Zr-97
Nb-97

Mo-99
Tc-99m
Ru-103
Rh-105
Te-131
Te-131m
I-131
Te-132
I-132
I-133
Xe-133
I-135
Xe-135
Ba-140
La-140
Ce-141
Ce-143
Pm-151
Sm-153

The presence of these radionuclides was confirmed by the computational models used to analyze the spectra. However, since the computational models are void of human judgment, they are unable to determine any additional information. On the other hand, as

the Appendix 8 derivation shows, several other radionuclides are identified as possibly present. These radionuclides are shown below.

Table 32: Additional Radionuclides:

Anthropogenic Radionuclides Possibly Present
Nb-95
Nb-98
Ru-105
Xe-133m
Xe-135m
Nd-147
Pm-149

The origin of the radionuclide sample analyzed is known to be inauthentic, and the radionuclides known to be and possibly present have been identified. Therefore, there is no need to continue analysis through the environment, possible sources, and chains of events. As a result, no additional sections will be evaluated within this case study.

Chapter VI: CASE STUDY 4 -- ERRANT DATA PROCESSING

Highlights

Section 1, Initial Condition: The initial condition was the detection of several anomalous gamma-ray peaks that could not be associated by the automated processing system measured at a radionuclide detection facility in Charlottesville, Virginia.

Section 2, Validate and Superficially Correct Data: The model novelty revealed in this section is the model's ability to process errant data to generate an accurate conclusion. Automated processes that attempted to determine the cause for the atypical peaks were unable to do so. A senior radionuclide modeler was quoted as saying "garbage in, garbage out." In many cases, the model developed is able to process inaccurate or incomplete data as if it were valid.

Sections 3 - 9 were not needed in order to complete this analysis.

1. Initial Condition -- Obtain Radionuclide Data Measurement

The initial condition for this case study occurred on May 27, 1997 when several anomalous gamma-ray peaks were measured in addition to the peaks customarily present within spectra at the US001 monitoring station located on the campus of the University of Virginia in Charlottesville, Virginia. The total number of gamma-ray peaks identified was twice the normal amount -- a total of 30 extra peaks. Table 33 lists all of the peaks that were identified within the spectrum. In addition, the table contrasts the gamma-rays generally present in US001 spectra with the atypical peaks that serve as the initial

conditions for this case study. An additional anomaly with this spectrum was that the peaks typically measured in US001 spectra appeared to be present, but with much lower peak areas.

Table 33: Gamma-Rays Present in US001 Spectrum

Generally Present Peaks	**Atypical Peaks**
Energy (keV)	Energy (keV)
238.56	
	241.18
252.67	
277.30	
	280.31
288.16	
	291.09
300.05	
	303.37
327.96	
	355.65
452.90	
	457.76
477.61	
	482.85

510.77	
	516.37
583.21	
	589.61
609.41	
	615.96
727.37	
	735.35
763.46	
	771.91
785.58	
	794.12
860.58	
	870.06
893.42	
	903.24
	921.29
951.96	
	962.58
	968.50
1078.89	
	1090.66
1093.76	

	1105.82
1119.84	
	1132.95
	1194.04
1460.79	
	1476.75
1512.81	
	1529.33
1592.53	
	1609.98
1620.66	
	1638.36
	1649.62
1764.06	
	1783.95
2103.28	
	2126.34
2614.42	
	2643.11

2. Evaluate Accuracy of Measurement, Highlight Anomalies, and Make Superficial Corrections as Needed

Much of the relevant data regarding this anomalous spectrum was not preserved, so evaluating the accuracy of the accompanying data is not possible. However, it is interesting to note that most of the typical and atypical peaks seem to occur in an alternating pattern. Closer scrutiny of the spectrum clarifies the pattern even further. A number of Type I and Type II peaks are present in this spectrum. These peaks seem to be the ones that disrupt the apparent pattern. If they are corrected, additional information about the pattern may be revealed. The type I errors include false peaks identified at 921.29 keV, 968.50 keV, 1194.04, and 1649 keV. The Type II errors include gamma-rays with energies 255.9 keV (atypical), 331.4 keV (atypical), and 351.9 keV (typical). Removing the Type I errors from Table 33 and including the Type II errors results in a pattern consistent throughout the entire spectrum.

Besides the simple pattern of alternating typical and atypical peaks, a more advanced pattern appears to be present. As the peak energies increase, the spacing between each atypical peak and its closest lower energy neighbor (a typical peak) seem to steadily increase. As a matter of fact, simple mathematical analysis reveals that all of the atypical peaks are located at energies that are 1.097% greater than their lower energy neighbors. Therefore, the simple solution to the anomalous detection is that a gain shift occurred during counting.

Because the cause for the anomalous detection has been identified, there is no need to continue analysis through the environment, possible sources, and chains of events. As a result, no additional sections will be evaluated within this case study.

Chapter VII: CONCLUSIONS

This study effectively developed and validated a radionuclide analysis model that relates the generation, emission, transport, collection, and measurement of anomalous anthropogenic radionuclides. The principal difference between this model and existing models is that this model integrates human judgment throughout the entire analytical process. Because of this revolutionary new approach in analysis, this model has several distinguishing features that set it apart from existing models. This list of features, each of which was demonstrated through one or more of the four case studies, includes the model's ability to:

- thoroughly characterize radionuclide sites while other models are limited to merely interpreting measured data;
- effectively process both quantitative and qualitative data, as compared to existing models, which are only able to effectively address quantitative data inputs;
- analyze complex radionuclide data without computational models; and
- compensate for errant and incomplete data during processing, as opposed to other models that generate errant results if the input data is not complete and accurate.

As a result of these features, this model offers many associated benefits. One benefit of the model is that it standardizes the radionuclide analysis process, which enables analysts of varying experience levels to normalize their assumptions and comprehensive consideration of relevant data. The primary effect of this benefit is that junior level analysts are able to perform senior level analysis to develop meaningful, accurate results. Another useful feature of this model is that it enables definitive conclusions to be reached

through analysis since it allows for the incorporation of qualitative, "ground truth" data. Through this model, radionuclide analysis output that is more comprehensive, accurate, and precise can be achieved. The development of this model represents a meaningful advancement in the state of the art.

Appendix A: GRAPHICAL DEPICTIONS OF SPECTRAL FILES

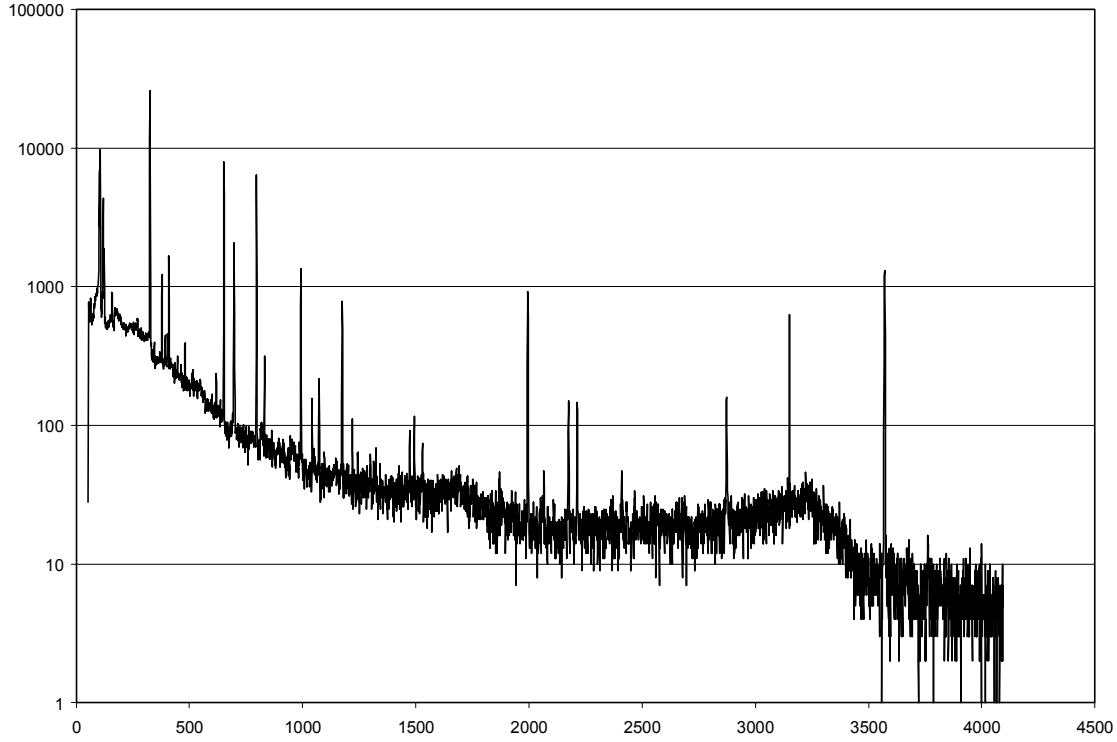

Figure A1: CA002 Spectrum Collected 14 March 2004

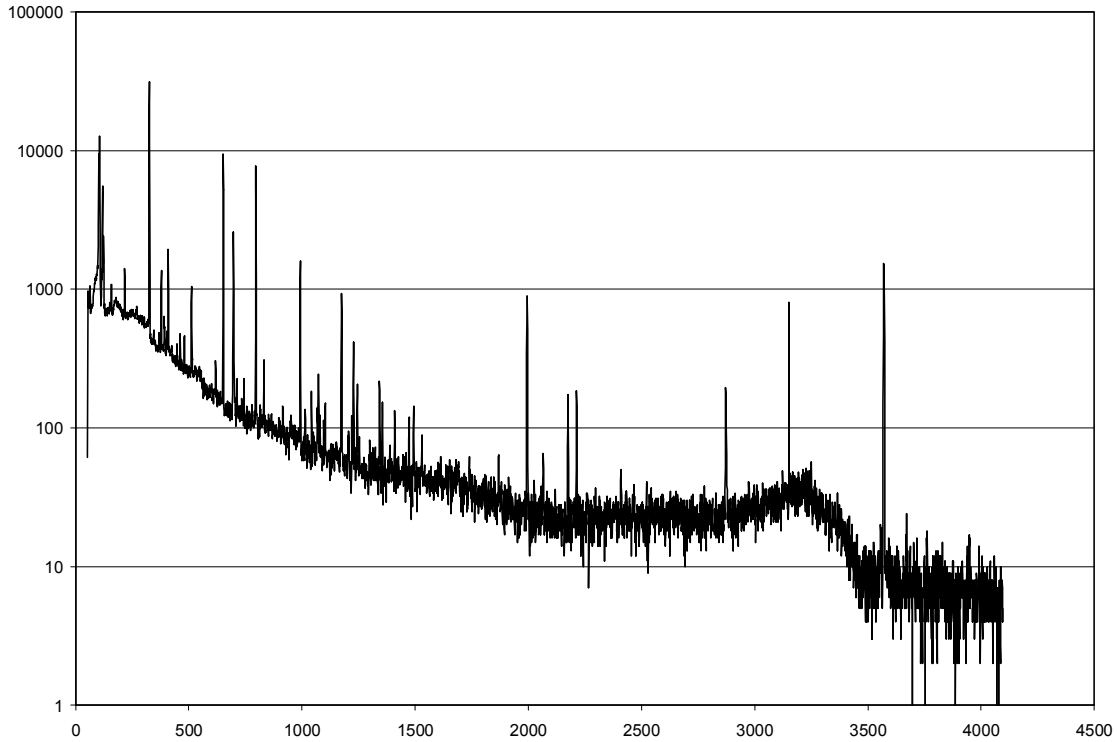

Figure A2: CA002 Spectrum Collected 15 March 2004

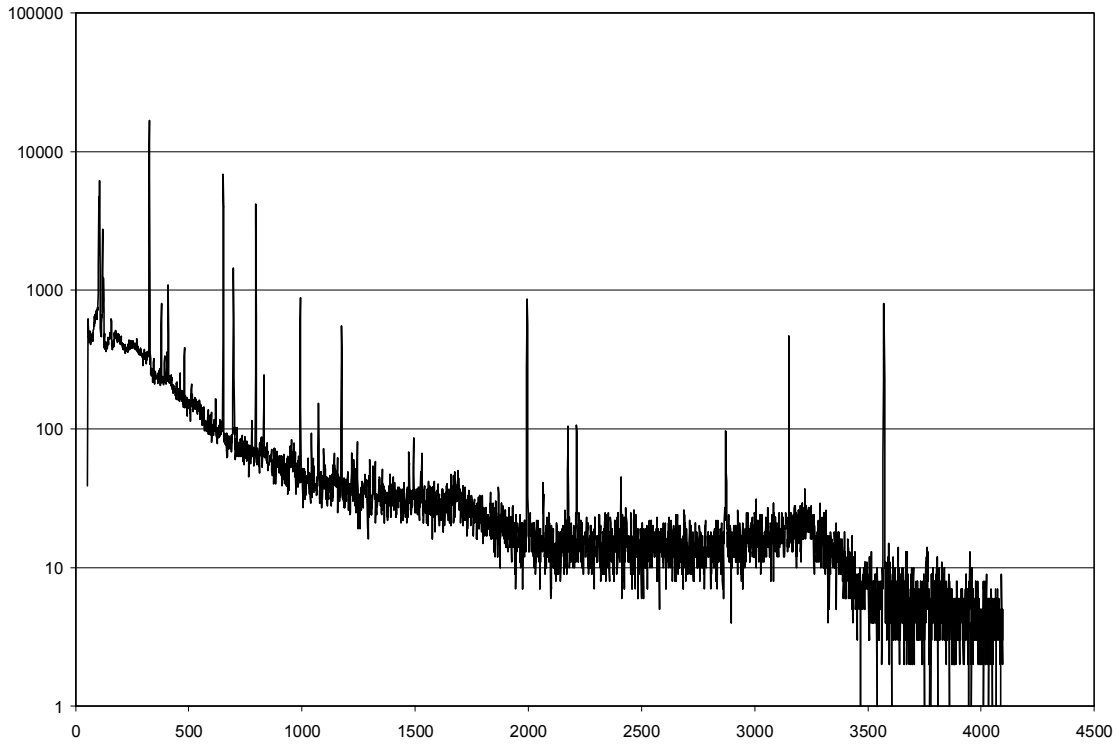

Figure A3: CA002 Spectrum Collected 16 March 2004

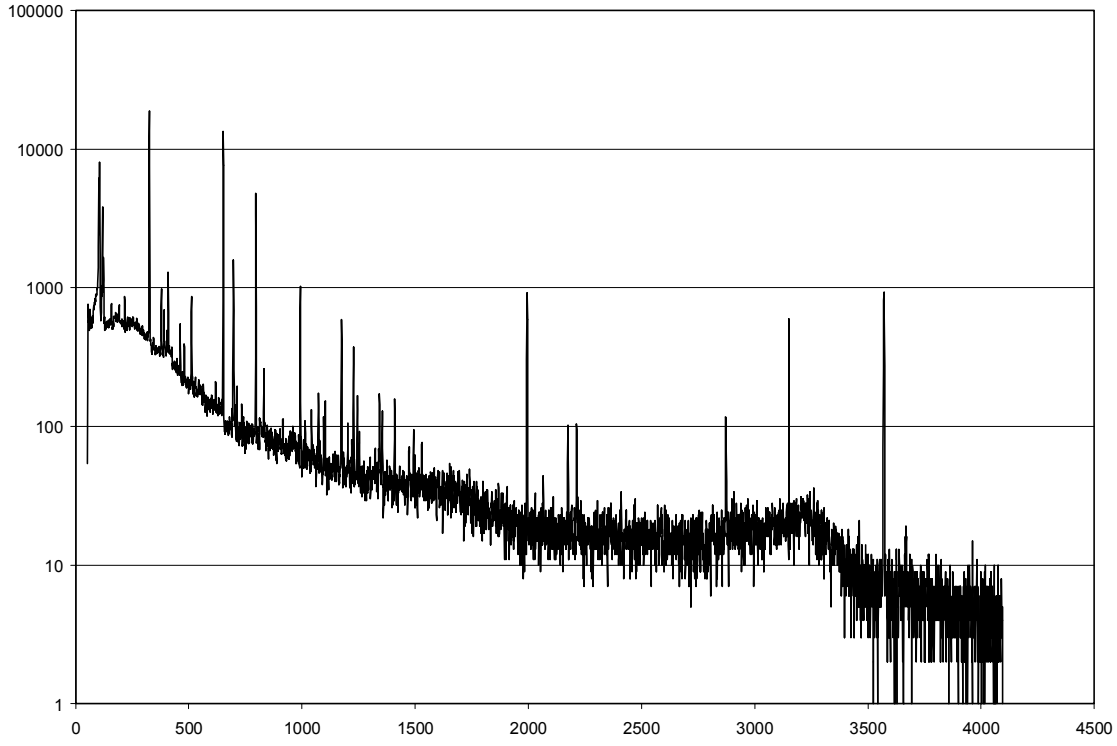

Figure A4: CA002 Spectrum Collected 17 March 2004

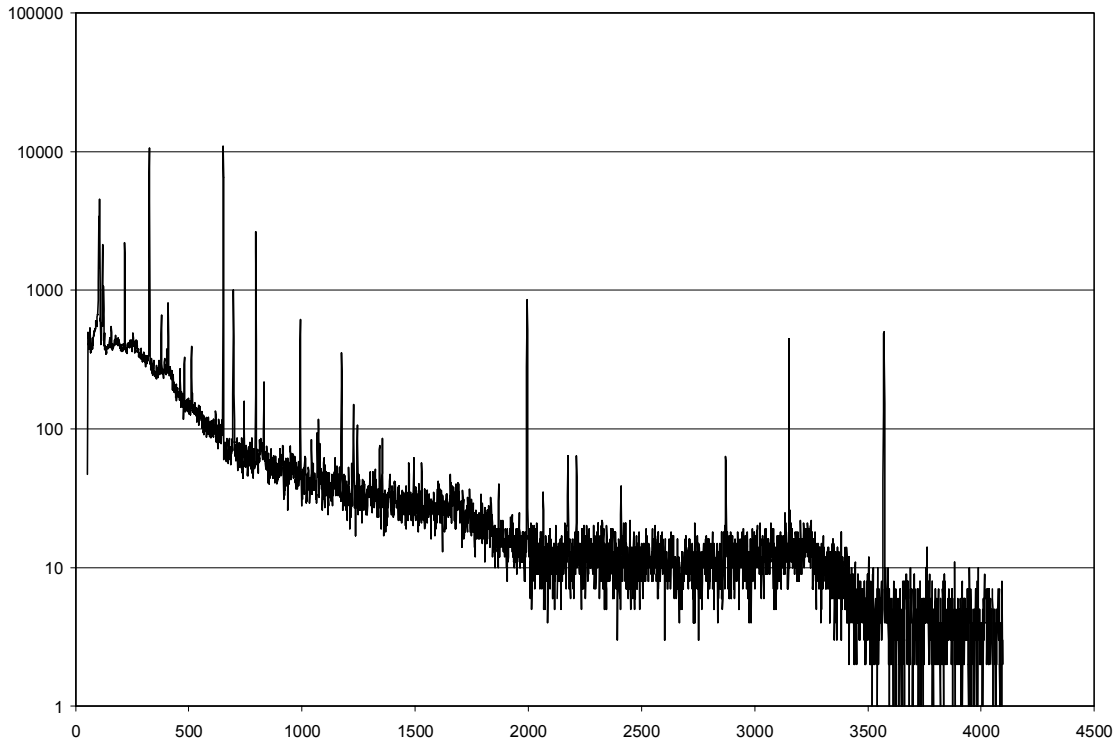

Figure A5: CA002 Spectrum Collected 18 March 2004

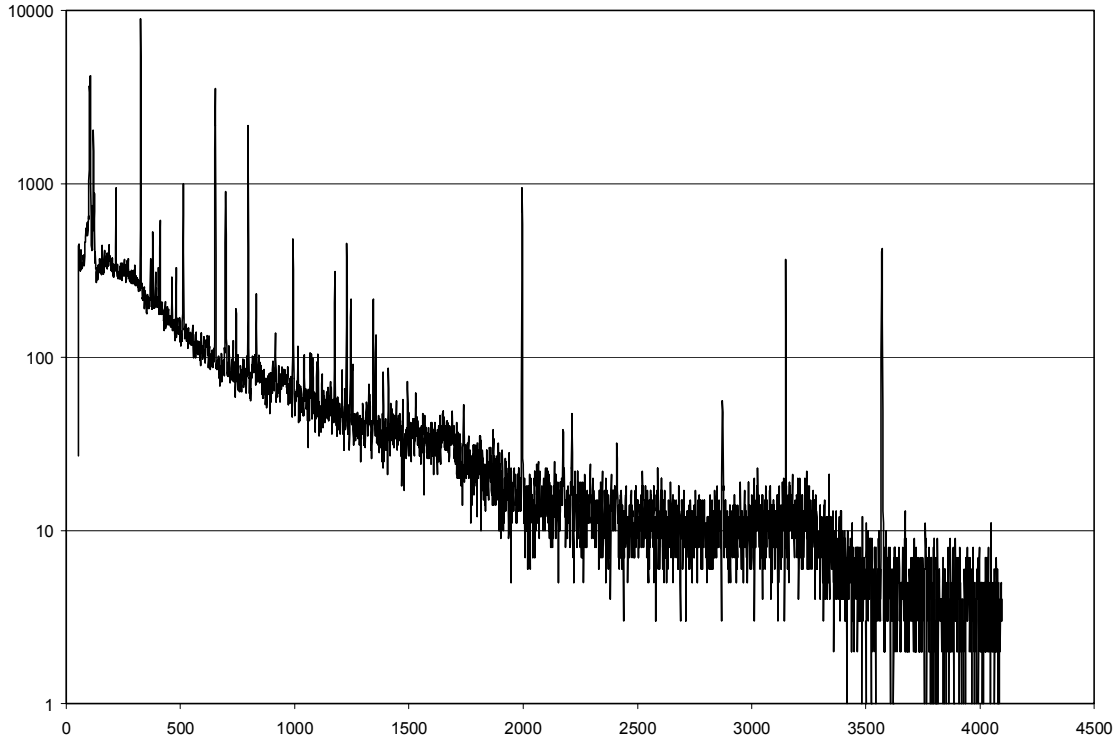

Figure A6: CA002 Spectrum Collected 19 March 2004

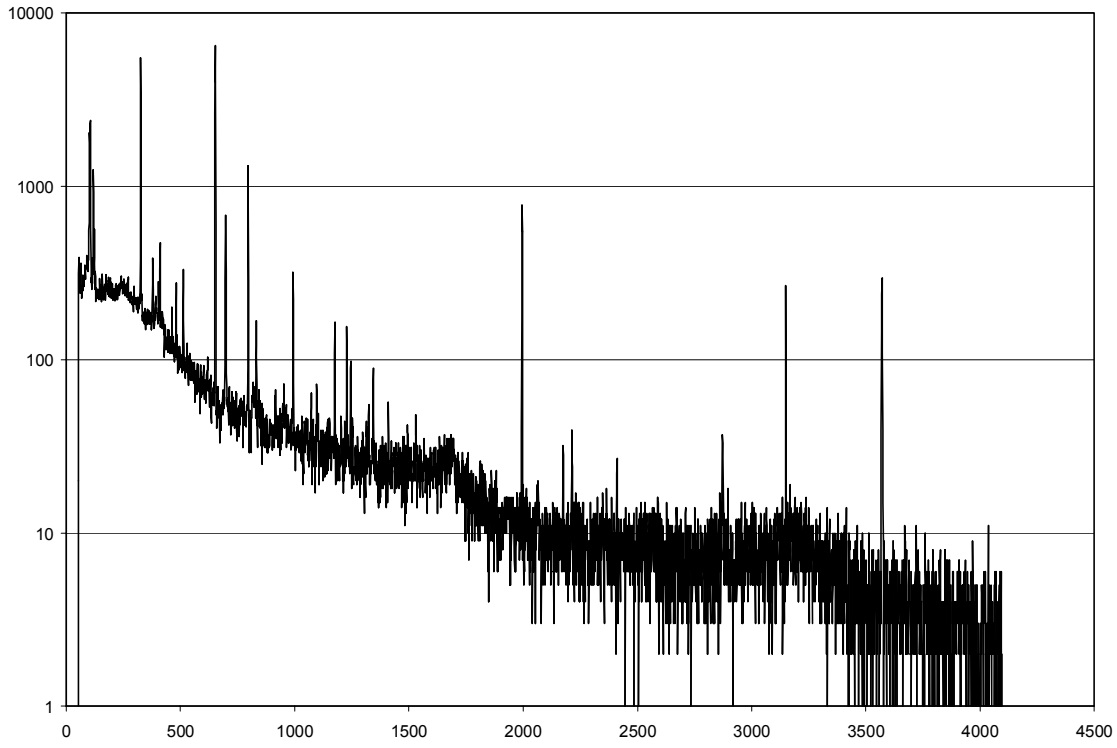

Figure A7: CA002 Spectrum Collected 20 March 2004

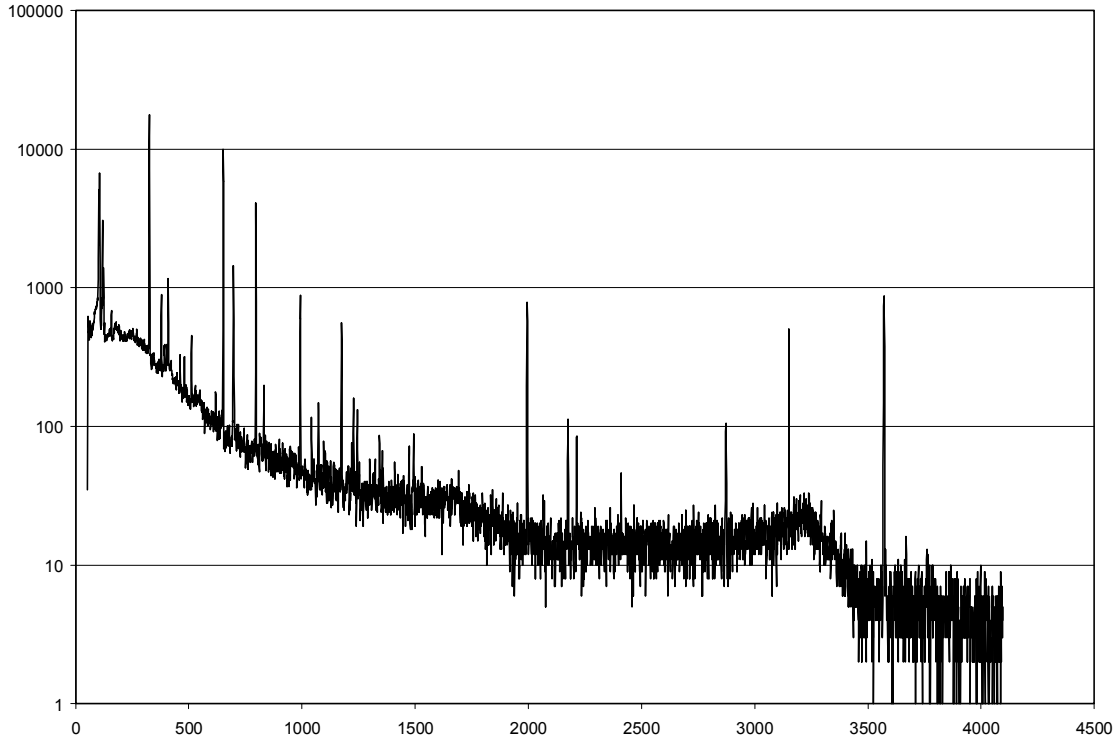

Figure A8: CA002 Spectrum Collected 21 March 2004

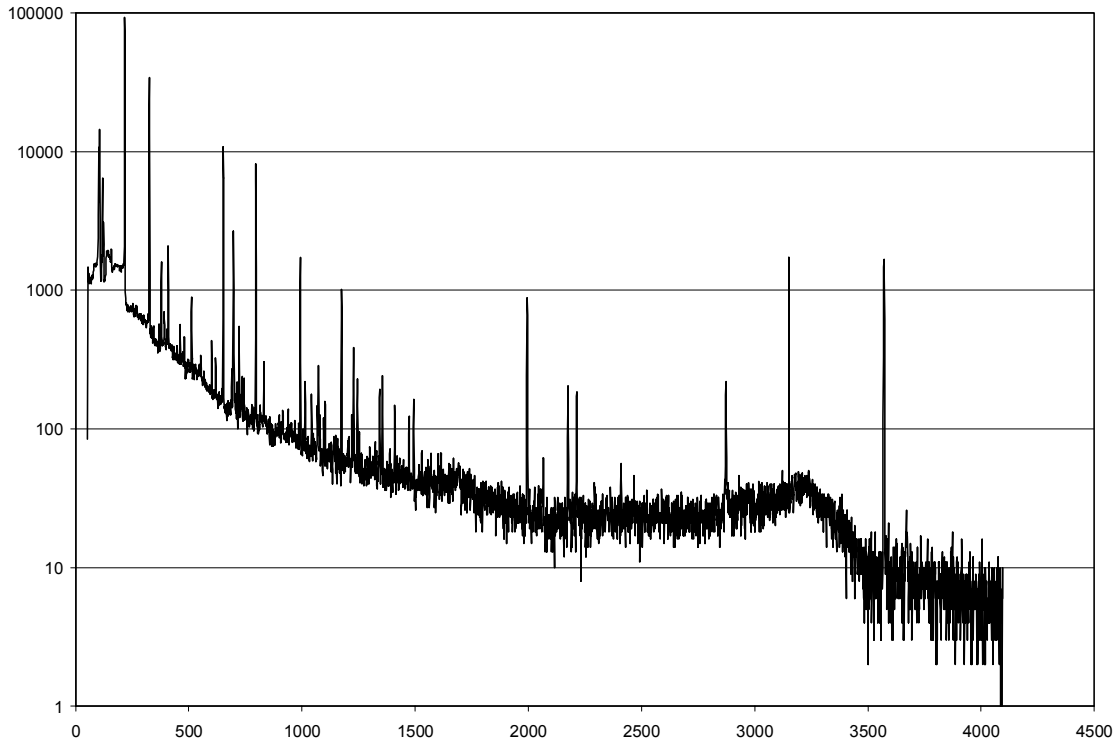

Figure A9: CA002 Spectrum Collected 22 March 2004

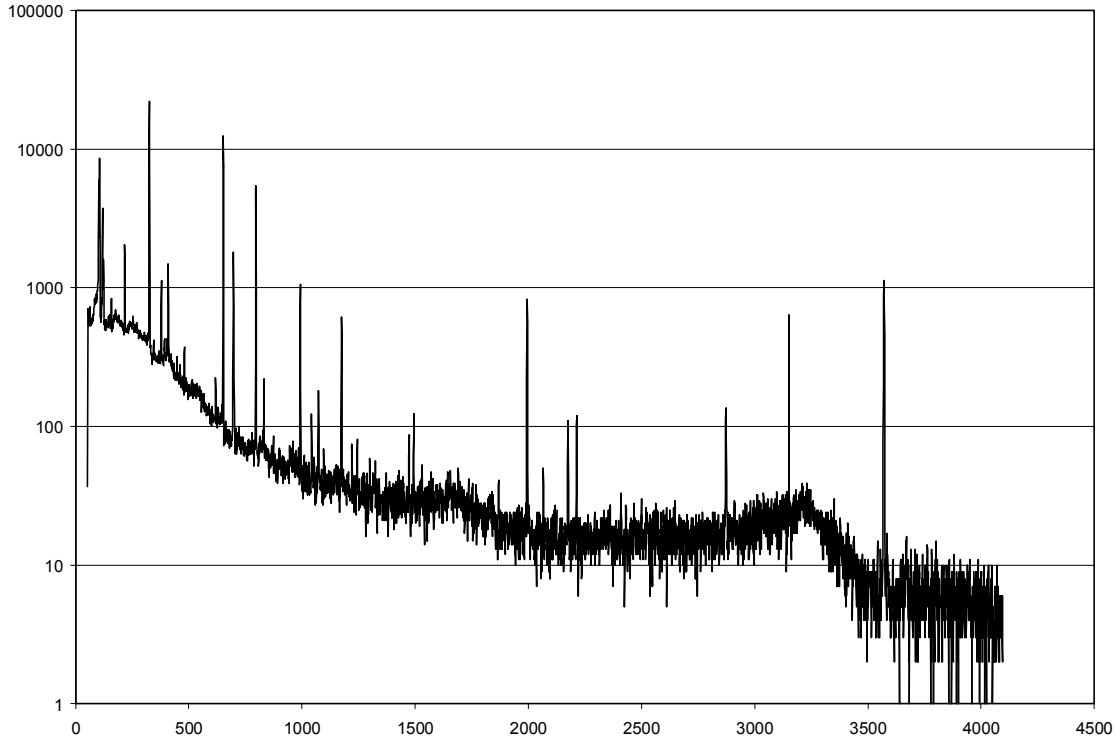

Figure A10: CA002 Spectrum Collected 23 March 2004

Appendix B: CA002 ATMOSPHERIC RADIONUCLIDE MONITORING REPORTS DURING PERIOD IN QUESTION

ATMOSPHERIC RADIONUCLIDE MEASUREMENT REPORT
Particulate Version

SAMPLE INFORMATION==========

Station ID:	CA002	Detector ID:	CAA2
Station Type:	ISAR2	Detector Type:	

Station Location: Vancouver, Canada
Detector Description: Detector A in Vancouver, Canada

Sample ID:	0022595	Sample Geometry:	DISK
Sample Quantity:	23689.00 m3	Sample Type:	Filter

Collection Start:	1997/03/13 18:30	Sampling Time:	24.17 hours
Collection Stop:	1997/03/14 18:40	Decay Time:	4.26 hours
Acquisition Start:	1997/03/14 22:55	Acquisition Time:	19.50 hours
Acquisition Stop:	1997/03/15 18:25	Avg Flow Rate:	980.10 m3/hr

Collection Station Comments:
goshka - Detector 1 Ranger (14-MAR-1997)

IDC Analysis General Comments:
Calibration Update Performed. Certificate file
/data/gold1/rmsuser/genie/defaults/short_decay.cer

MEASUREMENT CATEGORIZATION==========

Categorization Legend

Level 1 = Normal Natural Rad. Meas.
Level 2 = Abnormal Natural Rad. Meas.
Level 3 = Normal Anthropogenic Rad. Meas.
Level 4 = Abnormal Anthropogenic Rad. Meas.

Spectrum Category (1) -- Normal Natural Rad. Meas.

ACTIVITY SUMMARY==========

NATURAL RADIOACTIVITY:

Nuclides Identified: BI-212, BI-214, K-40, PB-214, TL-208

Nuclides Quantified:

Nuclide	Half-Life	Conc(uBq/m3)	%RelErr	Notes
BE-7	53.3 D	2.2E+03	2.62	
PB-212	10.64 H	3.9E+03	10.28	

ACTIVATION-PRODUCT RADIOACTIVITY:

None Found

FISSION-PRODUCT RADIOACTIVITY:

None Found

MINIMUM DETECTABLE CONCENTRATION FOR KEY NUCLIDES==========

Nuclide	Half-Life	MDC(uBq/m3)
BA-140	12.75 D	10.29
CE-143	1.4 D	8.56
CS-134	2.06135 Y	2.88
CS-136	13.16 D	2.88
CS-137	30.0197 Y	2.92
I-131	8.04 D	3.33
I-133	20.8 H	6.13
MO-99	65.94 H	26.41
NB-95	35.15 D	3.10
RU-103	39.26 D	2.55
TE-132	78.2 H	3.04
ZR-95	64.02 D	4.55
ZR-97	17 H	7.01

PEAK SEARCH RESULTS==========

36 peaks found in spectrum by automated peak search.
34 peaks associated with nuclides by automated processing.
2 peaks not associated with nuclides by automated processing.
94 percent of peaks were associated with nuclides.

Note: "*" indicates that a peak was a component of a multiplet.

Energy	Centroid	Width	FWHM	%Eff	Net Area	%RelErr	Nuclide	Nts
74.81	102.40 *	17	1.26	10.53	13296.21	1.19	PB-212	
74.81	102.40 *	17	1.26	10.53	13296.21	1.19	PB-214	
74.81	102.40 *	17	1.26	10.53	13296.21	1.19	TL-208	
77.09	105.51 *	17	1.27	10.63	20522.99	1.02	BI-214	
77.09	105.51 *	17	1.27	10.63	20522.99	1.02	PB-212	
77.09	105.51 *	17	1.27	10.63	20522.99	1.02	PB-214	
87.17	119.26 *	18	1.38	10.91	8033.26	1.91	PB-212	
87.17	119.26 *	18	1.38	10.91	8033.26	1.91	PB-214	
89.85	122.92 *	18	1.39	10.95	2552.86	3.06	BI-214	
89.85	122.92 *	18	1.39	10.95	2552.86	3.06	PB-212	
115.18	157.48	10	1.08	10.90	735.35	18.21	PB-212	
238.64	325.97	16	1.29	7.94	48152.86	0.69	PB-212	
252.56	344.97	12	1.50	7.63	218.30	29.65	TL-208	
277.34	378.79	13	1.27	7.12	1819.45	4.84	TL-208	
288.22	393.63	13	1.45	6.91	365.60	18.73	BI-212	
295.20	403.17 *	20	1.29	6.78	304.67	12.08	PB-214	
300.14	409.90 *	20	1.29	6.70	2613.09	3.76	PB-212	
327.85	447.73	17	1.10	6.23	141.65	39.76	BI-212	
351.88	480.54	12	1.63	5.87	506.43	12.69	PB-214	
376.98	514.79	13	0.91	5.53	83.10	63.96	PB212XR2	
452.74	618.23	7	1.46	4.69	248.51	19.03	BI-212	
477.57	652.11	14	1.45	4.46	16754.71	1.17	BE-7	
510.74	697.40	19	1.82	4.19	5427.17	2.23	TL-208	
583.15	796.27	16	1.55	3.69	14879.86	1.23	TL-208	
609.32	832.00	15	1.50	3.54	517.00	9.56	BI-214	

632.05	863.05	8	0.94	3.42	38.95	52.01		1
727.27	993.07	20	1.65	2.99	3112.30	2.87	BI-212	
763.17	1042.08	9	1.38	2.85	204.89	16.91	TL-208	
785.49	1072.57	17	1.50	2.77	427.03	9.83	BI-212	
785.49	1072.57	17	1.50	2.77	427.03	9.83	BI-214	
785.49	1072.57	17	1.50	2.77	427.03	9.83	PB-214	
860.52	1175.04	16	1.75	2.54	1844.78	3.86	TL-208	
893.42	1219.97	9	1.38	2.45	135.41	21.62	BI-212	
969.07	1323.30	14	1.37	2.28	75.00	33.43		2
1078.77	1473.12	16	1.97	2.06	169.47	18.85	BI-212	
1093.75	1493.59	10	1.63	2.04	210.22	15.59	TL-208	
1120.07	1529.55	17	1.89	2.00	104.85	27.66	BI-214	
1460.72	1994.87	17	2.09	1.59	2723.17	3.05	K-40	
1512.82	2066.05	9	1.33	1.55	52.45	34.54	BI-212	
1592.29	2174.60	15	2.31	1.49	422.88	9.31	TL-208	
1620.66	2213.35	13	2.19	1.47	410.39	9.37	BI-212	
1764.53	2409.89	20	3.17	1.38	126.28	22.08	BI-214	
2103.43	2872.81	26	3.34	1.23	697.81	7.06	TL-208	
2614.52	3570.69	24	2.68	1.10	5048.52	2.13	TL-208	

PEAK SEARCH NOTES==========

NOTE 1:
Date Entered: 1997/03/17 11:56:53
Analyst: dwilliam
False peak detection; Type I error in peak processing.

==========

NOTE 2:
Date Entered: 1997/03/17 11:58:14
Analyst: dwilliam
False peak detection; Type I error in peak processing.

==========

CALIBRATION EQUATIONS==========

Energy vs. Channel

$$E(c) = -0.2407 + 0.733*c - 4.522E-07*c^2 + 7.292E-11*c^3$$

E = energy (keV)
c = channel number

Resolution vs. Energy

$$FWHM(E) = 0.89 + 0.03064*SQRT(E)$$

FWHM = Full Width Half Max (keV)
E = energy (keV)

Efficiency vs. Energy

$$e(E) = \exp \{ -3.776 + 0.9255*\ln(962.1/E) + 0.1003*[\ln(962.1/E)]^2 - 0.0896*[\ln(962.1/E)]^3 \}$$

e = efficiency (counts/gamma)
E = energy (keV)

ATMOSPHERIC RADIONUCLIDE MEASUREMENT REPORT
Particulate Version

SAMPLE INFORMATION==========

Station ID:	CA002	Detector ID:	CAA2
Station Type:	ISAR2	Detector Type:	

Station Location: Vancouver, Canada
Detector Description: Detector A in Vancouver, Canada

Sample ID:	0022635	Sample Geometry:	DISK
Sample Quantity:	24461.00 m3	Sample Type:	Filter

Collection Start:	1997/03/14 18:41	Sampling Time:	24.95 hours
Collection Stop:	1997/03/15 19:38	Decay Time:	4.23 hours
Acquisition Start:	1997/03/15 23:52	Acquisition Time:	19.50 hours
Acquisition Stop:	1997/03/16 19:22	Avg Flow Rate:	980.40 m3/hr

Collection Station Comments:
goshka - Detector 1 Ranger (15-MAR-1997)

IDC Analysis General Comments:
This spectrum contains the following activation products: Bi-204, Po-206, Po-207 and At-209. These nuclides have contributed to the net peak areas associated with AC-228 in this spectrum; therefore, the presence of AC-228 is overestimated. A potential source of their injection is a medical facility (accelerator) near the IMS station. Leonid Vladimirski 3/20/97

I-123 is present in this spectrum and is seen at this site on occasion.

Calibration Update Performed. Certificate file
/data/gold1/rmsuser/genie/defaults/short_decay.cer

MEASUREMENT CATEGORIZATION==========

Categorization Legend

Level 1	= Normal Natural Rad. Meas.
Level 2	= Abnormal Natural Rad. Meas.
Level 3	= Normal Anthropogenic Rad. Meas.
Level 4	= Abnormal Anthropogenic Rad. Meas.

Spectrum Category (3) -- Normal Anthropogenic Rad. Meas.

Categorization Summary:

Name	Category	Categorization Comment
I-123	3	Within Statistical Range

ACTIVITY SUMMARY==========

NATURAL RADIOACTIVITY:

Nuclides Identified: AC-228, BI-212, BI-214, K-40, NA-24, PB-214, TL-208, UNKNAT01

Nuclides Quantified:

Nuclide	Half-Life	Conc(uBq/m3)	%RelErr	Notes
BE-7	53.3 D	2.5E+03	2.58	
PB-212	10.64 H	4.6E+03	10.27	
ACTIVATION-PRODUCT RADIOACTIVITY:				
I-123	13.13 H	36	7.84	
FISSION-PRODUCT RADIOACTIVITY:				
None Found				

MINIMUM DETECTABLE CONCENTRATION FOR KEY NUCLIDES==========

Nuclide	Half-Life	MDC(uBq/m3)
BA-140	12.75 D	12.32
CE-143	1.4 D	9.34
CS-134	2.06135 Y	3.18
CS-136	13.16 D	3.30
CS-137	30.0197 Y	3.50
I-131	8.04 D	3.80
I-133	20.8 H	7.27
MO-99	65.94 H	33.81
NB-95	35.15 D	3.47
RU-103	39.26 D	2.99
TE-132	78.2 H	3.38
ZR-95	64.02 D	5.35
ZR-97	17 H	6.85

PEAK SEARCH RESULTS==========

55 peaks found in spectrum by automated peak search.
45 peaks associated with nuclides by automated processing.
10 peaks not associated with nuclides by automated processing.
82 percent of peaks were associated with nuclides.

Note: "*" indicates that a peak was a component of a multiplet.

Energy	Centroid	Width	FWHM	%Eff	Net Area	%RelErr	Nuclide	Nts
74.85	102.39 *	17	1.26	10.53	17979.61	1.03	PB-212	
74.85	102.39 *	17	1.26	10.53	17979.61	1.03	PB-214	
74.85	102.39 *	17	1.26	10.53	17979.61	1.03	TL-208	
77.13	105.50 *	17	1.26	10.63	26988.13	0.89	BI-214	
77.13	105.50 *	17	1.26	10.63	26988.13	0.89	PB-212	
77.13	105.50 *	17	1.26	10.63	26988.13	0.89	PB-214	
84.93	116.14 *	19	1.36	10.86	662.79	10.14	TL-208	
87.23	119.28 *	19	1.36	10.91	9953.69	1.74	PB-212	
87.23	119.28 *	19	1.36	10.91	9953.69	1.74	PB-214	
89.93	122.97 *	19	1.37	10.95	3353.40	2.69	AC-228	
89.93	122.97 *	19	1.37	10.95	3353.40	2.69	BI-214	
89.93	122.97 *	19	1.37	10.95	3353.40	2.69	PB-212	
115.24	157.50	10	0.93	10.90	696.16	38.34	PB-212	
159.04	217.28	13	1.19	9.95	1429.38	7.44	I-123	1

159.04	217.28	13	1.19	9.95	1429.38	7.44	TE-123M	2
238.65	325.95	16	1.29	7.94	57815.91	0.63	PB-212	
269.85	368.54	11	0.36	7.27	27917.27	0.64	AC-228	3
277.35	378.78	13	1.40	7.12	2104.42	4.78	TL-208	
287.42	392.52	13	3.20	6.93	929.41	12.02	BI-212	4
295.39	403.39 *	20	1.33	6.78	200.90	19.80	PB-214	
300.12	409.86 *	20	1.34	6.70	3174.46	3.49	PB-212	
328.09	448.04	13	1.43	6.23	221.61	27.99	AC-228	
328.09	448.04	13	1.43	6.23	221.61	27.99	BI-212	
338.42	462.13	13	1.63	6.07	490.44	14.67	AC-228	5
351.90	480.53	10	1.53	5.87	508.99	13.79	PB-214	
374.81	511.81	14	1.48	5.56	1773.45	4.99	PB212XR1	6
452.74	618.20	14	1.52	4.69	307.36	18.02	BI-212	
477.56	652.07	18	1.46	4.46	19755.57	1.08	AC-228	
477.56	652.07	18	1.46	4.46	19755.57	1.08	BE-7	
510.79	697.44	17	1.79	4.19	6572.18	2.04	TL-208	
522.45	713.36	9	1.75	4.10	229.87	22.47	AC-228	7
545.10	744.28	7	1.58	3.94	270.94	17.80		8
583.15	796.22	19	1.55	3.69	17731.93	1.13	AC-228	
583.15	796.22	19	1.55	3.69	17731.93	1.13	TL-208	
609.32	831.96	13	1.57	3.54	473.48	11.09	BI-214	
670.28	915.19	12	1.89	3.23	152.36	28.83	TL208XR4	9
727.28	993.01	10	1.65	2.99	3714.63	2.67	AC-228	
727.28	993.01	10	1.65	2.99	3714.63	2.67	BI-212	
742.76	1014.15	12	1.89	2.93	186.64	21.73	BI-214	10
742.76	1014.15	12	1.89	2.93	186.64	21.73	ZR-97	11
763.20	1042.05	9	1.47	2.85	236.37	17.12	TL-208	
781.85	1067.51 *	21	1.77	2.79	184.92	13.68	AC-228	12
785.50	1072.50 *	21	1.77	2.77	507.90	8.64	BI-212	
785.50	1072.50 *	21	1.77	2.77	507.90	8.64	BI-214	
785.50	1072.50 *	21	1.77	2.77	507.90	8.64	PB-214	
790.30	1079.05 *	21	1.78	2.76	172.50	14.01		13
803.06	1096.48 *	22	1.48	2.72	125.42	19.47	UNKNAT01	
807.50	1102.53 *	22	1.49	2.70	209.05	16.19		14
860.52	1174.94	12	1.73	2.54	2227.36	3.53	TL-208	
884.00	1206.99	14	1.61	2.48	94.09	33.66		15
893.51	1219.98 *	16	1.75	2.45	162.74	13.32	BI-212	
899.12	1227.64 *	16	1.76	2.44	921.77	6.18		16
911.56	1244.62 *	17	2.01	2.41	450.13	10.06	AC-228	17
918.27	1253.79 *	17	2.01	2.39	101.14	20.46		18
951.03	1298.52	12	3.17	2.32	102.18	28.21		19
969.29	1323.45	8	0.54	2.27	43.84	403.74	AC-228	
983.93	1343.45	14	1.95	2.24	480.85	9.58		20
992.39	1355.00	13	1.67	2.23	277.76	13.87		21
1032.39	1409.62	10	1.81	2.15	236.46	16.04		22
1078.93	1473.17	12	1.86	2.06	215.72	16.63	BI-212	
1093.74	1493.39	15	2.17	2.04	337.15	12.28	TL-208	
1120.53	1529.98	14	1.03	1.99	67.77	28.15	BI-214	
1368.50	1868.62	16	1.32	1.68	79.62	30.88	NA-24	
1460.88	1994.79	16	2.13	1.59	2588.85	3.22	K-40	
1512.68	2065.53	14	2.76	1.55	157.60	19.91	BI-212	
1592.76	2174.90	12	2.14	1.49	455.27	9.02	TL-208	
1620.82	2213.23	17	2.22	1.47	501.89	8.52	BI-212	
1764.57	2409.58	16	2.50	1.38	108.96	25.38	BI-214	
2103.57	2872.62	23	3.39	1.23	827.65	6.46	TL-208	
2614.48	3570.48	13	2.67	1.10	6157.97	1.89	TL-208	

PEAK SEARCH NOTES==========

NOTE 1:
Date Entered: 1997/03/19 17:17:06
Analyst: dwilliam

The peak is real and the association is correct.

==========

NOTE 2:
Date Entered: 1997/03/19 17:16:20
Analyst: dwilliam
This nuclide was removed from the Activity Summary section because in the analyst's judgment the nuclide was not present; some nuclides may be removed because their activity calculations are not meaningful (they are identified, not quantified).

Date Entered: 1997/03/19 17:16:53
Analyst: dwilliam
This peak is associated with I-123.

==========

NOTE 3:
Date Entered: 1997/03/19 17:48:23
Analyst: dwilliam
This peak may be associated with the 270.0 keV gamma line of Po-204 and the 270.2 keV gamma line of Ac-228.

==========

NOTE 4:
Date Entered: 1997/03/19 17:42:52
Analyst: dwilliam
The actual centroid of this peak appears to be slightly different than the centroid calculated by the automated spectral processing application.
Therefore, this peak may be associated with the 286.5 keV gamma line of Po-206.

==========

NOTE 5:
Date Entered: 1997/03/19 17:44:34
Analyst: dwilliam
This peak may be associated with the 338.4 keV gamma line of Po-206 and the 338.3 keV gamma line of Ac-228.

==========

NOTE 6:
Date Entered: 1997/03/19 17:51:35
Analyst: dwilliam
This peak may be associated with the 374.8 keV gamma line of Bi-204.

==========

NOTE 7:
Date Entered: 1997/03/19 17:46:01
Analyst: dwilliam
This peak may be associated with the 522.4 keV gamma line of Po-206 and the 523.1 keV gamma line of Ac-228.

==========

NOTE 8:
Date Entered: 1997/03/19 17:30:27
Analyst: dwilliam
This peak is likely associated with the 545.0 keV gamma line of At-209.

==========

NOTE 9:
Date Entered: 1997/03/19 17:52:38
Analyst: dwilliam
This peak may be associated with the 670.7 keV gamma line of Bi-204.

==========

NOTE 10:
Date Entered: 1997/03/19 17:20:31
Analyst: dwilliam
This peak is likely associated with the 742.6 keV gamma line of Po-207.

==========

NOTE 11:
Date Entered: 1997/03/19 17:18:40
Analyst: dwilliam
This nuclide was removed from the Activity Summary section because in the analyst's judgment the nuclide was not present; some nuclides may be removed because their activity calculations are not meaningful (they are identified, not quantified).

Date Entered: 1997/03/19 17:20:31
Analyst: dwilliam
This peak is likely associated with the 742.6 keV gamma line of Po-207.

==========

NOTE 12:
Date Entered: 1997/03/19 17:35:29
Analyst: dwilliam
This peak may be associated with the 781.9 keV gamma line of At-209 and the 782.14 keV gamma line of Ac-228.

==========

NOTE 13:
Date Entered: 1997/03/19 17:36:19
Analyst: dwilliam
This peak may be associated with the 790.2 keV gamma line of At-209.

==========

NOTE 14:
Date Entered: 1997/03/19 17:46:44
Analyst: dwilliam
This peak may be associated with the 807.5 keV gamma line of Po-206.

==========

NOTE 15:
Date Entered: 1997/03/19 17:49:30
Analyst: dwilliam
This peak may be associated with the 883.9 keV gamma line of Po-204.

==========

NOTE 16:
Date Entered: 1997/03/19 17:53:05
Analyst: dwilliam
This peak may be associated with the 899.1 keV gamma line of Bi-204.

==========

NOTE 17:
Date Entered: 1997/03/19 17:27:18
Analyst: dwilliam
This peak is likely associated with the 911.2 keV gamma line of Ac-228, the 911.8 keV gamma line of Po-207, and the 911.8 keV gamma line of Bi-204.

==========

NOTE 18:
Date Entered: 1997/03/19 17:53:40
Analyst: dwilliam
This peak may be associated with the 918.3 keV gamma line of Bi-204.

==========

NOTE 19:
Date Entered: 1997/03/19 17:56:02
Analyst: dwilliam
The actual centroid of this peak appears to be slightly different than the centroid calculated by the automated spectral processing application. Therefore, this peak may be associated with the 952.1 keV gamma line of Bi-212.

==========

NOTE 20:
Date Entered: 1997/03/19 17:54:06
Analyst: dwilliam
This peak may be associated with the 983.9 keV gamma line of Bi-204.

==========

NOTE 21:
Date Entered: 1997/03/19 17:28:53
Analyst: dwilliam
This peak is likely associated with the 992.1 keV gamma line of Po-207.

==========

NOTE 22:
Date Entered: 1997/03/19 17:47:14
Analyst: dwilliam
This peak may be associated with the 1032.3 keV gamma line of Po-206.

==========

CALIBRATION EQUATIONS==========

Energy vs. Channel

$$E(c) = -0.169 + 0.7328*c - 2.024E-07*c^2 + 2.111E-11*c^3$$

E = energy (keV)
c = channel number

Resolution vs. Energy

$$FWHM(E) = 0.89 + 0.03064*SQRT(E)$$

FWHM = Full Width Half Max (keV)
E = energy (keV)

Efficiency vs. Energy

$$e(E) = \exp \{ -3.776 + 0.9255*\ln(962.1/E) + 0.1003*[\ln(962.1/E)]^2 - 0.0896*[\ln(962.1/E)]^3 \}$$

e = efficiency (counts/gamma)
E = energy (keV)

ATMOSPHERIC RADIONUCLIDE MEASUREMENT REPORT
Particulate Version

SAMPLE INFORMATION==========

Station ID:	CA002	Detector ID:	CAA2
Station Type:	ISAR2	Detector Type:	

Station Location: Vancouver, Canada
Detector Description: Detector A in Vancouver, Canada

Sample ID:	0022677	Sample Geometry:	DISK
Sample Quantity:	21661.00 m3	Sample Type:	Filter

Collection Start:	1997/03/15 19:40	Sampling Time:	23.83 hours
Collection Stop:	1997/03/16 19:30	Decay Time:	4.25 hours
Acquisition Start:	1997/03/16 23:44	Acquisition Time:	19.50 hours
Acquisition Stop:	1997/03/17 19:14	Avg Flow Rate:	908.98 m3/hr

Collection Station Comments:
goshka - Detector 1 Ranger (16-MAR-1997)

IDC Analysis General Comments:
Calibration Update Performed. Certificate file
/data/gold1/rmsuser/genie/defaults/short_decay.cer

MEASUREMENT CATEGORIZATION==========

Categorization Legend

Level 1 = Normal Natural Rad. Meas.
Level 2 = Abnormal Natural Rad. Meas.
Level 3 = Normal Anthropogenic Rad. Meas.
Level 4 = Abnormal Anthropogenic Rad. Meas.

Spectrum Category (1) -- Normal Natural Rad. Meas.

ACTIVITY SUMMARY==========

NATURAL RADIOACTIVITY:

Nuclides Identified: AC-228, BI-212, BI-214, K-40, NA-24, PB-214, TL-208

Nuclides Quantified:

Nuclide	Half-Life	Conc(uBq/m3)	%RelErr	Notes
BE-7	53.3 D	2.1E+03	2.65	
PB-212	10.64 H	2.7E+03	10.29	

ACTIVATION-PRODUCT RADIOACTIVITY:

None Found

FISSION-PRODUCT RADIOACTIVITY:

None Found

MINIMUM DETECTABLE CONCENTRATION FOR KEY NUCLIDES==========

Nuclide	Half-Life	MDC(uBq/m3)
BA-140	12.75 D	10.54
CE-143	1.4 D	8.40
CS-134	2.06135 Y	2.99
CS-136	13.16 D	2.96
CS-137	30.0197 Y	3.01
I-131	8.04 D	3.27
I-133	20.8 H	6.08
MO-99	65.94 H	26.13
NB-95	35.15 D	2.97
RU-103	39.26 D	2.59
TE-132	78.2 H	2.90
ZR-95	64.02 D	4.71
ZR-97	17 H	7.21

PEAK SEARCH RESULTS==========

36 peaks found in spectrum by automated peak search.
35 peaks associated with nuclides by automated processing.
1 peaks not associated with nuclides by automated processing.
97 percent of peaks were associated with nuclides.

Note: "*" indicates that a peak was a component of a multiplet.

Energy	Centroid	Width	FWHM	%Eff	Net Area	%RelErr	Nuclide	Nts
74.84	102.36 *	17	1.27	10.53	8740.16	1.49	PB-212	
74.84	102.36 *	17	1.27	10.53	8740.16	1.49	PB-214	
74.84	102.36 *	17	1.27	10.53	8740.16	1.49	TL-208	
77.14	105.50 *	17	1.27	10.63	13070.77	1.29	BI-214	
77.14	105.50 *	17	1.27	10.63	13070.77	1.29	PB-212	
77.14	105.50 *	17	1.27	10.63	13070.77	1.29	PB-214	
87.20	119.23 *	18	1.41	10.91	5004.23	2.50	PB-212	
87.20	119.23 *	18	1.41	10.91	5004.23	2.50	PB-214	
89.89	122.90 *	18	1.42	10.95	1637.66	3.99	AC-228	
89.89	122.90 *	18	1.42	10.95	1637.66	3.99	BI-214	
89.89	122.90 *	18	1.42	10.95	1637.66	3.99	PB-212	
115.23	157.48	10	0.62	10.90	399.59	123.48	PB-212	
238.65	325.96	14	1.30	7.94	31101.53	0.87	PB-212	
277.40	378.86	13	1.36	7.12	1158.33	6.53	TL-208	
287.79	393.04	8	1.99	6.92	269.23	24.94	BI-212	
295.19	403.15 *	16	1.26	6.78	250.80	13.16	PB-214	
300.11	409.86 *	16	1.27	6.70	1596.01	5.03	PB-212	
338.21	461.87	12	1.39	6.07	155.55	31.04	AC-228	
351.91	480.58	10	1.30	5.87	465.74	12.62	PB-214	
452.96	618.53	12	1.26	4.69	147.77	29.53	BI-212	
477.54	652.09	15	1.48	4.46	14626.85	1.25	BE-7	
510.73	697.40	19	1.84	4.19	3648.85	2.79	TL-208	
569.33	777.41	13	0.53	3.78	95.24	226.93		1
583.12	796.25	15	1.53	3.69	9445.24	1.58	AC-228	
583.12	796.25	15	1.53	3.69	9445.24	1.58	TL-208	
609.16	831.79	14	1.70	3.54	423.55	10.99	BI-214	
727.25	993.03	15	1.63	2.99	1932.37	3.75	AC-228	
727.25	993.03	15	1.63	2.99	1932.37	3.75	BI-212	
763.06	1041.93	8	1.86	2.85	152.27	21.13	TL-208	
785.49	1072.56	17	1.71	2.77	306.18	12.50	BI-212	

785.49	1072.56	17	1.71	2.77	306.18	12.50	BI-214
785.49	1072.56	17	1.71	2.77	306.18	12.50	PB-214
860.49	1174.97	13	1.62	2.54	1185.05	5.12	TL-208
911.36	1244.43	13	1.85	2.41	132.48	21.59	AC-228
952.14	1300.12	16	1.42	2.31	62.18	36.07	BI-212
969.22	1323.44	7	0.96	2.28	44.04	109.99	AC-228
1078.90	1473.22	9	2.26	2.06	98.25	30.44	BI-212
1093.64	1493.34	17	1.80	2.04	154.30	18.76	TL-208
1120.44	1529.95	11	1.28	1.99	64.64	32.35	BI-214
1368.50	1868.71	11	1.57	1.68	47.37	40.15	NA-24
1460.86	1994.86	14	2.07	1.59	2607.43	3.11	K-40
1512.98	2066.04	10	2.11	1.55	61.35	33.31	BI-212
1592.55	2174.71	14	2.10	1.49	251.63	12.57	TL-208
1620.77	2213.25	14	1.89	1.47	267.80	11.55	BI-212
1764.31	2409.30	10	1.43	1.38	55.40	35.02	BI-214
2103.45	2872.51	23	3.42	1.23	421.47	9.31	TL-208
2614.52	3570.53	22	2.65	1.10	3160.19	2.74	TL-208

PEAK SEARCH NOTES==========

NOTE 1:
Date Entered: 1997/03/20 09:21:43
Analyst: dwilliam
False peak detection; Type I error in peak processing.

==========

CALIBRATION EQUATIONS==========

Energy vs. Channel

$$E(c) = -0.1532 + 0.7327*c - 1.764E-07*c^2 + 2.041E-11*c^3$$

E = energy (keV)
c = channel number

Resolution vs. Energy

$$FWHM(E) = 0.89 + 0.03064*SQRT(E)$$

FWHM = Full Width Half Max (keV)
E = energy (keV)

Efficiency vs. Energy

$$e(E) = \exp \{ -3.776 + 0.9255*\ln(962.1/E) + 0.1003*[\ln(962.1/E)]^2 - 0.0896*[\ln(962.1/E)]^3 \}$$

e = efficiency (counts/gamma)
E = energy (keV)

ATMOSPHERIC RADIONUCLIDE MEASUREMENT REPORT
Particulate Version

SAMPLE INFORMATION==========

Station ID:	CA002	Detector ID:	CAA2
Station Type:	ISAR2	Detector Type:	

Station Location: Vancouver, Canada
Detector Description: Detector A in Vancouver, Canada

Sample ID:	0022792	Sample Geometry:	DISK
Sample Quantity:	23572.00 m3	Sample Type:	Filter

Collection Start:	1997/03/16 19:31	Sampling Time:	24.16 hours
Collection Stop:	1997/03/17 19:41	Decay Time:	4.27 hours
Acquisition Start:	1997/03/17 23:57	Acquisition Time:	19.50 hours
Acquisition Stop:	1997/03/18 19:27	Avg Flow Rate:	975.66 m3/hr

Collection Station Comments:
goshka - Detector 1 Ranger (17-MAR-1997)

IDC Analysis General Comments:
This spectrum contains the following activation products: Bi-204, Bi-206, Po-206, Po-207 and At-209. These nuclides have contributed to the net peak areas associated with AC-228 in this spectrum; therefore, the presence of AC-228 is overestimated. A potential source of their injection is a medical facility (accelerator) near the IMS station. Leonid Vladimirski 3/20/97

I-123 is present in this spectrum and is seen at this site on occasion.

Calibration Update Performed. Certificate file
/data/gold1/rmsuser/genie/defaults/short_decay.cer

MEASUREMENT CATEGORIZATION==========

Categorization Legend

Level 1	= Normal Natural Rad. Meas.
Level 2	= Abnormal Natural Rad. Meas.
Level 3	= Normal Anthropogenic Rad. Meas.
Level 4	= Abnormal Anthropogenic Rad. Meas.

Spectrum Category (3) -- Normal Anthropogenic Rad. Meas.

Categorization Summary:

Name	Category	Categorization Comment
I-123	3	Within Statistical Range

ACTIVITY SUMMARY==========

NATURAL RADIOACTIVITY:

Nuclides Identified: AC-228, BI-212, BI-214, K-40, PB-214, TH-228, TL-208, UNKNAT01

Nuclides Quantified:

Nuclide	Half-Life	Conc(uBq/m3)	%RelErr	Notes
BE-7	53.3 D	3.8E+03	2.51	
PB-212	10.64 H	2.8E+03	10.29	
ACTIVATION-PRODUCT RADIOACTIVITY:				
I-123	13.13 H	15	21.57	
FISSION-PRODUCT RADIOACTIVITY:				
None Found				

MINIMUM DETECTABLE CONCENTRATION FOR KEY NUCLIDES==========

Nuclide	Half-Life	MDC(uBq/m3)
BA-140	12.75 D	7.27
CE-143	1.4 D	9.36
CS-134	2.06135 Y	3.03
CS-136	13.16 D	3.09
CS-137	30.0197 Y	3.27
I-131	8.04 D	3.48
I-133	20.8 H	6.34
MO-99	65.94 H	31.82
NB-95	35.15 D	3.17
RU-103	39.26 D	2.64
TE-132	78.2 H	3.12
ZR-95	64.02 D	5.05
ZR-97	17 H	6.50

PEAK SEARCH RESULTS==========

48 peaks found in spectrum by automated peak search.
38 peaks associated with nuclides by automated processing.
10 peaks not associated with nuclides by automated processing.
79 percent of peaks were associated with nuclides.

Note: "*" indicates that a peak was a component of a multiplet.

Energy	Centroid	Width	FWHM	%Eff	Net Area	%RelErr	Nuclide	Nts
74.85	102.42 *	16	1.26	10.53	11885.74	1.29	PB-212	
74.85	102.42 *	16	1.26	10.53	11885.74	1.29	PB-214	
74.85	102.42 *	16	1.26	10.53	11885.74	1.29	TL-208	
77.11	105.50 *	16	1.26	10.63	16855.96	1.14	BI-214	
77.11	105.50 *	16	1.26	10.63	16855.96	1.14	PB-212	
77.11	105.50 *	16	1.26	10.63	16855.96	1.14	PB-214	
84.86	116.07 *	19	1.35	10.86	746.13	7.71	TH-228	
84.86	116.07 *	19	1.35	10.86	746.13	7.71	TL-208	
87.21	119.29 *	19	1.35	10.91	6763.09	2.11	PB-212	
87.21	119.29 *	19	1.35	10.91	6763.09	2.11	PB-214	
89.86	122.90 *	19	1.35	10.95	2206.79	3.35	AC-228	
89.86	122.90 *	19	1.35	10.95	2206.79	3.35	BI-214	
89.86	122.90 *	19	1.35	10.95	2206.79	3.35	PB-212	
115.23	157.52	12	0.86	10.90	429.60	82.20	PB-212	

140.26	191.69		14	0.75	10.42	232.96	168.87	GE-75M	
140.26	191.69		14	0.75	10.42	232.96	168.87	TC-99M	1
159.09	217.38		7	1.03	9.95	583.03	21.43	I-123	2
159.09	217.38		7	1.03	9.95	583.03	21.43	TE-123M	3
238.65	325.96		16	1.31	7.94	35182.75	0.82	PB-212	
277.37	378.81		12	1.35	7.12	1272.28	6.72	TL-208	
286.50	391.28		13	1.53	6.94	764.75	10.70		4
295.16	403.10	*	20	1.30	6.79	226.64	17.13	PB-214	
300.09	409.83	*	20	1.31	6.70	1871.05	4.93	PB-212	
311.60	425.54		7	0.52	6.50	201.67	223.06		5
338.45	462.19		13	1.31	6.07	589.65	11.02	AC-228	6
351.80	480.42		13	1.46	5.87	426.27	14.82	PB-214	
374.74	511.73		13	1.41	5.56	1426.52	5.52	PB212XR1	7
452.91	618.44		9	1.12	4.69	143.77	40.73	BI-212	
477.57	652.09		14	1.46	4.46	28327.91	0.89	AC-228	
477.57	652.09		14	1.46	4.46	28327.91	0.89	BE-7	
510.83	697.51	*	35	1.93	4.19	4454.38	2.50	TL-208	
516.24	704.89	*	35	1.14	4.15	88.96	21.47		8
522.42	713.33	*	35	1.15	4.10	205.44	11.21	AC-228	9
537.49	733.91		8	1.14	3.99	93.60	31.96	BA-140	10
583.14	796.22		19	1.54	3.69	10827.94	1.47	AC-228	
583.14	796.22		19	1.54	3.69	10827.94	1.47	TL-208	
609.23	831.84		15	1.83	3.54	445.31	11.54	BI-214	
727.25	992.99		19	1.59	2.99	2217.60	3.56	AC-228	
727.25	992.99		19	1.59	2.99	2217.60	3.56	BI-212	
742.59	1013.93		14	1.51	2.93	112.27	29.70	BI-214	11
742.59	1013.93		14	1.51	2.93	112.27	29.70	ZR-97	12
763.26	1042.15		13	1.66	2.85	173.36	21.15	TL-208	
785.60	1072.65		10	1.70	2.77	273.07	15.08	BI-212	
785.60	1072.65		10	1.70	2.77	273.07	15.08	BI-214	
785.60	1072.65		10	1.70	2.77	273.07	15.08	PB-214	
803.03	1096.46	*	18	1.72	2.72	199.60	13.16	UNKNAT01	13
807.48	1102.53	*	18	1.72	2.70	305.91	11.26		14
860.55	1175.00		17	1.81	2.54	1368.15	4.77	TL-208	
881.05	1202.99		16	1.39	2.49	115.16	25.38		15
899.22	1227.80		14	1.66	2.44	789.10	6.78		16
911.78	1244.95	*	20	1.83	2.41	356.75	11.01	AC-228	17
918.29	1253.84	*	20	1.84	2.39	114.63	17.69		18
968.80	1322.81		10	1.38	2.28	60.72	41.06	AC-228	
983.80	1343.31	*	25	1.91	2.24	360.93	10.09		19
992.07	1354.60	*	25	1.92	2.23	243.15	11.59		20
1032.35	1409.61		10	1.96	2.15	347.62	11.52		21
1093.73	1493.42		13	2.05	2.04	182.09	18.25	TL-208	
1120.15	1529.50		13	1.49	2.00	93.63	29.68	BI-214	
1460.84	1994.81		11	2.04	1.59	2739.09	3.02	K-40	
1512.64	2065.56		13	2.19	1.55	78.22	30.20	BI-212	
1592.50	2174.64		10	2.03	1.49	263.97	12.17	TL-208	
1620.83	2213.33		13	2.12	1.47	270.45	11.93	BI-212	
2103.59	2872.73		21	3.21	1.23	456.23	9.01	TL-208	
2614.49	3570.53		22	2.67	1.10	3617.52	2.51	TL-208	

PEAK SEARCH NOTES==========

NOTE 1:
Date Entered: 1997/03/20 10:05:08
Analyst: dwilliam
This nuclide was removed from the Activity Summary section because in the analyst's judgment the nuclide was not present; some nuclides may be removed because their activity calculations are not meaningful (they are identified, not quantified).

Date Entered: 1997/03/20 10:06:41

Analyst: dwilliam
This peak is likely associated with Ge-75m.

==========

NOTE 2:
Date Entered: 1997/03/20 09:34:40
Analyst: dwilliam
The peak is real and the association is correct.

==========

NOTE 3:
Date Entered: 1997/03/20 09:31:55
Analyst: dwilliam
This nuclide was removed from the Activity Summary section because in the analyst's judgment the nuclide was not present; some nuclides may be removed because their activity calculations are not meaningful (they are identified, not quantified).

Date Entered: 1997/03/20 09:33:48
Analyst: dwilliam
This peak is associated with I-123.

==========

NOTE 4:
Date Entered: 1997/03/20 09:56:09
Analyst: dwilliam
This peak may be associated with the 286.5 keV gamma line of Po-206.

==========

NOTE 5:
Date Entered: 1997/03/20 09:57:23
Analyst: dwilliam
This peak may be associated with the 311.5 keV gamma line of Po-206.

==========

NOTE 6:
Date Entered: 1997/03/20 09:58:00
Analyst: dwilliam
This peak may be associated with the 338.4 keV gamma line of Po-206 and the 338.3 keV gamma line of Ac-228.

==========

NOTE 7:
Date Entered: 1997/03/20 09:48:37
Analyst: dwilliam
This peak may be associated with the 374.8 keV gamma line of Bi-204.

==========

NOTE 8:
Date Entered: 1997/03/20 09:52:48
Analyst: dwilliam
This peak may be associated with the 516.2 keV gamma line of Bi-206.

==========

NOTE 9:

Date Entered: 1997/03/20 10:00:39
Analyst: dwilliam
This peak is likely associated with the 522.4 keV gamma line of Po-206 and may also be associated with the 523.1 keV gamma line of Ac-228.

==========

NOTE 10:
Date Entered: 1997/03/20 09:53:16
Analyst: dwilliam
This peak may be associated with the 537.4 keV gamma line of Bi-206.

Date Entered: 1997/03/20 10:07:21
Analyst: dwilliam
This nuclide was removed from the Activity Summary section because in the analyst's judgment the nuclide was not present; some nuclides may be removed because their activity calculations are not meaningful (they are identified, not quantified).

==========

NOTE 11:
Date Entered: 1997/03/20 10:04:40
Analyst: dwilliam
This peak is likely associated with the 742.6 keV gamma line of Po-207.

==========

NOTE 12:
Date Entered: 1997/03/20 10:04:16
Analyst: dwilliam
This nuclide was removed from the Activity Summary section because in the analyst's judgment the nuclide was not present; some nuclides may be removed because their activity calculations are not meaningful (they are identified, not quantified).

Date Entered: 1997/03/20 10:04:40
Analyst: dwilliam
This peak is likely associated with the 742.6 keV gamma line of Po-207.

==========

NOTE 13:
Date Entered: 1997/03/20 09:54:01
Analyst: dwilliam
This peak may be associated with the 803.0 keV gamma line of Bi-206.

==========

NOTE 14:
Date Entered: 1997/03/20 10:01:30
Analyst: dwilliam
This peak is likely associated with the 807.5 keV gamma line of Po-206.

==========

NOTE 15:
Date Entered: 1997/03/20 09:54:30
Analyst: dwilliam
This peak may be associated with the 881.0 keV gamma line of Bi-206.

==========

NOTE 16:
Date Entered: 1997/03/20 09:49:20
Analyst: dwilliam
This peak may be associated with the 899.1 keV gamma line of Bi-204.

==========

NOTE 17:
Date Entered: 1997/03/20 09:50:29
Analyst: dwilliam
This peak is likely associated with the 911.2 keV gamma line of Ac-228, the 911.8 keV gamma line of Po-207, and the 911.8 keV gamma line of Bi-204.

==========

NOTE 18:
Date Entered: 1997/03/20 09:50:49
Analyst: dwilliam
This peak may be associated with the 918.3 keV gamma line of Bi-204.

==========

NOTE 19:
Date Entered: 1997/03/20 09:51:27
Analyst: dwilliam
This peak may be associated with the 983.9 keV gamma line of Bi-204.

==========

NOTE 20:
Date Entered: 1997/03/20 10:03:41
Analyst: dwilliam
This peak is likely associated with the 992.1 keV gamma line of Po-207.

==========

NOTE 21:
Date Entered: 1997/03/20 10:02:10
Analyst: dwilliam
This peak is likely associated with the 1032.3 keV gamma line of Po-206.

==========

CALIBRATION EQUATIONS==========

Energy vs. Channel

E(c) = -0.2001 + 0.7328*c - 2.733E-07*c^2 + 3.489E-11*c^3

E = energy (keV)
c = channel number

Resolution vs. Energy

FWHM(E) = 0.89 + 0.03064*SQRT(E)

FWHM = Full Width Half Max (keV)
E = energy (keV)

Efficiency vs. Energy

```
e(E) = exp { -3.776 + 0.9255*ln(962.1/E) + 0.1003*[ln(962.1/E)]^2
 - 0.0896*[ln(962.1/E)]^3 }

      e = efficiency (counts/gamma)
      E = energy (keV)
```

ATMOSPHERIC RADIONUCLIDE MEASUREMENT REPORT
Particulate Version

SAMPLE INFORMATION==========

Station ID:	CA002	Detector ID:	CAA2
Station Type:	ISAR2	Detector Type:	

Station Location: Vancouver, Canada
Detector Description: Detector A in Vancouver, Canada

Sample ID:	0022872	Sample Geometry:	DISK
Sample Quantity:	22735.00 m3	Sample Type:	Filter

Collection Start:	1997/03/17 19:45	Sampling Time:	23.78 hours
Collection Stop:	1997/03/18 19:32	Decay Time:	4.24 hours
Acquisition Start:	1997/03/18 23:46	Acquisition Time:	18.21 hours
Acquisition Stop:	1997/03/19 17:59	Avg Flow Rate:	956.06 m3/hr

Collection Station Comments:
goshka - Detector 1 Ranger (18-MAR-1997)

IDC Analysis General Comments:
This spectrum contains the following activation products: Bi-204, Bi-206 (weak), Po-206 (weak), Po-207 and At-209. A potential source of their injection is a medical facility (accelerator) near the IMS station. Leonid Vladimirski. 03/20/97.

I-123 is present in this spectrum and is seen at this site on occasion.

Calibration Update Performed. Certificate file
/data/gold1/rmsuser/genie/defaults/short_decay.cer

MEASUREMENT CATEGORIZATION==========

Categorization Legend

Level 1	= Normal Natural Rad. Meas.
Level 2	= Abnormal Natural Rad. Meas.
Level 3	= Normal Anthropogenic Rad. Meas.
Level 4	= Abnormal Anthropogenic Rad. Meas.

Spectrum Category (3) -- Normal Anthropogenic Rad. Meas.

Categorization Summary:

Name	Category	Categorization Comment
I-123	3	Within Statistical Range

ACTIVITY SUMMARY==========

NATURAL RADIOACTIVITY:

Nuclides Identified: BI-212, BI-214, K-40, NA-24, PB-214, TL-208

Nuclides Quantified:

Nuclide	Half-Life	Conc(uBq/m3)	%RelErr	Notes
BE-7	53.3 D	3.5E+03	2.54	
PB-212	10.64 H	1.7E+03	10.32	
ACTIVATION-PRODUCT RADIOACTIVITY:				
I-123	13.13 H	1E+02	4.03	
FISSION-PRODUCT RADIOACTIVITY:				
None Found				

MINIMUM DETECTABLE CONCENTRATION FOR KEY NUCLIDES==========

Nuclide	Half-Life	MDC(uBq/m3)
BA-140	12.75 D	9.96
CE-143	1.4 D	9.00
CS-134	2.06135 Y	2.97
CS-136	13.16 D	3.05
CS-137	30.0197 Y	3.07
I-131	8.04 D	3.25
I-133	20.8 H	6.07
MO-99	65.94 H	29.57
NB-95	35.15 D	3.00
RU-103	39.26 D	2.51
TE-132	78.2 H	2.91
ZR-95	64.02 D	4.83
ZR-97	17 H	7.78

PEAK SEARCH RESULTS==========

41 peaks found in spectrum by automated peak search.
31 peaks associated with nuclides by automated processing.
10 peaks not associated with nuclides by automated processing.
76 percent of peaks were associated with nuclides.

Note: "*" indicates that a peak was a component of a multiplet.

Energy	Centroid	Width	FWHM	%Eff	Net Area	%RelErr	Nuclide	Nts
74.87	102.38 *	17	1.29	10.53	6193.22	1.82	PB-212	
74.87	102.38 *	17	1.29	10.53	6193.22	1.82	PB-214	
74.87	102.38 *	17	1.29	10.53	6193.22	1.82	TL-208	
77.15	105.49 *	17	1.29	10.63	9413.60	1.56	BI-214	
77.15	105.49 *	17	1.29	10.63	9413.60	1.56	PB-212	
77.15	105.49 *	17	1.29	10.63	9413.60	1.56	PB-214	
87.22	119.25 *	22	1.30	10.91	3409.03	3.15	PB-212	
87.22	119.25 *	22	1.30	10.91	3409.03	3.15	PB-214	
89.91	122.92 *	22	1.31	10.95	1255.25	4.75	BI-214	
89.91	122.92 *	22	1.31	10.95	1255.25	4.75	PB-212	
93.02	127.16 *	22	1.31	10.98	187.88	20.69		1
115.10	157.30	9	1.24	10.90	302.47	24.98	PB-212	
159.06	217.31	15	1.23	9.95	3600.22	3.19	I-123	2
159.06	217.31	15	1.23	9.95	3600.22	3.19	TE-123M	3
238.66	325.95	16	1.32	7.94	19746.24	1.11	PB-212	
277.44	378.89	14	1.44	7.12	852.71	8.58	TL-208	
295.32	403.30 *	16	1.32	6.78	206.25	17.28	PB-214	

300.12	409.86	*	16	1.32	6.70	1053.46	7.13	PB-212	
338.42	462.14		7	1.25	6.07	181.26	25.21		4
351.97	480.64		12	1.59	5.87	436.45	13.11	PB-214	
374.76	511.75		15	1.54	5.56	563.86	10.46	PB212XR1	5
477.56	652.10		14	1.47	4.46	23591.65	0.97	BE-7	
510.78	697.45		19	2.03	4.19	2761.60	3.28	TL-208	
544.95	744.11		11	1.57	3.94	181.61	21.43		6
583.13	796.23		15	1.54	3.69	5977.21	2.00	TL-208	
609.26	831.90		9	1.75	3.54	408.48	11.36	BI-214	
727.25	993.00		10	1.63	2.99	1344.73	4.76	BI-212	
763.12	1041.99		10	1.78	2.85	103.86	29.46	TL-208	
781.85	1067.56	*	26	1.83	2.79	147.54	14.97		7
785.52	1072.57	*	26	1.83	2.77	216.93	12.69	BI-212	
785.52	1072.57	*	26	1.83	2.77	216.93	12.69	BI-214	
785.52	1072.57	*	26	1.83	2.77	216.93	12.69	PB-214	
790.23	1079.00	*	26	1.83	2.76	140.11	14.63		8
839.70	1146.55		6	0.45	2.60	33074.20	0.01	PB-214	
860.58	1175.07		9	1.76	2.54	782.97	6.71	TL-208	
899.15	1227.73		15	1.77	2.44	320.35	11.89		9
911.45	1244.53		13	2.05	2.41	214.52	16.55		10
984.05	1343.66		9	2.00	2.24	143.70	20.40		11
992.38	1355.05		18	1.09	2.23	81.40	23.53		12
1094.09	1493.94		11	1.51	2.04	77.21	30.45	TL-208	
1119.92	1529.22		7	1.52	2.00	73.53	30.46	BI-214	
1368.45	1868.63		10	1.68	1.68	51.22	38.30	NA-24	
1460.85	1994.83		15	2.10	1.59	2532.16	3.17	K-40	
1512.74	2065.69		10	1.85	1.55	68.37	27.60	BI-212	
1592.44	2174.54		12	2.08	1.49	160.25	15.95	TL-208	
1620.67	2213.10		9	2.03	1.47	145.14	16.90	BI-212	
1718.30	2346.45		6	0.57	1.41	21.35	28.48		13
1764.54	2409.60		11	2.14	1.38	83.74	24.01	BI-214	
2103.54	2872.63		16	3.25	1.23	252.73	12.33	TL-208	
2614.50	3570.50		13	2.64	1.10	1982.01	3.48	TL-208	

PEAK SEARCH NOTES==========

NOTE 1:
Date Entered: 1997/03/20 15:24:25
Analyst: dwilliam
Many radionuclides emit gamma rays with energies similar to this one. Therefore, this peak may be due to natural radiation or one of the noted atypical nuclides present in this spectrum.

==========

NOTE 2:
Date Entered: 1997/03/20 10:29:12
Analyst: dwilliam
The peak is real and the association is correct.

==========

NOTE 3:
Date Entered: 1997/03/20 10:28:59
Analyst: dwilliam
This nuclide was removed from the Activity Summary section because in the analyst's judgment the nuclide was not present; some nuclides may be removed because their activity calculations are not meaningful (they are identified, not quantified).

Date Entered: 1997/03/20 10:29:40
Analyst: dwilliam

This peak may be associated with I-123.

==========

NOTE 4:
Date Entered: 1997/03/20 14:40:30
Analyst: dwilliam
This peak is likely associated with the 338.4 keV gamma line of Po-206.

==========

NOTE 5:
Date Entered: 1997/03/20 14:32:00
Analyst: dwilliam
This peak is likely associated with the 374.8 keV gamma line of Bi-204.

==========

NOTE 6:
Date Entered: 1997/03/20 14:44:06
Analyst: dwilliam
This peak is likely associated with the 545.0 keV gamma line of At-209.

==========

NOTE 7:
Date Entered: 1997/03/20 14:45:02
Analyst: dwilliam
This peak is likely associated with the 781.9 keV gamma line of At-209.

==========

NOTE 8:
Date Entered: 1997/03/20 14:47:53
Analyst: dwilliam
This peak is likely associated with the 790.2 keV gamma line of At-209.

==========

NOTE 9:
Date Entered: 1997/03/20 14:32:42
Analyst: dwilliam
This peak is likely associated with the 899.1 keV gamma line of Bi-204.

==========

NOTE 10:
Date Entered: 1997/03/20 14:36:46
Analyst: dwilliam
This peak is likely associated with the 911.8 keV gamma line of Bi-204. It may
also be associated with the 911.2 keV gamma line of Ac-228.

==========

NOTE 11:
Date Entered: 1997/03/20 14:37:47
Analyst: dwilliam
This peak is likely associated with the 983.9 keV gamma line of Bi-204.

==========

NOTE 12:
Date Entered: 1997/03/20 14:43:26

Analyst: dwilliam
This peak is likely associated with the 992.1 keV gamma line of Po-207.

==========

NOTE 13:
Date Entered: 1997/03/20 14:48:22
Analyst: dwilliam
False peak detection; Type I error in peak processing.

==========

CALIBRATION EQUATIONS==========

Energy vs. Channel

$$E(c) = -0.1455 + 0.7327*c - 1.946E-07*c^2 + 2.317E-11*c^3$$

E = energy (keV)
c = channel number

Resolution vs. Energy

$$FWHM(E) = 0.89 + 0.03064*SQRT(E)$$

FWHM = Full Width Half Max (keV)
E = energy (keV)

Efficiency vs. Energy

$$e(E) = \exp \{ -3.776 + 0.9255*\ln(962.1/E) + 0.1003*[\ln(962.1/E)]^2 - 0.0896*[\ln(962.1/E)]^3 \}$$

e = efficiency (counts/gamma)
E = energy (keV)

ATMOSPHERIC RADIONUCLIDE MEASUREMENT REPORT
Particulate Version

SAMPLE INFORMATION==========

Station ID:	CA002	Detector ID:	CAA2
Station Type:	ISAR2	Detector Type:	

Station Location: Vancouver, Canada
Detector Description: Detector A in Vancouver, Canada

Sample ID:	0022910	Sample Geometry:	DISK
Sample Quantity:	21336.00 m3	Sample Type:	Filter

Collection Start:	1997/03/18 19:35	Sampling Time:	22.42 hours
Collection Stop:	1997/03/19 18:00	Decay Time:	4.26 hours
Acquisition Start:	1997/03/19 22:15	Acquisition Time:	19.50 hours
Acquisition Stop:	1997/03/20 17:45	Avg Flow Rate:	951.65 m3/hr

Collection Station Comments:
goshka - Detector 1 Ranger (19-MAR-1997)

IDC Analysis General Comments:
This spectrum contains the following activation products: Bi-203, Bi-204, Po-204, Bi-206, Po-206, Po-207 and At-209. A potential source of their injection is a medical facility (accelerator) near the IMS station. Leonid Vladimirski. 03/20/97.

I-123 is present in this spectrum and is seen at this site on occasion.

Calibration Update Performed. Certificate file
/data/gold1/rmsuser/genie/defaults/short_decay.cer

MEASUREMENT CATEGORIZATION==========

Categorization Legend

Level 1	= Normal Natural Rad. Meas.
Level 2	= Abnormal Natural Rad. Meas.
Level 3	= Normal Anthropogenic Rad. Meas.
Level 4	= Abnormal Anthropogenic Rad. Meas.

Spectrum Category (3) -- Normal Anthropogenic Rad. Meas.

Categorization Summary:

Name	Category	Categorization Comment
I-123	3	Within Statistical Range

ACTIVITY SUMMARY==========

NATURAL RADIOACTIVITY:

Nuclides Identified: BI-212, BI-214, K-40, NA-22, PB-214, TH-228, TL-208, UNKNAT01

Nuclides Quantified:

Nuclide	Half-Life	Conc(uBq/m3)	%RelErr	Notes
BE-7	53.3 D	1.1E+03	2.96	
PB-212	10.64 H	1.4E+03	10.33	
ACTIVATION-PRODUCT RADIOACTIVITY:				
I-123	13.13 H	34	7.23	
FISSION-PRODUCT RADIOACTIVITY:				
None Found				

MINIMUM DETECTABLE CONCENTRATION FOR KEY NUCLIDES==========

Nuclide	Half-Life	MDC(uBq/m3)
BA-140	12.75 D	11.52
CE-143	1.4 D	7.99
CS-134	2.06135 Y	3.21
CS-136	13.16 D	3.46
CS-137	30.0197 Y	3.59
I-131	8.04 D	3.18
I-133	20.8 H	6.52
MO-99	65.94 H	35.32
NB-95	35.15 D	3.34
RU-103	39.26 D	2.74
TE-132	78.2 H	2.67
ZR-95	64.02 D	5.41
ZR-97	17 H	6.78

PEAK SEARCH RESULTS==========

49 peaks found in spectrum by automated peak search.
33 peaks associated with nuclides by automated processing.
16 peaks not associated with nuclides by automated processing.
67 percent of peaks were associated with nuclides.

Note: "*" indicates that a peak was a component of a multiplet.

Energy	Centroid	Width	FWHM	%Eff	Net Area	%RelErr	Nuclide	Nts
72.75	99.62 *	17	1.27	10.43	1427.71	4.19	TL-208	
74.81	102.42 *	17	1.27	10.53	6954.14	1.71	PB-212	
74.81	102.42 *	17	1.27	10.53	6954.14	1.71	PB-214	
74.81	102.42 *	17	1.27	10.53	6954.14	1.71	TL-208	
77.07	105.51 *	17	1.27	10.63	8642.87	1.58	BI-214	
77.07	105.51 *	17	1.27	10.63	8642.87	1.58	PB-212	
77.07	105.51 *	17	1.27	10.63	8642.87	1.58	PB-214	
84.81	116.07 *	19	1.31	10.86	414.18	11.55	TH-228	
84.81	116.07 *	19	1.31	10.86	414.18	11.55	TL-208	
87.17	119.29 *	19	1.31	10.91	3342.28	3.17	PB-212	
87.17	119.29 *	19	1.31	10.91	3342.28	3.17	PB-214	
89.79	122.86 *	19	1.32	10.95	1088.47	5.03	BI-214	
89.79	122.86 *	19	1.32	10.95	1088.47	5.03	PB-212	
137.06	187.38	9	0.48	10.49	152.59	289.67		1
158.99	217.30	15	1.22	9.95	1225.75	6.80	I-123	2
158.99	217.30	15	1.22	9.95	1225.75	6.80	TE-123M	3

238.62	325.98	16	1.30	7.94	16357.48	1.23	PB-212	
277.37	378.87	11	1.41	7.12	670.69	9.63	TL-208	
287.04	392.07	13	3.83	6.93	372.96	23.53		4
295.20	403.20 *	20	1.25	6.78	181.77	17.36	PB-214	
300.10	409.89 *	20	1.25	6.70	790.49	7.75	PB-212	
338.41	462.18	13	1.43	6.07	279.04	18.56		5
351.92	480.62	8	1.43	5.87	400.47	13.86	PB-214	
374.74	511.77	17	1.42	5.56	1777.50	4.47	PB212XR1	6
477.56	652.12	14	1.47	4.46	7477.52	1.80	BE-7	
510.84	697.56	19	2.09	4.19	2592.58	3.44	TL-208	
545.07	744.29	9	1.55	3.94	278.08	15.52		7
583.14	796.27	19	1.58	3.69	4952.36	2.26	TL-208	
609.29	831.97	9	1.46	3.54	323.12	13.66	BI-214	
670.61	915.69	10	1.92	3.23	187.40	22.17	TL208XR4	
727.30	993.09	14	1.67	2.99	1000.65	5.90	BI-212	
742.67	1014.08	11	1.60	2.93	143.93	24.26	BI-214	8
742.67	1014.08	11	1.60	2.93	143.93	24.26	ZR-97	9
762.88	1041.67	13	1.68	2.85	136.53	24.68	TL-208	
781.79	1067.49 *	25	1.72	2.79	134.78	19.38		10
785.55	1072.63 *	25	1.72	2.77	121.41	20.14	BI-212	
785.55	1072.63 *	25	1.72	2.77	121.41	20.14	BI-214	
785.55	1072.63 *	25	1.72	2.77	121.41	20.14	PB-214	
790.36	1079.19 *	25	1.72	2.76	127.22	19.31		11
803.29	1096.85 *	20	1.50	2.71	90.85	25.18	UNKNAT01	12
807.32	1102.36 *	20	1.50	2.70	114.91	23.49		13
820.11	1119.82	9	1.32	2.66	62.80	41.48		14
860.52	1174.99	20	1.81	2.54	696.67	7.32	TL-208	
883.97	1207.01	12	1.32	2.48	77.65	31.39		15
899.16	1227.76	12	1.78	2.44	1090.66	5.50		16
911.66	1244.83 *	20	1.81	2.41	465.17	9.23		17
918.01	1253.50 *	20	1.81	2.39	117.19	16.75		18
983.91	1343.50	14	1.79	2.24	509.58	8.71		19
992.33	1354.99	12	1.60	2.23	225.27	15.58		20
1016.20	1387.58	11	1.54	2.18	112.05	24.48		21
1032.54	1409.90	13	1.99	2.15	144.62	21.81		22
1078.34	1472.45	10	1.06	2.06	44.71	77.18	BI-212	
1093.81	1493.58	8	1.64	2.04	87.97	30.91	TL-208	
1120.39	1529.87	11	1.47	1.99	55.60	43.36	BI-214	
1273.92	1739.56	14	2.65	1.78	112.45	26.35	NA-22	
1460.88	1994.92	19	2.09	1.59	2744.67	3.04	K-40	
1620.79	2213.34	15	2.85	1.47	152.82	16.56	BI-212	
1764.77	2410.01	14	2.71	1.38	79.50	27.63	BI-214	
2103.69	2872.96	15	2.86	1.23	208.72	13.49	TL-208	
2614.54	3570.72	19	2.72	1.10	1738.10	3.68	TL-208	

PEAK SEARCH NOTES==========

NOTE 1:
Date Entered: 1997/03/21 15:55:20
Analyst: dwilliam
False peak detection; Type I error in peak processing.

==========

NOTE 2:
Date Entered: 1997/03/20 16:02:17
Analyst: dwilliam
The peak is real and the association is correct.

==========

NOTE 3:

Date Entered: 1997/03/20 16:01:08
Analyst: dwilliam
This nuclide was removed from the Activity Summary section because in the analyst's judgment the nuclide was not present; some nuclides may be removed because their activity calculations are not meaningful (they are identified, not quantified).

Date Entered: 1997/03/20 16:02:02
Analyst: dwilliam
This peak is associated with I-123.

==========

NOTE 4:
Date Entered: 1997/03/21 15:56:13
Analyst: dwilliam
This peak is likely associated with the 286.5 keV gamma line of Po-206.

==========

NOTE 5:
Date Entered: 1997/03/21 16:03:31
Analyst: dwilliam
This peak is likely associated with the 338.4 keV gamma line of Po-206. It may also be associated with the 338.3 keV gamma line of Ac-228.

==========

NOTE 6:
Date Entered: 1997/03/21 16:04:04
Analyst: dwilliam
This peak is likely associated with the 374.8 keV gamma line of Bi-204.

==========

NOTE 7:
Date Entered: 1997/03/21 16:16:20
Analyst: dwilliam
This peak is likely associated with the 545.0 keV gamma line of At-209.

==========

NOTE 8:
Date Entered: 1997/03/21 16:05:48
Analyst: dwilliam
This peak is likely associated with the 742.6 keV gamma line of Po-207.

==========

NOTE 9:
Date Entered: 1997/03/21 16:05:48
Analyst: dwilliam
This peak is likely associated with the 742.6 keV gamma line of Po-207.

Date Entered: 1997/03/21 16:05:53
Analyst: dwilliam
This nuclide was removed from the Activity Summary section because in the analyst's judgment the nuclide was not present; some nuclides may be removed because their activity calculations are not meaningful (they are identified, not quantified).

==========

NOTE 10:
Date Entered: 1997/03/21 16:16:40
Analyst: dwilliam
This peak is likely associated with the 781.9 keV gamma line of At-209.

==========

NOTE 11:
Date Entered: 1997/03/21 16:17:05
Analyst: dwilliam
This peak is likely associated with the 790.2 keV gamma line of At-209.

==========

NOTE 12:
Date Entered: 1997/03/21 16:06:27
Analyst: dwilliam
This peak is likely associated with the 803.0 keV gamma line of Bi-206.

==========

NOTE 13:
Date Entered: 1997/03/21 16:06:49
Analyst: dwilliam
This peak is likely associated with the 807.5 keV gamma line of Po-206.

==========

NOTE 14:
Date Entered: 1997/03/21 16:09:06
Analyst: dwilliam
This peak may be associated with the 820.2 keV gamma line of Bi-203.

==========

NOTE 15:
Date Entered: 1997/03/21 16:10:11
Analyst: dwilliam
This peak may be associated with the 884.0 keV gamma line of Po-204.

==========

NOTE 16:
Date Entered: 1997/03/21 16:10:37
Analyst: dwilliam
This peak is likely associated with the 899.1 keV gamma line of Bi-204.

==========

NOTE 17:
Date Entered: 1997/03/21 16:13:05
Analyst: dwilliam
This peak is likely associated with the 911.8 keV gamma line of Po-207, the
911.8 keV gamma line of Bi-204, and the 911.2 keV gamma line of Ac-228,

==========

NOTE 18:
Date Entered: 1997/03/21 16:13:50
Analyst: dwilliam
This peak is likely associated with the 918.3 keV gamma line of Bi-204.

==========

NOTE 19:
Date Entered: 1997/03/21 16:14:16
Analyst: dwilliam
This peak is likely associated with the 983.9 keV gamma line of Bi-204.

==========

NOTE 20:
Date Entered: 1997/03/21 16:14:28
Analyst: dwilliam
This peak is likely associated with the 992.1 keV gamma line of Po-207.

==========

NOTE 21:
Date Entered: 1997/03/21 16:18:40
Analyst: dwilliam
This peak is likely associated with the 1016.3 keV gamma line of Po-204.

==========

NOTE 22:
Date Entered: 1997/03/21 16:14:55
Analyst: dwilliam
This peak is likely associated with the 1032.3 keV gamma line of Po-206.

==========

CALIBRATION EQUATIONS==========

Energy vs. Channel

$$E(c) = -0.249 + 0.7329*c - 2.962E-07*c^2 + 3.723E-11*c^3$$

E = energy (keV)
c = channel number

Resolution vs. Energy

$$FWHM(E) = 0.89 + 0.03064*SQRT(E)$$

FWHM = Full Width Half Max (keV)
E = energy (keV)

Efficiency vs. Energy

$$e(E) = \exp \{ -3.776 + 0.9255*\ln(962.1/E) + 0.1003*[\ln(962.1/E)]^2 - 0.0896*[\ln(962.1/E)]^3 \}$$

e = efficiency (counts/gamma)
E = energy (keV)

ATMOSPHERIC RADIONUCLIDE MEASUREMENT REPORT
Particulate Version

SAMPLE INFORMATION==========

Station ID:	CA002	Detector ID:	CAA2
Station Type:	ISAR2	Detector Type:	

Station Location: Vancouver, Canada
Detector Description: Detector A in Vancouver, Canada

Sample ID:	0022953	Sample Geometry:	DISK
Sample Quantity:	16909.00 m3	Sample Type:	Filter

Collection Start:	1997/03/19 18:02	Sampling Time:	28.28 hours
Collection Stop:	1997/03/20 22:19	Decay Time:	4.24 hours
Acquisition Start:	1997/03/21 02:33	Acquisition Time:	17.23 hours
Acquisition Stop:	1997/03/21 19:47	Avg Flow Rate:	597.91 m3/hr

Collection Station Comments:
goshka - Detector 1 Ranger (20-MAR-1997)

IDC Analysis General Comments:
This spectrum contains the following activation products: Bi-204 and Po-206. These nuclides have contributed to the net peak areas associated with AC-228 in this spectrum; therefore, the presence of AC-228 is overestimated. A probable source of their injection is an accelerator near the IMS station. Leonid Vladimirski. 03/26/97.

Calibration Update Performed. Certificate file
/data/gold1/rmsuser/genie/defaults/short_decay.cer

MEASUREMENT CATEGORIZATION==========

Categorization Legend

Level 1 = Normal Natural Rad. Meas.
Level 2 = Abnormal Natural Rad. Meas.
Level 3 = Normal Anthropogenic Rad. Meas.
Level 4 = Abnormal Anthropogenic Rad. Meas.

Spectrum Category (1) -- Normal Natural Rad. Meas.

ACTIVITY SUMMARY==========

NATURAL RADIOACTIVITY:

Nuclides Identified: AC-228, BI-212, BI-214, K-40, PB-214, TL-208, UNKNAT01

Nuclides Quantified:

Nuclide	Half-Life	Conc(uBq/m3)	%RelErr	Notes
BE-7	53.3 D	2.9E+03	2.67	
PB-212	10.64 H	1.3E+03	10.37	

ACTIVATION-PRODUCT RADIOACTIVITY:

None Found

FISSION-PRODUCT RADIOACTIVITY:

None Found

MINIMUM DETECTABLE CONCENTRATION FOR KEY NUCLIDES=========================

Nuclide	Half-Life	MDC(uBq/m3)
BA-140	12.75 D	12.67
CE-143	1.4 D	10.93
CS-134	2.06135 Y	3.73
CS-136	13.16 D	3.93
CS-137	30.0197 Y	3.63
I-131	8.04 D	3.87
I-133	20.8 H	7.62
MO-99	65.94 H	36.40
NB-95	35.15 D	3.62
RU-103	39.26 D	3.05
TE-132	78.2 H	3.37
ZR-95	64.02 D	5.79
ZR-97	17 H	10.05

PEAK SEARCH RESULTS===

30 peaks found in spectrum by automated peak search.
26 peaks associated with nuclides by automated processing.
4 peaks not associated with nuclides by automated processing.
87 percent of peaks were associated with nuclides.

Note: "*" indicates that a peak was a component of a multiplet.

Energy	Centroid	Width	FWHM	%Eff	Net Area	%RelErr	Nuclide	Nts
74.75	102.36 *	17	1.28	10.53	3680.83	2.40	PB-212	
74.75	102.36 *	17	1.28	10.53	3680.83	2.40	PB-214	
74.75	102.36 *	17	1.28	10.53	3680.83	2.40	TL-208	
77.06	105.51 *	17	1.28	10.63	4758.72	2.20	BI-214	
77.06	105.51 *	17	1.28	10.63	4758.72	2.20	PB-212	
77.06	105.51 *	17	1.28	10.63	4758.72	2.20	PB-214	
87.11	119.23 *	18	1.33	10.90	2022.18	4.19	PB-212	
87.11	119.23 *	18	1.33	10.90	2022.18	4.19	PB-214	
89.86	122.98 *	18	1.33	10.95	572.54	7.47	AC-228	
89.86	122.98 *	18	1.33	10.95	572.54	7.47	BI-214	
89.86	122.98 *	18	1.33	10.95	572.54	7.47	PB-212	
238.61	325.99	16	1.31	7.94	10158.14	1.58	PB-212	
277.40	378.95	16	1.40	7.12	415.43	13.50	TL-208	
295.25	403.30 *	17	1.47	6.78	214.62	15.65	PB-214	
300.12	409.96 *	17	1.48	6.70	660.70	9.11	PB-212	
338.52	462.37	6	1.06	6.07	142.39	38.90	AC-228	1
351.91	480.65 *	13	1.44	5.87	402.76	11.98	PB-214	
355.65	485.75 *	13	1.45	5.82	63.25	34.93		2
374.66	511.70	12	1.63	5.56	563.33	9.44	PB212XR1	3
477.54	652.15	9	1.44	4.46	13774.68	1.27	BE-7	
510.79	697.55	19	1.98	4.19	1856.83	4.09	TL-208	
583.11	796.30	15	1.57	3.69	3097.14	2.93	AC-228	
583.11	796.30	15	1.57	3.69	3097.14	2.93	TL-208	
609.21	831.92	9	1.58	3.54	258.57	15.01	BI-214	

727.30	993.18	18	1.57	2.99	656.47	7.33	AC-228	
727.30	993.18	18	1.57	2.99	656.47	7.33	BI-212	
785.44	1072.57	9	1.45	2.77	66.86	37.10	BI-212	
785.44	1072.57	9	1.45	2.77	66.86	37.10	BI-214	
785.44	1072.57	9	1.45	2.77	66.86	37.10	PB-214	
802.85	1096.34	14	1.05	2.72	62.63	47.54	UNKNAT01	
860.57	1175.17	9	1.68	2.54	352.56	10.75	TL-208	
899.16	1227.87	13	1.56	2.44	280.66	12.44		4
911.39	1244.57	10	1.72	2.41	196.23	15.04	AC-228	5
969.21	1323.54	10	0.55	2.28	67.88	210.37	AC-228	
984.04	1343.78	19	1.45	2.24	143.07	17.74		6
1032.32	1409.73	11	1.46	2.15	71.45	30.60		7
1460.84	1995.03	22	2.04	1.59	2279.24	3.27	K-40	
1592.42	2174.77	10	2.11	1.49	75.58	25.07	TL-208	
1620.61	2213.28	18	2.10	1.47	79.17	24.93	BI-212	
2103.53	2872.92	18	3.02	1.23	137.25	17.54	TL-208	
2614.58	3570.88	17	2.55	1.10	1043.93	4.88	TL-208	

PEAK SEARCH NOTES==========

NOTE 1:
Date Entered: 1997/03/24 14:21:15
Analyst: dwilliam
This peak is likely associated with the 338.4 keV gamma line of Po-206 and the 338.3 keV gamma line of Ac-228.

==========

NOTE 2:
Date Entered: 1997/03/24 11:20:33
Analyst: dwilliam
False peak detection; Type I error in peak processing.

==========

NOTE 3:
Date Entered: 1997/03/24 14:19:07
Analyst: dwilliam
This peak may be associated with the 374.8 keV gamma line of Bi-204.

==========

NOTE 4:
Date Entered: 1997/03/24 10:42:44
Analyst: dwilliam
This peak is likely associated with the 899.1 keV gamma line of Bi-204.

==========

NOTE 5:
Date Entered: 1997/03/24 14:20:09
Analyst: dwilliam
This peak is likely associated with the 911.2 keV gamma line of Ac-228 and the 911.8 keV gamma line of Bi-204.

==========

NOTE 6:
Date Entered: 1997/03/24 10:41:51
Analyst: dwilliam
This peak is likely associated with the 983.9 keV gamma line of Bi-204.

```
================================================================================

NOTE 7:
Date Entered: 1997/03/24 10:42:24
Analyst: dwilliam
This peak is likely associated with the 1032.3 keV gamma line of Po-206.

================================================================================


CALIBRATION EQUATIONS=========================================================

Energy vs. Channel

       E(c) = -0.2624 + 0.7329*c - 3.425E-07*c^2 + 5.004E-11*c^3

              E = energy (keV)
              c = channel number


Resolution vs. Energy

       FWHM(E) = 0.89 + 0.03064*SQRT(E)

              FWHM = Full Width Half Max (keV)
              E = energy (keV)


Efficiency vs. Energy

       e(E) = exp { -3.776 + 0.9255*ln(962.1/E) + 0.1003*[ln(962.1/E)]^2
        - 0.0896*[ln(962.1/E)]^3 }

              e = efficiency (counts/gamma)
              E = energy (keV)
```

ATMOSPHERIC RADIONUCLIDE MEASUREMENT REPORT
Particulate Version

SAMPLE INFORMATION==========

Station ID:	CA002	Detector ID:	CAA2
Station Type:	ISAR2	Detector Type:	

Station Location: Vancouver, Canada
Detector Description: Detector A in Vancouver, Canada

Sample ID:	0022978	Sample Geometry:	DISK
Sample Quantity:	20936.00 m3	Sample Type:	Filter

Collection Start:	1997/03/20 22:21	Sampling Time:	21.48 hours
Collection Stop:	1997/03/21 19:49	Decay Time:	4.25 hours
Acquisition Start:	1997/03/22 00:04	Acquisition Time:	18.00 hours
Acquisition Stop:	1997/03/22 18:04	Avg Flow Rate:	974.67 m3/hr

Collection Station Comments:
goshka - Detector 1 Ranger (21-MAR-1997)

IDC Analysis General Comments:
This spectrum contains the following activation products: Bi-204, Po-206 and Po-207.. A probable source of their injection is an accelerator near the IMS station. Leonid Vladimirski. 03/26/97.

Calibration Update Performed. Certificate file
/data/gold1/rmsuser/genie/defaults/short_decay.cer

MEASUREMENT CATEGORIZATION==========

Categorization Legend

Level 1 = Normal Natural Rad. Meas.
Level 2 = Abnormal Natural Rad. Meas.
Level 3 = Normal Anthropogenic Rad. Meas.
Level 4 = Abnormal Anthropogenic Rad. Meas.

Spectrum Category (1) -- Normal Natural Rad. Meas.

ACTIVITY SUMMARY==========

NATURAL RADIOACTIVITY:

Nuclides Identified: BI-212, BI-214, K-40, PB-214, TL-208, UNKNAT01

Nuclides Quantified:

Nuclide	Half-Life	Conc(uBq/m3)	%RelErr	Notes
BE-7	53.3 D	3.4E+03	2.56	
PB-212	10.64 H	2.9E+03	10.28	

ACTIVATION-PRODUCT RADIOACTIVITY:

None Found

FISSION-PRODUCT RADIOACTIVITY:

None Found

MINIMUM DETECTABLE CONCENTRATION FOR KEY NUCLIDES==========

Nuclide	Half-Life	MDC(uBq/m3)
BA-140	12.75 D	11.84
CE-143	1.4 D	9.71
CS-134	2.06135 Y	3.17
CS-136	13.16 D	3.25
CS-137	30.0197 Y	3.47
I-131	8.04 D	3.72
I-133	20.8 H	6.73
MO-99	65.94 H	31.48
NB-95	35.15 D	3.41
RU-103	39.26 D	2.92
TE-132	78.2 H	3.37
ZR-95	64.02 D	5.32
ZR-97	17 H	8.08

PEAK SEARCH RESULTS==========

41 peaks found in spectrum by automated peak search.
33 peaks associated with nuclides by automated processing.
8 peaks not associated with nuclides by automated processing.
80 percent of peaks were associated with nuclides.

Note: "*" indicates that a peak was a component of a multiplet.

Energy	Centroid	Width	FWHM	%Eff	Net Area	%RelErr	Nuclide	Nts
74.74	102.39 *	17	1.26	10.53	9649.79	1.42	PB-212	
74.74	102.39 *	17	1.26	10.53	9649.79	1.42	PB-214	
74.74	102.39 *	17	1.26	10.53	9649.79	1.42	TL-208	
77.02	105.50 *	17	1.27	10.62	14219.20	1.24	BI-214	
77.02	105.50 *	17	1.27	10.62	14219.20	1.24	PB-212	
77.02	105.50 *	17	1.27	10.62	14219.20	1.24	PB-214	
84.83	116.16 *	20	1.32	10.86	545.84	9.42	TL-208	
87.12	119.27 *	20	1.32	10.90	5286.19	2.42	PB-212	
87.12	119.27 *	20	1.32	10.90	5286.19	2.42	PB-214	
89.82	122.96 *	20	1.33	10.95	1698.66	3.91	BI-214	
89.82	122.96 *	20	1.33	10.95	1698.66	3.91	PB-212	
92.73	126.93 *	20	1.33	10.98	141.81	29.68		1
115.18	157.56	11	0.81	10.90	425.88	107.58	PB-212	
238.61	325.99	12	1.29	7.94	32689.06	0.84	PB-212	
277.37	378.87	10	1.39	7.12	1265.18	6.44	TL-208	
286.55	391.41	16	0.49	6.94	149.06	299.77		2
295.14	403.12 *	18	1.27	6.79	181.04	18.76	PB-214	
300.08	409.87 *	18	1.27	6.70	1692.68	4.97	PB-212	
338.38	462.15	15	1.11	6.07	224.55	20.16		3
351.87	480.56	8	1.29	5.87	315.04	18.80	PB-214	
374.70	511.71	10	1.26	5.56	569.09	10.18	PB212XR1	4
452.91	618.48	13	1.01	4.69	152.26	45.02	BI-212	
477.56	652.13	14	1.45	4.46	20880.89	1.03	BE-7	
510.77	697.47	19	1.84	4.19	3834.46	2.71	TL-208	
583.15	796.30	17	1.57	3.69	9860.33	1.52	TL-208	
609.30	832.00	19	1.72	3.54	361.23	12.38	BI-214	

727.29	993.13	11	1.60	2.99	1986.51	3.70	BI-212	
763.19	1042.15	7	1.32	2.85	135.96	21.68	TL-208	
785.51	1072.64	10	1.45	2.77	241.47	14.72	BI-212	
785.51	1072.64	10	1.45	2.77	241.47	14.72	BI-214	
785.51	1072.64	10	1.45	2.77	241.47	14.72	PB-214	
802.99	1096.51	10	0.52	2.72	81.45	246.69	UNKNAT01	
860.51	1175.08	14	1.77	2.54	1344.55	4.56	TL-208	
893.20	1219.73 *	20	1.88	2.45	106.75	17.21	BI-212	
898.99	1227.63 *	20	1.89	2.44	326.72	11.50		5
911.39	1244.57	11	1.67	2.41	230.83	14.96		6
951.95	1299.98	13	1.22	2.31	46.69	40.26	BI-212	
983.71	1343.35	19	1.74	2.24	127.75	23.14		7
992.07	1354.77	14	1.31	2.23	71.58	32.19		8
1079.00	1473.53	11	1.75	2.06	118.36	22.56	BI-212	
1093.68	1493.58	15	1.81	2.04	167.61	18.05	TL-208	
1120.07	1529.63	7	1.18	2.00	41.63	59.43	BI-214	
1460.72	1995.02	15	2.06	1.59	2307.09	3.31	K-40	
1592.39	2174.91	10	2.25	1.49	314.35	10.69	TL-208	
1620.69	2213.57	16	1.98	1.47	221.13	12.75	BI-212	
1764.56	2410.12	7	1.34	1.38	63.72	27.54	BI-214	
1972.77	2694.55	10	0.57	1.28	25.60	54.43		9
2103.32	2872.87	16	3.13	1.23	418.77	9.27	TL-208	
2614.54	3570.90	13	2.68	1.10	3293.61	2.66	TL-208	

PEAK SEARCH NOTES==========

NOTE 1:
Date Entered: 1997/03/24 11:34:31
Analyst: dwilliam
Many radionuclides emit gamma rays with energies similar to this one. Therefore, this peak may be due to natural radiation or one of the noted atypical nuclides present in this spectrum.

==========

NOTE 2:
Date Entered: 1997/03/24 11:25:29
Analyst: dwilliam
False peak detection; Type I error in peak processing.

Date Entered: 1997/03/26 14:54:26
Analyst: dwilliam
Originally, this peak was thought to be false; however, after further review, this peak was found to be real. It is likely a multiplet associated with the 286.4 keV gamma line of Po-206, and the weak 288.1 keV gamma line of Bi-212.

==========

NOTE 3:
Date Entered: 1997/03/24 11:26:30
Analyst: dwilliam
This peak is likely associated with the 338.4 keV gamma line of Po-206. It may also be associated with the 338.3 keV gamma line of Ac-228.

==========

NOTE 4:
Date Entered: 1997/03/24 14:29:40
Analyst: dwilliam
This peak may be associated with the 374.8 keV gamma line of Bi-204.

==========

NOTE 5:
Date Entered: 1997/03/24 11:26:50
Analyst: dwilliam
This peak is likely associated with the 899.1 keV gamma line of Bi-204.

==========

NOTE 6:
Date Entered: 1997/03/24 11:28:13
Analyst: dwilliam
This peak is likely associated with the 911.8 keV gamma line of Po-207, the
911.8 keV gamma line of Bi-204, and the 911.2 keV gamma line of Ac-228,

==========

NOTE 7:
Date Entered: 1997/03/24 11:27:51
Analyst: dwilliam
This peak is likely associated with the 983.9 keV gamma line of Bi-204.

==========

NOTE 8:
Date Entered: 1997/03/24 11:28:02
Analyst: dwilliam
This peak is likely associated with the 992.1 keV gamma line of Po-207.

==========

NOTE 9:
Date Entered: 1997/03/24 11:29:20
Analyst: dwilliam
False peak detection; Type I error in peak processing.

==========

CALIBRATION EQUATIONS==========

Energy vs. Channel

$$E(c) = -0.3185 + 0.7331*c - 5.907E-07*c^2 + 9.742E-11*c^3$$

E = energy (keV)
c = channel number

Resolution vs. Energy

$$FWHM(E) = 0.89 + 0.03064*SQRT(E)$$

FWHM = Full Width Half Max (keV)
E = energy (keV)

Efficiency vs. Energy

$$e(E) = \exp \{ -3.776 + 0.9255*\ln(962.1/E) + 0.1003*[\ln(962.1/E)]^2 - 0.0896*[\ln(962.1/E)]^3 \}$$

e = efficiency (counts/gamma)
E = energy (keV)

ATMOSPHERIC RADIONUCLIDE MEASUREMENT REPORT
Particulate Version

SAMPLE INFORMATION==========

Station ID:	CA002	Detector ID:	CAA2
Station Type:	ISAR2	Detector Type:	

Station Location: Vancouver, Canada
Detector Description: Detector A in Vancouver, Canada

Sample ID:	0023016	Sample Geometry:	DISK
Sample Quantity:	21683.00 m3	Sample Type:	Filter

Collection Start:	1997/03/21 19:51	Sampling Time:	22.26 hours
Collection Stop:	1997/03/22 18:06	Decay Time:	4.24 hours
Acquisition Start:	1997/03/22 22:21	Acquisition Time:	19.50 hours
Acquisition Stop:	1997/03/23 17:51	Avg Flow Rate:	974.08 m3/hr

Collection Station Comments:
goshka - Detector 1 Ranger (22-MAR-1997)

IDC Analysis General Comments:
This spectrum contains the following activation products: Bi-204, Po-204, Po-206, Po-207 and At-209. These nuclides have contributed to the net peak areas associated with AC-228 in this spectrum; therefore, the presence of AC-228 is overestimated. A probable source of their injection is an accelerator near the IMS station. Leonid Vladimirski. 03/24/97.

This spectrum indicates the presence of I-123, which is observed from time to time at this station. Its source is known. The estimated concentration of I-123 exceeds the upper bound for this nuclide at this station. The cause of this unusual level of I-123 is under investigation. Leonid Vladimirski. 03/24/97.

I-123 is present in this spectrum and is seen at this site on occasion.

Calibration Update Performed. Certificate file
/data/gold1/rmsuser/genie/defaults/short_decay.cer

MEASUREMENT CATEGORIZATION==========

Categorization Legend

Level 1 = Normal Natural Rad. Meas.
Level 2 = Abnormal Natural Rad. Meas.
Level 3 = Normal Anthropogenic Rad. Meas.
Level 4 = Abnormal Anthropogenic Rad. Meas.

Spectrum Category (4) -- Abnormal Anthropogenic Rad. Meas.

Categorization Summary:

Name	Category	Categorization Comment
I-123	4	Above Statistical Range

ACTIVITY SUMMARY==

NATURAL RADIOACTIVITY:

Nuclides Identified: AC-228, BI-212, BI-214, K-40, PB-214, TL-208, UNKNAT01

Nuclides Quantified:

Nuclide	Half-Life	Conc(uBq/m3)	%RelErr	Notes
BE-7	53.3 D	3.3E+03	2.55	
PB-212	10.64 H	5.3E+03	10.27	

ACTIVATION-PRODUCT RADIOACTIVITY:

I-123	13.13 H	4.8E+03	2.48	

FISSION-PRODUCT RADIOACTIVITY:

None Found

MINIMUM DETECTABLE CONCENTRATION FOR KEY NUCLIDES=======================

Nuclide	Half-Life	MDC(uBq/m3)
BA-140	12.75 D	15.28
CE-143	1.4 D	10.69
CS-134	2.06135 Y	3.64
CS-136	13.16 D	3.83
CS-137	30.0197 Y	4.07
I-131	8.04 D	4.43
I-133	20.8 H	10.08
MO-99	65.94 H	40.57
NB-95	35.15 D	4.01
RU-103	39.26 D	3.44
TE-132	78.2 H	3.85
ZR-95	64.02 D	6.07
ZR-97	17 H	6.38

PEAK SEARCH RESULTS===

56 peaks found in spectrum by automated peak search.
44 peaks associated with nuclides by automated processing.
12 peaks not associated with nuclides by automated processing.
79 percent of peaks were associated with nuclides.

Note: "*" indicates that a peak was a component of a multiplet.

Energy	Centroid	Width	FWHM	%Eff	Net Area	%RelErr	Nuclide	Nts
74.79	102.39 *	17	1.28	10.53	20282.59	0.98	PB-212	
74.79	102.39 *	17	1.28	10.53	20282.59	0.98	PB-214	
74.79	102.39 *	17	1.28	10.53	20282.59	0.98	TL-208	
77.08	105.51 *	17	1.28	10.63	30344.94	0.85	BI-214	
77.08	105.51 *	17	1.28	10.63	30344.94	0.85	PB-212	
77.08	105.51 *	17	1.28	10.63	30344.94	0.85	PB-214	
84.98	116.29 *	16	1.32	10.86	429.80	17.54	TL-208	
87.18	119.29 *	16	1.32	10.91	10751.39	1.80	PB-212	
87.18	119.29 *	16	1.32	10.91	10751.39	1.80	PB-214	
89.87	122.96 *	16	1.33	10.95	3571.97	2.87	AC-228	
89.87	122.96 *	16	1.33	10.95	3571.97	2.87	BI-214	

89.87	122.96	*	16	1.33	10.95	3571.97	2.87	PB-212	
115.19	157.51		11	0.93	10.90	826.82	45.99	PB-212	
159.00	217.29		15	1.25	9.95	179387.95	0.35	I-123	1
159.00	217.29		15	1.25	9.95	179387.95	0.35	TE-123M	2
238.63	325.97		16	1.29	7.94	63092.29	0.61	PB-212	
270.04	368.84		7	1.26	7.26	308.67	22.29	AC-228	3
277.36	378.82		15	1.32	7.12	2327.08	4.50	TL-208	
287.20	392.26		13	2.82	6.93	997.29	11.04		4
295.17	403.13	*	20	1.34	6.78	192.30	21.14	PB-214	
300.13	409.90	*	20	1.34	6.70	3311.35	3.47	PB-212	
338.30	462.00		9	1.48	6.07	513.72	14.31	AC-228	5
351.86	480.52		13	1.40	5.87	400.35	17.79	PB-214	
374.77	511.79		13	1.51	5.56	1375.67	6.24	PB212XR1	6
405.58	553.84		13	1.33	5.18	190.52	28.95	BI-214	
440.01	600.85		8	1.29	4.81	476.72	11.73	AC-228	7
452.78	618.28		13	1.51	4.69	337.64	16.77	BI-212	
477.57	652.13		18	1.47	4.46	22872.23	1.00	AC-228	
477.57	652.13		18	1.47	4.46	22872.23	1.00	BE-7	
505.39	690.11	*	26	0.99	4.23	204.61	8.89		8
510.80	697.49	*	26	1.79	4.19	6912.02	1.25	TL-208	
522.46	713.42	*	17	1.44	4.10	201.50	14.30	AC-228	9
528.92	722.23	*	17	1.44	4.05	876.72	7.19	I-123	
538.51	735.33	*	24	0.50	3.98	66.41	161.99		10
545.21	744.47	*	24	0.51	3.94	214.05	160.09		11
583.15	796.27		14	1.55	3.69	18966.65	1.10	AC-228	
583.15	796.27		14	1.55	3.69	18966.65	1.10	TL-208	
609.17	831.81		15	1.47	3.54	418.42	12.13	BI-214	
687.83	939.21		8	1.22	3.15	91.31	37.12		12
727.30	993.12		10	1.65	2.99	4016.95	2.57	AC-228	
727.30	993.12		10	1.65	2.99	4016.95	2.57	BI-212	
742.71	1014.15		13	1.37	2.93	292.37	14.02	BI-214	13
742.71	1014.15		13	1.37	2.93	292.37	14.02	ZR-97	14
763.19	1042.12		9	1.84	2.85	267.80	16.83	TL-208	
781.91	1067.68	*	21	1.68	2.79	217.99	12.01	AC-228	15
785.43	1072.50	*	21	1.68	2.77	582.69	7.88	BI-212	
785.43	1072.50	*	21	1.68	2.77	582.69	7.88	BI-214	
785.43	1072.50	*	21	1.68	2.77	582.69	7.88	PB-214	
790.14	1078.93	*	21	1.68	2.76	128.82	17.33		16
802.91	1096.37	*	17	1.48	2.72	140.98	17.95	UNKNAT01	
807.39	1102.48	*	17	1.49	2.70	224.93	15.38		17
860.53	1175.05		11	1.75	2.54	2415.05	3.40	TL-208	
893.42	1219.98	*	23	1.73	2.45	188.15	12.17	BI-212	
899.15	1227.80	*	23	1.73	2.44	841.17	6.43		18
911.63	1244.85	*	23	1.92	2.41	494.10	9.47	AC-228	19
918.11	1253.70	*	23	1.92	2.39	95.91	21.21		20
968.60	1322.66		7	0.75	2.28	41.13	396.22	AC-228	
983.84	1343.48		17	1.84	2.24	382.33	11.39		21
992.31	1355.04		13	1.68	2.23	509.43	9.06		22
1032.31	1409.69		12	1.79	2.15	296.76	13.24		23
1078.73	1473.08		10	1.73	2.06	217.87	16.03	BI-212	
1093.69	1493.53		11	1.96	2.04	384.31	10.80	TL-208	
1120.17	1529.69		9	1.36	2.00	65.76	39.48	BI-214	
1460.79	1995.00		20	2.06	1.59	2618.99	3.15	K-40	
1512.72	2065.94		20	2.70	1.55	168.17	18.16	BI-212	
1592.38	2174.76		12	2.09	1.49	525.74	8.29	TL-208	
1620.66	2213.39		11	2.03	1.47	501.48	8.44	BI-212	
1764.13	2409.39		10	2.28	1.38	81.44	32.42	BI-214	
2103.38	2872.80		16	3.12	1.23	788.54	6.91	TL-208	
2614.50	3570.77		15	2.66	1.10	6386.32	1.89	TL-208	

PEAK SEARCH NOTES==========

NOTE 1:
Date Entered: 1997/03/24 14:53:34
Analyst: dwilliam
The peak is real and the association is correct.

==========

NOTE 2:
Date Entered: 1997/03/24 12:11:03
Analyst: dwilliam
This nuclide was removed from the Activity Summary section because in the analyst's judgment the nuclide was not present; some nuclides may be removed because their activity calculations are not meaningful (they are identified, not quantified).

Date Entered: 1997/03/24 12:11:30
Analyst: dwilliam
This peak is associated with I-123

==========

NOTE 3:
Date Entered: 1997/03/24 14:59:33
Analyst: dwilliam
This peak is likely associated with the 270.0 keV gamma line of Po-204 and the 270.24 keV gamma line of Ac-228.

==========

NOTE 4:
Date Entered: 1997/03/24 15:07:27
Analyst: dwilliam
This peak is likely associated with the 286.5 keV gamma line of Po-206.

==========

NOTE 5:
Date Entered: 1997/03/24 15:08:10
Analyst: dwilliam
This peak is likely associated with the 338.4 keV gamma line of Po-206. It may also be associated with the 338.3 keV gamma line of Ac-228.

==========

NOTE 6:
Date Entered: 1997/03/24 14:52:54
Analyst: dwilliam
This peak is likely associated with the 374.8 keV gamma line of Bi-204.

==========

NOTE 7:
Date Entered: 1997/03/24 14:49:29
Analyst: dwilliam
This peak is likely associated with the 440.0 keV gamma line of I-123 and the 440.5 keV gamma line of Ac-228.

==========

NOTE 8:
Date Entered: 1997/03/24 14:45:25
Analyst: dwilliam
This peak is likely associated with the 505.3 keV gamma line of I-123.

==========

NOTE 9:
Date Entered: 1997/03/24 15:10:00
Analyst: dwilliam
This peak is likely associated with the 522.4 keV gamma line of Po-206. It may also be associated with the 523.1 keV gamma line of Ac-228.

==========

NOTE 10:
Date Entered: 1997/03/24 14:46:34
Analyst: dwilliam
This peak is real and is likely associated with a weak gamma line of I-123 at 538.54 keV.

==========

NOTE 11:
Date Entered: 1997/03/24 15:20:36
Analyst: dwilliam
This peak is likely associated with the 545.0 keV gamma line of At-209.

==========

NOTE 12:
Date Entered: 1997/03/24 15:27:20
Analyst: dwilliam
This peak is real and is likely associated with the 687.6 keV gamma line of Po-207.

==========

NOTE 13:
Date Entered: 1997/03/24 15:10:51
Analyst: dwilliam
This peak is likely associated with the 742.6 keV gamma line of Po-207.

==========

NOTE 14:
Date Entered: 1997/03/24 11:59:01
Analyst: dwilliam
This nuclide was removed from the Activity Summary section because in the analyst's judgment the nuclide was not present; some nuclides may be removed because their activity calculations are not meaningful (they are identified, not quantified).

Date Entered: 1997/03/24 15:10:51
Analyst: dwilliam
This peak is likely associated with the 742.6 keV gamma line of Po-207.

==========

NOTE 15:
Date Entered: 1997/03/24 15:22:17
Analyst: dwilliam
This peak is likely associated with the 781.9 keV gamma line of At-209. It may also be associated with the 782.1 keV gamma line of Ac-228.

==========

NOTE 16:
Date Entered: 1997/03/24 15:20:23
Analyst: dwilliam
This peak is likely associated with the 790.2 keV gamma line of At-209.

==========

NOTE 17:
Date Entered: 1997/03/24 15:17:59
Analyst: dwilliam
This peak is likely associated with the 807.5 keV gamma line of Po-206.

==========

NOTE 18:
Date Entered: 1997/03/24 14:55:26
Analyst: dwilliam
This peak is likely associated with the 899.1 keV gamma line of Bi-204.

==========

NOTE 19:
Date Entered: 1997/03/24 14:56:23
Analyst: dwilliam
This peak is likely associated with the 911.8 keV gamma line of Po-207, the
911.8 keV gamma line of Bi-204, and the 911.2 keV gamma line of Ac-228,

==========

NOTE 20:
Date Entered: 1997/03/24 14:55:47
Analyst: dwilliam
This peak is likely associated with the 918.3 keV gamma line of Bi-204.

==========

NOTE 21:
Date Entered: 1997/03/24 14:55:58
Analyst: dwilliam
This peak is likely associated with the 983.9 keV gamma line of Bi-204.

==========

NOTE 22:
Date Entered: 1997/03/24 15:19:22
Analyst: dwilliam
This peak is likely associated with the 992.1 keV gamma line of Po-207.

==========

NOTE 23:
Date Entered: 1997/03/24 15:18:34
Analyst: dwilliam
This peak is likely associated with the 1032.3 keV gamma line of Po-206.

==========

CALIBRATION EQUATIONS==========

Energy vs. Channel

$$E(c) = -0.2539 + 0.733*c - 4.631E-07*c^2 + 7.287E-11*c^3$$

E = energy (keV)
c = channel number

Resolution vs. Energy

FWHM(E) = 0.89 + 0.03064*SQRT(E)

FWHM = Full Width Half Max (keV)
E = energy (keV)

Efficiency vs. Energy

e(E) = exp { -3.776 + 0.9255*ln(962.1/E) + 0.1003*[ln(962.1/E)]^2
- 0.0896*[ln(962.1/E)]^3 }

e = efficiency (counts/gamma)
E = energy (keV)

ATMOSPHERIC RADIONUCLIDE MEASUREMENT REPORT
Particulate Version

SAMPLE INFORMATION==========

Station ID: CA002 Detector ID: CAA2
Station Type: ISAR2 Detector Type:

Station Location: Vancouver, Canada
Detector Description: Detector A in Vancouver, Canada

Sample ID: 0023073 Sample Geometry: DISK
Sample Quantity: 25277.00 m3 Sample Type: Filter

Collection Start: 1997/03/22 18:07 Sampling Time: 25.96 hours
Collection Stop: 1997/03/23 20:04 Decay Time: 4.26 hours
Acquisition Start: 1997/03/24 00:20 Acquisition Time: 18.38 hours
Acquisition Stop: 1997/03/24 18:43 Avg Flow Rate: 973.69 m3/hr

Collection Station Comments:
goshka - Detector 1 Ranger (23-MAR-1997)

IDC Analysis General Comments:
I-123 is present in this spectrum and is seen at this site on occasion.

Calibration Update Performed. Certificate file
/data/gold1/rmsuser/genie/defaults/short_decay.cer

MEASUREMENT CATEGORIZATION==========

Categorization Legend

Level 1 = Normal Natural Rad. Meas.
Level 2 = Abnormal Natural Rad. Meas.
Level 3 = Normal Anthropogenic Rad. Meas.
Level 4 = Abnormal Anthropogenic Rad. Meas.

Spectrum Category (3) -- Normal Anthropogenic Rad. Meas.

Categorization Summary:

Name	Category	Categorization Comment
I-123	3	Within Statistical Range

ACTIVITY SUMMARY==========

NATURAL RADIOACTIVITY:

Nuclides Identified: BI-212, BI-214, K-40, NA-24, PB-214, TL-208, UNKNAT01

Nuclides Quantified:

Nuclide	Half-Life	Conc(uBq/m3)	%RelErr	Notes

BE-7	53.3 D	3.5E+03	2.52
PB-212	10.64 H	3.4E+03	10.28

ACTIVATION-PRODUCT RADIOACTIVITY:

I-123	13.13 H	82	4.51

FISSION-PRODUCT RADIOACTIVITY:

None Found

MINIMUM DETECTABLE CONCENTRATION FOR KEY NUCLIDES==========

Nuclide	Half-Life	MDC(uBq/m3)
BA-140	12.75 D	9.69
CE-143	1.4 D	8.86
CS-134	2.06135 Y	2.63
CS-136	13.16 D	2.74
CS-137	30.0197 Y	2.75
I-131	8.04 D	3.27
I-133	20.8 H	6.00
MO-99	65.94 H	25.33
NB-95	35.15 D	2.83
RU-103	39.26 D	2.42
TE-132	78.2 H	3.02
ZR-95	64.02 D	4.14
ZR-97	17 H	7.02

PEAK SEARCH RESULTS==========

37 peaks found in spectrum by automated peak search.
36 peaks associated with nuclides by automated processing.
1 peaks not associated with nuclides by automated processing.
97 percent of peaks were associated with nuclides.

Note: "*" indicates that a peak was a component of a multiplet.

Energy	Centroid	Width	FWHM	%Eff	Net Area	%RelErr	Nuclide	Nts
74.73	102.38 *	17	1.26	10.53	11542.04	1.28	PB-212	
74.73	102.38 *	17	1.26	10.53	11542.04	1.28	PB-214	
74.73	102.38 *	17	1.26	10.53	11542.04	1.28	TL-208	
77.03	105.53 *	17	1.27	10.62	17829.29	1.10	BI-214	
77.03	105.53 *	17	1.27	10.62	17829.29	1.10	PB-212	
77.03	105.53 *	17	1.27	10.62	17829.29	1.10	PB-214	
87.11	119.28 *	18	1.43	10.90	6918.96	2.10	PB-212	
87.11	119.28 *	18	1.43	10.90	6918.96	2.10	PB-214	
89.79	122.93 *	18	1.43	10.95	2211.18	3.37	BI-214	
89.79	122.93 *	18	1.43	10.95	2211.18	3.37	PB-212	
115.19	157.57	8	1.26	10.90	646.54	15.48	PB-212	
158.95	217.28	13	1.34	9.95	3166.41	3.78	I-123	1
158.95	217.28	13	1.34	9.95	3166.41	3.78	TE-123M	2
238.62	325.98	14	1.31	7.94	41333.80	0.75	PB-212	
252.55	344.99	12	1.56	7.63	227.43	30.09	TL-208	
277.35	378.84	11	1.28	7.12	1578.88	5.39	TL-208	
288.03	393.41	13	1.48	6.92	256.27	27.39	BI-212	
295.16	403.14 *	20	1.31	6.78	173.61	20.74	PB-214	
300.11	409.90 *	20	1.31	6.70	2222.18	4.33	PB-212	
328.13	448.13	8	1.12	6.23	144.09	32.02	BI-212	
351.89	480.57	17	1.23	5.87	345.81	18.49	PB-214	
452.82	618.34	14	1.39	4.69	216.72	20.97	BI-212	

477.57	652.13	16	1.46	4.46	26483.91	0.91	BE-7	
510.77	697.45	19	1.82	4.19	4654.88	2.43	TL-208	
583.15	796.28	14	1.56	3.69	12600.73	1.34	TL-208	
609.24	831.90	16	1.48	3.54	338.58	12.66	BI-214	
727.29	993.12	12	1.63	2.99	2525.71	3.17	BI-212	
763.31	1042.31	13	1.74	2.85	208.62	16.86	TL-208	
785.51	1072.63	21	1.73	2.77	401.72	10.24	BI-212	
785.51	1072.63	21	1.73	2.77	401.72	10.24	BI-214	
785.51	1072.63	21	1.73	2.77	401.72	10.24	PB-214	
803.06	1096.61	9	1.20	2.72	59.20	47.48	UNKNAT01	
860.48	1175.04	15	1.73	2.54	1464.74	4.35	TL-208	
893.40	1220.00	12	1.96	2.45	124.19	24.12	BI-212	
911.07	1244.14	11	1.78	2.41	126.88	22.30		3
951.76	1299.72	12	1.62	2.31	68.96	34.03	BI-212	
1078.73	1473.19	13	1.56	2.06	145.35	18.86	BI-212	
1093.63	1493.53	11	1.74	2.04	206.05	15.74	TL-208	
1120.59	1530.37	8	1.22	1.99	51.46	47.05	BI-214	
1368.37	1868.91	10	2.46	1.68	84.03	29.20	NA-24	
1460.62	1994.95	17	2.06	1.59	2404.28	3.26	K-40	
1512.55	2065.91	11	1.82	1.55	86.66	25.78	BI-212	
1592.31	2174.88	10	2.21	1.49	337.30	10.04	TL-208	
1620.63	2213.57	13	2.14	1.47	337.54	10.21	BI-212	
2103.28	2872.90	15	3.32	1.23	559.50	7.91	TL-208	
2614.53	3570.83	18	2.70	1.10	4204.72	2.33	TL-208	

PEAK SEARCH NOTES==========

NOTE 1:
Date Entered: 1997/03/24 15:56:00
Analyst: dwilliam
The peak is real and the association is correct.

==========

NOTE 2:
Date Entered: 1997/03/24 15:55:28
Analyst: dwilliam
This nuclide was removed from the Activity Summary section because in the analyst's judgment the nuclide was not present; some nuclides may be removed because their activity calculations are not meaningful (they are identified, not quantified).

Date Entered: 1997/03/24 15:55:52
Analyst: dwilliam
This peak is associated with I-123.

==========

NOTE 3:
Date Entered: 1997/03/24 16:28:19
Analyst: dwilliam
This peak is likely associated with the 911.21 keV gamma line of Ac-228.

==========

CALIBRATION EQUATIONS==========

Energy vs. Channel

$$E(c) = -0.3356 + 0.7332*c - 7.074E-07*c^2 + 1.226E-10*c^3$$

E = energy (keV)
c = channel number

Resolution vs. Energy

FWHM(E) = 0.89 + 0.03064*SQRT(E)

FWHM = Full Width Half Max (keV)
E = energy (keV)

Efficiency vs. Energy

e(E) = exp { -3.776 + 0.9255*ln(962.1/E) + 0.1003*[ln(962.1/E)]^2
- 0.0896*[ln(962.1/E)]^3 }

e = efficiency (counts/gamma)
E = energy (keV)

Appendix C: REPRESENTATIVE CA002 ATMOSPHERIC RADIONUCLIDE MONITORING REPORTS DURING BASELINE PERIOD

ATMOSPHERIC RADIONUCLIDE MEASUREMENT REPORT
Particulate Version

SAMPLE INFORMATION==========

Station ID:	CA002	Detector ID:	CAA2
Station Type:	ISAR2	Detector Type:	

Station Location: Vancouver, Canada
Detector Description: Detector A in Vancouver, Canada

Sample ID:	0022467	Sample Geometry:	DISK
Sample Quantity:	23964.68 m3	Sample Type:	Filter

Collection Start:	1997/03/11 17:16	Sampling Time:	24.05 hours
Collection Stop:	1997/03/12 17:19	Decay Time:	4.42 hours
Acquisition Start:	1997/03/12 21:45	Acquisition Time:	19.50 hours
Acquisition Stop:	1997/03/13 17:15	Avg Flow Rate:	996.45 m3/hr

Collection Station Comments:
goshka - Detector 1 Ranger (12-MAR-1997)

IDC Analysis General Comments:
Calibration Update Performed. Certificate file
/data/gold1/rmsuser/genie/defaults/short_decay.cer

MEASUREMENT CATEGORIZATION==========

Categorization Legend

Level 1 = Normal Natural Rad. Meas.
Level 2 = Abnormal Natural Rad. Meas.
Level 3 = Normal Anthropogenic Rad. Meas.
Level 4 = Abnormal Anthropogenic Rad. Meas.

Spectrum Category (1) -- Normal Natural Rad. Meas.

ACTIVITY SUMMARY==========

NATURAL RADIOACTIVITY:

Nuclides Identified: BI-212, BI-214, K-40, PB-214, TL-208

Nuclides Quantified:

Nuclide	Half-Life	Conc(uBq/m3)	%RelErr	Notes
BE-7	53.3 D	2.4E+03	2.60	
PB-212	10.64 H	2.7E+03	10.29	

ACTIVATION-PRODUCT RADIOACTIVITY:

None Found

FISSION-PRODUCT RADIOACTIVITY:

None Found

MINIMUM DETECTABLE CONCENTRATION FOR KEY NUCLIDES==========

Nuclide	Half-Life	MDC(uBq/m3)
BA-140	12.75 D	9.11
CE-143	1.4 D	7.88
CS-134	2.06135 Y	2.56
CS-136	13.16 D	2.63
CS-137	30.0197 Y	2.68
I-131	8.04 D	3.05
I-133	20.8 H	5.52
MO-99	65.94 H	24.37
NB-95	35.15 D	2.65
RU-103	39.26 D	2.26
TE-132	78.2 H	2.69
ZR-95	64.02 D	4.28
ZR-97	17 H	6.54

PEAK SEARCH RESULTS==========

32 peaks found in spectrum by automated peak search.
31 peaks associated with nuclides by automated processing.
1 peaks not associated with nuclides by automated processing.
97 percent of peaks were associated with nuclides.

Note: "*" indicates that a peak was a component of a multiplet.

Energy	Centroid	Width	FWHM	%Eff	Net Area	%RelErr	Nuclide	Nts
74.80	102.39 *	17	1.26	10.53	9191.65	1.45	PB-212	
74.80	102.39 *	17	1.26	10.53	9191.65	1.45	PB-214	
74.80	102.39 *	17	1.26	10.53	9191.65	1.45	TL-208	
77.08	105.49 *	17	1.26	10.63	14348.59	1.24	BI-214	
77.08	105.49 *	17	1.26	10.63	14348.59	1.24	PB-212	
77.08	105.49 *	17	1.26	10.63	14348.59	1.24	PB-214	
87.17	119.27 *	18	1.39	10.91	5607.57	2.34	PB-212	
87.17	119.27 *	18	1.39	10.91	5607.57	2.34	PB-214	
89.87	122.95 *	18	1.39	10.95	1751.51	3.84	BI-214	
89.87	122.95 *	18	1.39	10.95	1751.51	3.84	PB-212	
115.22	157.54	12	0.90	10.90	441.27	52.44	PB-212	
238.63	325.97	16	1.30	7.94	34091.35	0.82	PB-212	
252.76	345.26	6	1.06	7.62	138.35	43.32	TL-208	
277.34	378.80	14	1.39	7.12	1260.87	6.38	TL-208	
288.21	393.64	7	1.21	6.91	228.83	28.40	BI-212	
295.21	403.20 *	21	1.26	6.78	162.87	20.21	PB-214	
300.10	409.87 *	21	1.27	6.70	1820.49	4.69	PB-212	
351.95	480.64	14	1.41	5.87	388.43	14.77	PB-214	
452.68	618.16	12	1.53	4.69	180.77	23.34	BI-212	
477.56	652.12	14	1.44	4.46	17975.68	1.12	BE-7	
510.73	697.41	19	1.89	4.19	4049.84	2.62	TL-208	
583.13	796.27	19	1.53	3.69	10457.65	1.48	TL-208	
609.31	832.01	10	1.39	3.54	331.75	12.69	BI-214	
727.29	993.11	12	1.62	2.99	2145.65	3.54	BI-212	
763.29	1042.28	14	1.81	2.85	176.72	18.74	TL-208	

785.43	1072.52	17	1.48	2.77	272.55	13.06	BI-212	
785.43	1072.52	17	1.48	2.77	272.55	13.06	BI-214	
785.43	1072.52	17	1.48	2.77	272.55	13.06	PB-214	
860.49	1175.02	13	1.73	2.54	1285.86	4.77	TL-208	
893.44	1220.03	9	1.38	2.45	102.65	24.14	BI-212	
911.13	1244.18	9	1.76	2.41	102.92	26.41		1
1078.68	1473.03	9	1.50	2.06	104.62	23.78	BI-212	
1093.93	1493.86	11	1.73	2.04	149.37	18.55	TL-208	
1120.12	1529.63	13	1.42	2.00	69.15	35.16	BI-214	
1460.71	1994.87	14	2.06	1.59	2409.91	3.23	K-40	
1512.69	2065.87	14	1.96	1.55	74.83	28.21	BI-212	
1592.48	2174.88	11	1.92	1.49	275.23	11.84	TL-208	
1620.72	2213.45	10	2.33	1.47	275.93	11.50	BI-212	
2103.41	2872.76	20	3.31	1.23	464.16	8.68	TL-208	
2614.51	3570.69	24	2.57	1.10	3513.51	2.61	TL-208	

PEAK SEARCH NOTES==========

NOTE 1:
Date Entered: 1997/03/14 12:12:12
Analyst: dwilliam
Known natural nuclide, but lack of ID due to decay: only strongest line(s) present, insufficient for ID.

==========

CALIBRATION EQUATIONS==========

Energy vs. Channel

$$E(c) = -0.236 + 0.7329*c - 4.158E-07*c^2 + 6.653E-11*c^3$$

E = energy (keV)
c = channel number

Resolution vs. Energy

$$FWHM(E) = 0.89 + 0.03064*SQRT(E)$$

FWHM = Full Width Half Max (keV)
E = energy (keV)

Efficiency vs. Energy

$$e(E) = \exp \{ -3.776 + 0.9255*\ln(962.1/E) + 0.1003*[\ln(962.1/E)]^2 - 0.0896*[\ln(962.1/E)]^3 \}$$

e = efficiency (counts/gamma)
E = energy (keV)

ATMOSPHERIC RADIONUCLIDE MEASUREMENT REPORT
Particulate Version

SAMPLE INFORMATION==========

Station ID:	CA002	Detector ID:	CAA2
Station Type:	ISAR2	Detector Type:	

Station Location: Vancouver, Canada
Detector Description: Detector A in Vancouver, Canada

Sample ID:	0023232	Sample Geometry:	DISK
Sample Quantity:	23261.00 m3	Sample Type:	Filter

Collection Start:	1997/03/25 19:22	Sampling Time:	24.20 hours
Collection Stop:	1997/03/26 19:34	Decay Time:	4.26 hours
Acquisition Start:	1997/03/26 23:49	Acquisition Time:	17.89 hours
Acquisition Stop:	1997/03/27 17:43	Avg Flow Rate:	961.20 m3/hr

Collection Station Comments:
goshka - Detector 1 Ranger (26-MAR-1997)

IDC Analysis General Comments:
Calibration Update Performed. Certificate file
/data/gold1/rmsuser/genie/defaults/short_decay.cer

MEASUREMENT CATEGORIZATION==========

Categorization Legend

Level 1 = Normal Natural Rad. Meas.
Level 2 = Abnormal Natural Rad. Meas.
Level 3 = Normal Anthropogenic Rad. Meas.
Level 4 = Abnormal Anthropogenic Rad. Meas.

Spectrum Category (1) -- Normal Natural Rad. Meas.

ACTIVITY SUMMARY==========

NATURAL RADIOACTIVITY:

Nuclides Identified: BI-212, BI-214, K-40, PB-214, TL-208

Nuclides Quantified:

Nuclide	Half-Life	Conc(uBq/m3)	%RelErr	Notes
BE-7	53.3 D	3.9E+03	2.52	
PB-212	10.64 H	3.8E+03	10.28	

ACTIVATION-PRODUCT RADIOACTIVITY:

None Found

FISSION-PRODUCT RADIOACTIVITY:

None Found

MINIMUM DETECTABLE CONCENTRATION FOR KEY NUCLIDES==========

Nuclide	Half-Life	MDC(uBq/m3)
BA-140	12.75 D	10.95
CE-143	1.4 D	9.64
CS-134	2.06135 Y	2.98
CS-136	13.16 D	2.97
CS-137	30.0197 Y	3.17
I-131	8.04 D	3.68
I-133	20.8 H	6.50
MO-99	65.94 H	28.22
NB-95	35.15 D	3.19
RU-103	39.26 D	2.78
TE-132	78.2 H	3.44
ZR-95	64.02 D	4.90
ZR-97	17 H	7.41

PEAK SEARCH RESULTS==========

31 peaks found in spectrum by automated peak search.
29 peaks associated with nuclides by automated processing.
2 peaks not associated with nuclides by automated processing.
94 percent of peaks were associated with nuclides.

Note: "*" indicates that a peak was a component of a multiplet.

Energy	Centroid	Width	FWHM	%Eff	Net Area	%RelErr	Nuclide	Nts
74.78	102.38 *	17	1.25	10.53	12200.42	1.25	PB-212	
74.78	102.38 *	17	1.25	10.53	12200.42	1.25	PB-214	
74.78	102.38 *	17	1.25	10.53	12200.42	1.25	TL-208	
77.08	105.51 *	17	1.25	10.63	19126.90	1.07	BI-214	
77.08	105.51 *	17	1.25	10.63	19126.90	1.07	PB-212	
77.08	105.51 *	17	1.25	10.63	19126.90	1.07	PB-214	
87.17	119.28 *	18	1.41	10.91	7313.30	2.03	PB-212	
87.17	119.28 *	18	1.41	10.91	7313.30	2.03	PB-214	
89.85	122.95 *	18	1.42	10.95	2387.64	3.24	BI-214	
89.85	122.95 *	18	1.42	10.95	2387.64	3.24	PB-212	
115.15	157.46	12	1.25	10.90	714.98	14.42	PB-212	
238.63	325.98	16	1.30	7.94	44693.01	0.72	PB-212	
277.34	378.82	14	1.42	7.12	1748.61	5.26	TL-208	
288.13	393.54	9	1.42	6.91	330.35	21.80	BI-212	
300.11	409.90	21	1.31	6.70	2296.71	4.26	PB-212	
338.44	462.21	9	1.15	6.07	149.62	34.07		1
351.94	480.64	17	1.25	5.87	363.39	16.53	PB-214	
452.87	618.43	11	1.48	4.69	256.36	18.57	BI-212	
477.56	652.13	13	1.46	4.46	26360.02	0.91	BE-7	
510.76	697.45	19	1.79	4.19	4815.73	2.40	TL-208	
583.15	796.29	12	1.54	3.69	13651.37	1.28	TL-208	
609.28	831.96	16	1.54	3.54	325.08	13.19	BI-214	
727.30	993.12	8	1.62	2.99	2874.12	2.97	BI-212	
763.43	1042.46	15	1.47	2.85	214.46	16.28	TL-208	
785.42	1072.49	15	1.82	2.77	409.66	10.26	BI-212	
785.42	1072.49	15	1.82	2.77	409.66	10.26	BI-214	
785.42	1072.49	15	1.82	2.77	409.66	10.26	PB-214	
860.51	1175.04	16	1.68	2.54	1766.80	3.86	TL-208	
893.18	1219.66	8	1.46	2.45	94.93	29.24	BI-212	
911.39	1244.52	14	1.61	2.41	88.00	30.39		2

1078.73	1473.08	10	1.55	2.06	177.79	16.89	BI-212
1093.81	1493.68	18	1.91	2.04	222.30	14.78	TL-208
1460.80	1994.98	15	2.12	1.59	2457.92	3.22	K-40
1512.71	2065.89	13	2.21	1.55	95.87	25.09	BI-212
1592.40	2174.76	15	2.24	1.49	380.51	9.66	TL-208
1620.75	2213.48	14	2.04	1.47	354.75	10.06	BI-212
1764.67	2410.09	14	1.85	1.38	61.49	33.36	BI-214
2103.41	2872.82	26	3.16	1.23	581.03	7.96	TL-208
2614.49	3570.83	20	2.61	1.10	4586.25	2.23	TL-208

PEAK SEARCH NOTES==========

NOTE 1:
Date Entered: 1997/03/27 16:48:19
Analyst: dwilliam
Known natural nuclide, but lack of ID due to decay: only strongest line(s) present, insufficient for ID.

Date Entered: 1997/03/27 16:48:19
Analyst: dwilliam
This peak is likely associated with the 338.32 keV gamma line of Ac-228.

==========

NOTE 2:
Date Entered: 1997/03/27 16:35:58
Analyst: dwilliam
Known natural nuclide, but lack of ID due to decay: only strongest line(s) present, insufficient for ID.

==========

CALIBRATION EQUATIONS==========

Energy vs. Channel

$$E(c) = -0.2519 + 0.7329*c - 4.063E-07*c^2 + 6.025E-11*c^3$$

E = energy (keV)
c = channel number

Resolution vs. Energy

$$FWHM(E) = 0.89 + 0.03064*SQRT(E)$$

FWHM = Full Width Half Max (keV)
E = energy (keV)

Efficiency vs. Energy

$$e(E) = \exp \{ -3.776 + 0.9255*\ln(962.1/E) + 0.1003*[\ln(962.1/E)]^2 - 0.0896*[\ln(962.1/E)]^3 \}$$

e = efficiency (counts/gamma)
E = energy (keV)

Appendix D: DISCRIMINATING MINIMAL PEAKS FROM BACKGROUND IN GAMMA-RAY SPECTROSCOPY

Abstract

The net peak detection threshold (PDT_n) is a concept that can be used to determine the presence of peaks in gamma-ray spectra where the signal-to-noise ratio is low (marginally greater than 1). This concept has traditionally been considered from a theoretical and statistical perspective; however, to date, it has not been empirically validated with field data. This study uses historic gamma-ray spectra that were environmentally obtained through the Prototype International Data Center (PIDC) in support of the Comprehensive [Nuclear] Test Ban Treaty to validate the PDT_n concept. Through this study, the PDT_n is shown to effectively and reliably identify the existence of subtle peaks amid relatively high background counts, even in situations where automated analytical tools were unable to identify the peaks and visual inspections were inconclusive. As a result, applying the PDT_n concept to the real-world spectra evaluated in this study enabled a more thorough evaluation of the spectra and highlighted the existence of anthropogenic radionuclides not identified through the PIDC's automated gamma-ray spectral processing system.

Introduction

Performing gamma-ray spectroscopy on environmentally obtained samples to determine the presence of minimally abundant radionuclides can be challenging due to the low peak areas encountered and interference caused by background counts. In fact, the signal-to-noise ratios can be so low that the presence of peaks is best determined by incorporating

statistical methods rather than by direct analytical judgment. In such cases, when the gross number of counts (background + net peak) is on the same order of magnitude as the background counts, determining a net peak detection threshold (PDT_n) can be helpful in evaluating whether the deviation from average background values is most likely due to statistical noise or the presence of a peak. The PDT_n represents the minimum number of net counts required within a peak atop a set number of background counts in order to state with confidence that the peak is real. The level of confidence is defined in terms of the Type I and Type II statistical error rates.[1] These and other key features related to the PDT_n are illustrated in Figure D1.

[1] A Type I error (α) occurs when the number of background counts is so high that they are more likely to mistakenly represent the presence of a peak. Conversely, a Type II error (β) occurs when the gross number of counts (background + net peak) is so low that they are more likely to be mistaken to be background alone.

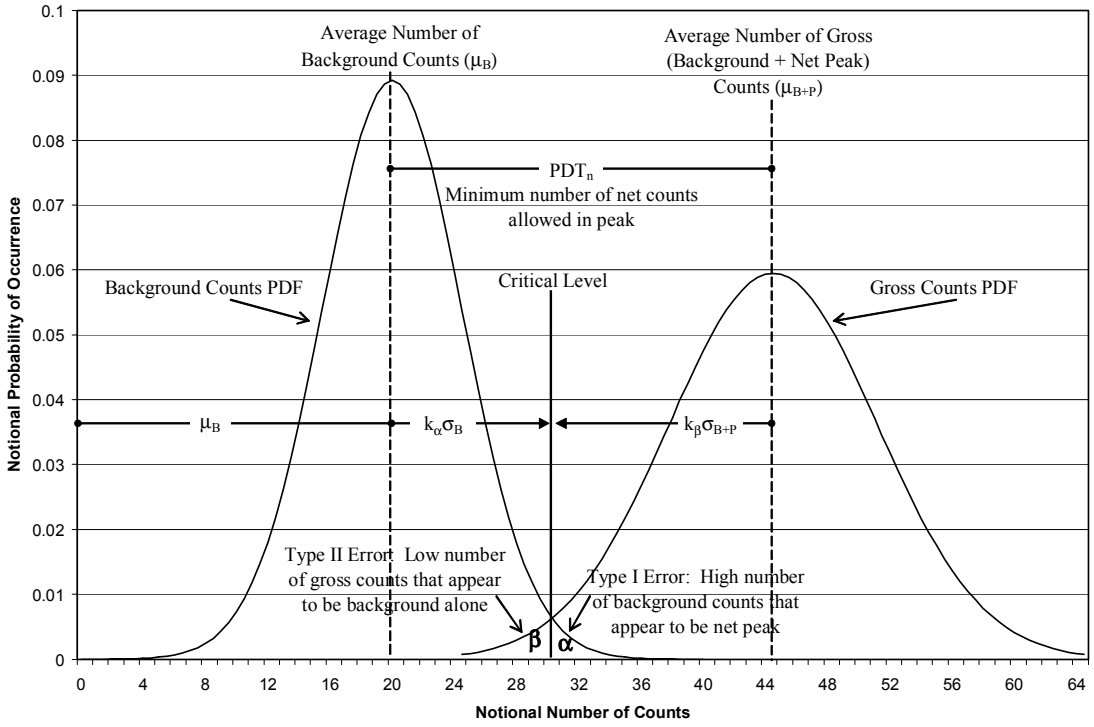

Figure D1: Key features related to PDT_n determination

Figure D1 shows two related probability distribution functions (PDFs) that would be expected when using a radiation detector to count radioactive particles. The steeper peak is representative of a background count distribution, while the lower, wider peak is representative of a gross counts (background + net peak) distribution. Naturally, the gross counts PDF is centered at a higher number of counts than the background PDF because a background with a net peak is expected to generate more counts than background alone.

The PDFs are both Poisson and Normal in nature. The Poisson attributes result from the principle that a large number of radioactive emissions give rise to a relatively small number of recorded counts (i.e., $p << 1$, a defining quality of Poisson distributions). The Normal qualities are the result of the Central Limit Theorem, which states that any random distribution tends to approximate a Normal distribution provided that the sample size is sufficiently large. In general, a sample size of 20 recorded counts is considered to be sufficiently large.

By definition, the peak of a Normal distribution (which corresponds to the greatest probability) occurs at its mean value (μ). Also, according to the definition of a Poisson distribution, the standard deviation equals the square root of the average ($\sigma = \sqrt{\mu}$). The relative sizes and shapes of the two distributions reflect these features.

The portions of the distributions corresponding to Type I and Type II errors are identified by α and β, respectively. Type I errors occur when the number of background counts are much higher than normal. Although no net peak is present, the number of counts is so high that they give the appearance of a "false peak". The reason for the "false peak" perception is centered upon the critical level – the number of counts that correspond to an equal probability for both distributions.[2] Correspondingly, Type II errors occur when the number of gross counts is so low that they give the appearance of background alone.

[2] At the critical level, the number of counts is just as likely the result of a background count as they are the result of a gross count. All counts that exceed the critical level are more likely to be associated with the combination of background with a net peak, while counts that are lower than the critical level are more likely to be associated with background alone.

The critical level is a value that can be specified according to the level of detection confidence that is desired. As the critical level is increased or decreased, the areas under the α and β sections of the respective PDFs are adjusted accordingly, which specify the error percentages. The critical level is usually defined as a function of a constant multiplied by the standard deviation (i.e., $k\sigma$). Since the percentage of area under a Normal PDF is commonly specified in terms of σ, by specifying the critical level as a function of σ, the critical level can be correlated to a percentage of area under the PDF curve. Values for k and corresponding areas under the Normal PDF are shown in Table D1.

Table D1: k Values and Corresponding Confidence Levels and Error Percentages

k	**$k\sigma$**	**Percentage of Normal PDF Area Covered (confidence level)**	**Error Percentage (α, β, respectively)**
0	0	0.500	0.500
0.253	0.253σ	0.600	0.400
0.500	0.5σ	0.692	0.308
0.524	0.524σ	0.700	0.300
0.674	0.674σ	0.750	0.250
0.842	0.842σ	0.800	0.200
1.000	σ	0.841	0.159
1.282	1.282σ	0.900	0.100
1.500	1.5σ	0.933	0.067

1.645	1.645σ	0.950	0.050
1.960	1.96σ	0.975	0.025
2.000	2σ	0.977	0.023
2.326	2.326σ	0.990	0.010
2.500	2.5σ	0.994	0.006
2.576	2.576σ	0.995	0.005
3.000	3σ	0.999	0.001
3.300	3.3σ	1.000	0.000

As Figure D1 shows, the PDT_n, which is the minimum number of net counts allowed in a reliable peak, is the difference between the average number of gross counts and the average number of background counts. This is expressed mathematically in Equation D1. However, in most practical situations, rarely are both average values known. Therefore, expressing the PDT_n in terms of one of the average values is more useful. The derivation below will result in an expression for the PDT_n in terms of the average number of background counts, μ_B.

$$PDT_n = \mu_{B+P} - \mu_B \qquad \text{Equation D1}$$

According to Figure D1, one way to evaluate the average number of gross counts is in terms of the standard deviations of the background and gross distributions.

$$\mu_{B+P} = \mu_B + k_\alpha \sigma_B + k_\beta \sigma_{B+P}$$ Equation D2

In cases where the Poisson distribution approximates the Normal distribution (i.e., when the number of measured counts exceeds 20), $\sigma_x = \sqrt{\mu_x}$, where x represents the distribution being evaluated. Making this substitution, while combining Equations D1 and D2, results in Equation D3.

$$PDT_n = k_\alpha \sqrt{\mu_B} + k_\beta \sqrt{\mu_{B+P}}$$ Equation D3

Making the same substitution into Equation D2 and rearranging yields Equation D4, which is quadratic in terms of the square root of the average number of gross counts ($\sqrt{\mu_{B+P}}$).

$$\mu_{B+P} - k_\beta \sqrt{\mu_{B+P}} - \left(\mu_B + k_\alpha \sqrt{\mu_B}\right) = 0$$ Equation D4

Solving for the principle root of Equation D4 generates Equation D5.

$$\sqrt{\mu_{B+P}} = \frac{k_\beta + \sqrt{k_\beta^2 + 4\left(\mu_B + k_\alpha \sqrt{\mu_B}\right)}}{2}$$ Equation D5

Substituting Equation D5 into Equation D1 results in Equation D6. This expression for the PDT_n has eliminated its dependence on μ_{B+P} and is a function of μ_B.

$$PDT_n(\mu_B) = \left[\frac{k_\beta + \sqrt{k_\beta^2 + 4\left(\mu_B + k_\alpha \sqrt{\mu_B}\right)}}{2} \right]^2 - \mu_B \qquad \text{Equation D6}$$

Simplifying and rearranging the Equation D6 produces Equation D7.

$$PDT_n(\mu_B) = k_\alpha \sqrt{\mu_B} + \frac{k_\beta^2}{2}\left[1 + \sqrt{1 + \frac{4}{k_\beta^2}\left(\mu_B + k_\alpha \sqrt{\mu_B}\right)}\right] \qquad \text{Equation D7}$$

When evaluating radiation count data, k_α and k_β are considered to be equal.[3] Setting $k_\alpha = k_\beta = k$ within Equation D7 leads to a highly simplified form of the PDT_n as a function of μ_B and k.

$$PDT_n(\mu_B, k) = k^2 + 2k\sqrt{\mu_B} \qquad \text{Equation D8}$$

This equation can be simplified further to hold the form of Equation D1.

$$PDT_n(\mu_B, k) = \left(\sqrt{\mu_B} + k\right)^2 - \mu_B \qquad \text{Equation D9}$$

Therefore, using Equation D9, the PDT_n can be calculated from the average number of recorded background counts and the confidence level constant, k. Furthermore, the form

of Equation D9 enables it to be used to determine whether a peak is real without actually calculating the PDT_n value. According to Equation D9, for a given number of background counts per channel and constant k, if the average gross number of counts per channel is at least $\left(\sqrt{\mu_B} + k\right)^2$, then the peak can be stated with confidence to be real. Table D2 and Figure D2 show selected background, PDT_n, and gross values when k = 1.645, which corresponds to a 95% confidence level.

Table D2: Selected Background, PDT_n, and Gross Values

If the number of background counts per channel is x,	**then the PDT_n (i.e., the required minimum number of net counts per channel within the peak) is y;**	**and the total number of gross counts per channel must be x+y.**
20	17.41935	37.41935
25	19.15603	44.15603
30	20.7261	50.7261
35	22.16993	57.16993
40	23.51381	63.51381
45	24.77602	69.77602
50	25.96984	75.96984
55	27.10532	82.10532
60	28.19026	88.19026

[3] A frequently used k value for $k_\alpha = k_\beta = k$ is 1.645. According to Table D1, this value for k corresponds to a 95% level of confidence (or a 5% error percentage).

65	29.23085	94.23085
70	30.23214	100.2321
75	31.19826	106.1983
80	32.13268	112.1327
85	33.03833	118.0383
90	33.91771	123.9177
95	34.77298	129.773
100	35.60603	135.606
105	36.41849	141.4185
110	37.21184	147.2118
115	37.98734	152.9873
120	38.74617	158.7462

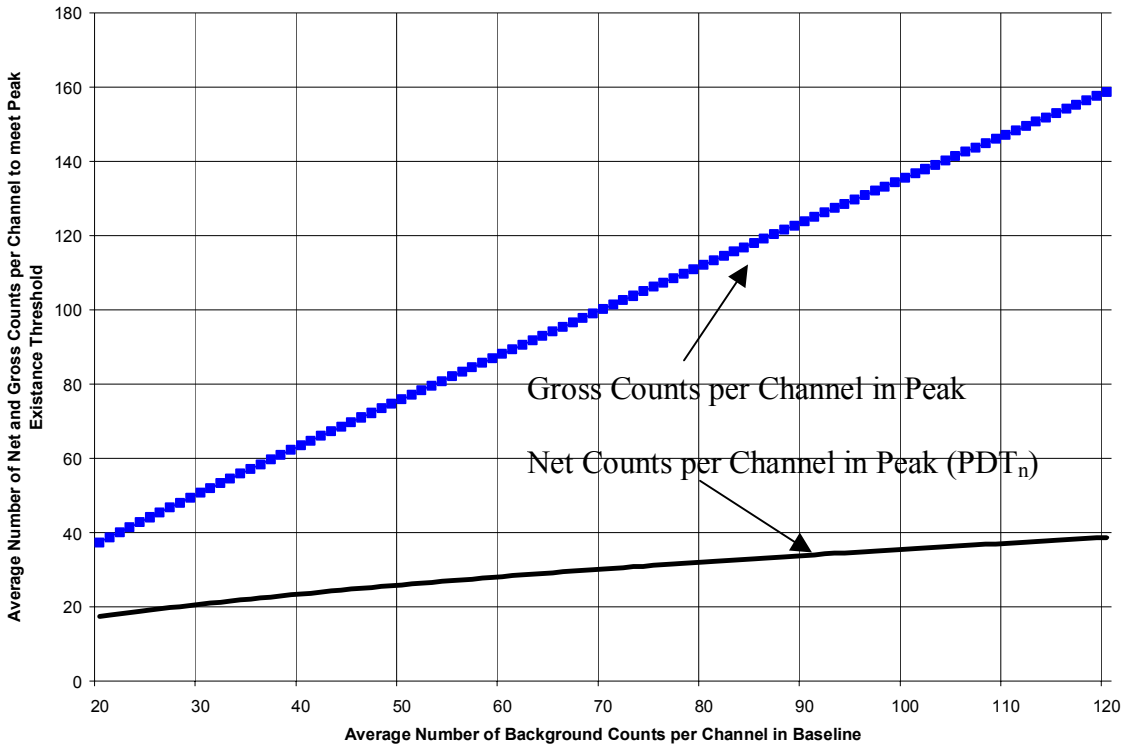

Figure D2: Graphical Depiction of Net and Gross Counts per Channel in Threshold Peaks

Analysis

Figure D3 is a gamma-ray spectrum that was acquired on 23 March 1997 through environmental sampling at the University of British Columbia in Vancouver, British Columbia, Canada. This representative spectrum demonstrates the difficulties that can be encountered in determining whether trace amounts of certain radionuclides are present. For example, in this spectrum, neither Bi-206 (with primary gamma-ray of 803.10 keV, which corresponds to channel 1097) nor Po-204 (with primary gamma-ray of 883.96 keV, which corresponds to channel 1207) is identified by the automated analysis system. Even so, as visual analysis will show, it is possible that both of these radionuclides are present in trace quantities. Figures D4a and D4b show enlargements of these two

regions with estimated baselines included. Figures D4c through D4j show enlargements of these two regions from other Vancouver spectra collected in March 1997.

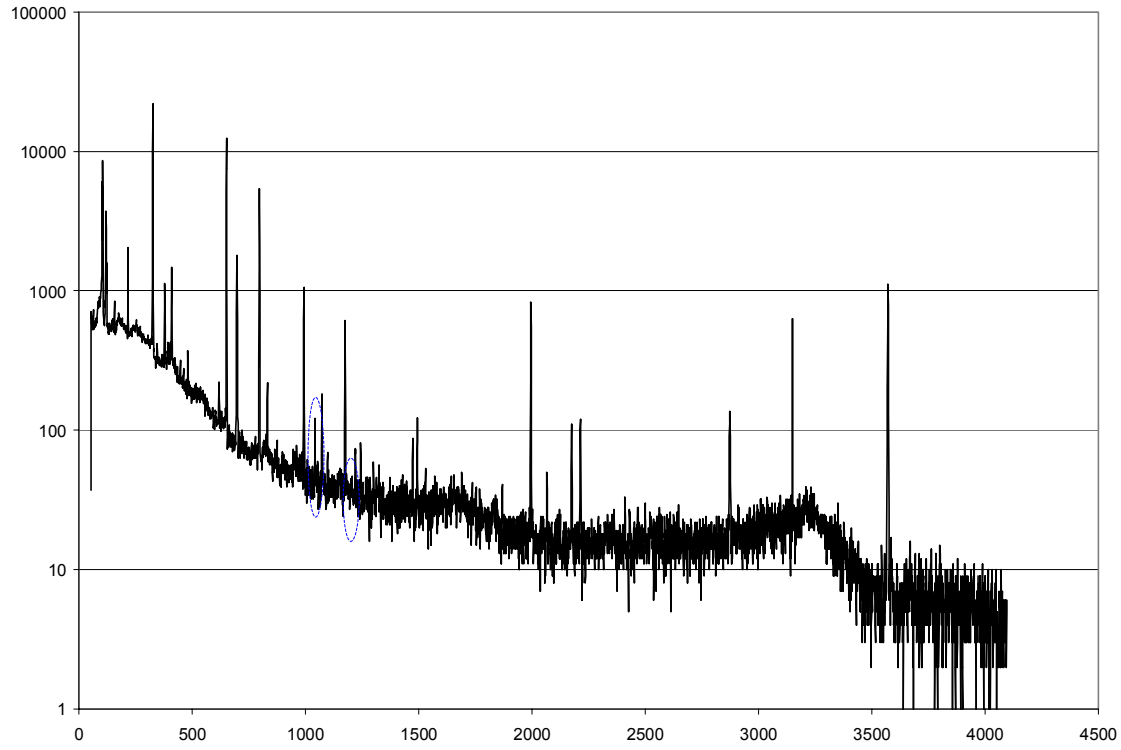

Figure D3: Gamma-Ray Spectrum from Vancouver, British Columbia, Canada collected 23 March 1997 Highlighting Regions where Bi-206 and Po-204 Peaks may be Present

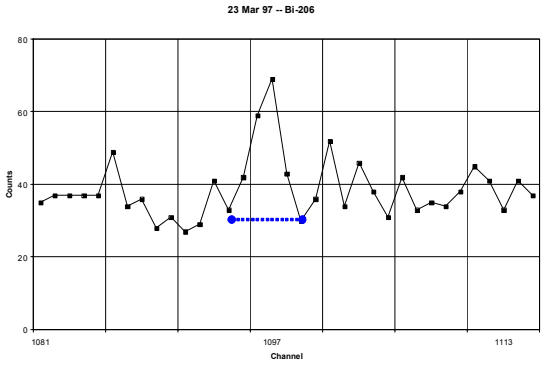

Figure D4a: Bi-206 Region -- 23 March 97

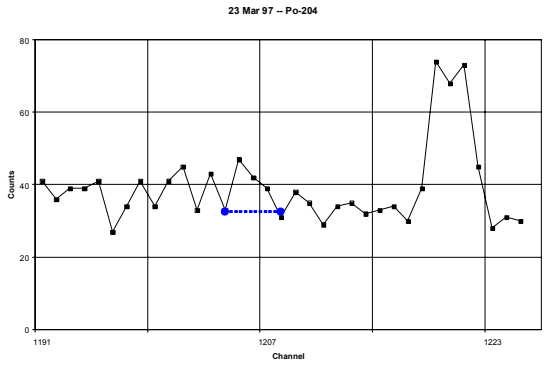

Figure D4b: Po-204 Region -- 23 March 97

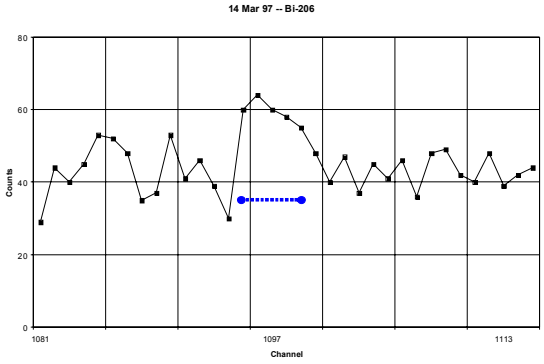

Figure D4c: Bi-206 Region -- 14 March 97

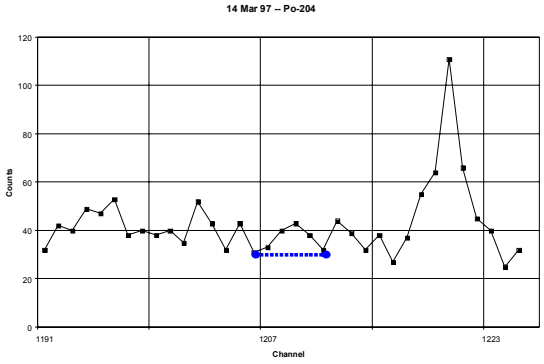

Figure D4d: Po-204 Region -- 14 March 97

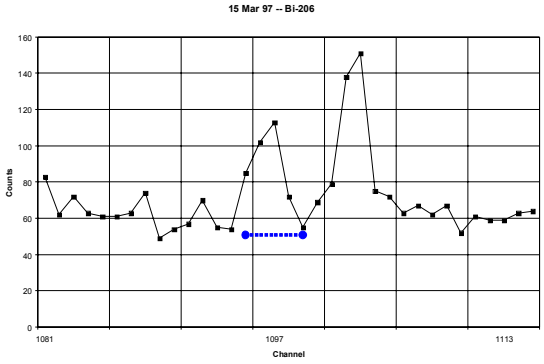

Figure D4e: Bi-206 Region -- 15 March 97

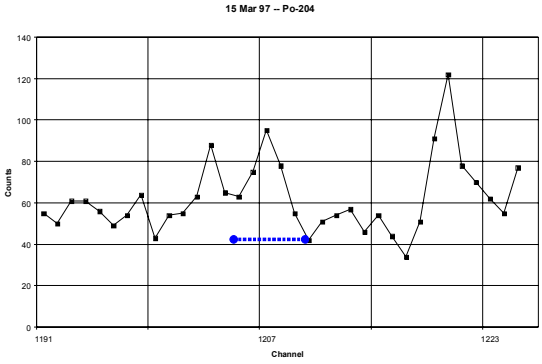

Figure D4f: Po-204 Region -- 15 March 97

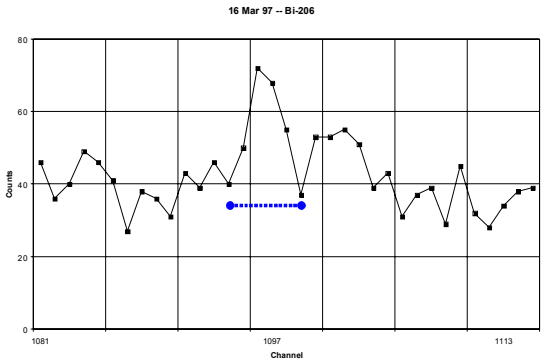

Figure D4g: Bi-206 Region -- 16 March 97

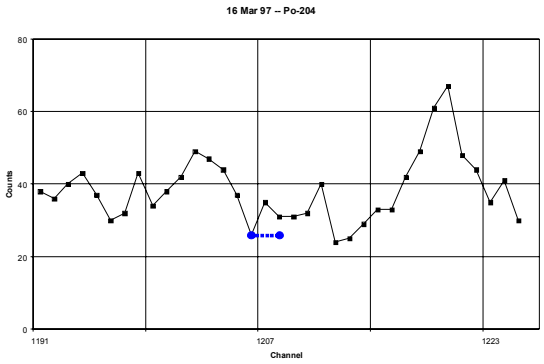

Figure D4h: Po-204 Region -- 16 March 97

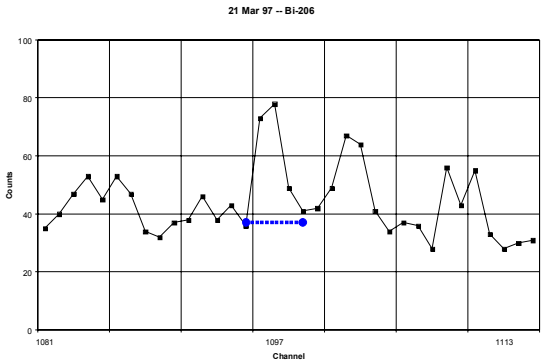

Figure D4i: Bi-206 Region -- 21 March 97

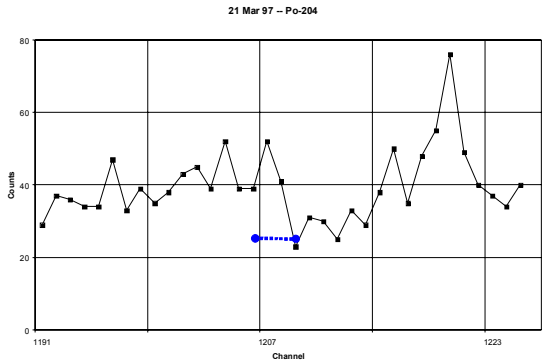

Figure D4j: Po-204 Region -- 21 March 97

Using the criteria described in Equation D9 and shown in Table D2 and Figure D2, the following conclusions can be drawn regarding the possible existence of peaks in the Bi-206 and Po-204 regions in Figures D4a through D4j.

Table D2: Determination Whether Figures 4a through 4j are Peaks or Background Counts

	Baseline Counts per Channel	**Average Net Counts per Channel in Peak (A)**	**Required Threshold Net Counts (PDT_n) per Channel for Peak to Exist (R)**	**Therefore, Does Peak Exist? (A>R, Yes; A<R, No)**	**Visual Inspection of Peak Existence (estimate based solely on figures D4a - D4j shown above)**
D4a	29	23.25	20.73	Yes	Yes, Definitely Peak
D4b	32	10.67	21.32	No	No, Definitely Not
D4c	36	23.4	22.45	Yes	Yes, Definitely Peak
D4d	30	8.5	20.73	No	No, Definitely Not

D4e	50	43	25.97	Yes	Yes, Definitely Peak
D4f	42	31.2	24.03	Yes	?, Probably Peak
D4g	34	32.25	21.89	Yes	Yes, Definitely Peak
D4h	26	9	19.48	No	No, Definitely Not
D4i	33	30.67	21.61	Yes	Yes, Definitely Peak
D4j	25	19	19.16	No	?, Probably Not

Conclusions

There are several conclusions that can be drawn from this study. The principal outcome is that the PDT_n is empirically shown to effectively and reliably determine the existence of peaks amongst background counts with a prescribed level of confidence. This study also highlights the value of the PDT_n in situations where visual inspections are inconclusive. Moreover, because the PDT_n concept is based upon an equation rooted in statistics, it can be a useful supplement to automated analytical tools that experience higher Type II error rates than desired.

Appendix E: REPRESENTATIVE METEOROLOGICAL DATA

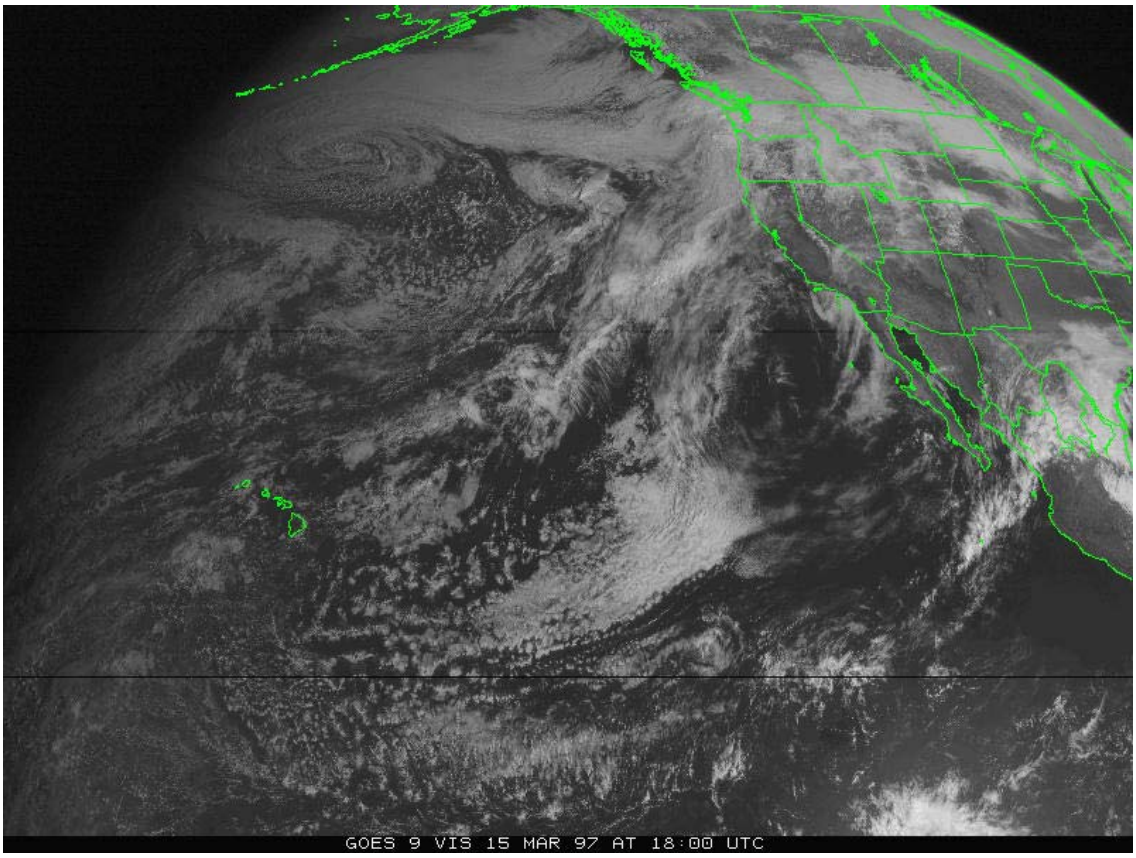

Figure E1: Satellite Imagery from 15 March 97

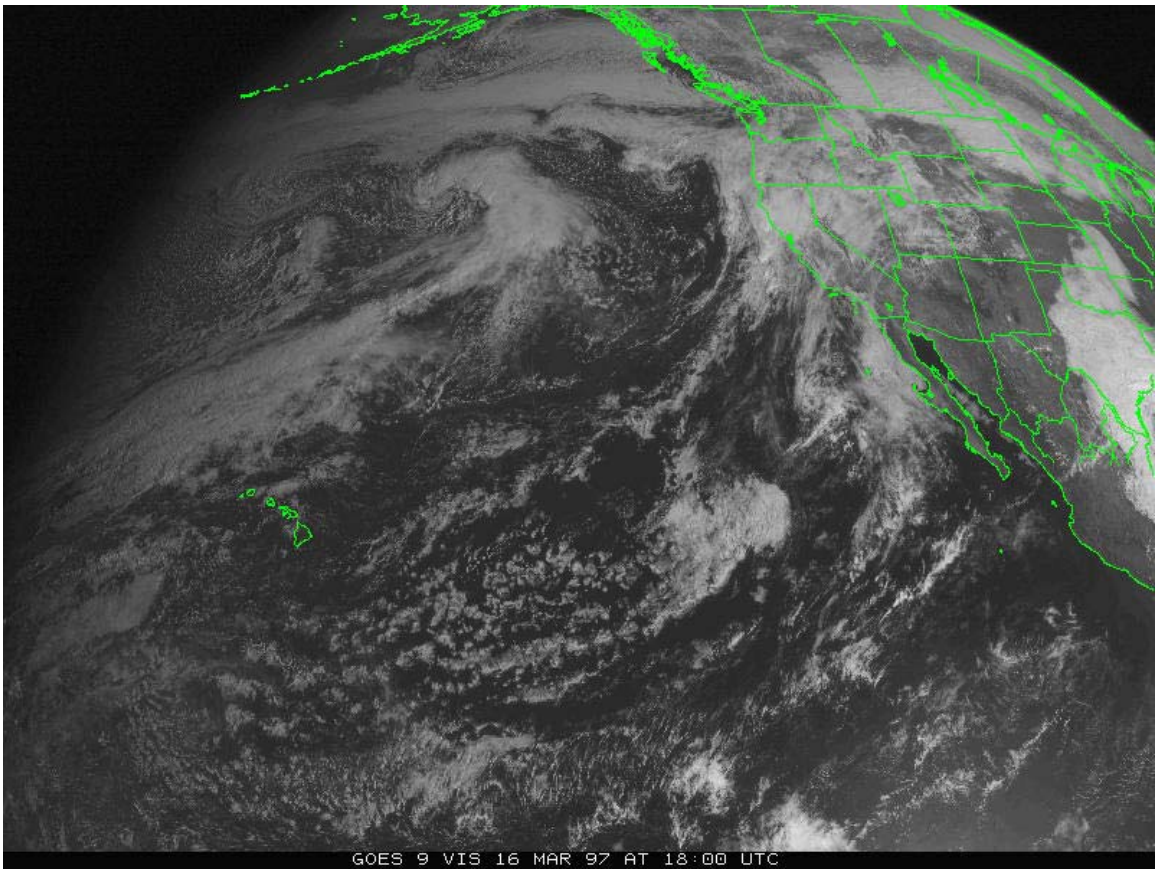

Figure E2: Satellite Imagery from 16 March 97

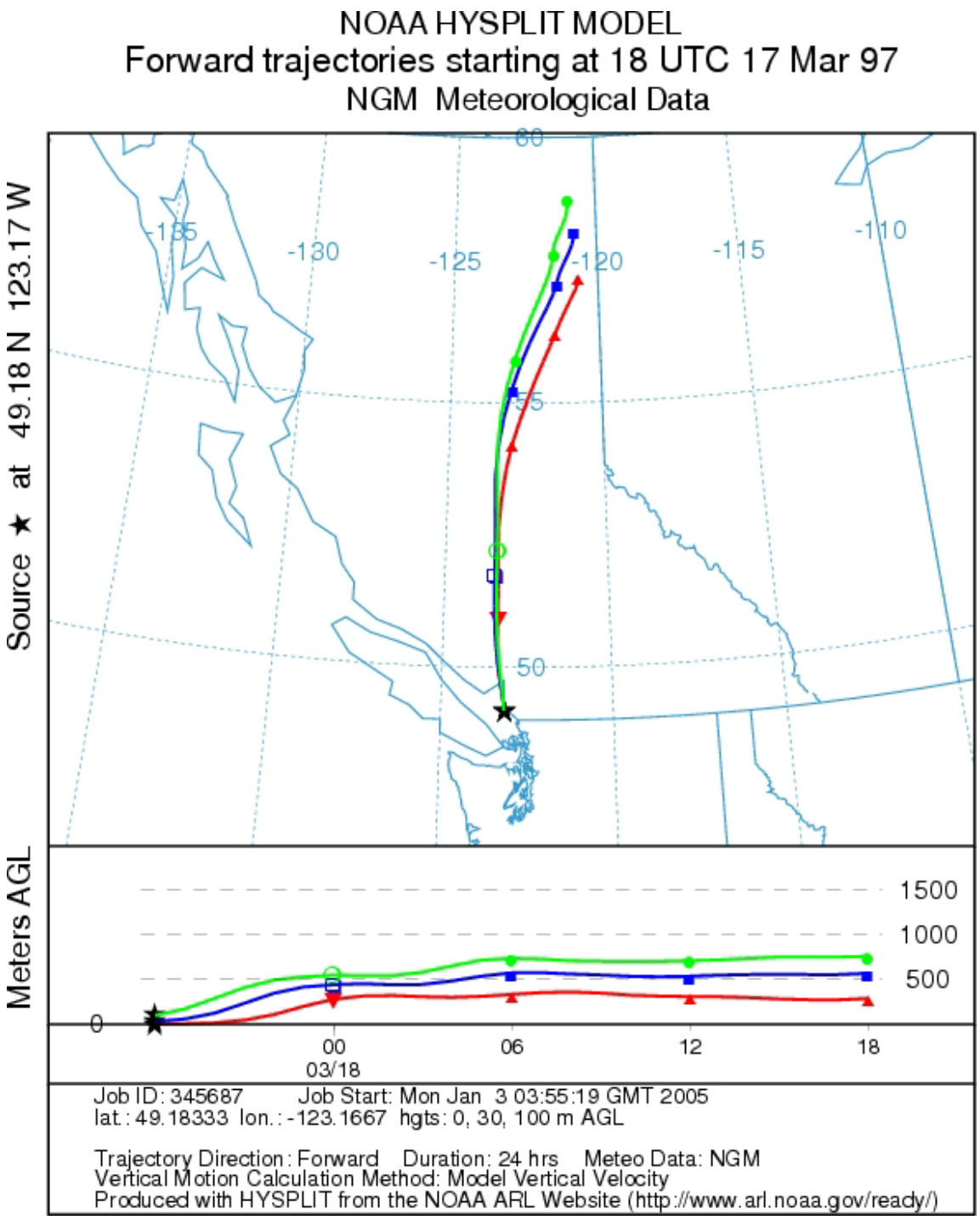

Figure E3: Forward Modeling Trajectory from 17 March 97

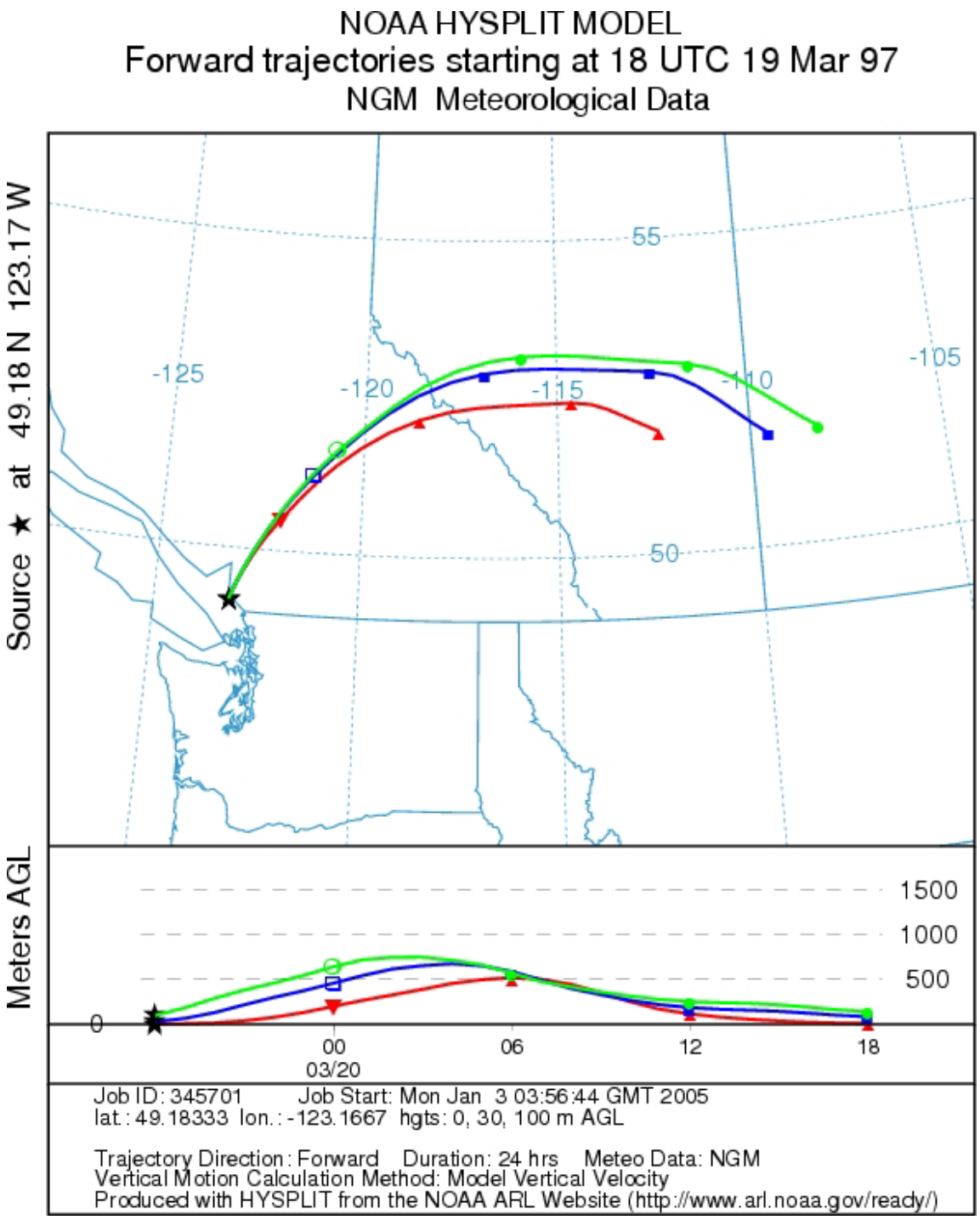

Figure E4: Forward Modeling Trajectory from 19 March 97

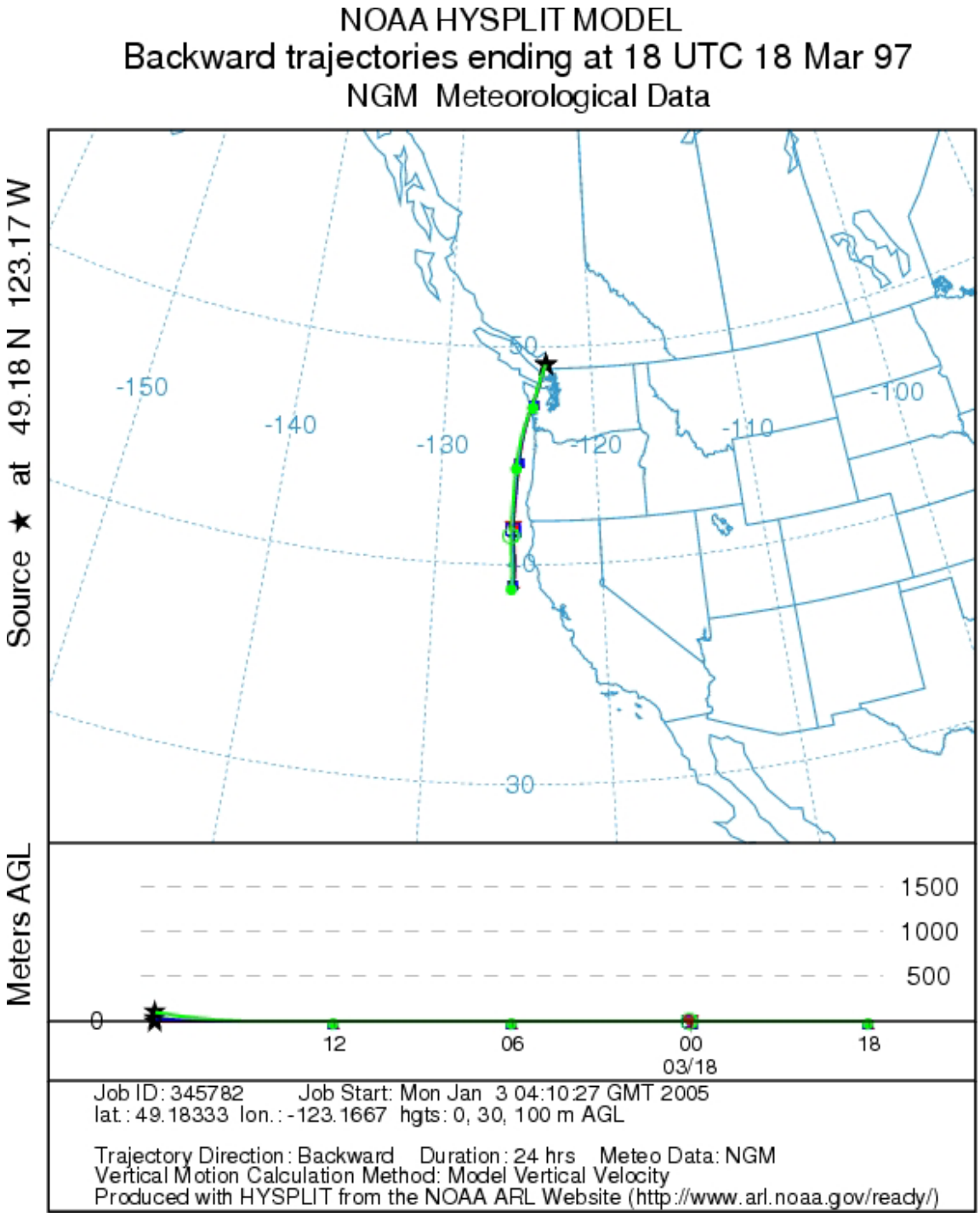

Figure E5: Backward Modeling Trajectory from 18 March 97

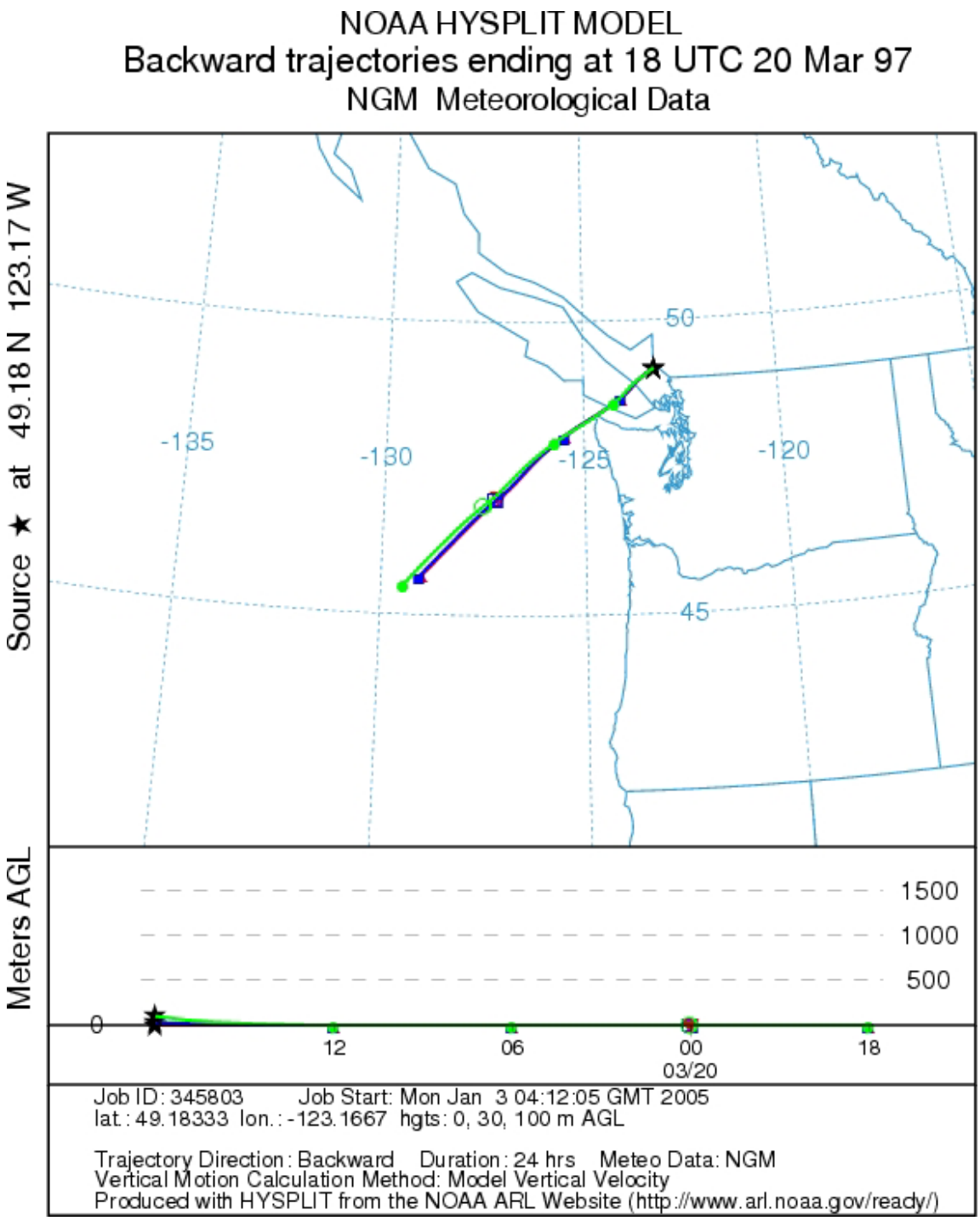

Figure E6: Backward Modeling Trajectory from 20 March 97

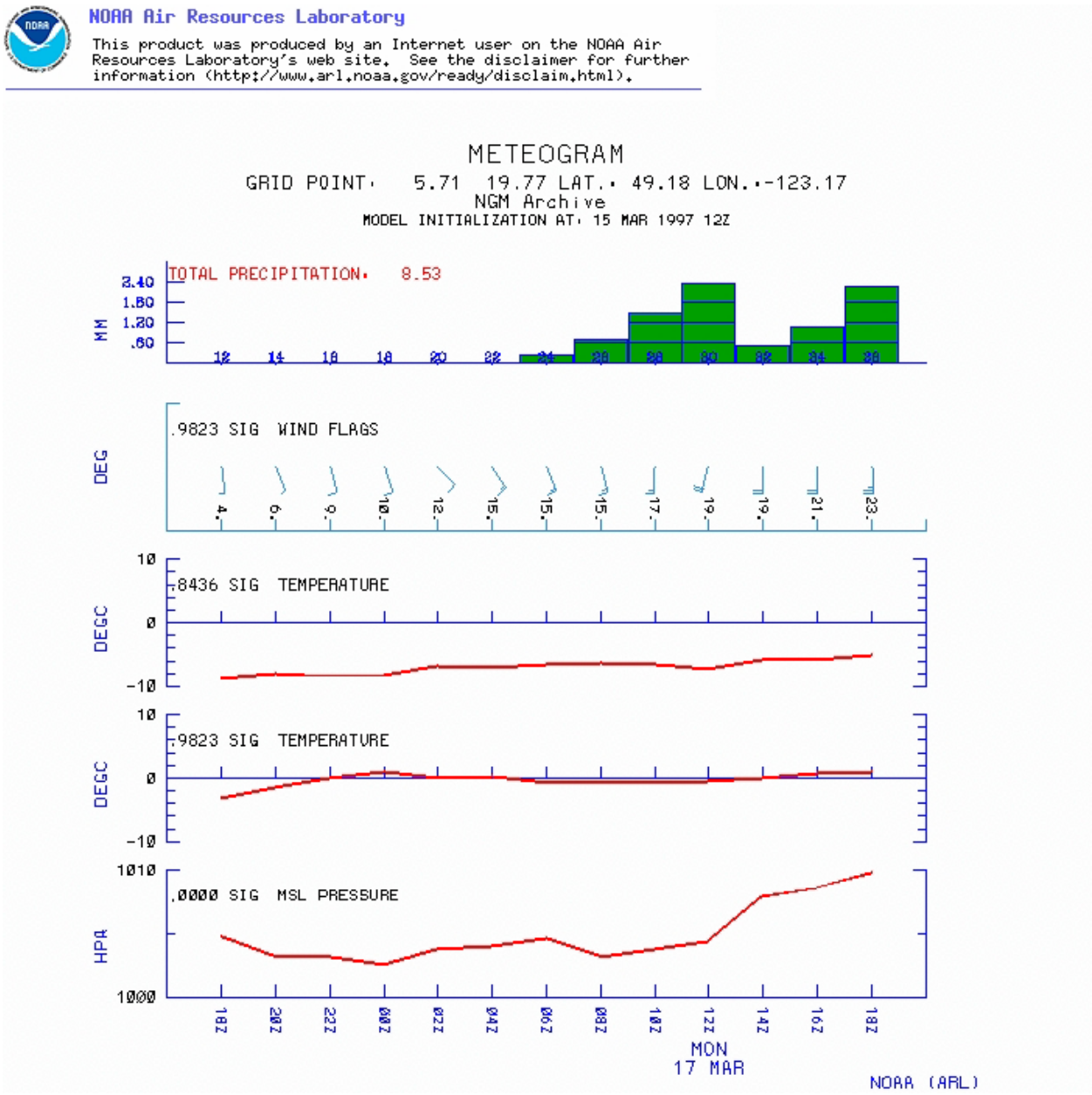

Figure E7: Meteogram from 16 March 97

Appendix F: LIST OF SELECTED EUROPEAN POTENTIAL RADIATION EMISSION FACILITIES

Armenia, Republic of: Nuclear Power Reactors

Operational **1**

Shut Down **1**

Annual Electrical Power Production for 2003

Total Power Production (including Nuclear)	Nuclear Power Production
5136 GWh(e)	**1822 GWh(e)**

				Capacity (MWe)		Date
Name	**Type**	**Status**	**Location**	**Net**	**Gross**	**Connected**
ARMENIA-1	WWER	Shut Down	ARMENIA	376	408	1976/12/28
ARMENIA-2	WWER	Operational	ARMENIA	376	408	1980/01/05

Belgium, Kingdom of : Nuclear Power Reactors

Operational **7**

Shut Down **1**

Annual Electrical Power Production for 2003

Total Power Production (including Nuclear)	Nuclear Power Production
*** Estimate**	*** Estimate**
80435 GWh(e)	**44613 GWh(e)**

				Capacity (MWe)		Date
Name	**Type**	**Status**	**Location**	**Net**	**Gross**	**Connected**
BR-3	PWR	Shut Down	BELGIUM-PROVINCE D'ANVERS	11	12	1962/10/10
DOEL-1	PWR	Operational	FLANDRE ORIENTALE	392	412	1974/08/28
DOEL-2	PWR	Operational	FLANDRE ORIENTALE	392	412	1975/08/21
DOEL-3	PWR	Operational	FLANDRE ORIENTALE	1006	1056	1982/06/23
DOEL-4	PWR	Operational	FLANDRE ORIENTALE	985	1041	1985/04/08

TIHANGE-1	PWR	Operational	LIEGE	962	1009	1975/03/07
TIHANGE-2	PWR	Operational	LIEGE	1008	1055	1982/10/13
TIHANGE-3	PWR	Operational	LIEGE	1015	1065	1985/06/15

Bulgaria, Republic of: Nuclear Power Reactors

Operational **4**

Shut Down **2**

Annual Electrical Power Production for 2003

Total Power Production (including Nuclear)	Nuclear Power Production
42534 GWh(e)	**16040 GWh(e)**

				Capacity (MWe)		Date
Name	**Type**	**Status**	**Location**	**Net**	**Gross**	**Connected**
KOZLODUY-1	WWER	Shut Down		408	440	1974/07/24
KOZLODUY-2	WWER	Shut Down		408	440	1975/09/27
KOZLODUY-3	WWER	Operational		408	440	1980/12/17
KOZLODUY-4	WWER	Operational		408	440	1982/05/17
KOZLODUY-5	WWER	Operational		953	1000	1987/11/29
KOZLODUY-6	WWER	Operational		953	1000	1991/08/02

Czech Republic: Nuclear Power Reactors

Operational **6**

Annual Electrical Power Production for 2003

Total Power Production (including Nuclear)	Nuclear Power Production
83227 GWh(e)	**25872 GWh(e)**

				Capacity (MWe)		Date
Name	**Type**	**Status**	**Location**	**Net**	**Gross**	**Connected**
DUKOVANY-1	WWER	Operational	TREBIC	412	440	1985/02/24
DUKOVANY-2	WWER	Operational	TREBIC	412	440	1986/01/30
DUKOVANY-3	WWER	Operational	TREBIC	412	440	1986/11/14
DUKOVANY-4	WWER	Operational	TREBIC	412	440	1987/06/11
TEMELIN-1	WWER	Operational	SOUTH	950	1000	2000/12/21

			BOHEMIA			
TEMELIN-2	WWER	Operational	SOUTH BOHEMIA	950	1000	2002/12/29

Finland, Republic of: Nuclear Power Reactors

Operational **4**

Annual Electrical Power Production for 2003

Total Power Production (including Nuclear)	Nuclear Power Production
79855 GWh(e)	**21819 GWh(e)**

				Capacity (MWe)		Date
Name	**Type**	**Status**	**Location**	**Net**	**Gross**	**Connected**
LOVIISA-1	WWER	Operational		488	510	1977/02/08
LOVIISA-2	WWER	Operational		488	510	1980/11/04
OLKILUOTO-1	BWR	Operational		840	870	1978/09/02
OLKILUOTO-2	BWR	Operational		840	870	1980/02/18

France (French Republic): Nuclear Power Reactors

Operational **59**

Shut Down **11**

Annual Electrical Power Production for 2003

Total Power Production (including Nuclear)	Nuclear Power Production
541600 GWh(e)	**420700 GWh(e)**

				Capacity (MWe)		Date
Name	**Type**	**Status**	**Location**	**Net**	**Gross**	**Connected**
BELLEVILLE-1	PWR	Operational		1310	1363	1987/10/14
BELLEVILLE-2	PWR	Operational		1310	1363	1988/07/06
BLAYAIS-1	PWR	Operational	GIRONDE	910	951	1981/06/12
BLAYAIS-2	PWR	Operational	GIRONDE	910	951	1982/07/17
BLAYAIS-3	PWR	Operational	GIRONDE	910	951	1983/08/17
BLAYAIS-4	PWR	Operational	GIRONDE	910	945	1983/05/16
BUGEY-1	GCR	Shut Down	AIN	540	555	1972/04/15

BUGEY-2	PWR	Operational	AIN	910	945	1978/05/10
BUGEY-3	PWR	Operational	AIN	910	917	1978/09/21
BUGEY-4	PWR	Operational	AIN	880	917	1979/03/08
BUGEY-5	PWR	Operational	AIN	880	937	1979/07/31
CATTENOM-1	PWR	Operational	MOSELLE	1300	1362	1986/11/13
CATTENOM-2	PWR	Operational	MOSELLE	1300	1362	1987/09/17
CATTENOM-3	PWR	Operational	MOSELLE	1300	1362	1990/07/06
CATTENOM-4	PWR	Operational	MOSELLE	1300	1362	1991/05/27
CHINON-A1	GCR	Shut Down	CHINON	70	80	1963/06/14
CHINON-A2	GCR	Shut Down	CHINON	210	230	1965/02/24
CHINON-A3	GCR	Shut Down	CHINON	480	480	1966/08/04
CHINON-B-1	PWR	Operational	CHINON	905	969	1982/11/30
CHINON-B-2	PWR	Operational	CHINON	905	969	1983/11/29
CHINON-B-3	PWR	Operational	CHINON	905	969	1986/10/20
CHINON-B-4	PWR	Operational	CHINON	905	969	1987/11/14
CHOOZ-A(ARDENNES)	PWR	Shut Down	ARDENNES	310	320	1967/04/03
CHOOZ-B-1	PWR	Operational	ARDENNES	1500	1520	1996/08/30
CHOOZ-B-2	PWR	Operational	ARDENNES	1500	1520	1997/04/10
CIVAUX-1	PWR	Operational		1495	1520	1997/12/24
CIVAUX-2	PWR	Operational		1495	1520	1999/12/24
CREYS-MALVILLE	FBR	Shut Down	ISERE	1200	1242	1986/01/14
CRUAS-1	PWR	Operational	ARDECHE	915	956	1983/04/29
CRUAS-2	PWR	Operational	ARDECHE	915	956	1984/09/06
CRUAS-3	PWR	Operational	ARDECHE	915	956	1984/05/14
CRUAS-4	PWR	Operational	ARDECHE	915	956	1984/10/27
DAMPIERRE-1	PWR	Operational	LOIRET	890	937	1980/03/23
DAMPIERRE-2	PWR	Operational	LOIRET	890	937	1980/12/10
DAMPIERRE-3	PWR	Operational	LOIRET	890	937	1981/01/30
DAMPIERRE-4	PWR	Operational	LOIRET	890	937	1981/08/18
EL-4 (MONTS D'ARREE)	HWGCR	Shut Down	MONTS ARREL	70	75	1967/07/09
FESSENHEIM-1	PWR	Operational	HAUT-RHINE	880	920	1977/04/06
FESSENHEIM-2	PWR	Operational	HAUT-RHINE	880	920	1977/10/07
FLAMANVILLE-1	PWR	Operational	MANCHE	1330	1382	1985/12/04

FLAMANVILLE-2	PWR	Operational	MANCHE	1330	1382	1986/07/18
G-2 (MARCOULE)	GCR	Shut Down		38	43	1959/04/22
G-3 (MARCOULE)	GCR	Shut Down		38	43	1960/04/04
GOLFECH-1	PWR	Operational	TARN ET GARONNE	1310	1363	1990/06/07
GOLFECH-2	PWR	Operational	TARN ET GARONNE	1310	1363	1993/06/18
GRAVELINES-1	PWR	Operational	DUNKERQUE	910	956	1980/03/13
GRAVELINES-2	PWR	Operational	DUNKERQUE	910	956	1980/08/26
GRAVELINES-3	PWR	Operational	DUNKERQUE	910	956	1980/12/12
GRAVELINES-4	PWR	Operational	DUNKERQUE	910	956	1981/06/14
GRAVELINES-5	PWR	Operational	DUNKERQUE	910	956	1984/08/28
GRAVELINES-6	PWR	Operational	DUNKERQUE	910	956	1985/08/01
NOGENT-1	PWR	Operational	AUBE	1310	1363	1987/10/21
NOGENT-2	PWR	Operational	AUBE	1310	1363	1988/12/14
PALUEL-1	PWR	Operational	SEINE MARITIME	1330	1382	1984/06/22
PALUEL-2	PWR	Operational	SEINE MARITIME	1330	1382	1984/09/14
PALUEL-3	PWR	Operational	SEINE MARITIME	1330	1382	1985/09/30
PALUEL-4	PWR	Operational	SEINE MARITIME	1330	1382	1986/04/11
PENLY-1	PWR	Operational	SEINE MARITIME	1330	1382	1990/05/04
PENLY-2	PWR	Operational	SEINE MARITIME	1330	1382	1992/02/04
PHENIX	FBR	Operational	GARD	233	250	1973/12/13
ST. ALBAN-1	PWR	Operational	ISERE	1335	1381	1985/08/30
ST. ALBAN-2	PWR	Operational	ISERE	1335	1381	1986/07/03
ST. LAURENT-A1	GCR	Shut Down	LOIR ET CHER	480	500	1969/03/14
ST. LAURENT-A2	GCR	Shut Down	LOIR ET CHER	515	530	1971/08/09
ST. LAURENT-B-1	PWR	Operational	LOIR ET CHER	915	937	1981/01/21
ST. LAURENT-B-2	PWR	Operational	LOIR ET CHER	915	937	1981/06/01
TRICASTIN-1	PWR	Operational	DROME	915	920	1980/05/31
TRICASTIN-2	PWR	Operational	DROME	915	920	1980/08/07
TRICASTIN-3	PWR	Operational	DROME	915	920	1981/02/10

TRICASTIN-4	PWR	Operational	DROME	915	920	1981/06/12

Germany, Federal Republic of: Nuclear Power Reactors

Operational	**18**
Shut Down	**18**

Annual Electrical Power Production for 2003

Total Power Production (including Nuclear)	Nuclear Power Production
560300 GWh(e)	**157443 GWh(e)**

				Capacity (MWe)		Date
Name	**Type**	**Status**	**Location**	**Net**	**Gross**	**Connected**
AVR JUELICH (AVR)	HTGR	Shut Down	NORDRHEIN-WESTFALEN	13	15	1967/12/17
BIBLIS-A (KWB A)	PWR	Operational	HESSEN	1167	1225	1974/08/25
BIBLIS-B (KWB B)	PWR	Operational	HESSEN	1240	1300	1976/04/06
BROKDORF (KBR)	PWR	Operational	SCHLESWIG-HOLSTEIN	1370	1440	1986/10/14
BRUNSBUETTEL (KKB)	BWR	Operational	SCHLESWIG-HOLSTEIN	771	806	1976/07/13
EMSLAND (KKE)	PWR	Operational	NIEDERSACHSEN	1329	1400	1988/04/19
GRAFENRHEINFELD (KKG)	PWR	Operational	BAYERN	1275	1345	1981/12/21
GREIFSWALD-1(KGR 1)	WWER	Shut Down		408	440	1973/12/17
GREIFSWALD-2 (KGR 2)	WWER	Shut Down		408	440	1974/12/23
GREIFSWALD-3 (KGR 3)	WWER	Shut Down		408	440	1977/10/24
GREIFSWALD-4 (KGR 4)	WWER	Shut Down		408	440	1979/09/03
GREIFSWALD-5 (KGR 5)	WWER	Shut Down		408	440	1989/04/24
GROHNDE (KWG)	PWR	Operational	NIEDERSACHSEN	1360	1430	1984/09/04
GUNDREMMINGEN-A (KRB A)	BWR	Shut Down	BAYERN	237	250	1966/12/01
GUNDREMMINGEN-B (GUN-B)	BWR	Operational	BAYERN	1284	1344	1984/03/16

GUNDREMMINGEN-C (GUN-C)	BWR	Operational	BAYERN	1288	1344	1984/11/02
HDR GROSSWELZHEIM	BWR	Shut Down	BAYERN	23	25	1969/10/14
ISAR-1 (KKI 1)	BWR	Operational	BAYERN	878	912	1977/12/03
ISAR-2 (KKI 2)	PWR	Operational	BAYERN	1400	1475	1988/01/22
KNK II	FBR	Shut Down	BADEN-WUERTTEMBERG	17	21	1978/04/09
KRUEMMEL (KKK)	BWR	Operational	SCHLESWIG-HOLSTEIN	1260	1316	1983/09/28
LINGEN (KWL)	BWR	Shut Down	NIEDERSACHSEN	250	268	1968/07/01
MUELHEIM-KAERLICH (KMK)	PWR	Shut Down	RHEINLAND-PFALZ	1219	1302	1986/03/14
MZFR	PHWR	Shut Down	BADEN-WUERTTEMBERG	52	57	1966/03/09
NECKARWESTHEIM-1 (GKN 1)	PWR	Operational	BADEN-WUERTTEMBERG	785	840	1976/06/03
NECKARWESTHEIM-2 (GKN 2)	PWR	Operational	BADEN-WUERTTEMBERG	1269	1365	1989/01/03
NIEDERAICHBACH (KKN)	HWGCR	Shut Down	BAYERN	100	106	1973/01/01
OBRIGHEIM (KWO)	PWR	Operational	BADEN-WUERTTEMBERG	340	357	1968/10/29
PHILIPPSBURG-1 (KKP 1)	BWR	Operational	BADEN-WUERTTEMBERG	890	926	1979/05/07
PHILIPPSBURG-2 (KKP 2)	PWR	Operational	BADEN-WUERTTEMBERG	1392	1458	1984/12/17
RHEINSBERG (KKR)	PWR	Shut Down	RHEINSBERG	62	70	1966/05/06
STADE (KKS)	PWR	Shut Down	NIEDERSACHSEN	640	672	1972/01/29
THTR-300	HTGR	Shut Down	NORDRHEIN-WESTFALEN	296	308	1985/11/16
UNTERWESER (KKU)	PWR	Operational	NIEDERSACHSEN	1345	1410	1978/09/29
VAK KAHL	BWR	Shut Down	BAYERN	15	16	1961/06/17
WUERGASSEN (KWW)	BWR	Shut Down	NORDRHEIN-WESTFALEN	640	670	1971/12/18

Spain, Kingdom of: Nuclear Power Reactors

Operational **9**

Shut Down **1**

Annual Electrical Power Production for 2003

Total Power Production (including Nuclear)	Nuclear Power Production
251050 GWh(e)	**59359 GWh(e)**

				Capacity (MWe)		Date
Name	**Type**	**Status**	**Location**	**Net**	**Gross**	**Connected**
ALMARAZ-1	PWR	Operational	CACERES	947	977	1981/05/01
ALMARAZ-2	PWR	Operational	CACERES	950	980	1983/10/08
ASCO-1	PWR	Operational	TARRAGONA	996	1033	1983/08/13
ASCO-2	PWR	Operational	TARRAGONA	992	1027	1985/10/23
COFRENTES	BWR	Operational	VALENCIA	1063	1095	1984/10/14
JOSE CABRERA-1(ZORITA)	PWR	Operational	GUADALAJARA	142	150	1968/07/14
SANTA MARIA DE GARONA	BWR	Operational	BURGOS	446	466	1971/03/02
TRILLO-1	PWR	Operational	GUADALAJARA	1003	1066	1988/05/23
VANDELLOS-1	GCR	Shut Down	TARAGONA	480	500	1972/05/06
VANDELLOS-2	PWR	Operational	TARAGONA	1045	1087	1987/12/12

Selected European Research Reactors

Country	Facility Name	Thermal Power (kW)	Type	Status	Criticality Date
Austria	ASTRA	500.00	POOL	SHUT	1960
Austria	TRIGA MARK II	250.00	TRIGA	OPER	1962/03/07
Belarus	IRT-M MINSK	4,000.00	POOL, IRT	DEC M	1962/04/01
Belgium	BR-02,POWER MOCKUP OF BR2	0.50	POOL	SHUT	1959/12/01
Belgium	BR-1	4,000.00	GRAPHITE	OPER	1956/05/11
Belgium	BR-2	100,000.00	TANK	OPER	1961/06/29
Belgium	BR-3	40,900.00	PWR POWER	SHUT	1962/08/29
Belgium	THETIS RR-BN-1	250.00	POOL	OPER	1967/04/07

Belgium	VENUS	0.50	CRIT ASSEMBLY	OPER	1964/04/30
Bulgaria	IRT-SOFIA	2,000.00	POOL, IRT	SHUT	1961/09/01
Czech Republic	LR-0	5.00	POOL-VAR	OPER	1982/12/19
Czech Republic	LWR-15 REZ	10,000.00	TANK WWR	OPER	1957/09/24
Czech Republic	SR-O	1.00	POOL	DEC M	1971/01/01
Czech Republic	TR-0	0.30	TANK	DEC M	1972/01/01
Czech Republic	VR-1 VRABEC	5.00	POOL	OPER	1990/03/12
Denmark	DR-1	2.00	HOMOG (L)	OPER	1957/08/15
Denmark	DR-2	5,000.00	POOL	DEC M	1958/12/18
Denmark	DR-3	10,000.00	HEAVY WATER	SHUT	1960/01/16
Finland	FIR-1	250.00	TRIGA MARK II	OPER	1962/03/27
Finland	SCA	0.00	SUBCRIT	DEC M	1963/07/30
France	CABRI	25,000.00	POOL	OPER	1963/01/01
Greece	DEMOKRITOS (GRR-1)	5,000.00	POOL	OPER	1961/07/27
Greece	GR-B SUBCRITICAL ASSEMBLY	0.00	CRIT ASSEMBLY	OPER	1971/08/04
Greece	NTU	0.10	SUBCRIT	SHUT	1970/10/10
Hungary	BUDAPEST RES. REACTOR	10,000.00	TANK WWR	OPER	1959/03/25
Hungary	NUCL. TRAINING REACTOR	100.00	POOL	OPER	1971/01/01
Hungary	ZR-6M	0.00	CRIT ASSEMBLY	DEC M	1972/11/28
Italy	AGN 201 COSTANZA	0.02	HOMOG (S)	OPER	1960/02/12

Italy	GALILEO GALILEI RTS-1	5,000.00	POOL	DEC M	1963/04/04
Italy	L-54 M	50.00	HOMOG (L)	DEC M	1959/11/20
Italy	LENA, TRIGA II PAVIA	250.00	TRIGA MARK II	OPER	1965/11/10
Italy	RANA	10.00	POOL	SHUT	1965/02/15
Italy	RB-1	20.00	CRIT GRAPHITE	SHUT	1962/07/01
Italy	RB-2	10.00	ARGONAUT	SHUT	1963/05/28
Italy	RB-3	0.10	ZERO POWER D2O	SHUT	1971/08/09
Italy	RITMO REACTOR (RC-4)	0.01	POOL	DEC M	1965/07/08
Italy	ROSPO 2	0.20	POOL	DEC M	1963/01/01
Italy	RSV TAPIRO	5.00	FAST SOURCE	OPER	1971/04/04
Italy	SM-1 SUBCRITICAL ASSEMBLY	0.00	SUBCRIT	OPER	1961/01/01
Italy	STRUTTURA SOTTOCRITICA	0.00	SUBCRIT	DEC M	1962/01/01
Italy	TRIGA RC-1	1,000.00	TRIGA MARK II	OPER	1960/06/11

Selected European Hospitals that may use Radioactive Sources

Netherlands

Academisch Medisch Centrum Universiteit van Amsterdam
Academisch Ziekenhuis Nijmegen St Radboud
Laurentius Ziekenhuis, Roermond
Leids Universitair Medisch Centrum
Mesos Medisch Centrum, Utrecht
Nederlands Kanker Instituut / Antoni van Leeuwenhoek Ziekenhuis, Amsterdam
Reinier de Graaf Groep
St. Antonius Ziekenhuis, Niewegein
The Digital Hospital
Westeinde Hospital, The Hague
Ziekenhuis Centrum Apeldoorn, Nijmegen

Ziekenhuis Gelderse Vallei
Ziekenhuis St. Jansdal, Harderwijk

Norway

Aker University Hospital, Olso
Harstad Sykehus
Haukeland Sykehus, Bergen
Kirkenes Sykehus
Kongsgard Sykehus, Kristiansand
Lofoten Sykehus
Lovisenberg Diakonale Sykehus, Oslo
Namdal Sykehus, Nord-Trøndelag
Narvik Sykehus - Narvik Sykehus
Nordland Sentralsykehus, Bodø
Rana Sentralsykehus
Statens Senter for Epilepsi, Sandvika
National Hospital, Rikshospitalet, Olso
University Hospital of Trondheim

Poland

Centralny Szpital Kliniczny Wojskowej Akademii Medycznej z Poliklinika
Kolejowy Szpital Dzieciecy
Specjalistyczny Szpital Miejski im. Miko³aja Kopernika
Szpital Damians, Warsaw
Szpital Kliniczny Wojskowej Akademii Medycznej
Szpital Wojewodzki, Koszalinie
Szpital Wojskowy z Przychodnia
Szpital Wojewodzki im. SW. Lukasza w Tarnowie
Wojewodzki Szpital Specjalistyczny, Wroclaw

Portugal

Centro Hospitalar de Coimbra
Hospitais da Universidade de Coimbra
Hospital de Nossa Senhora da Assuncao, Seia
Hospital de São João Baptista
Hospital de Santa Cruz, Carnaxide
Hospital São Sebastião
Hospital de São Teotónio de Viseu
Hospital Distrital de Santarém
Hospital Geral de Coimbra
Hospital Ortopédico Sant'Iago - Outão
Hospital Pediátrico de Coimbra
Hospital Sobral Cid

Maternidade Bissaya Barreto
Santa Maria Hospital, Lisbon

Sweden

Akademiska Sjukhuset, Uppsala University Hospital, Uppsala
Halsinglands Sjukhus
Huddinge Universitetssjukhus
Karolinska Institutet Danderyds Sjukhus, Stockholm
Karolinska Institutet, Institutionen Södersjukhuset, Stockholm
Linkoping University Hospital
Norrtälje Sjukhus
Sahlgrenska Universitetssjukhuset
Sodersjukhuset, Stockholm
Sodertalje Sjukhus
Skaraborgs Sjukhus
Sophiahemmet, Stockholm
St Görans Sjukhus AB

Switzerland

Bethesda-Spital, Basel
Hopital de la Tour
Inselspital Bern - University Hospital Bern
Kantonsspital Aarau
Kantonsspital St.Gallen
Kantonsspital Winterthur
Paracelsus Klink, Lustmühle
Rätischen Kantons- und Regionalspital, Chur
Spital Grabs
Spital Uster
Spital Wil
Stadtspital Waid Zürich
Tiefenauspital, Bern
Universitätsklinik Balgrist

Appendix G: SELECTED REPORTS REGARDING SPANISH FACILITY RADIONUCLIDE RELEASE

Legal Void Meant Costly Delay When Spanish Firm Melted Source

from a September 24, 1998, Nucleonics Week article

When a cesium-137 source was accidentally melted in a vat of scrap metal bought by the Spanish steel firm Acerinox, no regulations existed telling management what to do, a senior Spanish safety official said last week.

"This industrial activity is totally unregulated," said Jose Azuara, a commissioner of Spain's Nuclear Safety Council (CSN). "There was no legal responsibility for the company in the aftermath of the accident." The legal void, he said, eventually cost $25-million and led to a four-fold increase in the amount of contaminated material on one site before it was finally isolated.

At an IAEA-cosponsored conference on security of nuclear materials last week in Dijon, France (NW, 17 Sept., 1), Azuara recalled that, on May 30, an electric furnace at the firm's works near Cadiz melted down a Cs-137 source, venting radioactive emissions via the plant stack. The filtering system retained some matter, resulting in contamination of 270 metric tons (MT) of dust produced by the melting of the scrap. Azuara said that Acerinox, not realizing it had melted a source, moved 150 MT of the dust to another factory in Huelva, several hundred kilometers away. There, he said, the dust was unwittingly mixed with cement and sand into a "dough," which was then "spread out in layers" over a marshland, a process designed for conditioning conventional waste. That process increased the amount of contaminated material to 500 MT.

The first warning that the dust was contaminated came only on June 2, three days after the melting. Radioactivity was detected by a gate monitor at the Huelva factory as the truck that had brought the waste left the facility. CSN got the news only on June 9, Azuara said. The following day, the safety agency sent an inspection team to Acerinox. By June 12, CSN had cordoned off contaminated parts of the plant and begun checking for possible contamination of workers. It also reported the incident to the IAEA and counterpart agencies (NW, 18 June, 21).

On June 11, radiation monitors in southern France and northern Italy had begun detecting atmospheric Cs-137 levels up to 2,000 times higher than normal (2,000 microbecquerels per cubic meter compared to 2 Bq/m3). Because the isotopes were identical, the French and Italian findings were assumed to have originated in Acerinox.

Azuara said six people at the Spanish companies involved were slightly contaminated by the Cs-137 and the radiological impact of atmospheric Cs-137 was negligible. But because of the lack of rules and infrastructure, the environmental impact of the incident in Spain was "important," Azuara said. Ignorance of the presence of radioactivity in the

dust led to actions which increased the volume of the contaminated material by 400% at Huelva and irrevocably contaminated the marshland with cesium.

Economic damage caused by the accident was about $25-million, he said, due mostly to interruption of the factories' activities, but including $3-million for cleanup and $3-million for storage of the waste.

Spain was criticized for delays in reporting the contamination to both national and international bodies and in isolating the radioactive material. Azuara said delays arose because "neither scrap trade activities nor industrial processes using this material are submitted to any specific regulation to cope with the presence of improper active material." World trade in scrap metal is 400-million MT/year, the CSN official said. Spain alone buys and sells about 12-million MT/y, he said, about half of it imported.

What's more, under Spanish rules, Acerinox "is not obliged to have any systems installed to detect the presence of (such material) nor to make an early report of the incident to CSN." But the nine-day delay in reporting "was the cause of the main negative consequences" of the incident, he said. Underscoring the legal void, Azuara said, an investigation has concluded that Acerinox "should not have to face any legal responsibility" for its actions.

Azuara said that, since June, CSN has met with the Ministry of Industry and the National Scrap Traders Association and steel industry to seek a solution. But industry, he said, has ruled out continuous monitoring of steel production, analogous to monitoring conducted at nuclear installations, as inappropriate. Instead, he said, "control of key points in the process is equally effective" and "would not unduly increase burdens on enterprises."

Spain is expected to accept rules that concentrate on detecting sources at final destinations as well as controlling trade from point of origin.

Spain's industry has agreed to install detection systems at factory entrances to check incoming loads of scrap, although this approach will be less effective for sealed sources. Azuara said controls are expected to be set up at about 90 different destinations in Spain.

Right now, installation of detectors is voluntary, but the Ministry of Industry is considering making it compulsory. The work is being supported by Spanish radiation monitoring experts and will include programs to train steel company employees. Separately, studies are being done to define compulsory procedures to be followed when radioactive material is detected at a scrap metal-handling plant.

Spain can do little on its own to control radioactive sources at their origins. CSN Chairman Juan Manuel Kindelan said in July that his agency will lobby the European

Union for a new directive setting requirements for control of imported sources (NW, 30 July, 13). At the least, Azuara said last week, a system must be organized to alert foreign firms and authorities when sources are discovered stolen or missing. In addition, he argued, the world's steel industry must be familiarized with the characteristics of radiation sources, especially very old ones, which are most likely to be lost and cause a radiological accident.

ACERINOX

Recently the Council of Seguridad Nuclear (CSN) recognized that still they are left 1700 tons of radioactive ashes in the ACERINOX plant, where took place the fusion of a source of Cs-137 the 30 of May of 1988. According to Ecologists in Action this fact confirms that the decontamination of the plant was imperfect.

The initial process of decontamination of the factory of ACERINOX, dice by finalized by the CSN already was denounced like imperfect by Ecologists in Action. This organization esteem that radioactive doses m · ximas guaranteed for the workers was too high. The fact that in ACERINOX they are left still 1700 tons of radioactive ashes, with an average activity of 70 Bq/gr. (that is to say, 70 disintegrations per second and gram) it comes to confirm this asseveration. The CSN has been forced to review their appreciations and to evacuate these ashes. The radioactivity that contains comes to be between the 2 and 3% of the released one to the medio.ambiente in the fusion of the source of Cs-137. The own CSN still maintains in the factory a carp with the sign of the radioactivity, which sample that the decontamination has not been finalized.

On the other hand, the CSN tries to treat like inert these remainders, which is inadmissible. Ecologists in Action want to denounce in addition that a legal emptiness exists on the limits below which a remainder happens to be considered like inert instead of radioactive. This consideration allows the CSN to treat the remainders without no special precaution and to deposit them in some garbage dump of inert. Still the place of destiny of these substances has not been determined that happened to contaminate the place where they are deposited.

Introduction

At the end of May of 1998 a Cs-137 source was melted accidentally in one of the stainless steel production plant furnaces that the Acerinox company has in Cadiz (Spain).

Once the presence of radioactive contamination was detected, a number of organizations provided assistance. These included LAINSA, an expert company in decontamination and dismantling of radioactive and nuclear facilities with experience in radioactive emergencies, the regulatory body, CSN, and the waste management utility, ENRESA. They have evaluated the situation and implemented first radiological protection measures:

- Evaluation of the contamination in the plant

- Control of the access of people, vehicles and materials to the contaminated zones

- Delineation and signing of all areas where radioactivity was detected

- Control of radiation in the gases extracted by the smoke clearing system.

The recovery operation for the affected facilities began immediately: even before the formal approval from CSN of a Performance Plan, to decontaminate the affected facilities.

Decontamination took 5 months, and 50.000 man-hours were necessary to perform the whole work (20% corresponding to radiological protection activities). The total collective dose was about 60 man.mSv.

Objectives

The objectives established in the Performance Plan, previously mentioned, were:

- To avoid contamination outside the Plant.

- To guarantee the Radiological protection of the professionally exposed workers, the personnel of Acerinox and the public in general

- To control the decontamination activities according to the Radiological Protection standards.

- To ensure that the generated radioactive waste remained in safe conditions as far as their manipulation, storage and transport are concerned.

Affected facilities

Since the very beginning the contamination had affected the smoke dust that circulates through the conduits of the gas extraction system of the electrical arc furnace nº 1 and to the shared clearing system for furnaces no 1 and no 2 (Figure 1).

Table 1. Levels of initial radiation in the main areas

SYSTEM	Average Dose Rate mSv/h	Maximum Dose Rate mSv/h
Electrical arc furnace no 1 and gas ducts extractions	0.5	1.8
Natural Cooler and stark arrester	0.02	0.05
Bag filter nº1	0.05	0.1
Bag filter nº2	0.02	0.03
Silos A and B	0.03	0.1

Table 1 summarises the detected values of radiation in the affected systems. The measured activities in samples taken in the smoke dust, before the beginning of the decontamination were in the range 800 to 2000 Bq/g.

Radiological Criteria

According to the Performance Plan approved by the CSN the final state of the facilities would be such that:

- The maximum permissible dose in any zone of the factory did not exceed the value 1 mSv in an annual period.

- The derived values from surface contamination were such that they did not exceed 4 $Bq.cm^{-2}$, in those areas where their measurement was possible.

Due to the dimensions of the facility and the great number of affected zones it was not easy to establish a strict and unique access control. Thus, in the first phase those zones with higher dose rates and requiring greater movements of people were identified. The measures adopted were based on two general approaches:

- Immediate Intervention: action to remove radioactive material, decontaminating the zone, remove systems, equipment, etc, or.

- Isolation of these areas, by establishing alternative access and routes.

Works development

The objective established for the final state of the facilities had to fulfil two requirements; the production of the Steel Works had to continue and it was necessary to cope with the radiological protection principles.

Therefore, in the first phase decontamination was limited to clearing line no.1, allowing normal production to continue on the other clearing line. In that phase most of the very low activity contaminated wastes were generated

Next decontamination of the electrical Furnace no.1 was undertaken, followed by the Bag filter no.2 and silos. In these phases, less smoke dust wastes were extracted but metallic wastes, refractory bricks of the furnace, etc., were generated. Dry decontamination techniques (vacuum cleaning, grinding, etc.) were used to avoid the generation of liquid wastes that would have been difficult to treat in that facility.

Radiological control and ALARA studies

The main activities of LAINSA were as follow:

Control of effluents

Isokinetic samples were taken from the gas evacuation systems. The results showed that the values, prior to dispersion and diffusion in the atmosphere, were less than the lower limit of detection: 0.6 mBq/l. This monitoring was continuous until the decontamination of the smoke clearing systems was completed.

Radiological control of Decontamination work

The criteria for radiological protection control of the programme are summarised in the Table 2.

Table 2. Radiological protection criteria

Individual dose Constraints:

0.3 mSv per day; 1 mSv per week; 3 mSv per month

ALARA studies

If anticipated collective dose is higher than 10 mmanSv,

Use of electronic dosimeters

Works with dose rate greater than 30 μSv/h

Control of exposed time

In an ambient dose rate higher than 150 μSv/h.

Control of environmental contamination

Before and during the execution of the works with risk of producing dust.

With values between 3.75 % and 37.5 % of the LDCA, face mask will be used.

With values greater than 37.5 % of the LDCA air-fed equipment will be worn the ventilation conditions will be improved.

Control of surface contamination

Surface contamination limit in zones in which the measurement is feasible < 4 Bq/cm^2

The radiological state of areas, equipment or systems were described in the corresponding Radiation Work Permit, where a dose estimation was also made.

Controls of access

RP technicians from the UTPR - a specialised radiation protection company authorised to perform radiation protection tasks and provide specific activities such as decontamination - monitored the entrance and exit of personnel, materials and wastes, and controlled the accesses to the work zones. The controlled zones in the work places and the waste storage areas were periodically monitored, to assure that the established radiological conditions were fulfilled.

Occupational exposure

All the personnel involved in decontamination operations in Acerinox were classified as Professionally Exposed Personnel to ionizing radiation and used TLDs. The total collective dose was 60 man-mSv. For the 5 months period, the average individual dose was 0.6 mSv and the maximum individual dose was 3.5 mSv.

Table 3 shows the results of the operational dose (electronic dosimeters) for the critical tasks. 40 percent of the total collective dose was associated to the operations of decontamination of the electrical arc furnace nº 1 and of the gas ducts, where doses rates were the highest. The next critical group consists of the individuals dedicated to the wastes segregation and preparation (23% of the total collective dose). In this case, the number of people and the time used were more significant than the dose rates. As far as the internal dosimetry was concerned, two programs of monitoring were set up (whole body monitoring) , the first a few days after the start of works, to verify the suitability of the adopted protection measures. The second at the end of the work to confirm the absence of contamination. In the all cases the results were less than the recording level, 0.5 mSv.

Table 3. Operational doses for critical tasks

TASK	DOSES (man-mSv)
Electrical arc furnace nº1 and gas ducts extractions	16.1
Natural Coolers	3.1
Bag filter nº1	5.3
Bag filter nº2	2.3
Scaffolding installation and stripping	3.4
Silos	0.5
Wastes Handling	9.7
Total	40.4

Waste management

The wastes produced were put into two types of containers. The smoke dust was put into 1 m^3 big-bags, whereas metallic, plastic wastes, paper, etc., were put into 220 liters drums. Each waste was identified, labeled, and measured. The parameters registered for each container were the content, weight, size, origin, specific activity, etc. These wastes were stored within the facility in a place with the suitable radiological and physical security conditions. A significant percentage of the waste was checked with spectrometrical measures to determine the specific activity and to evaluate the decontamination process.

Conclusions

The incident in Acerinox in May 1998 did not involve illegal risks of exposure to ionizing radiation for the workers, or for the public, nor for the environment. The adopted radiological protection measures in the decontamination work were effective (no internal contamination). Also, the external doses remained at very low levels, thanks to the strict application of the established criteria of radiological protection from the beginning of the works.

Finally we would like to note that the immediate intervention made in Acerinox, has demonstrated the capacity of response and co-ordination between companies and institutions in an incident without precedent in Spain.

Approximately 2000 Ton of low level activity wastes were produced in the decontamination operation at Acerinox. (smoke dust 91%, fiber cement panel 4%, refractory bricks 2%, compressible waste 2%, metallic waste 1%).

Appendix H: HAND CALCULATIONS USED TO DETERMINE THE RADIONUCLIDES PRESENT

Beta decay radionuclides were considered because of their association with gamma-ray emissions. For each mass family, "x" indicates that the family is not seen. "*" indicates the radionuclides within a family that can be seen because of their half-lives, gamma emission abundances, etc.

x Z = 72 - 86; abundance percentages very low (<2.0%), therefore unlikely

x Z = 87 (2.55%); t1/2 too short until Rb-87 which emits no gammas

x Z = 88 (3.57%); t1/2 too short

x Z = 89 (4.76%); t1/2 too short until Sr-89 which emits very low abundance gammas (max < 0.01%) which decays into stable Y-89

x Z = 90 (5.8%); t1/2 too short until Sr-90 which has long t1/2 (29.2 a)

Z = 91 (5.84%); t1/2 too short until Sr-91 -> (57.6%) Y-91m & (42.4%) Y-91 -> Zr-91

*Sr-91, Y-91m

x Z = 92 (6.03%); t1/2 too short

Z = 93 (6.37%); t1/2 too short until Y-93 -> Zr-93 which has long t1/2 (1.5E6 a)

*Y-93

x Z = 94 (6.50%); t1/2 too short

Z = 95 (6.50%); t1/2 too short until Zr-95 -> (~100%) Nb-95 -> Mo-95

*Zr-95, Nb-95 keyline at 765.78 keV may be Type II partially hidden by 763.4 keV Tl-208 line

x Z = 96 (6.3%); t1/2 too short until Zr-96 which has long t1/2 (3.56E17 a)

Z = 97 (5.98%); t1/2 too short until Zr-97 -> (97.3%) Nb-97m & (2.7%) Nb-97 -> Mo-97

*Zr-97, Nb-97

Z = 98 (5.78%); t1/2 too short until Nb-98 -> Mo-98

*Nb-98 keyline at 787.4 keV may be Type II partially hidden by 785.6 keV Bi-212 line

Z = 99 (6.1%); t1/2 too short until Mo-99 -> (87.51%) Tc-99m & (12.29%) Tc-99 -> Ru-99

*Mo-99, Tc-99m

x Z = 100 (6.28%); t1/2 too short

x Z = 101 (5.18%); t1/2 too short

x Z = 102 (4.29%); t1/2 too short

Z = 103 (3.03%); t1/2 too short until Ru-103 -> (~100%) Rh-103m -> Rh-103

*Ru-103

x Z = 104 (1.88%) low abundance, therefore unlikely; t1/2 too short

Z = 105 (0.96%) low abundance, therefore unlikely; t1/2 too short until Ru-105 -> (28%) Rh-105m & (72%) Rh-105 -> Pd-105

*Rh-105, Ru-105 keyline at 724.3 keV may be hidden behind multiplet peaks from 722.25 keV to 727.4 keV

x Z = 106 - 128; abundance percentages very low (<0.5%), therefore unlikely

x Z = 129 (0.75%); t1/2 too short until I-129 which has long t1/2 (1.6E7 a)

x Z = 130 (1.81%); t1/2 too short until Te-130 which has long t1/2 (1E21 a)

Z = 131 (2.89%); t1/2 too short until Sb-131 (t1/2 too short) -> (6.8%) Te131m &
(93.2%) Te-131 -> I-131 -> Xe-131

*Te-131, Te-131m, I-131

Z = 132 (4.31%); t1/2 too short until Te-132 -> I-132 -> Xe-132

*Te-132, I-132

Z = 133 (6.69%); I-133 -> (2.88%) Xe-133m (most abundant gamma line within energy range of interest at 233.22 keV may be hidden under multiplet peaks from 228.33 keV to 253.71 keV) & (97.12%) Xe-133 -> Cs-133

*I-133, Xe-133m, Xe-133

x Z = 134 (7.87%); t1/2 too short

Z = 135 (6.54%); t1/2 too short until I-135 -> (15.5%) Xe-135m (keyline at 526.56 keV may be hidden under multiplet peaks from 507.66 keV to 537.37 keV) & (84.5%) Xe-135 -> Cs-135 -> Ba-135

*I-135, Xe-135m, Xe-135

x Z = 136 (6.32%); t1/2 too short, I expected to see Cs-136 but did not

x Z = 137 (6.19%); t1/2 too short until Cs-137 which has long t1/2 (30a)

x Z = 138 (6.71%); t1/2 too short

x Z = 139 (6.4%); t1/2 too short

Z = 140 (6.21%); t1/2 too short until Ba-140 -> La-140 -> Ce-140

*Ba-140, La-140

Z = 141 (5.8%); t1/2 too short until Ce-141 -> Pr-141 which has long t1/2 (2E16 a)

*Ce-141

x Z = 142 (5.84%); t1/2 too short until Ce-142 which has long t1/2 (5E16 a)

Z = 143 (5.95%); t1/2 too short until Ce-143 -> Pr-143 -> Nd-143

*Ce-143

x Z = 144 (5.50%); t1/2 too short until Ce-144 which has long t1/2 (285.8 d)

x Z = 145 (3.93%); t1/2 too short until Pr-145 which emits gammas of low abundance -> Nd-145 which has long t1/2 (1E17 a)

x Z = 146 (3.00%); t1/2 too short

Z = 147 (2.25%); t1/2 too short until Nd-147 (keyline at 531.02 keV may be hidden under multiplet peaks from 507.66 keV to 537.37 keV) -> Pm-147 (low abundance gammas only) -> Sm-147 which has long t1/2 (1.06E11 a)

*Nd-147

x Z = 148 (1.67%); t1/2 too short until Nd-148 which has long t1/2 (~1E18 a)

Z = 149 (1.08%); t1/2 too short until Pm-149 (keyline at 285.95 keV may exist as Type II within multiplet peaks from 288.08 keV to 305.84 keV) -> Sm-149

*Pm-149

x Z = 150 (0.653%); t1/2 too short until Nd-150 which has long t1/2 (>1.3E19 a)

Z = 151 (0.147%); t1/2 too short until Pm-151 -> Sm-151 which has long t1/2 (90 a)

*Pm-151

x Z = 152 (0.268%); t1/2 too short

Z = 153 (0.158%); t1/2 too short until Sm-153 -> Eu-153

*Sm-153

x Z > 153; abundance percentages very low (<0.1%), therefore unlikely

REFERENCES

Ahrens, C. (1994). Meteorology Today, 5th Edition. New York: West Publishing Company.

Benedict, M., et. al. (1981). Nuclear Chemical Engineering, 2nd Edition. New York: McGraw Hill.

Biegalski, K. et. al. (1999). Medical Industry Interference with CTBT Monitoring of Atmospheric Radionuclides. 21st Seismic Research Symposium Proceedings. Las Vegas, NV.

Biegalski, S. (1999). Distribution and Trends of Natural Radionuclide Concentrations at CTBT Radionuclide Monitoring Stations. 21st Seismic Research Symposium Proceedings. Las Vegas, NV.

Biegalski, S., et. al. (1999). Cesium-137 Distributions and Trends at CTBT Radionuclide Monitoring Stations and Their Implications on CTBT Monitoring. 21st Seismic Research Symposium Proceedings. Las Vegas, NV.

Black Forest -- Germany's Beautifully Forested Southwest web site (n.d.). Retrieved from http://www.tompgalvin.com/places/de/baden_wuerttemberg/black_forest.htm

Bohner, J., et. al. (1997). "Radonuclide Monitoring Operations Report of the Prototype International Data Center, Second Quarter, CY 1997." Arlington, VA: Pacific-Sierra Research Corporation.

Bohner, J., et. al. (1998). "Radonuclide Monitoring Operations Report of the Prototype International Data Center, Second Quarter, CY 1998." Arlington, VA: Pacific-Sierra Research Corporation.

Canada's National Meson Facility Associate Members (1998, April). "TRIUMF G Annual Report Scientific Activities, 1997."

Currie, L. (1968). Limits for Qualitative Detection and Quantitative Determination: Application to Radiochemistry. Journal of Analytical Chemistry, 40, 586-593.

East Tennessee State University Radioactive Materials License Application, Revision 1, Section 10: Radiation Detection Instruments. (n.d.). Retrieved from http://www.etsu.edu/ospa/rso/rso1/sup_lic_pdf/SECT-10R1.pdf

Eisenbud, M., and Gesell, T. (1997). Environmental Radioactivity, 4th Edition. New York: Academic Press.

Environmental Measurements Laboratory (1997, February). "HASL-300, 28th Edition, Vol. I, Section 2.1, Rev. 0," from http://www.eml.doe.gov/publications/procman/

Environmental Protection Agency web site. (n.d.). Retrieved from http://www.epa.gov

Evans, W. (1995). "Model for Assessment of Surveillance Strategies." Arlington, VA: Pacific-Sierra Research Corporation.

Examples of SEA Process: Algeciras, Spain Radionuclide Trigger (2001, January). Treaty Verification Office briefing. Arlington, VA.

Faw, R., and Shultis, J. (1993). Radiological Assessment. Upper Saddle River, New Jersey: PTR Prentice Hall, Inc.

Firestone, R. (2000, May 22). "The Berkeley Laboratory Isotopes Project's Exploring the Table of Isotopes." Earnest O. Lawrence Berkley National Laboratory, from http://ie.lbl.gov/education/isotopes.htm

Firestone, R. and Ekstrom, L. (2004, January). "WWW Table of Radioactive Isotopes Version 2.1." Lawrence Berkley National Laboratory Isotopes Project - LUNDS Universitet, from http://ie.lbl.gov/toi/images/tori.gif

Glasstone, S., and Dolan, P. (1977). The Effects of Nuclear Weapons, 3rd Edition. Washington, DC: U.S. Department of Defense.

Guide to the Nuclear Wall Chart -- Detectors. (2000, August 9). Retrieved from http://www.lbl.gov/abc/wallchart/chapters/12/2.html

Health Canada web site (n.d.). Retrieved from http://www.hc-sc.gc.ca/

Human Health Fact Sheet ANL (2002, July). "Natural Decay Series: Uranium, Radium, and Thorium," from www.ead.anl.gov/pub/doc/NaturalDecaySeries.pdf

Hospitals Around The World by Region - Europe (2004). Retrieved September 1, 2004, from http://www.escapeartist.com/Offshore_Health_Care/Europe.html

International Atomic Energy Agency (1999). "Nuclear Research Reactors in the World," from http://www.iaea.org/worldatom/rrdb

International Atomic Energy Agency (2000). "Power Reactor Information System (PRIS)," from http://www.iaea.org/programmes/a2/index.html

IUPAC Compendium of Chemical Terminology, 2nd Edition (1997). Retrieved from http://www.iupac.org/publications/compendium/index.html

Ivashkin, N., et. al. (1997). "Assessment of Information Content of radionuclide Monitoring Data during On-Site Inspection for Identification of 'Author' of Nuclear test in Sea Area." CTBT Technologies Workshop. Livermore, CA: Lawrence Livermore National Laboratory.

Knief, R., et. al. (1992). Nuclear Engineering, 2nd Edition. Washington, DC: Taylor and Francis.

Knoll, G. (1989). Radiation Detection and Measurement, 2nd Edition. New York: John Wiley and Sons, Inc.

Lamarsh, J., and Baratta, A. (2001). Introduction to Nuclear Engineering, 3rd Edition. Upper Saddle River, New Jersey: Prentice Hall, Inc.

Lougheed, R. (1997). "Nuclear Explosion Source Terms and Fractionation Effects." CTBT Technologies Workshop. Livermore, CA: Lawrence Livermore National Laboratory.

Lougheed, R., et. al. (1995). Report on the Peer Review of the Conference on Disarmament International Monitoring System Expert Group Report CD/NTB/WP.224 Part II: Radionuclide Monitoring; Washington, DC: U. S. Department of Energy.

Lucas, J. (1997). "Event Discrimination Methods." CTBT Technologies Workshop. Livermore, CA: Lawrence Livermore National Laboratory.

Martin Marietta Energy Systems, Inc. (1992, September). "Environmental Monitoring Plan for Airborne Radioactivity from Fugitive and Diffuse Sources," from http://www.epa.gov/radiation/docs/neshaps/nesh_sub_h_mon-pln-or_9-92.pdf

Mason, L., et. al. (1998, May). Ultra-Sensitive Environmental Monitoring of Emissions from a Radioisotope Production Facility. 11th Pacific Basin Nuclear Conference Proceedings, Volume 1. Banff, Canada.

Mazzola, C., and Addis, R. (1995, March). Atmospheric Dispersion Modeling Resources, Second Edition. Oak Ridge, TN: Oak Ridge Institute for Science and Education.

Measday, D., et. al. (2001, February). Detection of Anthropogenic Radionuclides by the CA002 Monitoring Station for the Comprehensive Test Ban Treaty. Health Physics, 80 (2).

Miley, H., et. al. (1998, June). Automated Aerosol Sampling and Analysis for the Comprehensive Test Ban Treaty. IEEE Transactions on Nuclear Science, 45 (3).

Miley, H., et. al. (1999). Evaluation of Fission Product Isotopes for Field or Laboratory Detection. 21st Seismic Research Symposium Proceedings. Las Vegas, NV.

Miley, H., et. al. (1999). Evaluation of Laboratory Detection Systems for Fission Product Detection. 21st Seismic Research Symposium Proceedings. Las Vegas, NV.

Moody, K. (1997). "Characteristics of an Attribution Database." CTBT Technologies Workshop. Livermore, CA: Lawrence Livermore National Laboratory.

Murray, R. (1993). Nuclear Energy, 4th Edition. New York: Butterworth Heinemann.

National Oceanic and Atmospheric Administration Air Resources Laboratory (n.d.). "Archived Meteorology (North America): Archived Model Graphics," from http://www.arl.noaa.gov/ready/ametus.html

National Oceanic and Atmospheric Administration Air Resources Laboratory (n.d.). "Archived Meteorology (World): Archived Model Graphics," from http://www.arl.noaa.gov/ready/amet.html

National Oceanic and Atmospheric Administration Air Resources Laboratory (n.d.). "NOAA ARL HYSPLIT Model: On-line (Internet-based) HYSPLIT," from http://www.arl.noaa.gov/ready/hysplit4.html

National Oceanic and Atmospheric Administration National Climatic Data Center (n.d.). "NCDC Historical GOES Browse Server," from http://cdo.ncdc.noaa.gov/GOESBrowser/goesbrowser

Nelson, S. (2003, September 30). "EENS 211 Earth Materials: Mineral Chemistry," from http://www.tulane.edu/~sanelson/eens211/mineral_chemistry.htm

Nuclear Energy Agency/Organisation for Economic Co-operation and Development (2002). Chernobyl: Assessment of Radiological and Health Impacts, from http://www.nea.fr/html/rp/chernobyl/chernobyl.html

Nuclear Regulatory Commission web site. (n.d.). Retrieved from http://www.nrc.gov

Nucleonics Week (1998, September 24). "Legal Void Meant Costly Delay When Spanish Firm Melted Source," from http://www.platts.com/Nuclear/Newsletters%20&%20Reports/Nucleonics%20Week/

Proteccion Ambiental (n.d.). Retrieved October 2004, from http://translate.google.com/translate?hl=en&sl=es&u=http://www.nodo50.org/ecologistas.cadiz/prt_amb.html&prev=/search%3Fq%3DACERINOX%2Bcsn%2B1700%26num%3D100%26hl%3Den%26lr%3D%26as_qdr%3Dall

Radiological Protection in the Radioactive Incident of ACERINOX in Spain (1998). "Actualite Internationale Du Nucleaire," from http://64.233.161.104/search?q=cache:jZs9abRM7kIJ:resosol.org:16080/InfoNuc/News/NewsNuc98.html+ACERINOX+csn+LAINSA&hl=en

Shchukin, V. (1997). "Identifying Originator of a Clandestine Nuclear Test in Ocean." CTBT Technologies Workshop. Livermore, CA: Lawrence Livermore National Laboratory.

Seinfeld, J., and Pandis, S. (1998). Atmospheric Chemistry and Physics. New York: John Wiley and Sons, Inc.

Shinohara, K, and Asano, T. (1992). Environmental Dose Assessment for Low-Level Radioactive Effluents discharged from Tokai Reprocessing Plant. Health Physics, 62 (1).

Slade D. (1968, July). "Meteorology and Atomic Energy." Oak Ridge, TN: U.S. Atomic Energy Comission.

The Daresbury Synchrotron Radiation Source (2004, November 4). "The World of Synchrotron Radiation," from http://www.srs.ac.uk/srs/SRworldwide/area3.htm

Thompson, R., et. al. (1995). "Technology for Cooperative In-Country Aerosol Monitoring of Radionuclides for Proliferation Detection." Richland, Washington: Pacific Northwest Laboratory.

Toivonen, H. (1997). "Xe-133m/Xe-133, Xe-135/Xe-133." CTBT Technologies Workshop. Livermore, CA: Lawrence Livermore National Laboratory.

Tourism British Columbia web site (n.d.) Retrieved from http://www.hellobc.com/en-CA/default.htm

Tourism Vancouver web site (n.d.). Retrieved from http://www.tourismvancouver.com/

TRIUMF web site (n.d.). Retrieved from http://www.triumf.info/

U.S. Army Corps of Engineers (1997, June 30). "Engineering and Design - Guidance For Low-Level Radioactive Waste (LLRW) and Mixed Waste (MW) Treatment and

Handling, EM 1110-1-4002," from http://www.usace.army.mil/inet/usace-docs/eng-manuals/em1110-1-4002/toc.htm

U.S. Department of Energy Radiological Control Technician Course (1995, May). "2.06: Air Sampling Program/Methods Lesson Outline -- Instructor's Notes," from http://cted.inel.gov/cted/eh_mat/206595lp.pdf

U.S. Department of Energy Radiological Control Technician Course (1995, May). "2.18: Air Sampling Equipment Lesson Outline -- Instructor's Notes," from http://cted.inel.gov/cted/eh_mat/218595lp.pdf

U.S. Environmental Protection Agency (1989, October). A Guide For Determining Compliance With The Clean Air Act Standards For Radionuclide Emissions From NRC-Licensed And Non-DOE Federal Facilities (Revision 2), EPA 520/1-89.002. Washington, DC

United Nations Scientific Committee on the Effects of Atomic Radiation (2000). "Report to the General Assembly with Scientific Annexes, Volume I: Sources, Annex C: Exposures to the public from man-made sources of radiation," from http://www.unscear.org/pdffiles/annexc.pdf

United Nations Scientific Committee on the Effects of Atomic Radiation (2000). "Report to the General Assembly with Scientific Annexes, Volume I: Sources, Annex D: Medical radiation exposures," from http://www.unscear.org/pdffiles/annexd.pdf

University of British Columbia web site (n.d.). Retrieved from http://www.ubc.ca/

Uranium Information Centre Ltd. (2004, December). "Research Reactors: UIC Nuclear Issues Briefing Paper # 66," http://www.uic.com.au/nip66.htm

Uslu, I., and Birol, E. (2000). "Detection Systems and Regulatory Issues for Illicit Trafficking ff Radioactive Materials." Ankara, Turkey: Turkish Atomic Energy Authority

Welcome to British Columbia! (2003). Retrieved August 2004, from http://www.cherrybouton.com/welcome.html

Wikipedia. (n.d.). Retrieved September 2004, from http://en.wikipedia.org/wiki/Main_Page

Wild, J. (1997). "Precursor and Fractionation Effects on Radionuclide Signatures." CTBT Technologies Workshop. Livermore, CA: Lawrence Livermore National Laboratory.

Williams, D., et. al. (1999). "Radonuclide Monitoring Operations Report of the Prototype International Data Center, First Quarter, CY 1999." Arlington, VA: Pacific-Sierra Research Corporation.

Williams, D., et. al. (1999). "Radonuclide Monitoring Operations Report of the Prototype International Data Center, Second Quarter, CY 1999." Arlington, VA: Pacific-Sierra Research Corporation.

Winter, M. (2003). "Chemistry: WebElements Periodic Table: Professional Edition: Definitions: Abundance in Earth's crust," from http://www.webelements.com/webelements/properties/text/image-intensity/abund-crust.html/